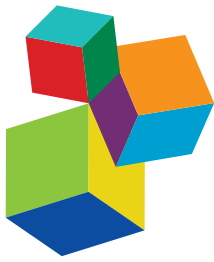


MICROBIAL ECOLOGY IN THE NORTH PACIFIC SUBTROPICAL GYRE

EDITED BY: Samuel T. Wilson and Matthew J. Church

PUBLISHED IN: Frontiers in Marine Science and Frontiers in Microbiology



Frontiers Copyright Statement

© Copyright 2007-2018 Frontiers Media SA. All rights reserved.

All content included on this site, such as text, graphics, logos, button icons, images, video/audio clips, downloads, data compilations and software, is the property of or is licensed to Frontiers Media SA ("Frontiers") or its licensees and/or subcontractors. The copyright in the text of individual articles is the property of their respective authors, subject to a license granted to Frontiers.

The compilation of articles constituting this e-book, wherever published, as well as the compilation of all other content on this site, is the exclusive property of Frontiers. For the conditions for downloading and copying of e-books from Frontiers' website, please see the Terms for Website Use. If purchasing Frontiers e-books from other websites or sources, the conditions of the website concerned apply.

Images and graphics not forming part of user-contributed materials may not be downloaded or copied without permission.

Individual articles may be downloaded and reproduced in accordance with the principles of the CC-BY licence subject to any copyright or other notices. They may not be re-sold as an e-book.

As author or other contributor you grant a CC-BY licence to others to reproduce your articles, including any graphics and third-party materials supplied by you, in accordance with the Conditions for Website Use and subject to any copyright notices which you include in connection with your articles and materials.

All copyright, and all rights therein, are protected by national and international copyright laws.

The above represents a summary only. For the full conditions see the Conditions for Authors and the Conditions for Website Use.

ISSN 1664-8714
ISBN 978-2-88945-646-8
DOI 10.3389/978-2-88945-646-8

About Frontiers

Frontiers is more than just an open-access publisher of scholarly articles: it is a pioneering approach to the world of academia, radically improving the way scholarly research is managed. The grand vision of Frontiers is a world where all people have an equal opportunity to seek, share and generate knowledge. Frontiers provides immediate and permanent online open access to all its publications, but this alone is not enough to realize our grand goals.

Frontiers Journal Series

The Frontiers Journal Series is a multi-tier and interdisciplinary set of open-access, online journals, promising a paradigm shift from the current review, selection and dissemination processes in academic publishing. All Frontiers journals are driven by researchers for researchers; therefore, they constitute a service to the scholarly community. At the same time, the Frontiers Journal Series operates on a revolutionary invention, the tiered publishing system, initially addressing specific communities of scholars, and gradually climbing up to broader public understanding, thus serving the interests of the lay society, too.

Dedication to Quality

Each Frontiers article is a landmark of the highest quality, thanks to genuinely collaborative interactions between authors and review editors, who include some of the world's best academicians. Research must be certified by peers before entering a stream of knowledge that may eventually reach the public - and shape society; therefore, Frontiers only applies the most rigorous and unbiased reviews.

Frontiers revolutionizes research publishing by freely delivering the most outstanding research, evaluated with no bias from both the academic and social point of view. By applying the most advanced information technologies, Frontiers is catapulting scholarly publishing into a new generation.

What are Frontiers Research Topics?

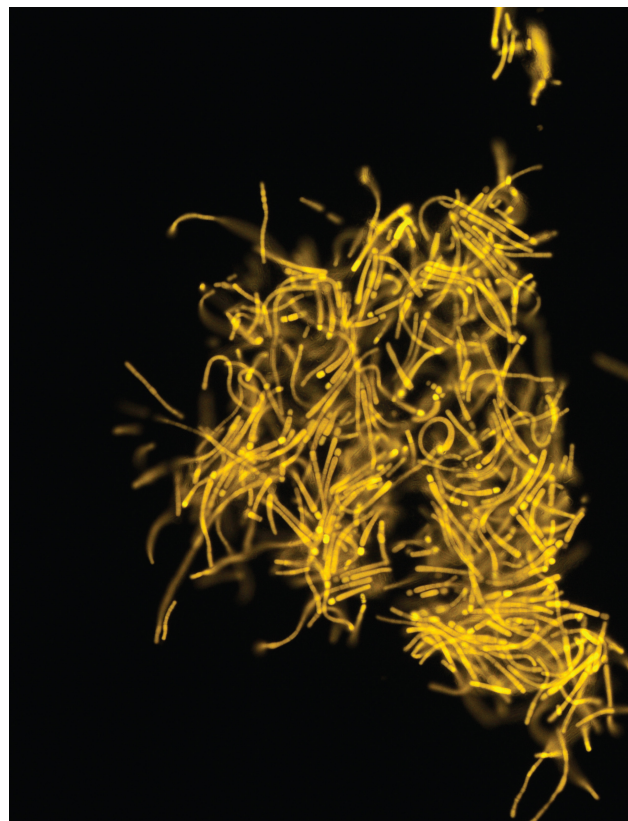
Frontiers Research Topics are very popular trademarks of the Frontiers Journals Series: they are collections of at least ten articles, all centered on a particular subject. With their unique mix of varied contributions from Original Research to Review Articles, Frontiers Research Topics unify the most influential researchers, the latest key findings and historical advances in a hot research area! Find out more on how to host your own Frontiers Research Topic or contribute to one as an author by contacting the Frontiers Editorial Office: researchtopics@frontiersin.org

MICROBIAL ECOLOGY IN THE NORTH PACIFIC SUBTROPICAL GYRE

Topic Editors:

Samuel T. Wilson, University of Hawai'i at Manoa, United States

Matthew J. Church, University of Montana, United States



Fluorescence micrograph of the heterocystous nitrogen-fixing cyanobacteria *Calothrix* sp. isolated from Station ALOHA.

Image courtesy of Christopher R. Schwarcz

The microbial community in the oligotrophic North Pacific Subtropical Gyre is dominated by unicellular microorganisms less than a few micrometers in size. Despite the persistent low nutrient concentrations, phytoplankton growth rates appear near maximal, sustained by the recycling of nutrients with plankton population sizes regulated by processes such as zooplankton grazing and viral lysis. Seasonal pulses of particle export to the deep sea and increases in phytoplankton abundance occur during the summer months; however, the factors that result in these imbalances in growth and loss processes are not well understood. Nonetheless, as a result of persistent fieldwork and development of sensitive methodologies, the biogeochemical and ecological dynamics occurring over timescales ranging from diel to interannual are being revealed. This Research Topic covers multiple aspects of microbial oceanography in the oligotrophic North Pacific Subtropical Gyre including

identification and isolation of microorganisms, quantification of microbial biomass and turnover, metabolism and physiological activities, and microbial-mediated biogeochemical cycling.

All of the papers use field data collected by either the Hawaii Ocean Time-series (HOT) program, the Center for Microbial Oceanography: Research and Education (C-MORE) or the Simons Collaboration on Ocean Processes and Ecology (SCOPE). These three programs have greatly increased our understanding of microbial ecology and biogeochemical cycling in the NPSG, in part by providing unparalleled access to the NPSG on oceanographic research vessels.

Citation: Wilson, S. T., Church, M. J., eds (2018). *Microbial Ecology in the North Pacific Subtropical Gyre*. Lausanne: Frontiers Media. doi: 10.3389/978-2-88945-646-8

Table of Contents

- 05 Editorial: Microbial Ecology in the North Pacific Subtropical Gyre**
Samuel T. Wilson and Matthew J. Church
- 08 Distinct Siderophores Contribute to Iron Cycling in the Mesopelagic at Station ALOHA**
Randelle M. Bundy, Rene M. Boiteau, Craig McLean, Kendra A. Turk-Kubo, Matt R. McIlvin, Mak A. Saito, Benjamin A. S. Van Mooy and Daniel J. Repeta
- 23 Light-Enhanced Microbial Organic Carbon Yield**
John R. Casey, Sara Ferrón and David M. Karl
- 32 ALOHA From the Edge: Reconciling Three Decades of in Situ Eulerian Observations and Geographic Variability in the North Pacific Subtropical Gyre**
Maria T. Kavanaugh, Matthew J. Church, Curtiss O. Davis, David M. Karl, Ricardo M. Letelier and Scott C. Doney
- 46 Bacterial Succession on Sinking Particles in the Ocean's Interior**
Erik A. Pelve, Kristina M. Fontanez and Edward F. DeLong
- 61 Differential Responses of Eukaryotic Phytoplankton to Nitrogenous Nutrients in the North Pacific Subtropical Gyre**
Yoshimi M. Rii, Robert R. Bidigare and Matthew J. Church
- 78 Isolation and Characterization of Bacteria That Degrade Phosphonates in Marine Dissolved Organic Matter**
Oscar A. Sosa, Daniel J. Repeta, Sara Ferrón, Jessica A. Bryant, Daniel R. Mende, David. M. Karl and Edward F. DeLong
- 94 In Situ Diazotroph Population Dynamics Under Different Resource Ratios in the North Pacific Subtropical Gyre**
Kendra A. Turk-Kubo, Paige Connell, David Caron, Mary E. Hogan, Hanna M. Farnelid and Jonathan P. Zehr
- 112 Dynamics of Prochlorococcus and Synechococcus at Station ALOHA Revealed Through Flow Cytometry and High-Resolution Vertical Sampling**
Ger J. van den Engh, Joseph K. Doggett, Anne W. Thompson, Martina A. Doblin, Carla N. G. Gimpel and David M. Karl
- 126 Temporal Variability of *Trichodesmium* spp. and Diatom-Diazotroph Assemblages in the North Pacific Subtropical Gyre**
Angelicque E. White, Katie S. Watkins-Brandt and Matthew J. Church



Editorial: Microbial Ecology in the North Pacific Subtropical Gyre

Samuel T. Wilson^{1*} and Matthew J. Church²

¹ Department of Oceanography, Daniel K. Inouye Center for Microbial Oceanography: Research and Education, University of Hawaii at Manoa, Honolulu, HI, United States, ² Flathead Lake Biological Station, University of Montana, Polson, MT, United States

Keywords: microbial ecology, microbiology, North Pacific Subtropical Gyre, oligotrophic, biogeochemical cycling, bacteria, oceanography

Editorial on the Research Topic

Microbial Ecology in the North Pacific Subtropical Gyre

Microorganisms play a critical role in controlling the source-sink behavior and cycling of major and minor elements in the biosphere. This occurs through cellular metabolic processes such as photosynthesis, respiration, oxidation-reduction, assimilation, and exudation, and via interactions with other constituents of the food web including predation and viral lysis. In the open ocean, microbes influence key processes such as the uptake of carbon dioxide from the atmosphere and the export of carbon from the sunlit waters to the seafloor. The subtropical ocean gyres are large expansive ecosystems that play globally important roles in carbon cycling (Martin et al., 1987; Emerson et al., 1997). Our knowledge of these habitats was transformed through initiation of shipboard time-series programs in the late 1980s in both the Sargasso Sea and the North Pacific Subtropical Gyre (NPSG). In the NPSG, Station ALOHA was established as the field outpost for the Hawaii Ocean Time-series (HOT) program (Figure 1). After 30 years of near-monthly measurements at Station ALOHA, the seasonal and interannual variability associated with key ecosystem processes are now well-described (Figure 2). However, assessment of the contributions of specific microorganisms to the ecology and metabolic activity of the NPSG ecosystem remain less understood. Since recognition of the key role that the microbial food web plays in nutrient recycling and the flux of organic matter (Azam et al., 1983), numerous studies have highlighted the need to link the identity of specific microorganisms to cellular-level processes for insight into ecosystem-scale dynamics (e.g., Follows et al., 2007).

OPEN ACCESS

Edited and reviewed by:

Hongyue Dang,
Xiamen University, China

*Correspondence:

Samuel T. Wilson
stwilson@hawaii.edu

Specialty section:

This article was submitted to
Aquatic Microbiology,
a section of the journal
Frontiers in Marine Science

Received: 07 August 2018

Accepted: 29 August 2018

Published: 21 September 2018

Citation:

Wilson ST and Church MJ (2018)
Editorial: Microbial Ecology in the
North Pacific Subtropical Gyre.
Front. Mar. Sci. 5:334.
doi: 10.3389/fmars.2018.00334

This Research Topic invited contributions on all aspects of microbial ecology in the NPSG. Consistent with the oligotrophic nature of this habitat, the majority of publications focus on light and nutrient acquisition by key groups of microbial populations. For example, van den Engh et al. examine the vertical depth distribution of *Prochlorococcus* and *Synechococcus* and show how these two groups of cyanobacteria are distributed in the lower euphotic zone. Casey et al. investigate how sunlight influences the metabolism of microorganisms in this ecosystem. Using glycolate as the experimental carbon compound, the authors quantify rates of photoheterotrophic metabolism. Two of the articles in this issue focus specifically on the ecology of nitrogen-fixing microorganisms in the NPSG. In particular, White et al. quantify the abundance of large nitrogen-fixing microorganisms ("diazotrophs") over a 2 year period in the NPSG from both direct cell counts and quantitative polymerase chain reaction amplification of nitrogenase (*nifH*) genes. Turk-Kubo et al. provide measurements of microzooplankton grazing on diazotrophs in the near surface ocean. Their work helps constrain grazing of diazotrophs as a loss mechanism balancing growth of these microorganisms. This is a key term required for the improvement of representation

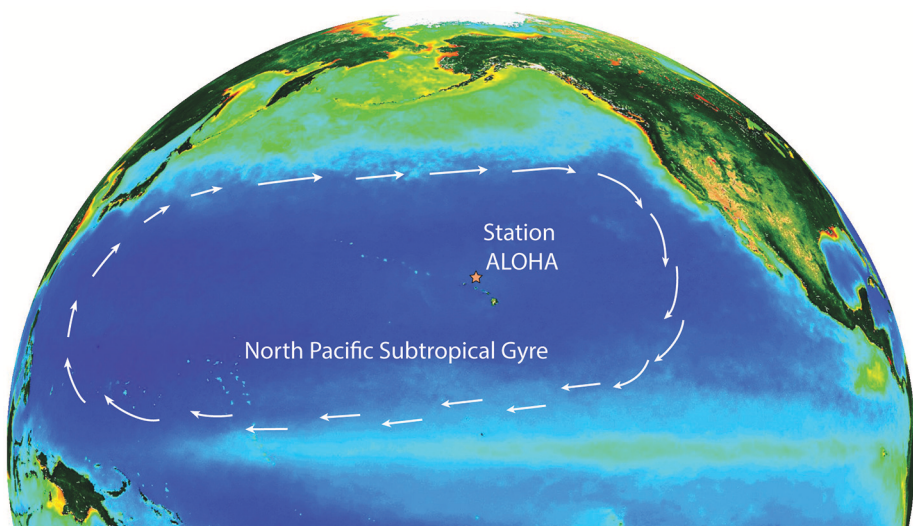


FIGURE 1 | Map of the North Pacific Ocean showing the North Pacific Subtropical Gyre and the location of Station ALOHA. The arrows depict the areal extent of the North Pacific Subtropical Gyre and show the direction of geostrophic flow. The background colors depict summer chlorophyll a distributions as determined by the SeaWiFS satellite mission (<https://oceancolor.gsfc.nasa.gov/SeaWiFS/>).

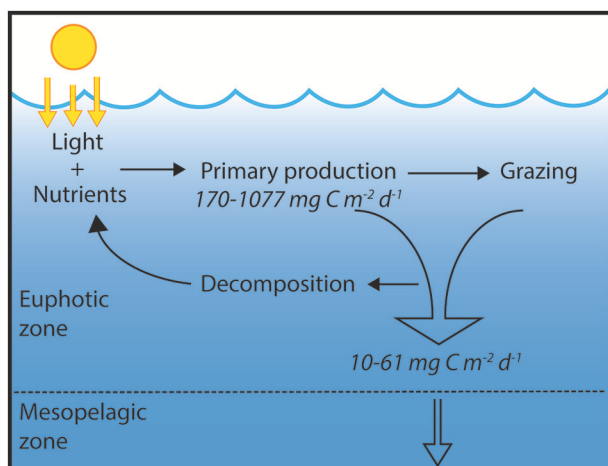


FIGURE 2 | Schematic of ecosystem process in the upper ocean, highlighting the central roles of primary production, grazing, remineralization, and export. The microorganisms and metabolic activity that regulates these fluxes form the basis of this Research Topic. The values depicted represent the range of carbon input via primary production (as measured by ^{14}C assimilation) and carbon export via sinking particles (as measured by particle interceptor traps); all data were obtained from the Hawaii Ocean Time-series program (<http://hahana.soest.hawaii.edu/hot/hot-dogs/interface.html>).

of diazotrophs in ecosystems models (Monteiro et al., 2010). Other papers in this issue evaluate how specific nutrient substrates influence the growth of microorganisms. Rii et al. investigate the response of naturally-occurring photosynthetic picoeukaryotes and larger ($>3\text{ }\mu\text{m}$) phytoplankton to both nitrate and ammonium. These authors identify that phylogenetically distinct groups of phytoplankton demonstrate seasonally-dependent responses to nitrogen availability.

Sosa et al. highlight microbial acquisition of carbon and phosphorus from high molecular weight dissolved organic material. Their observations link widespread members of the bacterioplankton, including members of the Roseobacter and Gammaproteobacteria, to semi-labile dissolved organic material cycling and aerobic production of methane in the ocean. Bundy et al. examined acquisition of dissolved iron by marine microorganisms, identifying, and quantifying vertical distributions of iron-binding siderophores in the NPSG. Their results demonstrate that the vast majority of iron in this ecosystem is organically complexed, and highlight a possible role for complexed iron in regulating microbial utilization of organic matter in this ecosystem. Pelve et al. utilized metagenomics to characterize microbial communities associated with sinking particles. Through the use of preserved (i.e., poisoned) and non-preserved collection of sinking particles, they identify successional patterns in microorganisms that facilitate the degradation of particles as they sink from the upper ocean to the deep sea. Finally, Kavanaugh et al. leverage satellite remote sensing observations to assess how interannual variability in the spatial extent of the oligotrophic NPSG influences the time series observations at Station ALOHA. The resulting analyses provide new insights into how gyre-scale spatial heterogeneity influences the fixed point observations conducted at Station ALOHA.

In summary, the papers included in this Research Topic focused on novel aspects of the ecology and biogeochemical role of microorganisms in the NPSG, with particular focus on linking the identities and functions of microorganisms to ecosystem-scale patterns. These contributions provide new information on ecological interactions occurring among the microbial community of the NPSG, ultimately helping to resolve key aspects of ocean ecosystems necessary for improving predictive models on the role of ocean biology on Earth's climate system.

AUTHOR CONTRIBUTIONS

All authors listed have made a substantial, direct and intellectual contribution to the work and approved it for publication.

ACKNOWLEDGMENTS

Papers featured in this Special Issue leveraged the field data and/or scientific infrastructure of the Hawaii Ocean Time-series

(HOT) program, the Center for Microbial Oceanography: Research and Education (C-MORE), and the Simons Collaboration on Ocean Processes and Ecology (SCOPE). Together, these programs have increased our understanding of the interconnections between microbial ecology and biogeochemical cycling in the NPSG. The U.S. National Science Foundation provided funding for both HOT and C-MORE (awards OCE-1260164 and EF-0424599, respectively), while the Simons Foundation funds the SCOPE program (award #329108).

REFERENCES

- Azam, F., Fenchel, T., Field, J. G., Gray, J. S., Meyer-Reil, L. A., and Thingstad, F. (1983). The ecological role of water-column microbes in the sea. *Mar. Ecol. Prog. Ser.* 10, 257–263. doi: 10.3354/meps010257
- Emerson, S., Quay, P., Karl, D., Winn, C., Tupas, L., and Landry, M. (1997). Experimental determination of the organic carbon flux from open-ocean surface waters. *Nature* 389, 951–954. doi: 10.1038/40111
- Follows, M. J., Dutkiewicz, S., Grant, S., and Chisholm, S. W. (2007). Emergent biogeography of microbial communities in a model ocean. *Science* 315, 1843–1846. doi: 10.1126/science.1138544
- Martin, J. H., Knauer, G. A., Karl, D. M., and Broenkow, W. W. (1987). VERTEX: carbon cycling in the northeast Pacific. *Deep Sea Res.* 34, 267–285. doi: 10.1016/0198-0149(87)90086-0

Monteiro, F. M., Follows, M. J. and Dutkiewicz, S. (2010). Distribution of diverse nitrogen fixers in the global ocean. *Global Biogeochem. Cycles* 24:GB3017. doi: 10.1029/2009GB003731

Conflict of Interest Statement: The authors declare that the research was conducted in the absence of any commercial or financial relationships that could be construed as a potential conflict of interest.

Copyright © 2018 Wilson and Church. This is an open-access article distributed under the terms of the Creative Commons Attribution License (CC BY). The use, distribution or reproduction in other forums is permitted, provided the original author(s) and the copyright owner(s) are credited and that the original publication in this journal is cited, in accordance with accepted academic practice. No use, distribution or reproduction is permitted which does not comply with these terms.



Distinct Siderophores Contribute to Iron Cycling in the Mesopelagic at Station ALOHA

Randelle M. Bundy^{1,2}, Rene M. Boiteau^{1,3}, Craig McLean¹, Kendra A. Turk-Kubo⁴, Matt R. McIlvin¹, Mak A. Saito¹, Benjamin A. S. Van Mooy¹ and Daniel J. Repeta^{1*}

¹ Marine Chemistry and Geochemistry, Woods Hole Oceanographic Institution, Woods Hole, MA, United States, ² School of Oceanography, University of Washington, Seattle, WA, United States, ³ Environmental Molecular Sciences Laboratory, Pacific Northwest National Laboratory, Richland, WA, United States, ⁴ Physical and Biological Sciences, University of California, Santa Cruz, Santa Cruz, CA, United States

OPEN ACCESS

Edited by:

Samuel Wilson,
University of Hawaii at Manoa,
United States

Reviewed by:

Martha Gledhill,
University of Southampton,
United Kingdom
Oliver Baars,
Princeton University, United States

*Correspondence:

Daniel J. Repeta
drepeta@whoi.edu

Specialty section:

This article was submitted to
Aquatic Microbiology,
a section of the journal
Frontiers in Marine Science

Received: 07 December 2017

Accepted: 09 February 2018

Published: 01 March 2018

Citation:

Bundy RM, Boiteau RM, McLean C, Turk-Kubo KA, McIlvin MR, Saito MA, Van Mooy BAS and Repeta DJ (2018)

Distinct Siderophores Contribute to Iron Cycling in the Mesopelagic at Station ALOHA. *Front. Mar. Sci.* 5:61.

doi: 10.3389/fmars.2018.00061

The distribution of dissolved iron (Fe), total organic Fe-binding ligands, and siderophores were measured between the surface and 400 m at Station ALOHA, a long term ecological study site in the North Pacific Subtropical Gyre. Dissolved Fe concentrations were low throughout the water column and strong organic Fe-binding ligands exceeded dissolved Fe at all depths; varying from 0.9 nmol L⁻¹ in the surface to 1.6 nmol L⁻¹ below 150 m. Although Fe does not appear to limit microbial production, we nevertheless found siderophores at nearly all depths, indicating some populations of microbes were responding to Fe stress. Ferrioxamine siderophores were most abundant in the upper water column, with concentrations between 0.1 and 2 pmol L⁻¹, while a suite of amphibactins were found below 200 m with concentrations between 0.8 and 11 pmol L⁻¹. The distinct vertical distribution of ferrioxamines and amphibactins may indicate disparate strategies for acquiring Fe from dust in the upper water column and recycled organic matter in the lower water column. Amphibactins were found to have conditional stability constants ($\log K_{FeL_1,Fe}^{cond}$) ranging from 12.0 to 12.5, while ferrioxamines had much stronger conditional stability constants ranging from 14.0 to 14.4, within the range of observed L₁ ligands by voltammetry. We used our data to calculate equilibrium Fe speciation at Station ALOHA to compare the relative concentration of inorganic and siderophore complexed Fe. The results indicate that the concentration of Fe bound to siderophores was up to two orders of magnitude higher than inorganic Fe, suggesting that even if less bioavailable, siderophores were nevertheless a viable pathway for Fe acquisition by microbes at our study site. Finally, we observed rapid production of ferrioxamine E by particle-associated bacteria during incubation of freshly collected sinking organic matter. Fe-limitation may therefore be a factor in regulating carbon metabolism and nutrient regeneration in the mesopelagic.

Keywords: iron, siderophores, Station ALOHA, organic ligands, iron limitation

INTRODUCTION

Iron (Fe) is an essential trace metal for many cellular processes in marine phytoplankton and bacteria, including nitrogen fixation and photosynthesis (Morel and Price, 2003). The Hawaii Ocean Time-series (HOT) at Station ALOHA has been a major study site to evaluate the annual and interannual variability in Fe chemistry and its influence on oligotrophic marine ecosystems. These time-series measurements have revealed a dynamic Fe cycle, with atmospheric dust deposition and mixing of deeper waters into the photic zone acting as a fluctuating source of bioavailable Fe (Boyle et al., 2005; Fitzsimmons et al., 2015). Although Fe is not considered to be a limiting nutrient in the oligotrophic North Pacific, competition for Fe among microorganisms may still impact community dynamics (Rue and Bruland, 1995; Johnson et al., 2007; Fitzsimmons et al., 2015). *Prochlorococcus* for example, the dominant photoautotroph at Station ALOHA, can thrive even under the low Fe conditions in the oligotrophic ocean (Johnson and Lin, 2009; Thompson et al., 2011). However, larger, more transiently abundant taxa such as diatoms and nitrogen fixing photoautotrophs such as *Trichodesmium* spp. often have high cellular Fe quotas (Berman-Frank et al., 2001; Kustka et al., 2003; Roe et al., 2012). These microbes could face Fe stress at times when the atmospheric delivery of Fe is low. Indeed, Fitzsimmons et al. (2015) observed an increase in internalization of Fe by diatoms following Fe inputs to the region either from dust or mesoscale eddies (Rue and Bruland, 1995; Johnson et al., 2007; Fitzsimmons et al., 2015). While oligotrophic ecosystems such as the one at Station ALOHA may not show a chlorophyll *a* or biomass response to Fe amendments, the traditional way by which Fe limitation is defined, the cycling of Fe within the community may nevertheless be important in determining the success of specific groups of microbes and for the ecosystem as a whole.

Confounding our understanding of Fe cycling is the observation that almost all dissolved Fe in the ocean is associated with organic ligands of largely unknown identity (see review by Gledhill and Buck, 2012). Voltammetric techniques, such as competitive ligand exchange adsorptive cathodic stripping voltammetry (CLE-ACSV), have been used to measure the concentrations and binding strengths of Fe-binding organic ligands across ocean basins (GEOTRACES; Buck et al., 2015, in press; Gerringa et al., 2015), on smaller seasonal studies of Fe cycling (Bundy et al., 2014; Fitzsimmons et al., 2015), and on numerous process cruises completed over the past two decades (Gledhill and Buck, 2012). These studies have established that nanomolar concentrations of Fe-binding organic compounds occur throughout the water column, and that a fraction of these ligands have an extremely high affinity for Fe (Gledhill and Buck, 2012; Buck et al., 2015, in press; Gerringa et al., 2015; Bundy et al., 2016). These ligands are generally referred to as either strong (L_1 -type) or weaker (L_2 -type) ligands, though several additional ligand classes have also been reported (Gledhill and Buck, 2012; Bundy et al., 2014, 2016; Buck et al., 2015). These ligands may be the by-product of routine organic matter cycling by microbes, however based on their similar binding strengths for Fe, it has been inferred that a fraction of natural ligands is composed of

siderophores, high-affinity organic Fe-binding ligands used by bacteria to acquire Fe from their environment (Haygood et al., 1993; Reid et al., 1993; Butler, 1998, 2005; Hutchins et al., 1999; Martinez et al., 2000, 2001, 2003; Ito and Butler, 2005; Vraspir and Butler, 2009; Boiteau et al., 2013, 2016; Boiteau and Repeta, 2015). The presence of siderophores within the Fe-ligand pool is significant, in that it entails a direct intervention in dissolved Fe cycling and speciation by marine microbes.

Recent advances in mass spectrometry and sample processing have enabled the picomolar detection of siderophores in seawater (Gledhill et al., 2004; Mawji et al., 2008; Velasquez et al., 2011; Boiteau et al., 2013, 2016; Boiteau and Repeta, 2015), and dissolved siderophores have been successfully characterized from surface waters of the Atlantic (Mawji et al., 2008) and Pacific (Boiteau et al., 2016). CLE-ACSV does not provide molecular-level information on ligand composition and it is not yet known what fraction of the strong ligands in the water column might be siderophores. Very few direct measurements of siderophores have been made in seawater (Mawji et al., 2008; Boiteau et al., 2016). Nevertheless, the distribution and cycling of siderophores can potentially be inferred from the very strong (L_1) class of Fe-binding organic ligands measured by CLE-ACSV. Elevated L_1 concentrations have been found in oceanic regions with elevated macronutrients relative to dissolved Fe (high nitrate:Fe; Buck and Bruland, 2007; Wagener et al., 2008; Ibisani et al., 2011; Bundy et al., 2014, 2016) and have also been linked with the subsurface chlorophyll maximum (Rue and Bruland, 1995; van den Berg, 1995; Boye et al., 2001, 2006; Croot et al., 2004; Gerringa et al., 2006, 2008; Tian et al., 2006; Buck and Bruland, 2007; Wagener et al., 2008; Ibisani et al., 2011; Bundy et al., 2016), which in many regions of the ocean may be co-limited by Fe and light (Sunda and Huntsman, 1997; Holm-Hansen et al., 2005; Hopkinson et al., 2007; Hopkinson and Barbeau, 2008; Boyd and Ellwood, 2010). L_1 production has also been observed in macronutrient amendment experiments that have evolved into Fe-limiting conditions, or in incubation experiments when external Fe is added (Buck et al., 2007, 2010; Kondo et al., 2008; King and Barbeau, 2011; Bundy et al., 2014, 2016; Adly et al., 2015). CLE-ACSV-based studies therefore suggest a potentially broad role for siderophores in Fe cycling, however, there have been no studies to quantitatively compare mass spectrometric measurements of dissolved siderophores with Fe-binding ligands (L) measured by voltammetric techniques. It is therefore unknown if siderophores are among the strong ligands produced when microbial communities are Fe-limited in experimental mesocosms, or if they are present in regions where Fe is not the primary limiting nutrient.

Here we report the distribution of dissolved siderophores in the water column near Station ALOHA, a well-studied system with respect to microbial community dynamics (Karl and Lukas, 1996; Karl and Church, 2014) and Fe cycling (Boyle et al., 2005; Fitzsimmons et al., 2015). In order to capture a more complete picture of Fe speciation and cycling, we coupled our mass spectrometric analyses of siderophores with measurements of the ligand pool using traditional voltammetry. The profile data is also complemented with an Fe speciation model, as well as an incubation experiment that examines siderophore

production from particle-associated bacteria, in order to inform the mechanisms leading to rapid Fe cycling at Station ALOHA. This work is the first study to date that begins to quantitatively assess the contribution of siderophores to the overall organic pool binding Fe in seawater, and to explore the mechanisms for their depth distributions. The evidence presented also argues that siderophores play a role in the dynamic and rapid cycling of Fe at Station ALOHA by the microbial community, and suggests siderophores may contribute disproportionately to Fe cycling in the mesopelagic in this region.

METHODS

Sampling and Storage

Sampling was done on-board the R/V *Ka'imikai-O-Kanaloa* (KOK) from July 26-August 2, 2015. Water column samples for siderophore analysis were collected from 7 depths in the Station ALOHA circle (22.75°N , 158°W ; July 28, 2015) using a deckboard Teflon diaphragm pump for the 15 m sample (Cole Parmer) and a trace metal clean X-Niskin rosette (Ocean Test Equipment) for all other depths. Samples for flow cytometry were taken directly from the Niskin bottles, fixed with 0.1% paraformaldehyde, incubated in the dark for 15 min then flash-frozen with liquid nitrogen and stored at -80°C . Samples for macronutrients, dissolved Fe, total Fe-binding ligands, and siderophore analyses were filtered (0.2 μm Acropak 200 capsule filter) into trace metal clean 20 L polycarbonate carboys (Nalgene) and double bagged in heavy duty trash bags before processing. Fe samples were immediately acidified to pH 1.8 with 6 N Optima HCl (4 mL L^{-1}) and stored for 3 months before laboratory analyses. Samples for total Fe-binding ligands (measured by voltammetry) and nutrients were stored frozen at -20°C . Siderophores were extracted on board as described in the section Siderophore Identification in Station ALOHA Seawater, and the solid phase extraction columns were frozen at -20°C .

Nutrients and Flow Cytometry

Dissolved nutrients were analyzed in the Woods Hole Oceanographic Institution Nutrient Analytical Facility using a SEAL AA3 four-channel segmented flow analyzer. Nitrate (nitrate+nitrite), silicate and phosphate were analyzed with 0.01, 0.016, and 0.025 $\mu\text{mol L}^{-1}$ detection limits for each nutrient, respectively. Flow cytometry samples were enumerated for heterotrophic bacteria as well as *Prochlorococcus*, *Synechococcus*, and photosynthetic picoeukaryote cells using a BD Biosciences Influx Cell Sorter as described in Shilova et al. (2017). *Synechococcus* were enumerated based on the presence of phycoerythrin, and all other non-phycoerythrin cells were identified using forward scatter as a proxy for cell size and red fluorescence (chlorophyll *a* content). Half of the sample was stained with SYBR^{VR} Green I nucleic acid stain (Lonza, Allendale, New Jersey, USA) based on Marie et al. (1999) to determine the abundance of heterotrophic bacteria. Cell count data was processed using FlowJo v10.0.7 (Tree Star, Ashland, Oregon, USA).

Isolation and Purification of Amphibactins From *Vibrio cyclitrophicus* 1F-53

Several *Vibrio* strains containing the non-ribosomal peptide synthases encoding genes putatively identified for amphibactin production (Kem and Butler, 2015; Kem et al., 2015; Boiteau et al., 2016) were cultured in 25 mL Fe-limiting media (2.01 g casamino acids, 0.13 g ultrapure glycerophosphate disodium hydrate, and 1.03 g ultrapure ammonium chloride in 1 L of filtered South Pacific seawater). The strains assessed for amphibactin production included; *Vibrio cyclitrophicus* FF75 (FF75), *Vibrio splendidus* ZS-139 (ZS-139), *Vibrio tasmaniensis* ZS-17 (ZS-17), *Vibrio tasmaniensis* 5F-79 (5F-79), and *Vibrio cyclitrophicus* 1F-53 (1F-53). Cultures were screened for siderophore production through initial, log, and stationary phases using the chrome azurol S (CAS) colorimetric assay (Schwyn and Neilands, 1987). One liter cultures of *Vibrio cyclitrophicus* 1F-53, the strongest responder to CAS, were harvested during late log phase by centrifuging the cultures and extracting the supernatant onto a polystyrene divinyl benzene (Bond Elut ENV, Agilent Technologies) solid phase extraction (SPE) column. The column was eluted in 10 mL distilled methanol and the eluent reduced in volume to ~ 1 mL after drying down for 4 h at 35°C on a SpeedVac concentrator coupled to a refrigerated vapor trap (Thermo Scientific). Siderophores were separated by reverse phase high pressure liquid chromatography (HPLC), using an Agilent 1200 series LC and a C₁₈ column (4.2 \times 150 mm, 5 μm particle size; Agilent Zorbax), and detected by electrospray ionization quadrupole mass spectrometry (ESI-MS; Agilent 6130 series). Amphibactins were separated using a flow rate of 1 mL min^{-1} using a 98/2 gradient elution (% A/B) for 5 min, 90/10 for 15 min, 2/98 for 10 min, and 98/2 for 1 min (A = LCMS grade H₂O with 0.1% formic acid; B = LCMS grade acetonitrile with 0.1% formic acid). Fractions were collected at 30 s intervals for 35 min into acid-cleaned and methanol rinsed deep 96-well plates, concentrated for 2 h under vacuum and analyzed by LC-ESIMS (see section Siderophore Identification in Station ALOHA Seawater) to confirm the presence of each amphibactin in individual wells (Supplementary Figure 1).

Dissolved Iron and Iron-Binding Ligand Determination by Voltammetry

Dissolved Fe concentrations were determined using adsorptive cathodic stripping voltammetry (CSV) on a 663 VA Stand controlled growth mercury electrode connected to an Eco-Chemie μ Autolab-III analyzer (Metrohm USA). Briefly, 100 mL of the filtered and acidified sample was UV-irradiated for 2 h using a 909 UV Digester (Metrohm USA) in acid cleaned and Milli-Q conditioned quartz tubes. The samples were then slowly neutralized to approximately pH 8 using 1 N ammonium hydroxide (Optima, Fisher Scientific) then placed in conditioned Teflon bottles along with 5 $\mu\text{mol L}^{-1}$ salicylaldoxime (SA) and 100 μL of 1.5 mol L^{-1} boric acid in 0.4 N ammonium hydroxide (pH 8.2, NBS scale). Samples were equilibrated overnight (>12 h) to ensure all Fe was associated with SA before analyses, then analyzed using standard additions and triplicate

measurements using CSV as described previously (Buck et al., 2007).

Conditional stability constants of pure amphibactins, ferrioxamines B and E, as well as organic Fe-binding ligand concentrations and strengths from water column profiles, were determined using competitive ligand exchange adsorptive cathodic stripping voltammetry (CLE-ACSV) with SA as the competing ligand (Abualhaija and van den Berg, 2014). For the determination of the conditional stability constants of the isolated amphibactins, 4 L of filtered low Fe seawater was collected from 15 m depth at Station ALOHA and was UV-irradiated for 2 h in acid cleaned quartz tubes as described above. After irradiation, the seawater was slowly passed through clean Chelex-100 resin (Bio-Rad) and irradiated a second time to ensure the seawater was metal and organic-free. For each amphibactin ligand titration, 12 separate 10 mL aliquots of UV-irradiated seawater were placed in acid-cleaned and conditioned Teflon vials. Then 50 μ L of 1.5 mol L⁻¹ boric acid in 0.4 N ammonium hydroxide was added to each vial (final pH = 8.2, NBS scale), along with 12.5 μ L SA (final concentration of 5 μ mol L⁻¹). A 5 μ L aliquot from the well containing the isolated amphibactin was added to each Teflon vial, along with 10 Fe additions up to 25 nmol L⁻¹. These were equilibrated overnight before being analyzed by CLE-ACSV. Purging with nitrogen has been found to decrease the sensitivity of CLE-ACSV titrations on 663 VA stand electrodes (Abualhaija and van den Berg, 2014), so each aliquot was not purged when analyzed, and the nitrogen blanket was switched off, and vials were run in triplicate. Triplicate titrations were performed for each amphibactin and analyzed using ProMCC (Omanović et al., 2015), using an optimized sensitivity and updated Fe-SA side reaction coefficients (Abualhaija and van den Berg, 2014). Ligand strengths represent the average of the triplicate titrations analyzed using the chemical speciation fitting mode in ProMCC at the 95% confidence interval. A secondary check on the approximate concentration of each amphibactin was determined by spiking the bulk *Vibrio* media extract containing amphibactins with 3 different concentrations of Fe and an internal standard and analyzing the aliquots by LC-ICPMS (see section Siderophore Identification in Station ALOHA Seawater). Concentrations determined by CLE-ACSV were within ~1 nmol L⁻¹ of the estimates made using LC-ICPMS. Organic Fe-binding ligand samples from the water column were analyzed using CLE-ACSV as described above, using 12 titration points and overnight equilibration with 5 μ mol L⁻¹ SA and boric acid buffer. Titrations were also interpreted using ProMCC in chemical speciation fitting mode with optimized sensitivity (Omanović et al., 2015) and solved for a single ligand class.

Siderophore Identification in Station ALOHA Seawater

Between 16–20 L of filtered seawater was pumped at 15 mL min⁻¹ through a 6 mL Bond-Elut ENV column (1 g, 6 mL, Agilent Technologies) that had been cleaned with pH 2 Milli-Q (Optima HCl), rinsed with Milli-Q, and activated with distilled methanol before a final rinse with Milli-Q. Columns were

wrapped in aluminum foil to prevent photochemical degradation of the concentrated organic material during sample processing. Columns were washed with three column volumes of Milli-Q and frozen at -20°C. Prior to analyses, columns were thawed and eluted with 10 mL distilled methanol into acid-cleaned 15 mL falcon tubes. The eluent was reduced in volume to ~500–1000 μ L, and divided into equal volumes. One half of the sample was spiked with 2 μ L of 100 μ mol L⁻¹ cyanocobalamin. The other half was placed in a separate tube and both sample splits frozen at -20°C until analysis.

All samples were analyzed by liquid chromatography inductively coupled plasma mass spectrometry (LC-ICPMS) on a quadrupole ICPMS (iCap Q; Thermo Scientific) connected to a Dionex Ultimate 3000 bioinert LC (Thermo Scientific). Aliquots of the spiked and unspiked samples (with the internal standard) were analyzed on a polyetheretherketone (PEEK) LC column (2.1 × 100 mm, 3- μ m particle size C₈ resin; Hamilton) and eluted using a 20-min gradient (5 to 90% B), followed by an isocratic gradient for 10 min at 90% B, a 5 min gradient from 90 to 95% B, and an isocratic gradient at 95% B for 5 min at 200 μ L min⁻¹ (solvent A: 5 mmol L⁻¹ ammonium formate, solvent B: 5 mmol L⁻¹ ammonium formate in methanol). A post-column PEEK flow splitter directed 50 μ L min⁻¹ of the flow into a perfluoroalkoxy micronebulizer (PFA-ST; Elemental Scientific) and a cyclonic spray chamber that was cooled to 0°C. Oxygen was added to the sample gas at a flow of 25 mL min⁻¹ to prevent the formation of reduced organic compounds onto the platinum sampler and skimmer cones. Measurements were made in kinetic energy discrimination mode with a helium collision gas that was introduced at a rate of 4.2 mL min⁻¹ to remove isobaric ArO⁺ interferences with ⁵⁶Fe. Several metals were monitored, including ⁵⁶Fe, ⁵⁷Fe, and ⁵⁹Co at an integration time of 0.05 s each. Siderophore concentrations were determined using a four-point calibration curve using ferrioxamine E as a standard. Signals were normalized between each sample run using the peak height of ⁵⁹Co from the internal standard cyanocobalamin to account for matrix effects and sensitivity changes during instrument runs. Naturally occurring cyanocobalamin was not present in detectable concentrations in any of the samples.

The HPLC system was subsequently coupled to an electrospray ionization mass spectrometer (ESI-MS; Orbitrap Fusion, Thermo Scientific). The ESI-MS was equipped with a heated electrospray ionization source and was set to a capillary voltage of 3,500 V, sheath gas 12 (arbitrary units), auxiliary gas 6 units, and sweep gas 2 units, along with ion transfer tube and vaporizer pressure temperatures of 300 and 75°C. Scans were collected in high resolution (450K) positive mode, and high energy collisional dissociation (HCD). MS² spectra were collected on the ion trap mass analyzer by decision making tree using a targeted siderophore list (ChelomEx; Baars et al., 2014) and the most abundant masses. Ions were trapped using an isolation window of 1 m/z and fragmented using a collision energy of 35%.

The ESI-MS data was converted to an open source mzML format using MSconvert (Proteowizard) and processed using in house R script based on the XCMS data structure (<https://cran.r-project.org/>; Tautenhahn et al., 2012b). A constant time

offset was applied to align the retention time of the internal standard (cyanocobalamin; $m/z = 678$) mass peak from the ESI-MS to the ^{59}Co peak from the ICP-MS. An isotope pattern search algorithm (Boiteau et al., 2016) was used to identify potential Fe-containing compounds that matched the abundance ratio of ^{56}Fe and ^{54}Fe , appeared as coherent peaks in the scans, and also matched an ^{56}Fe peak in the ICP-MS data. Masses indicative of the apo (metal free) form were present for some siderophores. Siderophore identifications were confirmed by matching MS² spectra with those of the authentic standards (Tautenhahn et al., 2012a).

Particle Incubation Experiment

To investigate mechanisms of dissolved siderophore production below the euphotic zone, an incubation experiment was conducted using settling particles collected from Lagrangian style net traps (Peterson et al., 2005; Edwards et al., 2015) and water collected from the X-Niskin rosette. One hour prior to the incubation experiment, 16 trace metal clean 250 mL PC bottles were filled with Milli-Q and microwave-sterilized until boiling. The bottles were kept closed and allowed to cool to room temperature. Particles for the incubation experiment were collected over a 24-h net trap deployment at 150 m in the Station ALOHA sampling circle. Upon recovery, trapped particles were divided into 8 equal splits in acid-cleaned 500 mL HDPE bottles. In a trace metal clean van, one split was immediately added to 4 L of unfiltered 150 m trace metal clean seawater that had been collected in a clean 10 L polycarbonate (PC) carboy within 1 h of the incubation set-up, and had been kept at 15°C in the dark. After the particles had been added, the carboy was gently inverted three times to ensure an even distribution of the particles before dispensing into 250 mL bottles. The sixteen separate 250 mL PC bottles were divided into three treatments. The treatments were a no-particle control (only containing unfiltered 150 m water, denoted as Control A and B), a sterilized control (150 m seawater and particles and microwave sterilized, denoted as Sterilized Control A and B), and a particle addition treatment (denoted as + Particles A and B). Each treatment was completed in duplicate. Bottles were incubated in a Percival-style incubator at 15°C in the dark. The incubation was terminated after 3 days, and at each time point ($t = 0, 1$, and 3 days) an entire 250 mL sample bottle from each replicate was sacrificed. The $t = 0$ time-point was processed immediately after placing the remaining bottles in the incubator, and the control with no added particles was only sampled on day 3. Each bottle was sampled for flow cytometry cell counts and dissolved siderophore analyses.

RESULTS

Nutrients, Dissolved Iron, and Flow Cytometry at Station ALOHA

Depth profiles of macronutrient concentrations, *Synechococcus*, *Prochlorococcus*, heterotrophic bacteria, and photosynthetic picoeukaryote cell abundances were typical of summer conditions at Station ALOHA. Nitrate (equal to nitrate+nitrite) varied 10-fold from $\sim 0.1 \mu\text{mol L}^{-1}$ in surface waters, to $1 \mu\text{mol L}^{-1}$

L^{-1} in the nitracline at 300 m (Figure 1; Table 1). Phosphate also increased to $\sim 0.1 \mu\text{mol L}^{-1}$ from our detection limit in surface waters, while silicate concentrations remained relatively constant at $\sim 1.2 \mu\text{mol L}^{-1}$ to 400 m (Figure 1). Concentrations of dissolved Fe also remained relatively constant between 0.15 nmol L^{-1} (15 m) and 0.12 nmol L^{-1} (400 m), with potentially a slight decrease immediately below the deep chlorophyll maximum (DCM; 125 m), where values ranged from 0.06 nmol L^{-1} (150 m) to 0.08 nmol L^{-1} (200 m) before recovering to 0.10 nmol L^{-1} at 300 m. (Table 1). Flow cytometry counts also showed typical conditions at Station ALOHA, with a dominance of *Prochlorococcus* in surface waters ($1.14 \times 10^5 \text{ cell mL}^{-1}$, Table 1), as well as elevated *Synechococcus* (Figure 1; Table 1). Cell counts decreased throughout the water column, and *Prochlorococcus*, *Synechococcus*, and other phototrophic picoeukaryotes were non-detectable below 200 m (Figure 1). Heterotrophic bacteria were also abundant in surface waters, with numbers ranging from 2 to $6 \times 10^5 \text{ cells mL}^{-1}$ in the upper 125 m, and dropping to $5 \times 10^4 \text{ cells mL}^{-1}$ at 400 m. These cell numbers are also typical for heterotrophic bacteria at Station ALOHA during summer months (Campbell and Vault, 1993).

Siderophores and the Total Iron-Binding Ligand Pool

Siderophores

Siderophore abundances and distributions varied considerably with depth, despite only small changes in Fe and macronutrient concentrations (Figure 2). Nine different siderophores were identified in samples collected between 15 and 400 m (Table 2), including the hydroxamate siderophores ferrioxamine G and E (Figure 2). Ferrioxamine G was present in low concentrations in 6 of 7 samples (Table 2), and was only absent in the 200 m sample. Ferrioxamine E was identified at 15 and 125 m (the DCM), but was below the limit of detection in the other samples. The concentrations of ferrioxamines G and E ranged from 0.1 to 1.3 pmol L^{-1} and were highest in samples above 150 m. Deep samples (300 and 400 m), were characterized by a suite of amphibactins (Figure 2). These siderophores all have a common head group that binds Fe, and only differ in the structure of their side chains (Figure 2B). Amphibactins were present in higher concentrations than ferrioxamines, with concentrations ranging from 0.1 to 6 pmol L^{-1} , with the highest concentrations (6 pmol L^{-1}) observed at 300 m (Table 2). To confirm our compound assignments, MS² data was collected for ferrioxamine E, amphibactin T, S, D, and H (Figure 3; Table 2). The abundance of ions from ferrioxamine G and other amphibactins were too low to permit MS² data acquisition, and compound identification rests on MS and retention time data alone. Fragmentation data for ferrioxamine E showed characteristic fragments at m/z 537.3 and 295.2 (Figure 3C), corresponding to neutral losses of $\text{C}_{20}\text{H}_{45}\text{N}_{10}\text{O}_7$ and $\text{C}_{10}\text{H}_{27}\text{N}_6\text{O}_4$ and matching those of a ferrioxamine E standard. Likewise, MS² spectra of amphibactins T, S, D, and H also showed characteristic fragments due to common neutral losses of 218 ($\text{C}_8\text{H}_{14}\text{N}_2\text{O}_5$), 277 ($\text{C}_{10}\text{H}_{19}\text{N}_3\text{O}_6$), and 305

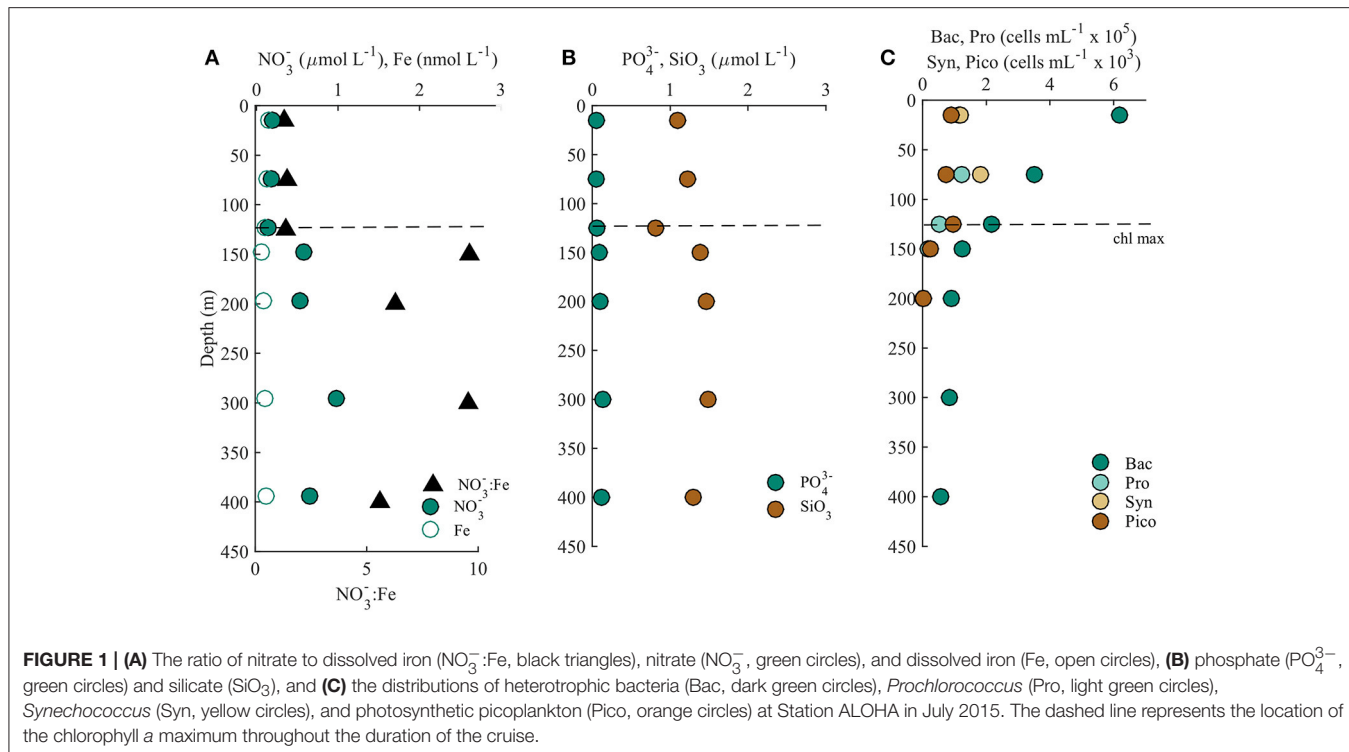


TABLE 1 | Macro (nitrate, phosphate, silicate) and micro (dissolved iron) nutrient concentrations and cell counts (heterotrophic bacteria, *Prochlorococcus*, *Synechococcus*, and photosynthetic picoeukaryotes) determined from 15 to 400 m at Station ALOHA.

Depth m	Nitrate $\mu\text{mol L}^{-1}$	Phosphate $\mu\text{mol L}^{-1}$	Silicate $\mu\text{mol L}^{-1}$	Fe nmol L^{-1}	+/-	Total Bacteria cells mL^{-1}	<i>Prochlorococcus</i> cells mL^{-1}	<i>Synechococcus</i> cells mL^{-1}	Photosynthetic picoeukaryotes cells mL^{-1}
15	0.19	0.05	1.10	0.15	0.08	6.19E+05	1.14E+05	1.19E+03	8.98E+02
75	0.18	0.05	1.22	0.13	0.02	3.51E+05	1.23E+05	1.82E+03	7.39E+02
125	0.14	0.06	0.81	0.10	0.01	2.17E+05	5.26E+04	nd	9.59E+02
150	0.58	0.09	1.39	0.06	0.01	1.25E+05	1.76E+04	nd	2.48E+02
200	0.53	0.10	1.46	0.08	0.00	9.05E+04	1.35E+03	nd	2.58E+01
300	0.98	0.14	1.49	0.10	0.02	8.43E+04	nd	nd	nd
400	0.65	0.12	1.30	0.12	0.03	5.69E+04	nd	nd	nd

The “nd” notation means not determined.

($\text{C}_{11}\text{H}_{19}\text{N}_3\text{O}_7$, **Figure 3F**) as seen in previous analyses (Boiteau et al., 2016) and in the MS^2 spectra of authentic amphibactins (Supplementary Figure 2).

Our LC-ICPMS analyses measures siderophores that are bound to Fe. To measure total siderophores (both with and without Fe), $5 \mu\text{mol L}^{-1}$ of Fe was added to the sample in the form of Fe-citrate, and was left overnight to equilibrate with the Fe-free natural ligands. We observed similar concentrations of total siderophores in samples from surface depths (**Table 3**), but total siderophore concentrations in the 300 and 400 m samples increased to 11 and 3 pmol L^{-1} respectively. In addition, the uncharacterized organic matter, appearing as the unresolved baseline rise in each of the chromatograms, also increased upon the addition of Fe at each depth, signifying there is organic matter at each of our sampling depths that is under-saturated with Fe. Below 150 m, unresolved organic

matter containing organic Fe-binding sites increased much more than in samples from shallower depths, indicating higher “excess” ligands in these samples. Taken together, the 300 and 400 m sample contained much higher concentrations of both siderophores and uncharacterized organic Fe-binding ligands that were under-saturated with Fe compared to upper water column samples. The total Fe-L (siderophores and unresolved baseline, **Table 3**) measured by LC-ICPMS represents about 10–30% of the total dissolved Fe (**Figure 4**; **Table 3**). A large fraction of dissolved Fe was not captured by our solid phase extraction method.

Strong Iron-Binding Organic Ligand Pool Measured by CLE-ACSV

Fe-binding organic ligands at Station ALOHA were also characterized by CLE-ACSV (**Figure 4**; **Table 3**). Using a single

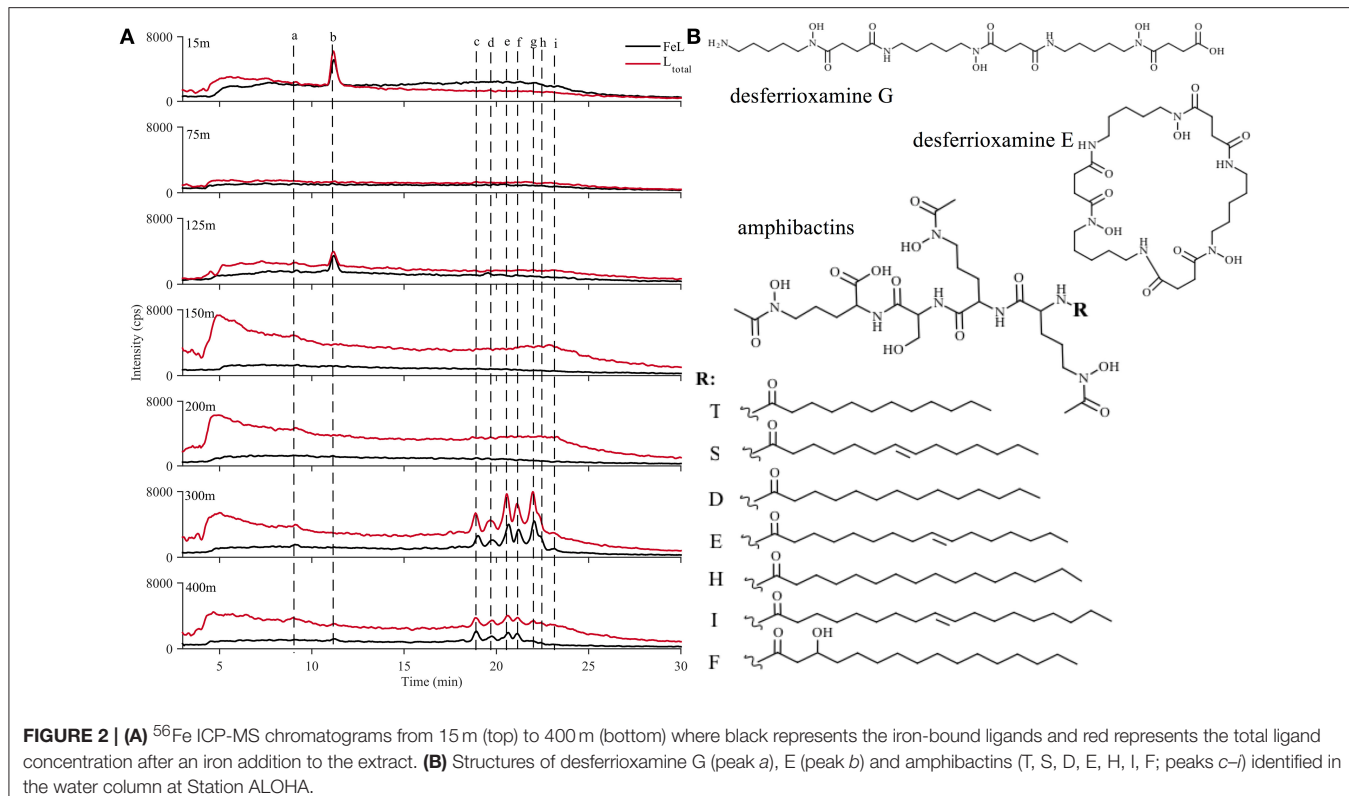


TABLE 2 | Siderophore peak identities in each sample as presented in Figure 2, with the siderophore name, retention time (min), apo mass (iron free), ^{54}Fe and ^{56}Fe mass, and the dominant fragments from the MS^2 fragmentation spectra.

Peak	Siderophore	Retention time (min)	Apo mass	^{54}Fe mass	^{56}Fe mass	Dominant fragments
A	ferrioxamine G	9.05	619.367	670.283	672.278	nd
b	ferrioxamine E	11.07	601.356	652.272	654.268	654.39, 295.2
c	amphibactin T	18.82	804.472	855.388	857.383	552.3, 580.3
d	amphibactin S	20.34	830.488	881.404	883.399	371.2, 719.3
e	amphibactin D	20.59	832.503	883.419	885.415	580.3, 608.3
f	amphibactin E	21.11	858.519	909.435	911.430	nd
g	amphibactin H	22.01	860.534	911.450	913.445	608.3, 636.3
h	amphibactin I	22.31	874.514	925.430	927.425	nd
i	amphibactin F	22.45	876.529	927.446	929.441	490.3, 467.2

The notation "nd" means not determined. See Supplementary Figures 2–7 for fragmentation spectra.

analytical window, one ligand class was detected at all depths. These ligands were in excess of Fe at every depth, and had a $\log K_{\text{Fe}L_1,\text{Fe}'}^{\text{cond}}$ that would place them in the stronger (L_1 or L_2 ; $\log K_{\text{Fe}L_1,\text{Fe}'}^{\text{cond}} \sim 12$) class of ligands (Table 3). Since volume was limited and only a single analytical window was employed, the strength of the ligands detected likely represent the average conditional stability constants of one or more ligand classes. Total Fe-binding ligands ranged from 0.9 nmol L⁻¹ in surface waters to ~1.6 nmol L⁻¹ at 300 and 400 m. The $\log K_{\text{Fe}L_1,\text{Fe}'}^{\text{cond}}$ was relatively consistent with depth, with slightly stronger conditional stability constants in surface waters.

Conditional Stability Constants of Model Ligands

To determine the contribution of the siderophores to Fe complexation at Station ALOHA, the conditional stability constants of amphibactins T, S, D, E, and C purified from *Vibrio cyclitrophicus* 1F-53 along with ferrioxamines B and E were measured using CLE-ACSV. All amphibactins had very similar conditional stability constants, ranging from 12.0 to 12.4 (Table 4). Ferrioxamines B and E were found to have conditional stability constants of 14.4 and 14.0 respectively, consistent with other studies ($\log K_{\text{Fe}L_1,\text{Fe}'}^{\text{cond}}$ 13–14; Rue and Bruland, 1995; Witter et al., 2000).

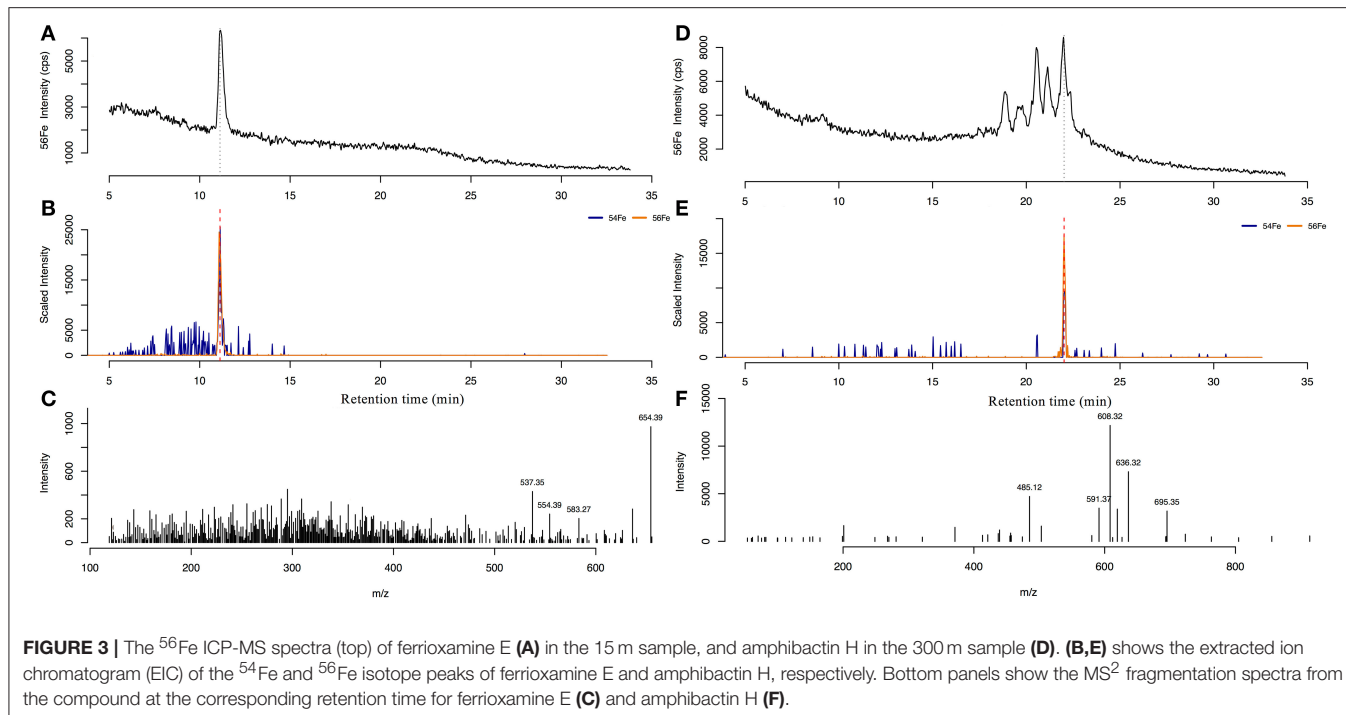


FIGURE 3 | The ^{56}Fe ICP-MS spectra (top) of ferrioxamine E (**A**) in the 15 m sample, and amphibactin H in the 300 m sample (**D**). (**B,E**) shows the extracted ion chromatogram (EIC) of the ^{54}Fe and ^{56}Fe isotope peaks of ferrioxamine E and amphibactin H, respectively. Bottom panels show the MS^2 fragmentation spectra from the compound at the corresponding retention time for ferrioxamine E (**C**) and amphibactin H (**F**).

TABLE 3 | Siderophore and total iron binding ligand parameters determined at Station ALOHA.

Depth m	Fe nmol L ⁻¹	L nmol L ⁻¹	logK	Fe' pmol L ⁻¹	FeL pmol L ⁻¹	Fe(Ferrioxamine) pmol L ⁻¹	Fe(Amphibactin) pmol L ⁻¹	Ferrioxamine Total pmol L ⁻¹	Amphibactin Total pmol L ⁻¹
15	0.15	0.88	12.44	0.07	41.73	1.35	0.16	2.16	0.27
75	0.13	0.90	12.19	0.11	13.53	0.03	0.17	0.06	0.20
125	0.10	0.96	12.00	0.12	21.00	0.86	0.77	0.92	0.77
150	0.06	1.61	11.89	0.05	12.66	0.04	0.15	0.07	0.15
200	0.08	1.41	11.90	0.08	12.98	nd	0.65	nd	0.83
300	0.10	1.57	11.93	0.08	23.29	1.20	6.30	1.20	11.05
400	0.12	1.55	11.76	0.14	12.46	0.13	2.60	0.13	2.96

Dissolved iron (Fe), total iron-binding ligands (L), and conditional stability constants (logK) were determined using cathodic stripping voltammetry, and Fe' (inorganic Fe) was calculated by $\text{Fe}' = \text{Fe}/(\text{L} - \text{Fe}) \times K$. Siderophore parameters were determined using LC-ICPMS and include a calculation of total iron-binding ligands (FeL; measured as the area under the chromatographic curve in ICP-MS analyses), iron bound to ferrioxamine-type siderophores [Fe(Ferrioxamine)], iron bound to amphibactins-type siderophores [Fe(Amphibactin)], as well as the total concentration of ferrioxamines (Ferrioxamine Total) and amphibactins (Amphibactin Total) after adding Fe to the sample and analyzing again by LC-ICPMS. The notation "nd" refers to not determined.

Siderophore Production During Particle Regeneration Incubations

To assess the potential contribution of particle regeneration to the high concentrations of siderophores measured at 300 and 400 m, we measured siderophore production from particle-associated bacteria during organic matter regeneration of sinking particles (Figure 5). Very low concentrations of siderophores were observed in the water column at 150 m, just below the DCM (Figure 2), and in all treatments at the beginning of the particle incubation experiments (Figure 5A; t = 0). The only siderophore detected in the initial conditions of the incubation with no particles added was ferrioxamine E (0.02 pmol L⁻¹). After 1 day, significantly higher concentrations of ferrioxamine E (0.4 pmol L⁻¹, t-test, $p < 0.05$) were detected in the particle amended treatment, but not in the non-amended or sterilized controls

(Figure 5A). After 3 days, concentrations of ferrioxamine E had not changed in the controls of sterilized treatments, while concentrations in the +Particles treatments remained high, within the range observed on day 1 (Figure 5A). The production of ferrioxamine E in +Particle treatments was also accompanied by an increase in heterotrophic bacteria compared to control treatments (Figure 5B). However, no amphibactins were observed in the experiment.

DISCUSSION

Siderophores at Station ALOHA

Dissolved Fe concentrations in the upper water column (<500 m) at Station ALOHA are generally low (0.1–0.5 nmol L⁻¹; Fitzsimmons et al., 2015), but not limiting (Boyle et al., 2005).

At the time of our sampling, dissolved Fe concentrations were $>0.06 \text{ nmol L}^{-1}$, but nevertheless siderophores were present at several depths between 5 and 400 m, with strikingly different distributions in the upper and lower portions of our profile. Ferrioxamine E was by far the most abundant siderophore in the euphotic zone, with picomolar concentrations in the surface (15 m) and in the DCM (125 m). We found small amounts of ferrioxamine G at these depths as well. Both ferrioxamine E and G have been found to be produced by the marine heterotroph *Pseudomonas* spp. (Meyer and Abdallah, 1980; Essén et al., 2007), and ferrioxamine G has been identified in cultures of marine *Vibrio* species (Martinez et al., 2001). Ferrioxamines have also been observed in the Atlantic (Mawji et al., 2008), and the coastal Pacific (Boiteau et al., 2016). Summertime rates of primary production and nitrogen fixation at Station ALOHA are highest in the surface mixed layer ($<50 \text{ m}$; Karl and Church, 2014; Böttjer et al., 2017), where microbial Fe demand would be expected to reach a maximum as well. Nitrogen fixing cyanobacteria such as *Trichodesmium* and diatoms (*Hemiaulus*, *Rhizoselenia*), hosting endosymbiotic diazotrophs (*Richelia*), are common in the upper water column in summer (Karl et al., 2012), and may experience Fe stress due to their higher Fe requirements and larger cell sizes. A large fraction of Fe in ALOHA surface waters is supplied by the deposition of atmospheric dust, which may include Fe in a mineral form (Boyle et al., 2005; Fitzsimmons et al., 2015). Ferrioxamines have very strong stability constants ($\log K_{\text{FeL}_1,\text{Fe}'}^{\text{cond}} > 14$), and have been shown to be particularly effective at dissolving Fe minerals (Akafia et al., 2014). Ferrioxamines E and G have also been reported in surface waters of the oligotrophic North Atlantic Ocean (Mawji et al., 2008), a region with moderately high concentrations of Fe largely sourced from atmospheric dust (Jickells et al., 2005; Mahowald et al., 2005; Conway and John, 2014) that supports abundant *Trichodesmium* spp. and *Richelia*-diatom nitrogen fixers. Heterotrophic bacteria associated with these nitrogen-fixing cyanobacteria are an additional possible source of ferrioxamines at Station ALOHA, and perhaps at other oligotrophic sites where *Trichodesmium* and diatom-diazotroph associations are abundant, however direct evidence of siderophore production from these assemblages has not been observed.

Rates of primary production and nitrogen fixation fall rapidly between 15 and 75 m (Karl and Church, 2014; Böttjer et al., 2017), while Fe concentrations remain relatively stable ($\sim 0.1 \text{ nmol L}^{-1}$). Only trace amounts of ferrioxamine G were detected in our 75 m sample, suggesting depth dependent changes in bacteria species, microbial activity or Fe concentrations that may decrease Fe stress. It is possible the bacteria responsible for producing siderophores were absent at 75 m, or perhaps the combination of sufficient dissolved Fe and low(er) rates of primary productivity and nitrogen fixation, may have reduced the demand for Fe at 75 m, making the synthesis of siderophores unnecessary. Using similar reasoning, even though Fe concentrations were at a minimum (0.06–0.08 nmol L $^{-1}$) in the 150 and 200 m samples, the number of bacterial cells, particularly photoautotrophs, falls rapidly below 125 m (**Figure 1**). The near absence of siderophores between 150 and

200 m may indicate a decrease in Fe demand, or Fe stress overall, within the community.

The highest concentration of siderophores in our profile was found at 300 m, where we detected a suite of seven amphibactins. Amphibactins are hybrid compounds composed of a peptidic, Fe-complexing portion, and a lipid portion that allows these siderophores to form strong associations with cell membranes (reviewed in Vraspir and Butler, 2009). These membrane associations may reduce diffusive loss of amphibactins to the environment, creating a more favorable energy balance between Fe uptake and loss of siderophore to the environment. Although dissolved Fe concentrations between 300 and 400 m were $\sim 0.1 \text{ nmol L}^{-1}$, nearly half the amphibactins in both samples were not complexed to Fe. Addition of Fe to our 300 m sample increased the total Fe-amphibactin by $\sim 45\%$, from ~ 6 to $\sim 11 \text{ pmol L}^{-1}$. Total amphibactin concentrations at depth at ALOHA were similar to the values reported for surface waters of the HNLC eastern tropical Pacific Ocean (Boiteau et al., 2016).

Amphibactins at 300 m were most likely produced at depth, and not passively introduced from the regeneration of sinking particles or laterally from advection. Amphibactins were not detected in any samples collected above 300 m. Shipboard incubations of sinking particles collected in sediment traps only yielded small amounts of ferrioxamine E, but no amphibactins were produced. Although the time scales of amphibactin cycling at 300 m may integrate longer periods than captured by our euphotic zone sampling and particle incubation experiments, we found no evidence of amphibactin production in the euphotic zone and subsequent transport to depth. Therefore, we inferred that amphibactins were synthesized by bacteria at 300 and 400 m. Such high concentrations of amphibactins in the mesopelagic were surprising. Although there is some evidence for Fe limitation of heterotrophic production in surface waters of the Southern Ocean (Church et al., 2000), low rates of bacterial production coupled to high dissolved Fe concentrations characteristic of meso- and bathypelagic regions were not expected to induce production of siderophores in higher concentrations than in the euphotic zone.

We note that at Station ALOHA, water between 300 and 400 m forms the upper portion of the North Pacific Intermediate Water (NPIW) salinity minimum, which outcrops in the low Fe region of the northwest subpolar gyre (Talley, 1993). Concentrations of dissolved Fe transported with NPIW are expected to be low, and bioavailable Fe may represent only a fraction of the total dissolved Fe. Low Fe bioavailability may be one factor inducing Fe stress within the 300–400 m zone. We expected that much of the bioavailable Fe in the 300–400 m region was supplied from remineralization of Fe-containing proteins in sinking particulate organic matter. Some Fe from this sinking organic matter is bound by the $\sim 1.5 \text{ nmol L}^{-1}$ strong ligands measured by CLE-ACSV (discussed in the next section). Amphibactins have conditional stability constants that are much weaker than ferrioxamines, but are nevertheless strong enough to compete with the other organic ligands for some portion of the dissolved Fe. The distinct sources of Fe from dust and sinking particles to the upper and lower regions of the Station ALOHA water column

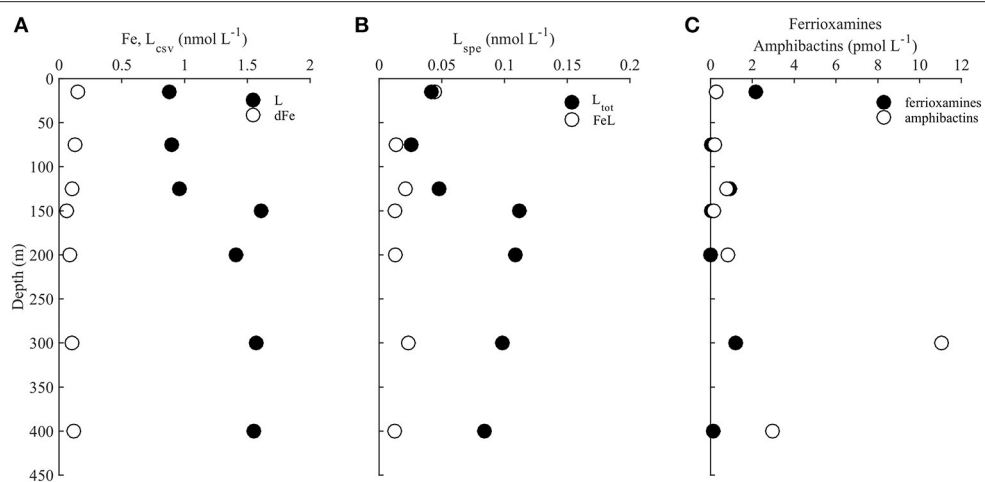


FIGURE 4 | (A) Dissolved iron (Fe, open circles) and total ligands determined using electrochemical methods (L_{csv} , black circles), **(B)** iron-bound ligands (FeL, open circles) and total ligands (L_{tot} , black circles) determined by solid phase extraction, **(C)** and total concentrations (iron bound and excess) of ferrioxamines (ferrioxamine G+E, black circles) and amphibactins (amphibactins T+S+D+E+H+I+F, open circles) throughout the water column at station ALOHA.

TABLE 4 | Conditional stability constants ($\log K$) of isolated amphibactins from *Vibrio cyclitrophicus* 1F-53, as well as model siderophores ferrioxamine E and B.

Ligand	$\log K$	+/-
amphibactin T	12.40	0.03
amphibactin S	12.48	0.07
amphibactin D	12.07	0.15
amphibactin E	12.06	0.08
amphibactin C*	12.00	0.03
ferrioxamine E	14.05	0.09
ferrioxamine B**	14.42	0.08

*Amphibactin C was not observed in the water column, but was effectively isolated from *Vibrio cyclitrophicus* 1F-53.

**Ferrioxamine B was not observed in the water column, but was used as a model siderophore for ferrioxamine G.

may influence the types of siderophores microbes produce in and below the euphotic zone.

Comparison of Ligand Distribution Determined by CLE-ACSV and Siderophores Measured by LC-ICPMS

Efforts to model Fe cycling and bioavailability have largely focused on parameterizing the distribution of strong Fe-binding ligands (L_1) measured by CLE-ACSV (Tagliabue et al., 2014, 2016, 2017). It has long been assumed that siderophores are a component of L_1 (Gledhill and Buck, 2012). However, no direct comparisons of siderophore and L_1 concentrations have been made. In this study we used CLE-ACSV with a single analytical window rather than the multiple windows used in some other studies (Bundy et al., 2014, 2015, 2016; Hogle et al., 2016a). Thus, the ligands measured here likely represent an average of the very strong (L_1 ; $\log K_{\text{Fe}L_1,\text{Fe}'}^{\text{cond}} > 12$) and relatively strong (L_2 ; $\log K_{\text{Fe}L_1,\text{Fe}'}^{\text{cond}} < 12$) ligands measured by others (Gledhill and Buck,

2012; Bundy et al., 2014, 2016; Hogle et al., 2016a). Both L_1 and L_2 are considered to be “strong” Fe-binding ligands, thus we will refer to the ligands characterized by our measurements as strong ligands.

Beyond simply comparing their distributions, there are two important considerations for determining whether or not the siderophores are detected as strong ligands by voltammetry. The first is to consider whether or not siderophores fall within the analytical window of CLE-ACSV. The analytical window of the voltammetric measurements is defined by α'_{CL} , which is the side reaction coefficient of the competitive ligand (CL) used in the measurements. The side reaction coefficient is defined by,

$$\alpha'_{L'} = [L'] \times K_{\text{Fe}L,\text{Fe}'}^{\text{cond}} \quad (1)$$

where $\alpha'_{L'}$ represents the side reaction coefficient of the ligand (L') being considered, $[L']$ is the concentration of the free ligand, and $K_{\text{Fe}L,\text{Fe}'}^{\text{cond}}$ is the conditional stability constant (binding strength to Fe). If $\alpha'_{L'}$ is greater than or less than 10 times that of the competing ligand (α'_{CL}) then the detection of that particular ligand (in this case, the siderophore) is outside of the analytical window of the voltammetric measurement (van den Berg and Donat, 1992). We used salicylaldoxime (SA) as the competing ligand in our analyses, which has $\alpha'_{SA} = 17.9$. The $\alpha'_{\text{ferrioxamine}}$ is ~ 200 , more than 10 times α'_{SA} . The ferrioxamines we measured at Station ALOHA by ICP-MS therefore, likely do not contribute to the concentration of L determined by voltammetry. However, the $\alpha'_{\text{amphibactins}}$ do fall within the range of the analytical window used, so our measurement of L likely includes a contribution from amphibactins.

The second important aspect that determines whether or not siderophores were captured in the voltammetric measurements is the kinetics of Fe exchange. Since the majority of the ferrioxamines, as well as a portion of the amphibactins detected in this profile were bound to Fe (Figure 2), it is possible the

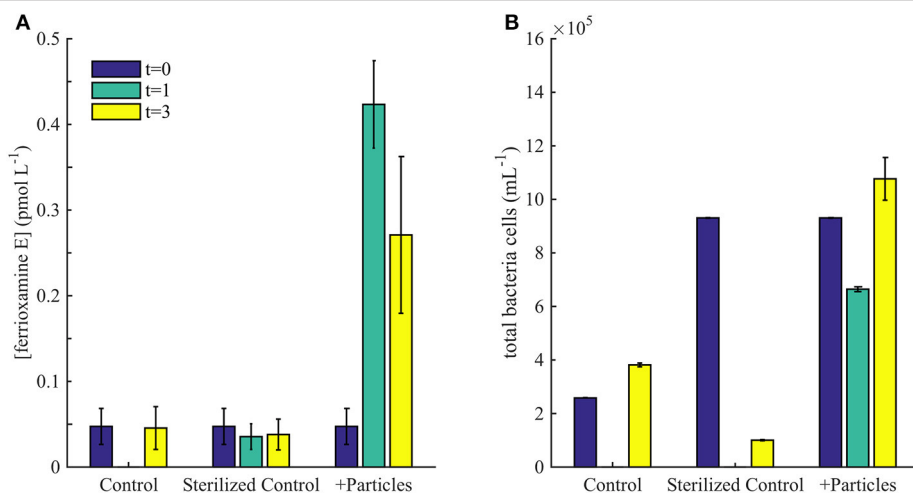


FIGURE 5 | (A) Concentrations of ferrioxamine E observed in particle incubation experiment on day 0, 1, and 3. **(B)** Flow cytometry cell counts during the incubation experiment.

natural Fe bound to these compounds did not exchange with the added Fe in the voltammetry titrations. If no exchange occurs, those ligands will not be detected as a separate and distinct ligand class by voltammetry (Gledhill and Buck, 2012), but will be accounted for in the average ligand parameters. Laboratory experiments of ⁵⁶Fe:⁵⁷Fe exchange between ferrioxamine E and natural organic ligands in seawater suggest very slow exchange kinetics (Boiteau, 2016). Coupled to the high value of $\alpha'_{\text{ferrioxamine}}$, our voltammetric measurements largely missed any contribution of ferrioxamines to the total L pool. Fe exchange kinetics for amphibactins are somewhat faster, but are still slow relative to the equilibration times used in our measurements (Boiteau, 2016). This exchange reaction may be accelerated to some extent in the presence of high concentrations of SA used in the titration via an associative mechanism. Our voltammetric measurements therefore likely captured ~45% of apo-amphibactins at depth, and a small fraction of Fe-amphibactins. Despite the encouraging coherence between the concentration profiles of siderophores and L measured by voltammetry (Figures 4A,B), the ligand pools measured by these two methods only partially overlap. Many Fe-siderophores are likely missed by traditional voltammetric techniques (Hawkes et al., 2013), while LC-ICPMS only measures the fraction of ligands captured by solid phase extraction.

Estimating the Contribution of Siderophores to Iron Cycling at Station ALOHA

Previous work at Station ALOHA has shown that Fe varies seasonally and interannually in the upper 250 m, and that organic Fe-binding ligands often vary along with dissolved Fe with a time lag on the order of days (Fitzsimmons et al., 2015). The covariation in dissolved Fe and ligands suggests a dynamic interaction between Fe and organic ligand production, as well as active mediation of Fe cycling by the microbial community (Adly

et al., 2015). To estimate the potential availability of siderophore bound Fe, we compared their concentration to inorganic Fe (Fe') which is thought to be the most bioavailable form of Fe (Table 3; Shaked et al., 2005; Shaked and Lis, 2012; Lis et al., 2015).

In order to determine the relative contribution of siderophore bound Fe, Fe', and FeL to total dissolved Fe, we can consider the equilibrium Fe speciation at Station ALOHA in our profile using the following relationship,

$$K_{\text{FeL}, \text{Fe}'}^{\text{cond}} = \frac{[\text{FeL}]}{[\text{Fe}'] [\text{L}']} \quad (2)$$

From this equation and values of L and K determined by voltammetry, we can calculate the distribution of Fe' and compare that to the concentration of Fe bound by siderophores determined by ICP-MS in order to infer the relative importance of these species in biological Fe uptake. The amount of Fe bound to siderophores at 15 m is twice as high as inorganic Fe (Fe'; Table 3). However, at 300 m siderophore-bound Fe is approximately two orders of magnitude higher (~10 pmol L⁻¹) than inorganic Fe concentrations (0.1 pmol L⁻¹; Shaked et al., 2005; Shaked and Lis, 2012; Lis et al., 2015). Even at the lower concentrations of siderophores present in surface waters (0.1–2 pmol L⁻¹), Fe-siderophore concentrations are still greater than Fe' due to the stronger conditional stability constants determined at these depths (Table 3). Fe bound to unknown ligands (L) in the chemical speciation calculations represent the vast majority (99%) of the dissolved Fe. Although Fe' is thought to be the most bioavailable form of Fe (Lis et al., 2015), the very low concentrations of Fe' present in seawater suggest that organic pools of Fe are very important. Based on data from phytoplankton Fe uptake experiments (Lis et al., 2015), we can infer that on average, FeL is taken up by phytoplankton at 1–10% the rate of Fe' uptake, while FeL concentrations are >100 greater than Fe' concentrations (Table 3).

Dynamic Iron Cycling at Station ALOHA

The presence of siderophores in the upper water column indicates that even though Fe is not thought to be limiting at Station ALOHA, some populations of microbes are likely responding to Fe stress, perhaps in response to low Fe concentrations and high biological demand. Biological responses to low Fe are not unprecedented at our study site, and have been observed in surface waters due to dust events or passing mesoscale eddies that contain elevated Fe (Fitzsimmons et al., 2015). Our results show that the microbial response to low Fe was not uniform throughout the Station ALOHA water column. Siderophore concentrations and types changed rapidly with depth. If Fe stress arises from a combination of Fe bioavailability, concentration, and microbial Fe demand, the rapidly changing profile of siderophores at Station ALOHA suggests these factors are dynamic, and at least vertically, can change over spatial scales of only a few tens of meters. The two major classes of siderophores we observed, ferrioxamines and amphibactins, have strikingly different conditional stability constants and abilities to form associations with cell membranes. Their distribution in the water column could be due to many factors, but it may reflect subtle differences in the nature of Fe available for complexation.

Dynamic responses to Fe have primarily been observed in surface waters, and the effects of Fe on mesopelagic communities have been relatively understudied. The high concentrations of siderophores between 300 and 400 m, as well as the rapid production of ferrioxamine E in our particle incubation experiment at a rate of $0.08 \text{ pmol L}^{-1} \text{ day}^{-1}$ (Figure 5), indicate that Fe bioavailability is a factor in organic matter degradation below the euphotic zone. Our incubation results confirm results from other studies (Boyd et al., 2010; Bundy et al., 2016; Velasquez et al., 2016), and demonstrate that siderophores are produced by bacteria associated with sinking particles. Sinking particles are a microenvironment where macronutrients are elevated, but Fe could be in forms that are not readily available (Hogle et al., 2016b). It was surprising that no amphibactins were produced in our experiment, however it may be that the short

duration of the incubation favored fast-growing, copiotrophic bacteria that produce ferrioxamines (Cordero et al., 2012). Regardless, the high concentrations of siderophores in this profile, as well as the strong ligands observed in voltammetry studies throughout the deep ocean (Buck et al., 2015; Gerrings et al., 2015) suggests that bacteria are actively interacting with Fe on sinking particles during the regeneration processes.

AUTHOR CONTRIBUTIONS

RaB was responsible for sample collection, experimental design, sample analyses, and data interpretation. ReB and CM isolated amphibactins from culture and contributed to data acquisition and analyses. KT-K analyzed flow cytometry samples. BV helped design and implement the sediment trap collections and particle incubation experiments. MM assisted with mass spectral data analyses. MS and DR contributed to experimental design, analyses, and data interpretation. RaB wrote the paper with assistance from all coauthors.

ACKNOWLEDGMENTS

We thank Chief Scientists Tara Clemente and Sam Wilson for leading the SCOPE Diel cruises. We also thank the Captain and crew of the R/V *Ka'imiaki-O-Kanaloa*, as well as Paul Henderson in the Woods Hole Oceanographic Nutrient Analytical Facility for nutrient analyses. This work was funded by the Woods Hole Oceanographic Postdoctoral Fellowship for RaB, the Simons Foundation (Award 329108), and the National Science Foundation (OCE-1356747). We also thank two reviewers for helpful comments on the manuscript.

SUPPLEMENTARY MATERIAL

The Supplementary Material for this article can be found online at: <https://www.frontiersin.org/articles/10.3389/fmars.2018.00061/full#supplementary-material>

REFERENCES

- Abualhaija, M. M., and van den Berg, C. M. (2014). Chemical speciation of iron in seawater using catalytic cathodic stripping voltammetry with ligand competition against salicylaldoxime. *Mar. Chem.* 164, 60–74. doi: 10.1016/j.marchem.2014.06.005
- Adly, C. L., Tremblay, J. E., Powell, R. T., Armstrong, E., Peers, G., and Price, N. M. (2015). Response of heterotrophic bacteria in a mesoscale iron enrichment in the northeast subarctic Pacific Ocean. *Limnol. Oceanogr.* 60, 136–148. doi: 10.1002/lno.10013
- Akafia, M. M., Harrington, J. M., Bargar, J. R., and Duckworth, O. W. (2014). Metal oxyhydroxide dissolution as promoted by structurally diverse siderophores and oxalate. *Geochim. Cosmochim. Acta* 141, 258–269. doi: 10.1016/j.gca.2014.06.024
- Baars, O., Morel, F. M., and Perlman, D. H. (2014). ChelomEx: isotope-assisted discovery of metal chelates in complex media using high-resolution LC-MS. *Anal. Chem.* 86, 11298–11305. doi: 10.1021/ac503000e
- Berman-Frank, I., Cullen, J. T., Shaked, Y., Sherrell, R. M., and Falkowski, P. G. (2001). Iron availability, cellular iron quotas, and nitrogen fixation in *Trichodesmium*. *Limnol. Oceanogr.* 46, 1249–1260. doi: 10.4319/lo.2001.46.6.1249
- Boiteau, R. M. (2016). *Molecular Determination of Marine Iron Ligands by Mass Spectrometry*. Doctoral dissertation, Massachusetts Institute of Technology.
- Boiteau, R. M., Fitzsimmons, J. N., Repeta, D. J., and Boyle, E. A. (2013). Detection of iron ligands in seawater and marine cyanobacteria cultures by high-performance liquid chromatography-inductively coupled plasma-mass spectrometry. *Anal. Chem.* 85, 4357–4362. doi: 10.1021/ac3034568
- Boiteau, R. M., Mende, D. R., Hawco, N. J., McIlvin, M. R., Fitzsimmons, J. N., Saito, M. A., et al. (2016). Siderophore-based microbial adaptations to iron scarcity across the eastern Pacific Ocean. *Proc. Natl. Acad. Sci. U.S.A.* 113, 14237–14242. doi: 10.1073/pnas.1608594113
- Boiteau, R. M., and Repeta, D. J. (2015). An extended siderophore suite from *Synechococcus* sp PCC 7002 revealed by LC-ICPMS-ESIMS. *Metallomics* 7, 877–884. doi: 10.1039/C5MT00005
- Böttjer, D., Dore, J. E., Karl, D. M., Letelier, R. M., Mahaffey, C., Wilson, S. T., et al. (2017). Temporal variability of nitrogen fixation and particulate nitrogen export at Station ALOHA. *Limnol. Oceanogr.* 62, 200–216. doi: 10.1002/lno.10386

- Boyd, P. W., and Ellwood, M. J. (2010). The biogeochemical cycle of iron in the ocean. *Nat. Geosci.* 3, 675–682. doi: 10.1038/ngeo964
- Boyd, P. W., Ibsanmi, E., Sander, S. G., Hunter, K. A., and Jackson, G. A. (2010). Remineralization of upper ocean particles: implications for iron biogeochemistry. *Limnol. Oceanogr.* 55, 1271–1288. doi: 10.4319/lo.2010.55.3.1271
- Boye, M., Aldrich, A., van den Berg, C. M. G., de Jong, J. T. M., Nirmaier, H., Veldhuis, M., et al. (2006). The chemical speciation of iron in the northeast Atlantic Ocean. *Deep Sea Res. Part I Oceanogr. Res. Pap.* 53, 667–683. doi: 10.1016/j.dsr.2005.12.015
- Boye, M., van den Berg, C. M. G., de Jong, J. T. M., Leach, H., Croot, P., and de Baar, H. J. W. (2001). Organic complexation of iron in the Southern Ocean. *Deep Sea Res. Part I Oceanogr. Res. Pap.* 48, 1477–1497. doi: 10.1016/S0967-0637(00)00099-6
- Boyle, E. A., Bergquist, B. A., Kayser, R. A., and Mahowald, N. (2005). Iron, manganese, and lead at hawaii ocean time-series station ALOHA: temporal variability and an intermediate water hydrothermal plume. *Geochim. Cosmochim. Acta* 69, 933–952. doi: 10.1016/j.gca.2004.07.034
- Buck, K. N., and Bruland, K. W. (2007). The physicochemical speciation of dissolved iron in the Bering Sea, Alaska. *Limnol. Oceanogr.* 52, 1800–1808. doi: 10.4319/lo.2007.52.5.1800
- Buck, K. N., Lohan, M. C., Berger, C. J. M., and Bruland, K. W. (2007). Dissolved iron speciation in two distinct river plumes and an estuary: implications for riverine iron supply. *Limnol. Oceanogr.* 52, 843–855. doi: 10.4319/lo.2007.52.2.0843
- Buck, K. N., Sedwick, P. N., Sohst, B., and Carlson, C. A. (in press). Organic complexation of iron in the eastern tropical South Pacific: results from US GEOTRACES Eastern Pacific Zonal Transect (GEOTRACES cruise GP16). *Mar. Chem.* doi: 10.1016/j.marchem.2017.11.007
- Buck, K. N., Selph, K. E., and Barbeau, K. A. (2010). Iron-binding ligand production and copper speciation in an incubation experiment of Antarctic Peninsula shelf waters from the Bransfield Strait, Southern Ocean. *Mar. Chem.* 122, 148–159. doi: 10.1016/j.marchem.2010.06.002
- Buck, K. N., Sohst, B., and Sedwick, P. N. (2015). The organic complexation of dissolved iron along the US GEOTRACES (GA03) North Atlantic Section. *Deep Sea Res. Part II Top. Stud. Oceanogr.* 116, 152–165. doi: 10.1016/j.dsr2.2014.11.016
- Bundy, R. M., Abdulla, H. A. N., Hatcher, P. G., Biller, D. V., Buck, K. N., and Barbeau, K. A. (2015). Iron-binding ligands and humic substances in the San Francisco Bay estuary and estuarine-influenced shelf regions of coastal California. *Mar. Chem.* 173, 183–194. doi: 10.1016/j.marchem.2014.11.005
- Bundy, R. M., Biller, D. V., Buck, K. N., Bruland, K. W., and Barbeau, K. A. (2014). Distinct pools of dissolved iron-binding ligands in the surface and benthic boundary layer of the California Current. *Limnol. Oceanogr.* 59, 769–787. doi: 10.4319/lo.2014.59.3.0769
- Bundy, R. M., Jiang, M., Carter, M., and Barbeau, K. (2016). A. Iron-binding ligands in the southern California current system: mechanistic studies. *Front. Mar. Sci.* 3:27. doi: 10.3389/fmars.2016.00027
- Butler, A. (1998). Acquisition and utilization of transition metal ions by marine organisms. *Science* 281, 207–210. doi: 10.1126/science.281.5374.207
- Butler, A. (2005). Marine siderophores and microbial iron mobilization. *Biometals* 18, 369–374. doi: 10.1007/s10534-005-3711-0
- Campbell, L., and Vaultot, D. (1993). Photosynthetic picoplankton community structure in the subtropical North Pacific Ocean near Hawaii (station ALOHA). *Deep Sea Res. Part I Oceanogr. Res. Pap.* 40, 2043–2060. doi: 10.1016/0967-0637(93)90044-4
- Church, M. J., Hutchins, D. A., and Ducklow, H. W. (2000). Limitation of bacterial growth by dissolved organic matter and iron in the Southern Ocean. *Appl. Environ. Microbiol.* 66, 455–466. doi: 10.1128/AEM.66.2.455-466.2000
- Conway, T. M., and John, S. G. (2014). Quantification of dissolved iron sources to the North Atlantic Ocean. *Nature* 511, 212–215. doi: 10.1038/nature13482
- Cordero, O. X., Ventouras, L. A., DeLong, E. F., and Polz, M. F. (2012). Public good dynamics drive evolution of iron acquisition strategies in natural bacterioplankton populations. *Proc. Natl. Acad. Sci. U.S.A.* 109, 20059–20064. doi: 10.1073/pnas.1213344109
- Croot, P. L., Andersson, K., Ozturk, M., and Turner, D. R. (2004). The distribution and specification of iron along 6 degrees E in the Southern Ocean. *Deep Sea Res. Part II Top. Stud. Oceanogr.* 51, 2857–2879. doi: 10.1016/j.dsr2.2003.10.012
- Edwards, B. R., Bidle, K. D., and Van Mooy, B. A. (2015). Dose dependent regulation of microbial activity on sinking particles by polyunsaturated aldehydes: implications for the carbon cycle. *Proc. Natl. Acad. Sci. U.S.A.* 112, 5909–5914. doi: 10.1073/pnas.1422664112
- Essén, S. A., Johnsson, A., Bylund, D., Pedersen, K., and Lundström, U. S. (2007). Siderophore production by *Pseudomonas stutzeri* under aerobic and anaerobic conditions. *Appl. Environ. Microbiol.* 73, 5857–5864. doi: 10.1128/AEM.00072-07
- Fitzsimmons, J. N., Hayes, C. T., Al-Subiai, S. N., Zhang, R., Morton, P. L., Weisend, R. E., et al. (2015). Daily to decadal variability of size-fractionated iron and iron-binding ligands at the Hawaii Ocean time-series station ALOHA. *Geochim. Cosmochim. Acta* 171, 303–324. doi: 10.1016/j.gca.2015.08.012
- Gerringa, L. J. A., Blain, S., Laan, P., Sarthou, G., Veldhuis, M. J. W., Brussaard, C. P. D., et al. (2008). Fe-binding dissolved organic ligands near the Kerguelen Archipelago in the Southern Ocean (Indian sector). *Deep Sea Res. Part II Top. Stud. Oceanogr.* 55, 5–7. doi: 10.1016/j.dsr2.2007.12.007
- Gerringa, L. J. A., Veldhuis, M. J. W., Timmermans, K. R., Sarthou, G., and de Baar, H. J. W. (2006). Co-variance of dissolved Fe-binding ligands with phytoplankton characteristics in the Canary Basin. *Mar. Chem.* 102, 276–290. doi: 10.1016/j.marchem.2006.05.004
- Gerringa, L., Rijkenberg, M., Schoemann, V., Laan, P., and de Baar, H. (2015). Organic complexation of iron in the West Atlantic Ocean. *Mar. Chem.* 177, 434–446. doi: 10.1016/j.marchem.2015.04.007
- Gledhill, M., and Buck, K. N. (2012). The organic complexation of iron in the marine environment: a review. *Front. Microbiol.* 3:69. doi: 10.3389/fmicb.2012.00069
- Gledhill, M., McCormack, P., Ussher, S., Achterberg, E. P., Mantoura, R. F. C., and Worsfold, P. J. (2004). Production of siderophore type chelates by mixed bacterioplankton populations in nutrient enriched seawater incubations. *Mar. Chem.* 88, 75–83. doi: 10.1016/j.marchem.2004.03.003
- Hawkes, J. A., Gledhill, M., Connally, D. P., and Achterberg, E. P. (2013). Characterisation of iron binding ligands in seawater by reverse titration. *Anal. Chim. Acta* 766, 53–60. doi: 10.1016/j.aca.2012.12.048
- Haygood, M. G., Holt, P. D., and Butler, A. (1993). Aerobactin production by a planktonic marine vibrio sp. *Limnol. Oceanogr.* 38, 1091–1097. doi: 10.4319/lo.1993.38.5.1091
- Hogle, S. L., Bundy, R. M., Blanton, J. M., Allen, E. E., and Barbeau, K. A. (2016a). Copiotrophic marine bacteria are associated with strong iron-binding ligand production during phytoplankton blooms. *Limnol. Oceanogr. Lett.* 1, 36–43. doi: 10.1002/lo2.10026
- Hogle, S. L., Thrash, J. C., Dupont, C. L., and Barbeau, K. A. (2016b). Trace metal acquisition by marine heterotrophic bacterioplankton with contrasting trophic strategies. *Appl. Environ. Microbiol.* 82, 1613–1624. doi: 10.1128/AEM.03128-15
- Holm-Hansen, O., Kahru, M., and Hewes, C. D. (2005). Deep chlorophyll a maxima (DCMs) in pelagic Antarctic waters. II. Relation to bathymetric features and dissolved iron concentrations. *Mar. Ecol. Prog. Ser.* 297, 71–81. doi: 10.3354/meps297071
- Hopkinson, B. M., and Barbeau, K. A. (2008). Interactive influences of iron and light limitation on phytoplankton at subsurface chlorophyll maxima in the eastern North Pacific. *Limnol. Oceanogr.* 53, 1303–1318. doi: 10.4319/lo.2008.53.4.1303
- Hopkinson, B. M., Mitchell, B. G., Reynolds, R. A., Wang, H., Selph, K. E., Measures, C. I., et al. (2007). Iron limitation across chlorophyll gradients in the southern drake passage: phytoplankton responses to iron addition and photosynthetic indicators of iron stress. *Limnol. Oceanogr.* 52, 2540–2554. doi: 10.4319/lo.2007.52.6.2540
- Hutchins, D. A., Witter, A. E., Butler, A., and Luther, G. W. (1999). Competition among marine phytoplankton for different chelated iron species. *Nature* 400, 858–861. doi: 10.1038/23680
- Ibsanmi, E., Sander, S. G., Boyd, P. W., Bowie, A. R., and Hunter, K. A. (2011). Vertical distributions of iron-(III) complexing ligands in the Southern Ocean. *Deep Sea Res. Part II Top. Stud. Oceanogr.* 58, 2113–2125. doi: 10.1016/j.dsr2.2011.05.028
- Ito, Y., and Butler, A. (2005). Structure of synechobactins, new siderophores of the marine cyanobacterium *Synechococcus* sp. PCC 7002. *Limnol. Oceanogr.* 50, 1918–1923. doi: 10.4319/lo.2005.50.6.1918

- Jickells, T. D., An, Z. S., Andersen, K. K., Baker, A. R., Bergametti, G., Brooks, N., et al. (2005). Global iron connections between desert dust, ocean biogeochemistry, and climate. *Science* 308, 67–71. doi: 10.1126/science.1105959
- Johnson, K. S., Elrod, V., Fitzwater, S., Plant, J., Boyle, E., Bergquist, B., et al. (2007). Developing standards for dissolved iron in seawater. *Eos Trans. AGU* 88, 131–132. doi: 10.1029/2007EO110003
- Johnson, Z. I., and Lin, Y. (2009). Prochlorococcus: approved for export. *Proc. Natl. Acad. Sci. U.S.A.* 106, 10400–10401. doi: 10.1073/pnas.0905187106
- Karl, D. M., and Church, M. J. (2014). Microbial oceanography and the Hawaii Ocean Time-series programme. *Nat. Rev. Microbiol.* 12, 699–713. doi: 10.1038/nrmicro3333
- Karl, D. M., Church, M. J., Dore, J. E., Letelier, R. M., and Mahaffey, C. (2012). Predictable and efficient carbon sequestration in the North Pacific Ocean supported by symbiotic nitrogen fixation. *Proc. Natl. Acad. Sci. U.S.A.* 109, 1842–1849. doi: 10.1073/pnas.1120312109
- Karl, D. M., and Lukas, R. (1996). The Hawaii Ocean Time-series (HOT) program: background, rationale and field implementation. *Deep Sea Res. Part II Top. Stud. Oceanogr.* 43, 129–156. doi: 10.1016/0967-0645(96)00005-7
- Kem, M. P., and Butler, A. (2015). Acyl peptidic siderophores: structures, biosyntheses and post-assembly modifications. *Biometals* 28, 445–459. doi: 10.1007/s10534-015-9827-y
- Kem, M. P., Naka, H., Inishi, A., Haygood, M. G., and Butler, A. (2015). Fatty acid hydrolysis of acyl marinobactin siderophores by Marinobacter acylases. *Biochemistry* 54, 744–752. doi: 10.1021/bi5013673
- King, A. L., and Barbeau, K. A. (2011). Dissolved iron and macronutrient distributions in the southern California current system. *J. Geophys. Res. Oceans* 116:18. doi: 10.1029/2010JC006324
- Kondo, Y., Takeda, S., Nishioka, J., Obata, H., Furuya, K., Johnson, W. K., et al. (2008). Organic iron(III) complexing ligands during an iron enrichment experiment in the western subarctic North Pacific. *Geophys. Res. Lett.* 35:L12601. doi: 10.1029/2008GL033354
- Kustka, A. B., Sa-udo-Wilhelmy, S. A., Carpenter, E. J., Capone, D., Burns, J., and Sunda, W. G. (2003). Iron requirements for dinitrogen-and ammonium-supported growth in cultures of *Trichodesmium* (IMS 101): comparison with nitrogen fixation rates and iron: carbon ratios of field populations. *Limnol. Oceanogr.* 48, 1869–1884. doi: 10.4319/lo.2003.48.5.1869
- Lis, H., Shaked, Y., Kranzler, C., Keren, N., and Morel, F. M. (2015). Iron bioavailability to phytoplankton: an empirical approach. *ISME J.* 9, 1003–1013. doi: 10.1038/ismej.2014.199
- Mahowald, N. M., Baker, A. R., Bergametti, G., Brooks, N., Duce, R. A., Jickells, T. D., et al. (2005). Atmospheric global dust cycle and iron inputs to the ocean. *Glob. Biogeochem. Cycles* 19:GB4025. doi: 10.1029/2004GB002402
- Marie, D., Partensky, F., Vaultol, D., and Brussard, C. (1999). Enumeration of phytoplankton, bacteria, and viruses in marine samples. *Curr. Protoc. Cytom. Chapter 11:Unit 11.11.* doi: 10.1002/0471142956.cy111s10
- Martinez, J. S., Carter-Franklin, J. N., Mann, E. L., Martin, J. D., Haygood, M. G., and Butler, A. (2003). Structure and membrane affinity of a suite of amphiphilic siderophores produced by a marine bacterium. *Proc. Natl. Acad. Sci. U.S.A.* 100, 3754–3759. doi: 10.1073/pnas.0637444100
- Martinez, J. S., Haygood, M. G., and Butler, A. (2001). Identification of a natural desferrioxamine siderophore produced by a marine bacterium. *Limnol. Oceanogr.* 46, 420–424. doi: 10.4319/lo.2001.46.2.0420
- Martinez, J. S., Zhang, G. P., Holt, P. D., Hung, H. T., Carrano, C. J., Haygood, M. G., et al. (2000). Self-assembling amphiphilic siderophores from marine bacteria. *Science* 287, 1245–1247. doi: 10.1126/science.287.5456.1245
- Mawji, E., Gledhill, M., Milton, J. A., Tarran, G. A., Ussher, S., Thompson, A., et al. (2008). Hydroxamate siderophores: occurrence and importance in the Atlantic Ocean. *Environ. Sci. Technol.* 42, 8675–8680. doi: 10.1021/es801884r
- Meyer, J. M., and Abdallah, M. A. (1980). The siderochromes of non-fluorescent pseudomonads: production of nocardamine by *Pseudomonas stutzeri*. *Microbiology* 118, 125–129. doi: 10.1099/00221287-118-1-125
- Morel, F. M., and Price, N. M. (2003). The biogeochemical cycles of trace metals in the oceans. *Science* 300, 944–947. doi: 10.1126/science.1083545
- Omanović, D., Gamier, C., and Pizeta, I. (2015). ProMCC: an all-in-one tool for trace metal complexation studies. *Mar. Chem.* 173, 25–39. doi: 10.1016/j.marchem.2014.10.011
- Peterson, M. L., Wakeham, S. G., Lee, C., Askea, M. A., and Miquel, J. C. (2005). Novel techniques for collection of sinking particles in the ocean and determining their settling rates. *Limnol. Oceanogr. Methods* 3, 520–532. doi: 10.4319/lom.2005.3.520
- Reid, R. T., Live, D. H., Faulkner, D. J., and Butler, A. (1993). A siderophore from a marine bacterium with an exceptional ferric ion affinity constant. *Nature* 366, 455–458. doi: 10.1038/366455a0
- Roe, K. L., Barbeau, K., Mann, E. L., and Haygood, M. G. (2012). Acquisition of iron by *Trichodesmium* and associated bacteria in culture. *Environ. Microbiol.* 14, 1681–1695. doi: 10.1111/j.1462-2920.2011.02653.x
- Rue, E. L., and Bruland, K. W. (1995). Complexation of iron(III) by natural organic-ligands in the central North Pacific as determined by a new competitive ligand equilibration adsorptive cathodic stripping voltammetric method. *Mar. Chem.* 50, 117–138. doi: 10.1016/0304-4203(95)00031-L
- Schwyn, B., and Neilands, J. B. (1987). Universal chemical assay for the detection and determination of siderophores. *Anal. Biochem.* 160, 47–56. doi: 10.1016/0003-2697(87)90612-9
- Shaked, Y., Kustka, A. B., and Morel, F. M. M. (2005). A general kinetic model for iron acquisition by eukaryotic phytoplankton. *Limnol. Oceanogr.* 50, 872–882. doi: 10.4319/lo.2005.50.3.0872
- Shaked, Y., and Lis, H. (2012). Disassembling iron availability to phytoplankton. *Front. Microbiol.* 3:123. doi: 10.3389/fmicb.2012.00123
- Shilova, I. N., Mills, M. M., Robidart, J. C., Turk-Kubo, K. A., Björkman, K. M., Kolber, Z., et al. (2017). Differential effects of nitrate, ammonium, and urea as N sources for microbial communities in the North Pacific Ocean. *Limnol. Oceanogr.* 62, 2550–2574. doi: 10.1002/lno.10590
- Sunda, W. G., and Huntsman, S. A. (1997). Interrelated influence of iron, light and cell size on marine phytoplankton growth. *Nature* 390, 389–392. doi: 10.1038/37093
- Tagliabue, A., Aumont, O., and Bopp, L. (2014). The impact of different external sources of iron on the global carbon cycle. *Geophys. Res. Lett.* 41, 920–926. doi: 10.1002/2013GL059059
- Tagliabue, A., Aumont, O., DeAth, R., Dunne, J. P., Dutkiewicz, S., Galbraith, E., et al. (2016). How well do global ocean biogeochemistry models simulate dissolved iron distributions? *Glob. Biogeochem. Cycles* 30, 149–174. doi: 10.1002/2015GB005289
- Tagliabue, A., Bowie, A. R., Boyd, P. W., Buck, K. N., Johnson, K. S., and Saito, M. A. (2017). The integral role of iron in ocean biogeochemistry. *Nature* 543, 51–59. doi: 10.1038/nature21058
- Talley, L. D. (1993). Distribution and formation of North Pacific intermediate water. *J. Phys. Oceanogr.* 23, 517–537. doi: 10.1175/1520-0485(1993)023<0517:DAFONP>2.0.CO;2
- Tautenhahn, R., Cho, K., Uritboonthai, W., Zhu, Z., Patti, G. J., and Siuzdak, G. (2012a). An accelerated workflow for untargeted metabolomics using the METLIN database. *Nat. Biotechnol.* 30, 826–828. doi: 10.1038/nbt.2348
- Tautenhahn, R., Patti, G. J., Rinehart, D., and Siuzdak, G. (2012b). XCMS Online: a web-based platform to process untargeted metabolomic data. *Anal. Chem.* 84, 5035–5039. doi: 10.1021/ac300698c
- Thompson, A. W., Huang, K., Saito, M. A., and Chisholm, S. W. (2011). Transcriptome response of high- and low-light-adapted Prochlorococcus strains to changing iron availability. *ISME J.* 5, 1580–1594. doi: 10.1038/ismej.2011.49
- Tian, F., Frew, R. D., Sander, S., Hunter, K. A., and Ellwood, M. J. (2006). Organic iron. *Mar. Freshw. Res.* 57, 533–544. doi: 10.1071/MF05209
- van den Berg, C. M., and Donat, J. R. (1992). Determination and data evaluation of copper complexation by organic ligands in sea water using cathodic stripping voltammetry at varying detection windows. *Anal. Chim. Acta*, 257, 281–291. doi: 10.1016/0003-2670(92)85181-5
- van den Berg, C. M. G. (1995). Evidence for organic complexation of iron in seawater. *Mar. Chem.* 50, 139–157. doi: 10.1016/0304-4203(95)00032-M
- Velasquez, I. B., Ibisammi, E., Maas, E. W., Boyd, P. W., Nodder, S., and Sander, S. G. (2016). Ferrioxamine siderophores detected amongst iron binding ligands produced during the remineralization of marine particles. *Front. Mar. Sci.* 3:172. doi: 10.3389/fmars.2016.00172
- Velasquez, I., Nunn, B. L., Ibisammi, E., Goodlett, D. R., Hunter, K. A., and Sander, S. G. (2011). Detection of hydroxamate siderophores in coastal and

- Sub-Antarctic waters off the South Eastern Coast of New Zealand. *Mar. Chem.* 126, 97–107. doi: 10.1016/j.marchem.2011.04.003
- Vrapsir, J. M., and Butler, A. (2009). Chemistry of marine ligands and siderophores. *Ann. Rev. Mar. Sci.* 1, 43–63. doi: 10.1146/annurev.marine.010908.163712
- Wagener, T., Pulido-Villena, E., and Guieu, C. (2008). Dust iron dissolution in seawater: results from a one-year time-series in the Mediterranean Sea. *Geophys. Res. Lett.* 35:L16601. doi: 10.1029/2008GL034581
- Witter, A. E., Hutchins, D. A., Butler, A., and Luther, G. (2000). Determination of conditional stability constants and kinetic constants for strong model Fe-binding ligands in seawater. *Mar. Chem.* 69, 1–17. doi: 10.1016/S0304-4203(99)00087-0

Conflict of Interest Statement: The authors declare that the research was conducted in the absence of any commercial or financial relationships that could be construed as a potential conflict of interest.

Copyright © 2018 Bundy, Boiteau, McLean, Turk-Kubo, McIlvin, Saito, Van Mooy and Repeta. This is an open-access article distributed under the terms of the Creative Commons Attribution License (CC BY). The use, distribution or reproduction in other forums is permitted, provided the original author(s) and the copyright owner are credited and that the original publication in this journal is cited, in accordance with accepted academic practice. No use, distribution or reproduction is permitted which does not comply with these terms.



Light-Enhanced Microbial Organic Carbon Yield

John R. Casey*, Sara Ferrón and David M. Karl

Center for Microbial Oceanography, School of Ocean and Earth Science and Technology, University of Hawaii at Manoa, Honolulu, HI, United States

Molecular evidence for proteorhodopsin- and bacteriochlorophyll-based photoheterotrophy is widespread in oligotrophic marine microbial community metagenomes, and has been implicated in light-enhanced growth rates, substrate uptake rates, and anapleurotic carbon fixation, thus complicating the web of interactions within the ‘microbial loop.’ We quantified photoheterotrophic metabolism of the oxidized organic acid glycolate, a fast-turnover and exclusively phytoplankton-derived substrate at an oligotrophic site in the subtropical North Pacific Ocean. As expected, concentration-dependent changes in uptake rates were observed over the diel cycle, with maxima occurring at midday. Although no light-enhanced substrate uptake rates were observed, samples exposed to light altered the balance between assimilation and respiration, resulting in an approximately four-fold increase in glycolate-specific assimilation efficiency. Energy demand for such a metabolic adjustment was linearly related to light, consistent with photoheterotrophy.

OPEN ACCESS

Edited by:

Matthew J. Church,
University of Montana, United States

Reviewed by:

David L. Kirchman,
University of Delaware, United States

Yao Zhang,
Xiamen University, China

***Correspondence:**

John R. Casey
jrcasey@hawaii.edu

Specialty section:

This article was submitted to
Aquatic Microbiology,
a section of the journal
Frontiers in Microbiology

Received: 24 August 2017

Accepted: 20 October 2017

Published: 16 November 2017

Citation:

Casey JR, Ferrón S and Karl DM (2017) Light-Enhanced Microbial Organic Carbon Yield. *Front. Microbiol.* 8:2157.
doi: 10.3389/fmicb.2017.02157

INTRODUCTION

The web of microbially mediated transformations of carbon and energy in the oceans is intricate and dynamic. The conduit through which a great majority of oceanic respiration is channeled is the dissolved organic matter (DOM) reservoir. DOM is composed of thousands of unique molecules in widely varying concentrations (Mopper et al., 2007), and the spectrum of turnover spans from minutes (Fuhrman and Ferguson, 1986) to millennia (Ziolkowski and Druffel, 2010; Zigah et al., 2017). Among other physicochemical attributes, the thermodynamic properties of organic substrates governs their turnover, with high enthalpy substrates supporting sub-optimal microbial growth rates and therefore turning over more slowly than low enthalpy substrates (Casey et al., 2015). However, since the discovery of two unique light-harvesting systems widespread in marine bacteria and archaea, aerobic anoxygenic phototrophy (AAP; Shiba et al., 1979) and proteorhodopsin (PR) phototrophy (PRP; Béjà et al., 2000), the traditional view of a primary producer-DOM-secondary producer microbial loop (Azam et al., 1983) should be revised (Karl, 2014). Collectively, PR and aerobic anoxygenic phototrophic bacteria and archaea comprise most of the total heterotrophic microbial community in oligotrophic marine ecosystems (Rusch et al., 2007), and PRs have been found in diverse bacterial phyla (McCarren and DeLong, 2007), including the numerically dominant alphaproteobacterium SAR11 and marine archaea (Frigaard et al., 2006). While nutrient and ion transport have been associated with rhodopsins (Chan et al., 1981; Dimroth, 1990; Feng et al., 2013; Inoue et al., 2013; Kwon et al., 2013; Yoshizawa et al., 2014), both PR and the bacteriochlorophyll (BChl) complex are capable of generating a proton motive force

(pmf) to supplement the ATP demands of biosynthetic and maintenance functions. The PR pmf generated has been shown in monoclonal cultures to markedly stimulate growth rates (Gómez-Consarnau et al., 2007; Kimura et al., 2011; Palovaara et al., 2014), anapleurotic carbon fixation rates (Palovaara et al., 2014), substrate uptake rates (Alonso-Saez et al., 2006; Michelou et al., 2007; Mary et al., 2008), and to resuscitate carbon-starved cells (Gómez-Consarnau et al., 2010; Steindler et al., 2011). Whether the high abundance and diversity of AAP and PRP in the marine environment indicates a physiological cost-benefit solution to energy limitation of heterotrophic microbial growth on low-yield, thermodynamically efficient substrates remains unclear.

The PRP and AAP pmf may provide microbes with a reliable energy source to supplement, or perhaps to partly relieve oxidative phosphorylation demands (Johnston et al., 2005). Indeed, Koblížek et al. (2010) measured a 70% reduction in respiration rates of an AAP *Roseobacter* isolate when grown on glutamate as a sole carbon source in the presence of light. Accordingly, the 'shaft work' provided to facultative photoorganoheterotrophs by photochemical energy transduction should decouple substrate chemical energy potential from the anabolic yields of obligate chemoorganoheterotrophs (von Stockar et al., 2006). We hypothesized that light repression of photoorganoheterotrophic respiration improves substrate-specific growth yields within natural microbial assemblages, especially for substrates more oxidized than their anabolic end-products.

Light-enhanced nucleic acid and amino acid assimilation rates have been reported in whole communities (Church et al., 2004, 2006) and within flow cytometry sorted populations of *Prochlorococcus*, *Synechococcus*, and small, low nucleic acid bacterioplankton, including SAR11 (Michelou et al., 2007; Mary et al., 2008; Gómez-Pereira et al., 2012). However, sorted populations have not been directly linked to their respective respiration rates, and thus evidence for light-enhanced bacterial growth efficiency has necessarily been inferred from bulk oxygen consumption (Cottrell et al., 2008). A suitable substrate to evaluate light-enhanced heterotrophic growth yield is the hydroxy acid glycolate. Glycolate has long been recognized to be an important light-dependent excretory product of phytoplankton (Tolbert and Zill, 1957; Nalewajko et al., 1963), and featured at the center of a lively debate regarding its extracellular production (Sharp, 1977; Mague et al., 1980; Fogg, 1983; Bjørnsen, 1988) and consumption by heterotrophic bacteria (Wright and Shah, 1977). Glycolate is secreted as a result of photorespiration from photoautotrophic microbes like high-light adapted *Prochlorococcus* strains (Bertilsson et al., 2005), some of which lack a complete salvage pathway (Casey et al., 2016). Since photorespiration is likely the sole extracellular source of glycolate, and since glycolate permease transporters and glycolate oxidases and dehydrogenases are present in SAR11, glycolate represents a direct transfer of oxidized, newly fixed photosynthate to support heterotrophic carbon and energy demands. In this study, radiorespirometry experiments were conducted to determine the concentration-dependent kinetics of glycolate uptake, the diel cycle of glycolate uptake, and the effect of light within that cycle

and as a function of depth within the euphotic zone (5–100 m).

MATERIALS AND METHODS

Station Locations and Sample Collection

Samples were collected on two separate expeditions (Cruise 1 – September 2013 at 22° 75' N, 158° 00' W and Cruise 2 – July–August 2015 at 24° 25' N, 156° 45' W) in the North Pacific Subtropical Gyre north of the island of O'ahu. The kinetics experiment was carried out during Cruise 1. Cruise 2 followed a semi-Lagrangian track near the center of an anticyclonic mode-water eddy feature, facilitated by maintaining ship's position with World Ocean Circulation Experiment Surface Velocity Profile drifters with 15 m-depth drogues. Sampling for glycolate tracer incubation time-series was conducted at 4 h intervals, uninterrupted over the course of 2 days. Additionally, a depth profile of glycolate uptake rates was conducted using a surface-tethered array, designed to accommodate sample bottles suspended at 5, 25, 50, 75, and 100 m, which were deployed from dawn to dusk on the last day of the time-series experiments. Water samples were collected using polyvinyl chloride Niskin® bottles mounted on a rosette equipped with dual conductivity, temperature, pressure, and oxygen sensors, a transmissometer, and a triplet fluorometer (SBE 911plus, Sea-Bird Electronics, Inc.). Photosynthetically active radiation (PAR; 400–700 nm wavelength band) are measured both at the surface in time-series experiments by shipboard quantum cosine sensor (LI-190R; LI-COR Inc.) with data logger (LI-1000; LI-COR Inc.), and also in depth profiles (0–190 m) by a free-falling profiling hyperspectral radiometer (HyperPro, Satlantic LP.). Incubation time-integrated PAR was calculated by scaling shipboard PAR to incubator transmittance (50%).

Community Stocks, Production, and Respiration Data

Alongside glycolate incubations, samples were collected for chlorophyll a (Chl a), primary production (PP), and microbial community respiration (MCR). Chl a and PP measurements were conducted according to Hawaii Ocean Time-series standard protocols (Karl and Dore, 2001¹). Briefly, for Chl a, 125 ml samples were pressure filtered onto 25 mm glass fiber filters (Whatman GF/F) and stored in acetone at –20°C until analyzed fluorometrically. For PP, 500 ml samples were collected in triplicate at different depths and incubated *in situ* on a surface-tethered array deployed before sunrise and recovered after sunset. Prior to deployment, bottles were spiked with H¹⁴CO₃[–] to yield a final radioactivity of approximately 2 MBq L^{–1}. After a 14 h incubation, samples were filtered onto GF/F filters, acidified in glass scintillation vials with 1 ml 2M hydrochloric acid and allowed to vent for 24 h prior to the addition of 10 ml Ultima Gold LLN cocktail and liquid scintillation counting. Similarly, samples for gross oxygen production (GOP)

¹<http://hahana.soest.hawaii.edu/hot/methods/results.html>

and MCR were collected in triplicate in 125 ml Pyrex glass bottles, spiked with H₂¹⁸O (Medical Isotopes, 97.2% ¹⁸O) to a final δ¹⁸O(H₂O) of approximately 2300‰, and incubated *in situ* along with the PP array. After recovery, biological activity was stopped by adding 100 μL of saturated mercuric chloride solution. In addition, triplicate time-zero samples were collected at each depth and poisoned at the beginning of the deployment. Mass-to-charge (*m/z*) ratios of 32 (¹⁶O¹⁶O), 34 (¹⁸O¹⁶O), and 40 (Ar) were quantified using membrane inlet mass spectrometry (MIMS) following Ferrón et al. (2016). The system consists of a water inlet, described in detail by Kana et al. (1994), and an analyzer, consisting of a HiQuad™ quadrupole mass spectrometer (QMG 700) with a cross-beam ion source, a Faraday collector, and a 90° off-axis secondary electron multiplier (SEM), connected to a Pfeiffer Vacuum HiCube 80 Eco turbo pumping station. MCR was determined as the difference between GOP and the net O₂ change during the incubation (Ferrón et al., 2016).

Glycolate Kinetics and Uptake Experiments

Incubations for glycolate kinetics and diel uptake rates were conducted in semi-transparent acrylic (shaded to approximately match the 15 m depth of sampling) or darkened deckboard incubators flushed with circulating surface seawater to maintain *in situ* temperatures. Incubator bath temperatures were monitored by HOBO Pendant® Data Loggers (Onset Computer Corp.). We refer to samples incubated at simulated light levels of 15 m depth as ‘unshaded,’ and samples incubated in dark conditions as ‘shaded,’ so as not to be confused with nighttime. Accordingly, ‘light’ and ‘dark’ refer to daytime and nighttime.

Experimental procedures for glycolate incubations were described in Casey et al. (2015). Briefly, 60 ml samples were spiked with [U-¹⁴C]-glycolic acid calcium salt (¹⁴C-glycolate herein; American Radiolabeled Chemicals, Inc.) at a specific radioactivity of 1.48 TBq mol⁻¹. For the kinetics experiment, nine spike concentrations were added, ranging from 1 to 348 nM, spaced logarithmically. For all other incubations, spike concentrations were 10 nM. Uptake time series samples were collected at 4 h intervals for 2 days. Samples were incubated for 4.7 ± 0.4 h. All samples were incubated in triplicate and a 500 μL total activity aliquot was collected from each sample prior to incubation. For glycolate assimilation rates (*v_A*), samples were filtered under gentle vacuum (<70 mBar) directly after incubation onto 25 mm glass fiber filters (nominal pore size 0.3 μm; GF75, Sterlitech Corp.) and rinsed with three volumes of 20 ml 0.2 μm filtered seawater. Filters were transferred to 20 ml glass scintillation vials and submerged in 10 ml scintillation cocktail (Ultima Gold LLT, Perkin Elmer). To account for ¹⁴C-glycolate adsorbed to cells or glass fiber filters, a “killed-control” replicate sample poisoned with 2% final concentration paraformaldehyde was included prior to each incubation. Killed-controls were incubated alongside live samples and processed identically. Assimilation depth profiles were conducted alongside PP and MCR *in situ* arrays.

For glycolate respiration rates (*v_R*), 125 ml glass serum bottles were fitted with rubber sleeve stoppers pierced with center well cups containing a dry piece of fluted cellulose paper (Whatman #2) positioned in the headspace. Respiration incubations were terminated by first soaking the filter paper with 150 μL phenethylamine and then acidifying the sample with 4 ml 4.5 N sulfuric acid through the gas-tight stopper. The acidified sample was allowed to react for at least 48 h before removing the stoppers. This procedure is designed to completely capture the respired ¹⁴CO₂. Center well cups were transferred to 20 ml glass scintillation vials and submerged in 10 ml scintillation cocktail. A complete radiochemical mass balance (100 ± 4%) was achieved in the kinetics experiment, and recovery was independent of substrate concentration.

Glycolate uptake rates were calculated as the sum of assimilation and respiration rates. Glycolate-specific energy transduction was calculated as the difference in glycolate respiratory energy yield (*Y_E*) in shaded and unshaded samples incubated during daylight hours (*Y_{E,Shaded}* - *Y_{E,Unshaded}*). Glycolate energy yield was calculated as the product of the respiration rate and the standard molar enthalpy of combustion (*Y_E = v_R × ΔH_C^o*) of glycolate. Throughout, two-tailed *t*-tests were used to determine significant differences between treatments, and correlation coefficients were determined from model I or model II least-squares regressions, as appropriate for the experimental conditions (Laws, 1997).

RESULTS

Glycolate Kinetics Experiment

Two distinct kinetics profiles were observed for dark glycolate assimilation and respiration (Figure 1). Assimilation followed a

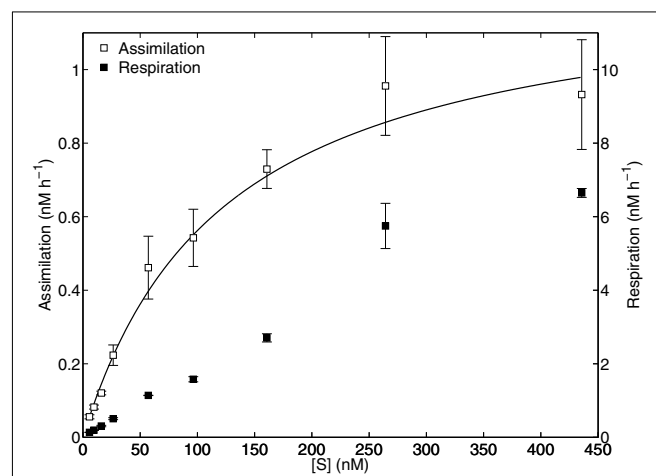


FIGURE 1 | Kinetics experiment. Glycolate assimilation and respiration as a function of added substrate. Error bars represent one standard deviation of the mean rates of three replicates at each concentration. Michaelis-Menten non-linear least-squares regression line is shown (solid line) for assimilation data.

monophasic Michaelis–Menten function with a resulting half-saturation concentration ($K_{m,A}$) of 118 nM and a maximum velocity ($V_{max,A}$) of 1.2 nM h⁻¹. Glycolate respiration did not appear to completely saturate over the concentration range tested, therefore $K_{m,R}$ and $V_{max,R}$ could not be determined. The resulting uptake parameters $K_{m,U}$ and $V_{max,U}$ were calculated to be 195 and 8.9 nM h⁻¹, respectively. Glycolate-specific assimilation efficiency ($100 * \mathcal{V}_A / \mathcal{V}_A + \mathcal{V}_R$) varied as a logistic function of substrate concentration added (S), with highest efficiencies ($29.3 \pm 0.9\%$) corresponding to $S < 57$ nM. At saturating substrate concentrations, the assimilation efficiency approached 12%. The glycolate turnover rate was 0.63 d⁻¹, a half-life of 26 h.

Glycolate Diel Time-Series Experiment

Glycolate uptake rates varied by roughly three-fold ($280 \pm 70\%$) over the diel cycle, in phase with the solar cycle, and no difference between shaded and unshaded uptake rates was observed (two-sample *t*-test with unequal variance; $p = 0.39$; **Figure 2**). Glycolate assimilation rates also followed a diel cycle ($310 \pm 110\%$), but with maximal rates occurring in unshaded samples in the morning or early afternoon (600–1400 h, local time). Assimilation rates in shaded samples were $35 \pm 7\%$ lower than in unshaded samples ($p = 0.007$) during daylight hours, and were similar to nighttime samples ($p = 0.42$). In contrast, glycolate respiration rates in shaded samples were $120 \pm 14\%$ higher than unshaded samples ($p < 0.001$) during daylight

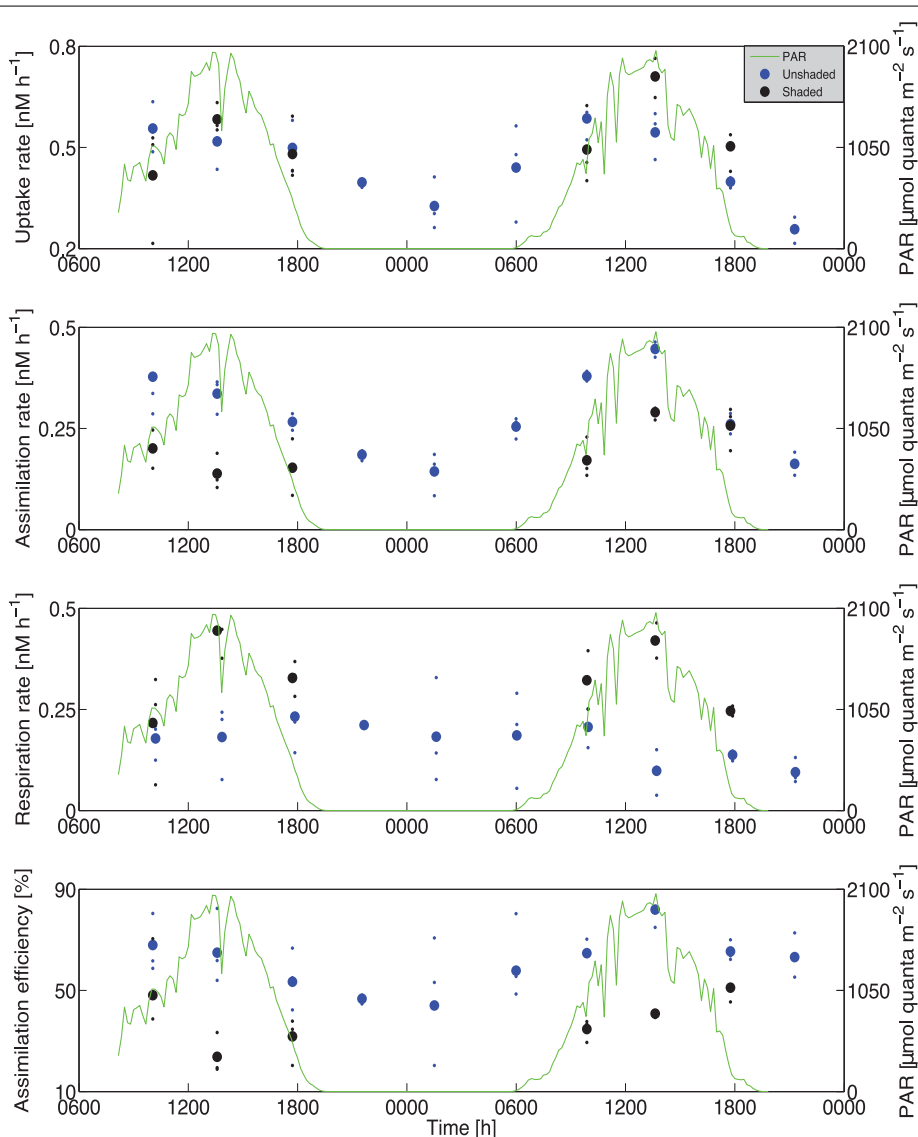


FIGURE 2 | Time-series experiment. Glycolate uptake (**Top**), assimilation (**Second**), respiration (**Third**), and specific assimilation efficiency (**Bottom**) for shaded and unshaded incubations over the course of the diel time-series experiment. Mean (large symbols) and individual data points (small symbols) are shown for clarity. Photosynthetically active radiation (PAR) data are overlaid (green line) in each panel and nighttime is indicated by shaded areas. Data points are aligned to the midpoint of each incubation.

hours, and unshaded samples were similar over the entire daylength ($p = 0.71$). The discrepancy between daytime light-dependent responses in glycolate assimilation and respiration rates resulted in glycolate-specific growth efficiencies ranging from $24 \pm 6\%$ in shaded daytime samples to $82 \pm 8\%$ in unshaded daytime samples ($p < 0.001$). Even if the glycolate taken up was quantitatively respired, the maximum potential contribution of phytoplankton uptake of respired $^{14}\text{CO}_2$ calculated from isotope dilution into the very large dissolved inorganic pool of seawater (approximately 0.006 DPM) would be negligible.

Glycolate Assimilation Depth Profile Experiment

Assimilation rates decreased exponentially with depth (Figure 3), and were more closely correlated with PAR (Model II geometric mean least-squares fit; $r = 0.997$) than with PP ($r = 0.88$), GOP ($r = 0.90$), or MCR ($r = 0.51$). Importantly, within the mixed layer (36 m; defined as the 0.125 kg m^{-3} offset from 0 m), PP and GOP were uniform, indicating a decoupling of glycolate cycling from PP. In consideration of the differences in incubation lengths between *in situ* and on-deck incubations, assimilation rates at 25 m on the array were similar to average diel time-series assimilation rates ($p = 0.71$).

Photoheterotrophic Energy Potential and Glycolate Respiration

Energy transduction, such as the pmf generated by PR or BChla-complex, should increase the adenylate energy charge

and thus increase the anabolic yield. Similarly, a quantitative substitution of the energy derived from dark glycolate respiration should be derived from light. Since numerous pathways for the assimilation of glycolate are possible, and the composition of each consumer may differ considerably, the free energy of glycolate anabolism cannot be estimated reliably. Instead, we introduce a quantity derived from the enthalpy generated by the respiration of glycolate in shaded and unshaded incubations during the daytime. This quantity, glycolate-specific energy transduction, reflects the maximum chemical potential energy derived from light-dependent processes. Glycolate-specific energy transduction was linearly correlated with PAR integrated over each daytime incubation ($r = 0.97$; $p < 0.001$; Figure 4). Accordingly, over the range of irradiances observed, the relationship between these two energy quantities (light and chemical energy) did not saturate.

DISCUSSION

Glycolate, a low molecular weight (76 Da) hydroxy acid, may constitute an important flux of both carbon and energy within the marine microbial community metabolism. Dark glycolate uptake kinetics indicated an upper bound ambient concentration of $30 \pm 6 \text{ nM}$, based on turnover time as a function of substrate added (Dietz et al., 1977). This estimate, though an upper bound (Laws, 1983), is roughly half the nighttime concentration measured by HPLC at an oligotrophic site ($60\text{--}70 \text{ ng Chl a L}^{-1}$) in the tropical eastern North Atlantic

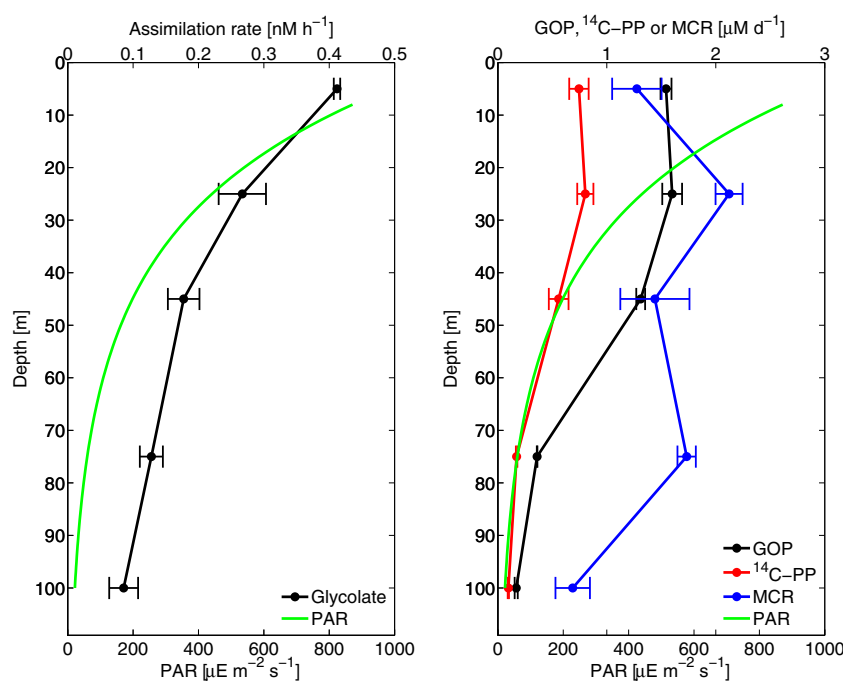


FIGURE 3 | Array profile. Depth profiles of glycolate assimilation rates (Left) and productivity [primary production (PP), gross oxygen production (GOP)] and microbial community respiration (MCR) (Right). Carbon units correspond to PP and oxygen units correspond to GOP and MCR. The accompanying PAR profile is shown in both panels. Error bars represent one standard deviation of the mean rates of three replicates at each depth.

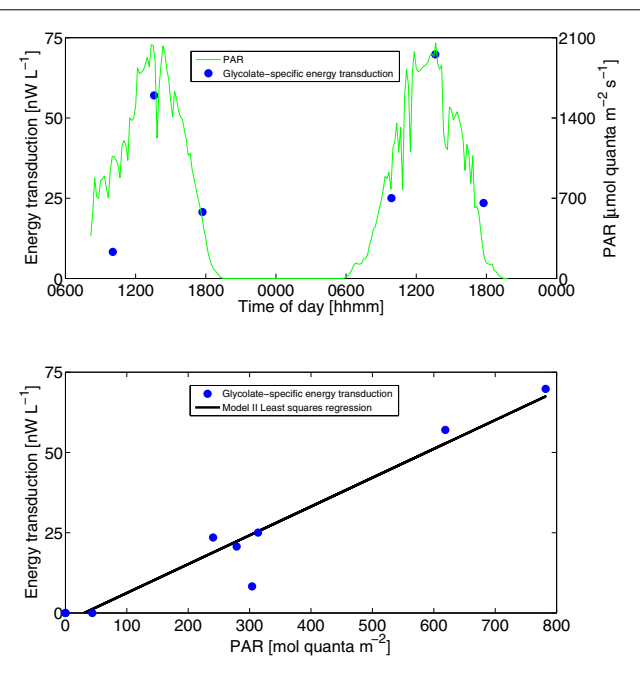


FIGURE 4 | Energy transduction. Calculated glycolate-specific energy transduction (see section “Materials and Methods” for description) and instantaneous PAR irradiance over the diel time-series experiment (**Top**) and as a function of incubation time-integrated PAR (**Bottom**). Model II geometric mean least-squares regression line is shown.

(66 nM; Leboulanger et al., 1997), and is well below the K_m, U (195 nM). During the dark kinetics incubation, the glycolate pool turned over approximately daily (1.1 ± 0.1 days); however, this is likely an underestimate due to disequilibrium with respect to production (which is exclusively during daylight hours).

Time-series incubations showed a characteristic diel cycle in uptake rates in phase with the solar cycle, independent of whether the sample was exposed to light. Taken together with our understanding of a photorespiratory source of glycolate, these results indicate ambient concentration-dependent rates, rather than light-enhanced uptake by heterotrophs. Although the time-series experiment and kinetics experiment were conducted on separate expeditions with somewhat different phytoplankton community stocks and rates (Cruise 1: Chl $a = 80$ ng L $^{-1}$, PP = 8.1 mg C L $^{-1}$ d $^{-1}$; Cruise 2: Chl $a = 137$ ng L $^{-1}$, PP = 9.9 mg C L $^{-1}$ d $^{-1}$), nighttime uptake rates (10 nM spike) collected during the time-series experiment closely matched the corresponding values from the kinetics curve ($p = 0.81$). With this caution, we conservatively estimate a two-fold change in ambient glycolate concentrations over the course of the diel cycle, which is consistent with estimates from the North Atlantic (2.4 ± 1.2 -fold; Leboulanger et al., 1998). Glycolate-specific respiration rates accounted for approximately 3% of total community oxygen consumption (respiration rates), and considering the glycolate respiration quotient, 6% of total community respired CO₂ (assuming a total community respiration quotient of 1.0; del Giorgio et al.,

2006; c.f., Berggren et al., 2011). On a carbon basis, glycolate production rates accounted for less than 4% of GOP in the time-series incubations, however, this can also be interpreted as an underestimate of gross photorespiration since salvage pathways are present in some photoautotrophs. Due to methodological challenges, photorespiration rates have only been indirectly measured in the oceans (Carrillo et al., 2004), and may be an important but largely ignored flux of carbon (Karl et al., 1996).

High-light adapted ‘ecotypes’ (eHL) of the marine cyanobacterium *Prochlorococcus*, the most abundant photoautotroph at Station ALOHA, lacks glycolate oxidase or glycolate dehydrogenase, an essential step in the salvage pathway for photorespiratory glycolate regeneration of 3-phosphoglycerate. Because the precursor 2-phosphoglycolate is toxic to central carbon fixation pathways, *Prochlorococcus* actively excretes glycolate via an ATP-binding cassette efflux transporter. In cultures of two eHL *Prochlorococcus* strains, glycolate excretion was 3% of carbon fixation (Bertilsson et al., 2005), remarkably close to our upper bound estimate. It should be noted that the diazotrophic cyanobacterium *Crocospaera*, which was relatively abundant during the time-series expedition (100–700 cells ml $^{-1}$; 3% of PP; calculated from Wilson et al., 2017), does have a complete photorespiratory salvage pathway. Therefore we cannot eliminate the possibility that *Crocospaera* could take up glycolate. Notwithstanding, *Prochlorococcus* was the dominant primary producer during the time-series expedition, and was likely the major glycolate producer. Interestingly, a major consumer of glycolate is likely the numerically dominant heterotroph at Station ALOHA, SAR11, a small alphaproteobacterium with an absolute growth requirement for pyruvate and either glycolate or one of several photorespiratory salvage pathway intermediate metabolites. SAR11 has both a glycolate transporter and glycolate oxidase which yields glyoxylate and hydrogen peroxide. In addition to the apparent co-evolution of these two dominant oligotrophs (Braakman et al., 2017), SAR11 and much of the heterotrophic microbial community at Station ALOHA (Rusch et al., 2007), have genes for proteorhodopsin-based phototrophy, prompting our investigation into the light-dependent metabolism of glycolate. With a respiration quotient (mol CO₂: mol O₂) of 2, a carbon redox number of 3, and a standard carbon molar enthalpy of combustion (ΔH°_c) of 340 KJ [C-mol] $^{-1}$, glycolate is a relatively poor energy substrate. Accordingly, heterotrophic growth on carboxylic and hydroxy acids like acetate and fatty acids typically requires the operation of the glyoxylate shunt (Kornberg, 1966), a bypass of two CO₂ evolving steps of the oxidative tricarboxylic acid pathway by way of isocitrate lyase and malate synthase which allows the net accumulation of carbon through acetyl-CoA. However, at least one alternative pathway utilizing glyoxylate is present in SAR11 and many other heterotrophs, consisting of a heterotrophic analog of the photorespiratory salvage pathway which can supply precursors for gluconeogenesis (by way of 3-phosphoglycerate) or a number of amino acid synthesis pathways (by way of L-glycine). These anabolic pathways cannot be sustained without a supplemental energy source, since

the ATP/NAD(P)H ratio and yield of the glyoxylate shunt using glycolate as a substrate does not satisfy the demands of e.g., protein synthesis (calculation based on iAF1260, a metabolic model of *Escherichia coli* K-12 MG1655; Feist et al., 2007).

The central finding of this study, that exposure to light enhances the glycolate-specific assimilation efficiency, points to the possibility that the pmf generated by PR or by the BChla-complex yields sufficient energy to divert glycolate flux from the mostly catabolic glyoxylate shunt to the mostly anabolic pathways. We cannot eliminate the possibility that another light-dependent process which is decoupled from PP and community respiration could reproduce our observations. However, the strong correspondence between light and glycolate-specific assimilation efficiency, independent of concentration, supports the notion that photoheterotrophy supplements cellular energy demands for growth on oxidized substrates. Furthermore, considering the ΔH° and the maximum chemical potential energy yield of glycolate respiration, the resulting energy yield was closely correlated with PAR irradiance integrated over each incubation, rather than PP or community respiration. Unfortunately, it is not possible to ‘scale’ glycolate-specific phototrophic energy yields to total photoheterotrophy, since the composition of the myriad additional growth substrates and their respective uptake rates and light-dependent growth efficiencies is not known. We suggest that light-enhanced biomass yields may play an important role in the co-evolution of *Prochlorococcus* and SAR11 (Braakman et al., 2017), a metabolic coupling supported by the exchange of low-yield, thermodynamically optimal substrates (glycolate and pyruvate;

thermodynamic efficiency = 20–24%; Westerhoff et al., 1983).

AUTHOR CONTRIBUTIONS

JRC, SF, and DMK planned the experiments, JRC and SF collected and processed the samples and analyzed the data. All authors contributed to the manuscript preparation and editing.

FUNDING

This work was supported by the National Science Foundation (OCE-1260164 and EF-0424599 awarded to DMK, Graduate Research Fellowship awarded to JRC), the Gordon and Betty Moore Foundation (grant #3794 awarded to DMK), the Simons Foundation (SCOPE Award ID 329108 awarded to DMK and Edward DeLong), and the Balzan Foundation (awarded to DMK).

ACKNOWLEDGMENTS

We would like to thank the captain and crew of the R/V Kilo Moana and chief scientist S. Wilson for their essential support during the “HOE” field campaign. We are grateful to the reviewers and to R. Bidigare, M. Church, P. Falkowski, T. Hemscheidt, and C. Nelson for their comments and helpful discussion.

REFERENCES

- Alonso-Saez, L., Gasol, J. M., Lefort, T., Hofer, J., and Sommaruga, R. (2006). Effect of natural sunlight on bacterial activity and differential sensitivity of natural bacterioplankton groups in northwestern Mediterranean coastal waters. *Appl. Environ. Microbiol.* 72, 5806–5813. doi: 10.1128/AEM.00597-06
- Azam, F., Fenchel, T., Field, J. G., and Gray, J. S. (1983). The ecological role of water-column microbes in the sea. *Mar. Ecol. Prog. Ser.* 10, 257–263. doi: 10.3354/meps010257
- Béjà, O., Aravind, L., Koonin, E. V., Suzuki, M. T., Hadd, A., Nguyen, L. P., et al. (2000). Bacterial rhodopsin: evidence for a new type of phototrophy in the sea. *Science* 289, 1902–1906. doi: 10.1126/science.289.5486.1902
- Berggren, M., Lapierre, J. F., and del Giorgio, P. A. (2011). Magnitude and regulation of bacterioplankton respiratory quotient across freshwaters environmental gradients. *ISME J.* 6, 984–993. doi: 10.1038/ismej.2011.157
- Bertilsson, S., Berglund, O., Pullin, M., and Chisholm, S. W. (2005). Release of dissolved organic matter by *Prochlorococcus*. *Vie Milieu* 55, 225–232.
- Bjørnsen, P. K. (1988). Phytoplankton exudation of organic matter: why do healthy cells do it? *Limnol. Oceanogr.* 33, 151–154. doi: 10.4319/lo.1988.33.1.0151
- Braakman, R., Follows, M. J., and Chisholm, S. W. (2017). Metabolic evolution and the self-organization of ecosystems. *Proc. Natl. Acad. Sci. U.S.A.* 114, E3091–E3100. doi: 10.1073/pnas.1619573114
- Carrillo, C. J., Smith, R. C., and Karl, D. M. (2004). Processes regulating oxygen and carbon dioxide in surface waters west of the Antarctic Peninsula. *Mar. Chem.* 84, 161–179. doi: 10.1016/j.marchem.2003.07.004
- Casey, J., Mardinoglu, A., Nielsen, J., and Karl, D. M. (2016). Adaptive evolution of phosphorus metabolism in *Prochlorococcus*. *mSystems* 1:e00065-16. doi: 10.1128/mSystems.00065-16
- Casey, J. R., Falkowski, P. G., and Karl, D. M. (2015). Substrate selection for heterotrophic bacterial growth in the sea. *Mar. Chem.* 177, 349–356. doi: 10.1016/j.marchem.2015.06.032
- Chan, W. Y., Mosca, P., and Rennert, O. M. (1981). Lithium nephrotoxicity: a review. *Ann. Clin. Lab. Sci.* 11, 343–349.
- Church, M. J., Ducklow, H. W., and Karl, D. M. (2004). Light dependence of [³H]Leucine incorporation in the oligotrophic North Pacific Ocean. *Appl. Environ. Microbiol.* 70, 4079–4087. doi: 10.1128/AEM.70.7.4079-4087.2004
- Church, M. J., Ducklow, H. W., Letelier, R. M., and Karl, D. M. (2006). Temporal and vertical dynamics in picoplankton photoheterotrophic production in the subtropical North Pacific Ocean. *Aquat. Microb. Ecol.* 45, 41–53. doi: 10.3354/ame045041
- Cottrell, M. T., Michelou, V. K., Nemcek, N., DiTullio, G., and Kirchman, D. L. (2008). Carbon cycling by microbes influenced by light in the Northeast Atlantic Ocean. *Aquat. Microb. Ecol.* 50, 239–250. doi: 10.3354/ame01173
- del Giorgio, P. A., Pace, M., and Fischer, D. (2006). Relationship of bacterial growth efficiency to spatial variation in bacterial activity in the Hudson River. *Aquat. Microb. Ecol.* 45, 55–67. doi: 10.3354/ame045055
- Dietz, A. S., Albright, L. J., and Tuominen, T. (1977). Alternative model and approach for determining microbial heterotrophic activities in aquatic systems. *Appl. Environ. Microbiol.* 33, 817–823.
- Dimroth, P. (1990). Mechanisms of sodium transport in bacteria. *Philos. Trans. R. Soc. Lond. B Biol. Sci.* 326, 465–477. doi: 10.1098/rstb.1990.0025
- Feist, A. M., Henry, C. S., Reed, J. L., Krummenacker, M., Joyce, A. R., Karp, P. D., et al. (2007). A genome-scale metabolic reconstruction for *Escherichia coli* K-12 MG1655 that accounts for 1260 ORFs and thermodynamic information. *Mol. Syst. Biol.* 3, 121. doi: 10.1038/msb4100155
- Feng, S., Powell, S. M., Wilson, R., and Bowman, J. P. (2013). Light-stimulated growth of proteorhodopsin-bearing sea-ice psychrophile *Psychroflexus torquis* is salinity dependent. *ISME J.* 7, 2206–2213. doi: 10.1038/ismej.2013.97

- Ferrón, S., del Valle, D. A., Björkman, K. M., Quay, P. D., Church, M. J., and Karl, D. M. (2016). Application of membrane inlet mass spectrometry to measure aquatic gross primary production by the ^{18}O *in vitro* method. *Limnol. Oceanogr. Methods* 14, 610–622. doi: 10.1002/lom3.10116
- Fogg, G. E. (1983). The ecological significance of extracellular products of phytoplankton photosynthesis. *Bot. Mar.* 26, 3–14. doi: 10.1515/botm.1983.26.1.3
- Frigaard, N.-U., Martinez, A., Mincer, T. J., and Delong, E. F. (2006). Proteorhodopsin lateral gene transfer between marine planktonic Bacteria and Archaea. *Nature* 439, 847–850. doi: 10.1038/nature04435
- Fuhrman, J. A., and Ferguson, R. L. (1986). Nanomolar concentrations and rapid turnover of dissolved free amino-acids in seawater—agreement between chemical and microbiological measurements. *Mar. Ecol. Prog. Ser.* 33, 237–242. doi: 10.3354/meps03323
- Gómez-Consarnau, L., Akram, N., Lindell, K., Pedersen, A., Neutze, R., Milton, D. L., et al. (2010). Proteorhodopsin phototrophy promotes survival of marine bacteria during starvation. *PLOS Biol.* 8:e1000358. doi: 10.1371/journal.pbio.1000358
- Gómez-Consarnau, L., González, J. M., Coll-Lladó, M., Gourdon, P., Pascher, T., Neutze, R., et al. (2007). Light stimulates growth of proteorhodopsin-containing marine flavobacteria. *Nature* 445, 210–213. doi: 10.1038/nature05381
- Gómez-Pereira, P. R., Hartmann, M., Grob, C., Tarhan, G. A., Martin, A. P., Fuchs, B. M., et al. (2012). Comparable light stimulation of organic nutrient uptake by SAR11 and *Prochlorococcus* in the North Atlantic subtropical gyre. *ISME J.* 7, 603–614. doi: 10.1038/ismej.2012.126
- Inoue, K., Ono, H., Abe-Yoshizumi, R., and Yoshizawa, S. (2013). A light-driven sodium ion pump in marine bacteria. *Nat. Commun.* 4:1678. doi: 10.1038/ncomms2689
- Johnston, W., Cooney, M., Schorlemmer, A., Pohl, S., Karl, D. M., and Bidigare, R. (2005). Carbon mass balance methodology to characterize the growth of pigmented marine bacteria under conditions of light cycling. *Bioprocess Biosyst. Eng.* 27, 163–174. doi: 10.1007/s00449-004-0395-8
- Kana, T. M., Darkangelo, C., Duane Hunt, M., Oldham, J. B., Bennett, G. E., and Cornwell, J. C. (1994). Membrane inlet mass spectrometer for rapid high-precision determination of N_2 , O_2 , and Ar in environmental water samples. *Anal. Chem.* 66, 4166–4170. doi: 10.1021/ac00095a009
- Karl, D. M. (2014). Solar energy capture and transformation in the sea. *Elem. Sci. Anth.* 2:21. doi: 10.12952/journal.elementa.000021
- Karl, D. M., Christian, J. R., Dore, J. E., and Letelier, R. M. (1996). “Microbiological oceanography in the region west of the Antarctic Peninsula: microbial dynamics, nitrogen cycle, and carbon flux,” in *Foundations for Ecological Research West of the Antarctic Peninsula. Antarctic Research Series*, Vol. 70, eds R. M. Ross, E. E. Hofmann, and L. B. Quetin (Washington, DC: American Geophysical Union), 303–332.
- Karl, D. M., and Dore, J. E. (2001). “Microbial ecology at sea: sampling, subsampling and incubation considerations,” in *Methods in Microbiology*, Vol. 30, ed. J. H. Paul (Cambridge, MA: Academic Press).
- Kimura, H., Young, C. R., Martinez, A., and Delong, E. F. (2011). Light-induced transcriptional responses associated with proteorhodopsin-enhanced growth in a marine flavobacterium. *ISME J.* 5, 1641–1651. doi: 10.1038/ismej.2011.36
- Kobližek, M., Mlèoušková, J., Kolber, Z., and Kopecký, J. (2010). On the photosynthetic properties of marine bacterium COL2P belonging to *Roseobacter* clade. *Arch. Microbiol.* 192, 41–49. doi: 10.1007/s00203-009-0529-0
- Kornberg, H. L. (1966). The role and control of the glyoxylate cycle in *Escherichia coli*. *Biochem. J.* 99, 1–11. doi: 10.1042/bj0990001
- Kwon, S. K., Kim, B. K., Song, J. Y., Kwak, M. J., Lee, C. H., Yoon, J. H., et al. (2013). Genomic makeup of the marine flavobacterium *Nonlabens (Donghaeania) dokdonensis* and identification of a novel class of rhodopsins. *Genome Biol. Evol.* 5, 187–199. doi: 10.1093/gbe/evs134
- Laws, E. A. (1983). Plots of turnover times versus added substrate concentrations provide only upper bounds to *in situ* substrate concentrations. *J. Theor. Biol.* 101, 147–150. doi: 10.1016/0022-5193(83)90278-3
- Laws, E. A. (1997). *Mathematical Methods for Oceanographers*. New York, NY: John Wiley and Sons.
- Leboulanger, C., Oriol, L., Jupin, H., and Desolas-Gros, C. (1997). Diel variability of glycolate in the eastern tropical Atlantic Ocean. *Deep Sea Res. I* 44, 2131–2139. doi: 10.1016/S0967-0637(97)00090-3
- Leboulanger, C., Serve, L., Comellas, L., and Jupin, H. (1998). Determination of glycolic acid released from marine phytoplankton by post-derivatization gas chromatography-mass spectrometry. *Phytochem. Anal.* 9, 5–9. doi: 10.1002/(SICI)1099-1565(199801/02)9:1<5::AID-PCA378>3.0.CO;2-#
- Mague, T. H., Friberg, E., Hughes, D. J., and Morris, I. (1980). Extracellular release of carbon by marine phytoplankton: physiological approach. *Limnol. Oceanogr.* 25, 262–279. doi: 10.4319/lo.1980.25.2.0262
- Mary, I., Tarhan, G. A., Warwick, P. E., Terry, M. J., Scanlan, D. J., Burkhill, P. H., et al. (2008). Light enhanced amino acid uptake by dominant bacterioplankton groups in surface waters of the Atlantic Ocean. *FEMS Microbiol. Ecol.* 63, 36–45. doi: 10.1111/j.1574-6941.2007.00414.x
- McCarren, J., and DeLong, E. F. (2007). Proteorhodopsin photosystem gene clusters exhibit co-evolutionary trends and shared ancestry among diverse marine microbial phyla. *Environ. Microbiol.* 9, 846–858. doi: 10.1111/j.1462-2920.2006.01203.x
- Michelou, V. K., Cottrell, M. T., and Kirchman, D. L. (2007). Light-stimulated bacterial production and amino acid assimilation by cyanobacteria and other microbes in the North Atlantic Ocean. *Appl. Environ. Microbiol.* 73, 5539–5546. doi: 10.1128/AEM.00212-07
- Mopper, K., Stubbins, A., Ritchie, J. D., Bialk, H. M., and Hatcher, P. G. (2007). Advanced instrumental approaches for characterization of marine dissolved organic matter: extraction techniques, mass spectrometry, and nuclear magnetic resonance spectroscopy. *Chem. Rev.* 107, 419–442. doi: 10.1021/cr050359b
- Nalewajko, C., Chowdhuri, N., and Fogg, G. E. (1963). “Excretion of glycolic acid and the growth of a planktonic *Chlorella*,” in *Microalgae and Photosynthetic Bacteria*, ed. The Japanese Society of Plant Physiologists (Tokyo: University of Tokyo Press), 171–183.
- Palovaara, J., Akram, N., Baltar, F., Bunse, C., Forsberg, J., Pedrós-Alió, C., et al. (2014). Stimulation of growth by proteorhodopsin phototrophy involves regulation of central metabolic pathways in marine planktonic bacteria. *Proc. Natl. Acad. Sci. U.S.A.* 111, E3650–E3658. doi: 10.1073/pnas.1402617111
- Rusch, D. B., Halpern, A. L., Sutton, G., Heidelberg, K. B., Williamson, S., Yooseph, S., et al. (2007). The Sorcerer II global ocean sampling expedition: northwest Atlantic through eastern tropical Pacific. *PLOS Biol.* 5:e77. doi: 10.1371/journal.pbio.0050077
- Sharp, J. H. (1977). Excretion of organic matter by marine phytoplankton: do healthy cells do it? *Limnol. Oceanogr.* 22, 381–399. doi: 10.4319/lo.1977.22.3.0381
- Shiba, T., Simidu, U., and Taga, N. (1979). Distribution of aerobic bacteria which contain bacteriochlorophyll a. *Appl. Environ. Microbiol.* 38, 43–45.
- Steindler, L., Schwalbach, M. S., Smith, D. P., and Chan, F. (2011). Energy starved *Candidatus Pelagibacter ubique* substitutes light-mediated ATP production for endogenous carbon respiration. *PLOS ONE* 6:e19725. doi: 10.1371/journal.pone.0019725
- Tolbert, N. E., and Zill, L. P. (1957). “Excretion of glycolic acid by *Chlorella* during photosynthesis,” in *Research in Photosynthesis*, ed. H. Gaffron (New York, NY: Interscience Publishers), 228–231.
- von Stockar, U., Maskow, T., Liu, J., and Marison, I. W. (2006). Thermodynamics of microbial growth and metabolism: an analysis of the current situation. *J. Biotechnol.* 121, 517–533. doi: 10.1016/j.jbiotec.2005.08.012
- Westerhoff, H. V., Hellingwerf, K. J., and Van Dam, K. (1983). Thermodynamic efficiency of microbial growth is low but optimal for maximal growth rate. *Proc. Natl. Acad. Sci. U.S.A.* 80, 305–309. doi: 10.1073/pnas.80.1.305
- Wilson, S. T., Aylward, F. O., Ribalet, F., Barone, B., Casey, J. R., Connell, P. E., et al. (2017). Coordinated regulation of growth, activity and transcription in natural populations of the unicellular nitrogen-fixing cyanobacterium *Crocospaera*. *Nat. Microbiol.* 2:17118. doi: 10.1038/nmicrobiol.2017.118
- Wright, R. T., and Shah, N. M. (1977). The trophic role of glycolic acid in coastal seawater. I. Heterotrophic metabolism in seawater and bacterial cultures. *Mar. Biol.* 33, 175–183. doi: 10.1007/BF00390723
- Yoshizawa, S., Kumagai, Y., Kim, H., Ogura, Y., Hayashi, T., Iwasaki, W., et al. (2014). Functional characterization of flavobacteria rhodopsins

reveals a unique class of light-driven chloride pump in bacteria. *Proc. Natl. Acad. Sci. U.S.A.* 111, 6732–6737. doi: 10.1073/pnas.1403051111

Zigah, P. K., McNichol, L., Xu, C., Johnson, C. S., Karl, D. M., and Repeta, D. J. (2017). Allochthonous sources and dynamic cycling of oceanic dissolved organic carbon cycle revealed by carbon isotopes. *Geophys. Res. Lett.* 44, 2407–2415.

Ziolkowski, L. A., and Druffel, E. R. M. (2010). Aged black carbon identified in marine dissolved organic carbon. *Geophys. Res. Lett.* 37:L16601. doi: 10.1029/2010GL043963

Conflict of Interest Statement: The authors declare that the research was conducted in the absence of any commercial or financial relationships that could be construed as a potential conflict of interest.

Copyright © 2017 Casey, Ferrón and Karl. This is an open-access article distributed under the terms of the Creative Commons Attribution License (CC BY). The use, distribution or reproduction in other forums is permitted, provided the original author(s) or licensor are credited and that the original publication in this journal is cited, in accordance with accepted academic practice. No use, distribution or reproduction is permitted which does not comply with these terms.



ALOHA From the Edge: Reconciling Three Decades of *in Situ* Eulerian Observations and Geographic Variability in the North Pacific Subtropical Gyre

Maria T. Kavanaugh^{1*}, Matthew J. Church², Curtiss O. Davis¹, David M. Karl³, Ricardo M. Letelier¹ and Scott C. Doney⁴

¹ College of Earth, Ocean and Atmospheric Sciences, Oregon State University, Corvallis, OR, United States, ² Flathead Lake Biological Station, University of Montana, Polson, MT, United States, ³ Daniel K. Inouye Center for Microbial Oceanography: Research and Education (C-MORE), University of Hawaii at Manoa, Honolulu, HI, United States, ⁴ Department of Environmental Sciences, University of Virginia, Charlottesville, VA, United States

OPEN ACCESS

Edited by:

Alison Buchan,
University of Tennessee, Knoxville,
United States

Reviewed by:

Jeffrey Polovina,
National Oceanic and Atmospheric
Administration (NOAA), United States
Andrew Irwin,
Mount Allison University, Canada

*Correspondence:

Maria T. Kavanaugh
mkavanaugh@ceoas.oregonstate.edu

Specialty section:

This article was submitted to
Aquatic Microbiology,
a section of the journal
Frontiers in Marine Science

Received: 06 December 2017

Accepted: 28 March 2018

Published: 20 April 2018

Citation:

Kavanaugh MT, Church MJ,
Davis CO, Karl DM, Letelier RM and
Doney SC (2018) ALOHA From the
Edge: Reconciling Three Decades of
in Situ Eulerian Observations and
Geographic Variability in the North
Pacific Subtropical Gyre.
Front. Mar. Sci. 5:130.

doi: 10.3389/fmars.2018.00130

Global analyses of satellite and modeled data suggest decreased phytoplankton abundance and primary productivity in oligotrophic gyres as they expand in response to increased surface temperatures, shoaling of surface mixed layers, and decreased supply of subsurface macronutrients. However, analogous changes in the phytoplankton have not been evident *in situ* at Hawaii Ocean Time-series (HOT) Station ALOHA (22°45'N, 158°00'W), suggesting that physiological or structural reorganization not observed from space, uncorrected sensor drift, or uncharacterized geographic variability may be responsible for the apparent discrepancy. To address the latter, we compared interannual patterns of *in situ* phytoplankton dynamics and mixed layer properties to gyre extent and boundary location based on multiple definitions including dynamic topography, a threshold of satellite surface chlorophyll (chl a) $\leq 0.07 \text{ mg m}^{-3}$, and multivariate biophysical seascapes using modeled or satellite data. Secular increases in gyre extent were apparent, although the rate of expansion was much slower than previously reported, whereas strong interannual oscillations were evident for all definitions of the gyre. Modeled and satellite-based multivariate seascapes agreed well in terms of expansion (surface area of seascapes) and isolation of Station ALOHA (distance to seascape boundary) resulting in a combined data record of nearly three decades. Isolation was associated positively with the North Pacific Gyre Oscillation (NPGO), and negatively with Multivariate ENSO Index (MEI), and Pacific Decadal Oscillation (PDO). The converse was true for the gyre's expansion. Expansion followed a shoaling and freshening of the surface mixed layer and declines of *in situ* net primary production (PP) suggesting that Station ALOHA may serve as an early indicator of gyre biogeographic patterns. Lags between geographic indicators and *in situ* conditions appear to partially explain past observed discrepancies between patterns from satellite remote sensing and those from *in situ* conditions at Station ALOHA.

Keywords: climate oscillations, North Pacific Subtropical Gyre, dynamic geography, seascapes ecology, Station ALOHA

INTRODUCTION

Covering over 20 million square kilometers, the North Pacific Subtropical Gyre (NPSG) is the largest ecosystem on the planet surface (Sverdrup et al., 1942; Karl, 2010). The permanently stratified surface layer in this system restricts the vertical fluxes of inorganic nutrients into the well-lit surface region, resulting in low primary production (PP) and export of carbon to the deep ocean. However, because of their size, open ocean regions like the NPSG are responsible for substantial oceanic primary and export production (Martin et al., 1987; Emerson et al., 1997). The debate is ongoing, however, as to how these processes are changing in response to longer term shifts in environmental forcing such as changes in ocean chemistry (Dore et al., 2009) and temperature (Karl et al., 2001; Corno et al., 2007; Saba et al., 2010). Accurate estimation of global ocean production and export, therefore, will require not only reliable estimation of NPSG ecosystem processes (Karl, 2010) but also a detailed understanding of the oceanographic context in which these processes are occurring, including an accurate characterization of gyre geography and the dynamics of gyre areal extent and boundary location.

Because of their immense size and age, oligotrophic gyres have been considered historically to support pelagic ecosystems in a climax state relatively resulting from stable environmental forcing in space and time; however, they are now recognized to display substantial spatial, seasonal, and interannual variability (Venrick, 1995; Karl, 2010; Karl and Church, 2017). While dominated by small phytoplankton and regenerated productivity (Letelier et al., 1996; Li et al., 2011), relatively short-lived perturbations in the NPSG contribute not only to momentary increases in net primary productivity (NPP) but also to the decoupling of autotrophic and heterotrophic processes and subsequent export of particulate carbon. These include deep vertical mixing events followed by water column restratification (DiTullio and Laws, 1991) associated with the passage of cyclonic eddies (Letelier et al., 2000; Wilson and Adamec, 2001), Rossby waves (Sakamoto et al., 2004), and the breaking of internal waves. On longer time scales, *in situ* PP and phytoplankton biomass (as determined by chlorophyll chl *a*) in the NPSG, measured during various programs such as CLIMAX and the Hawaii Ocean Time-series (HOT) have increased over the past four decades (Venrick et al., 1987; Karl et al., 2001; Corno et al., 2007). These increases have been linked to a shift in the phase of the Pacific Decadal Oscillation (PDO, Karl et al., 2001) or El Niño Southern Oscillation (ENSO)/PDO interactions (Corno et al., 2007) and resulting changes in stratification.

Station ALOHA (22.75°N, 158°W: A Long-term Oligotrophic Habitat Assessment) is a benchmark monitoring site in the NPSG where *in situ* sampling of ocean physical, biological, and chemical parameters has occurred since 1988 (Karl, 2010). However, the patterns of increased biomass and primary productivity found *in situ* are contrary to synoptic patterns observed through analyses of derived satellite products. Behrenfeld et al. (2006) observed that global ocean net PP and phytoplankton biomass (as defined by chl *a*) decreased from 1999 to 2006 in response to increased water column stratification. Hypothesized as an ecological response to an increase in the multivariate ENSO

index, the chl *a* trend was largely driven by changes in the subtropical gyres. Both Polovina et al. (2008) and Irwin and Oliver (2009) noted ENSO or PDO-associated increases in the areal extent of the most oligotrophic water in subtropical gyres. Finally, recent analyses of ocean color data from 1997 to 2010 and 1997 to 2013 suggest gradual, yet significant, decreases in surface chl *a* in subjectively defined polygons that encompassed the oligotrophic regions of the North Pacific as well as other basins (Signorini and McClain, 2012; Signorini et al., 2015). Conversely, Siegel et al. (2013) argue that the tropical/sub-tropical negative correlation between satellite chl *a* and sea surface temperature (SST) is primarily a physiological signal of variable chl *a* to carbon (C) ratio rather than a phytoplankton biomass signal, likely associated with photoacclimation (Letelier et al., 1993, 2017; Winn et al., 1993). While some analyses of long-term *in situ* data support the trend toward oligotrophy found in early large-scale studies (Boyce et al., 2010, 2011, 2014), the majority of *in situ* time series do not (Chavez et al., 2011; McQuatters-Gollop et al., 2011).

Contrary findings between gyre-scale and *in situ* analyses, attribution of change to differing climate modes, and the variations in the shape and extent of the gyre suggest that regional oceanographic context needs to be considered when examining the role of interannual variability and secular trends on large scale shifts in the subtropical gyres (e.g., Hammond et al., 2017). One such regional approach considers the temporal patterns of features as a composite of biophysical interactions (Oliver and Irwin, 2008; Kavanaugh et al., 2014b, 2016). Seasonally evolving satellite-derived seascapes describe regional variability in the North Pacific with differences in biogeochemical interactions (Kavanaugh et al., 2014b), and community structure (Kavanaugh et al., 2014a). Here, we use interannual varying seascapes to further our understanding of subtropical gyre dynamics and compare seascape variability relative to circulation-based or low-level chl *a*-based definitions of the gyre. We hypothesized that year-to-year variability in the size of the subtropical gyre and location of the gyre boundary is reflected in the patterns of phytoplankton abundance and productivity at Station ALOHA. The location of Station ALOHA is highlighted, with trends and oscillations of seascape area and isolation compared across definitions and analyzed in concert with *in situ* patterns. Specifically, we address the following questions:

1. What are the interannual trends across different metrics of gyre expansion?
2. To what degree are variations in subtropical seascape geography related to interannual to decadal climate modes?
3. Finally, how do variations in seascape geography relate to the interannual patterns of phytoplankton abundance and primary productivity observed at Station ALOHA?

METHODS

Oligotrophic Chl *a* Gyre Extent

Area of the extent of highly oligotrophic gyre (a threshold defined as chl *a* $\leq 0.07 \text{ mg m}^{-3}$; Polovina et al., 2008, hereafter oligotrophic threshold chl *a*) was calculated from monthly

SeaWiFS (R2017, completed January 2018) and Aqua-MODIS (R2017, completed December 2017) satellite ocean color derived chl *a* (**Figure 1A**). The SeaWiFS data record extends from autumn of 1997–2010 albeit with episodic gaps during 2008–2010 due to periodic sensor malfunction. Reprocessing (Franz et al., 2007; Franz, 2009) has removed much of the drift in the SeaWiFS and Aqua-MODIS instruments. Data were merged by comparing the per pixel seasonal cycle of SeaWiFS to that of MODIS-Aqua from 2003 to 2007, and then applying a seasonal correction to the historical SeaWiFS record. Merged data include seasonally adjusted SeaWiFS data until July of 2002, after which MODIS-Aqua data were used to December 2016. We also compared the trends between the OCI algorithm (Hu et al., 2012) to that of the previously standard OC3/OC4 (OCX) algorithms for SeaWiFS and MODIS-Aqua. The OCI algorithm is more accurate for [chl *a*] < 0.2 mg m⁻³, converges with the OCX values above 0.2 mg m⁻³, and has been the standard NASA chl *a* algorithm since 2014.

Circulation-Based Gyre Extent and Eddy Kinetic Energy

Near daily, gridded sea level anomalies (SLA) and absolute dynamic topography (ADT) fields derived from satellite altimetry were downloaded from AVISO (<https://www.aviso.altimetry.fr/en/data/products.html>). Eddy kinetic energy (EKE) was calculated from the near daily fields:

$$\text{EKE (m}^2 \text{s}^{-2}\text{)} = 0.5 \times [\text{u}^2 + \text{v}^2] \quad (1)$$

where *u* and *v* are the zonal and meridional velocities calculated from sea surface height anomalies. Monthly means of each field were calculated.

Because the determination of extent of features estimated from geostrophic flow lines can be confounded by the effect of steric sea level rise on ADT (Gille, 2014), we downloaded steric sea level anomalies (Levitus et al., 2012) for the upper 2,000 m from NOAA's National Center for Environmental Information (https://www.nodc.noaa.gov/OC5/3M_HEAT_CONTENT/index.html), and calculated the trend in steric sea-level rise from 1993 to 2015 on a per pixel basis. Dynamic height was adjusted by subtracting the interpolated steric sea-level trend from the monthly satellite dynamic height field. The gyre was then classified as the region contained within closing contours of original ADT and adjusted ADT (ADT_{adj}) at 1.05 m, the minimum height at which the contour lines recirculated (closed) completely to the western boundary (**Figure 1B**).

Seascape Classification

Seascapes were classified from Level 3 9-km merged chl *a* (described above), PAR, and SST from the Advanced Very High Resolution Radiometer (AVHRR) and MODIS-Aqua. Similar to chl *a*, monthly averages of PAR and SST were computed from the combined SeaWiFS and MODIS product; all three variables were binned to 1 degree to match model output. Model output of SST, PAR, and surface chl *a* from 1985 to 2005 were taken from the Biogeochemical Element Cycling Model embedded

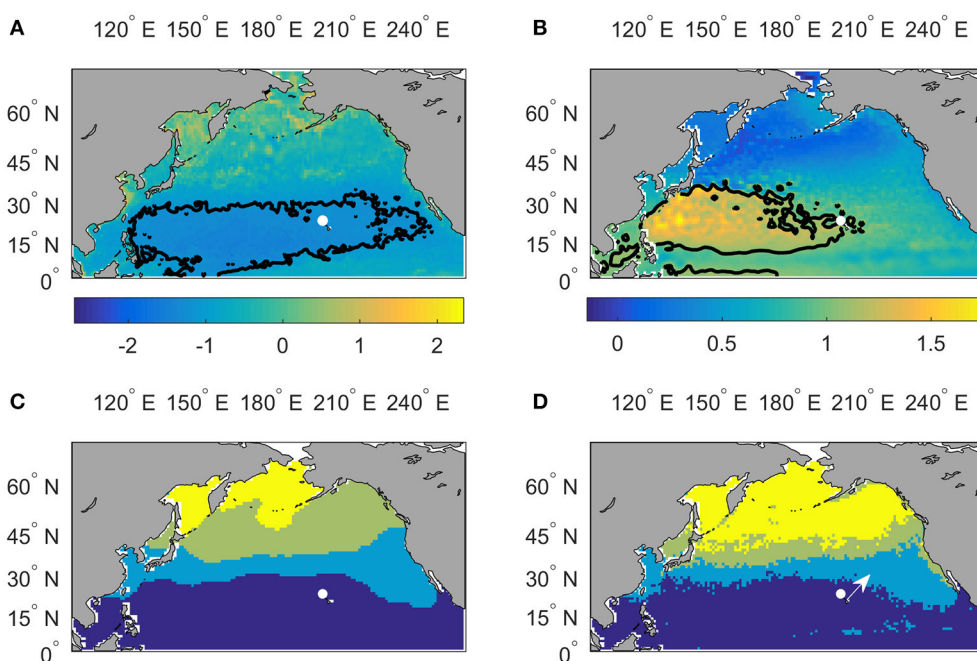


FIGURE 1 | Extent of the North Pacific Subtropical Gyre (NPSG) for June of 2003, showing **(A)** oligotrophic threshold ($\leq 0.07 \text{ mg m}^{-3}$) satellite ocean color derived surface chlorophyll, chl *a*; **(B)** geostrophic recirculation defined by the 1.05 m absolute dynamic height relative to the geoid; and multivariate seascapes classified from **(C)** CESM-BEC model output and **(D)** satellite data. Dark blue, subtropical seascapes; light blue, oligotrophic boundary seascapes; green, transition seascapes; yellow, subarctic seascapes. Arrow in **(D)** shows distance between Station ALOHA (white circle) and the boundary of the subtropical seascapes.

in the Community Earth System Model (CESM-BEC, Doney et al., 2009; Moore et al., 2013). Surface chl *a* concentration is sensitive to mixed layer depth in the subtropics (e.g., Letelier et al., 1996; Siegel et al., 2013); thus we chose the CESM-BEC because of its inclusion of photoacclimation. While this does not isolate the effect of photoacclimation, it assures that modeled chl *a* and satellite chl *a* are responding similarly to physical forcing, reflecting the phytoplankton physiological responses observed at Station ALOHA. All data sets were standardized prior to classification. Satellite and model seascapes were classified separately (**Figures 1C,D**).

Climatological seasonal means of PAR, SST, and chl *a* were defined for both data sets from 2003 to 2007. We used a probabilistic self-organizing mapping algorithm (PrSOM, Anouar et al., 1998) to reduce the 3-variable (SST_{x,y,m}, PAR_{x,y}, chl *a* _{x,y,m}) spatiotemporal data set onto a 15 × 15 neuronal map resulting in 225 classes, each with its own 3-D weight based on the maximum likelihood estimation (3-D MLEs). The neural net size (15 × 15 nodes) was chosen to maximize sensitivity to mesoscale processes while preventing underpopulated nodes (defined as <500 pixels). The 3-D MLEs were then further reduced using a hierarchical agglomerative clustering (HAC) with Ward linkages (Ward, 1963). This linkage method uses combinatorial, Euclidian distances that conserve the original data space with sequential linkages (McCune et al., 2002). Euclidian distances here are equivalent to within-group and total sum of squares.

Previously, we found that eight seascapes classified from seasonal climatologies of satellite-derived SST, chl *a*, and PAR represented seasonal shifts in biogeochemical patterns and planktonic assemblages (Kavanaugh et al., 2014a,b). Here, we followed the methodology of Kavanaugh et al. (2014b), with three exceptions. First, the seasonal variability of PAR was removed on a per-pixel basis to minimize discontinuities associated with the spring and fall transitions, with interannual and spatial variability remaining. Second, stepwise agglomerations were conducted using the Ward method until four seascapes for each of the model and satellite data sets were defined: a subtropical seashape, oligotrophic transition, a mesotrophic transition, and a subarctic seashape. These four regions bear the spatial signature of analogous seasonally evolving regions classified previously (Kavanaugh et al., 2014b) and represent a trade-off between variance explained in both the satellite and model records, and spatial match-up between satellite and modeled seascapes (**Figure S1**). Finally, once the seasonal and spatial vectors were classified, the means, variances and covariances within seascapes informed a multivariate Gaussian mixture model (GMM). Class assignments of individual months were then determined by their maximum posterior probabilities. New classes were then predicted from the CESM and satellite GMMs using the monthly means of chl *a*, SST, and PAR of the respective model and satellite time series.

Geographic Metrics

We focus on the dynamics of the subtropical seashape and the boundary between the subtropical and oligotrophic transition seashape. Total area of oligotrophy, recirculation, and multivariate subtropical seashape was assigned based on the

sum of the area of all pixels within the appropriate contour or identified seashape in the North Pacific. Surface area of each pixel was calculated by correcting for the spheroid-effect on distance between lines of longitude. For each time step, the distance from Station ALOHA to the subtropical seashape boundary was also calculated using the mean of the 5th quantile of all boundary distances in a quadrant 45° on either side of due NE from Station ALOHA (**Figure 1D**); encroachment of less oligotrophic waters from the NE was most common. When the oligotrophic boundary encroached beyond (south and/or east of) Station ALOHA, the distance values were negative. All area-based analyses were truncated at 10°N to minimize the effect of the equatorial upwelling region.

To understand the role of mesoscale variability on basin-scale geography, we examined the relationship between mean EKE and the difference in extent between the gyre defined by circulation and that defined by oligotrophy (see above). Pixels were categorized as belonging in (1) both the oligotrophic and physical gyres, (2) only in the physical gyre, or (3) only in the oligotrophic gyre. The mean EKE was calculated over the pixels for each of the three aforementioned groups.

Climatic Indices

To infer the effect of climatic forcing on the interannual dynamics of gyre geography, three different indices were used. The multivariate El Niño Southern Oscillation Index (MEI) is computed from a principal component analysis (PCA) of six variables including sea level pressure, zonal and meridional wind components, cloudiness, and sea surface and air temperatures (Wolter and Timlin, 1993). These data are available from NOAA (<http://www.esrl.noaa.gov/psd/enso/mei/>). The North Pacific Gyre Oscillation (NPGO, Di Lorenzo et al., 2008; <http://www.3d.org/npgc/>) is the second dominant mode calculated from North Pacific sea surface height anomalies and is associated with accelerated North Pacific, Alaska, and California Currents (Chavez et al., 2011). The Pacific Decadal Oscillation (PDO, Mantua et al., 1997; Zhang et al., 1997) is associated with the dominant mode of North Pacific SST anomalies and the data are available from the University of Washington (<http://jisao.washington.edu/pdo/>).

Station ALOHA Data

In situ NPP, Total chl *a* (Tchl *a*), the sum of divinyl and monovinyl chl *a*), and *in situ* physical patterns in the subtropical North Pacific were assessed using archived data from Station ALOHA (<http://hahana.soest.hawaii.edu/hot/hot-dogs/interface.html>). Net PP was determined by daytime incubation in bottles spiked with ¹⁴C bicarbonate incubated *in situ* to maintain natural light and temperature (Letelier et al., 1996). Chl *a* and photosynthetic accessory pigments were measured by high performance liquid chromatography (HPLC) according to Wright et al. (1991). Mean pigment concentrations and NPP patterns were quantified separately for the light-saturated surface (0–45 m) and light-limited region of the euphotic zone that contained the deep chlorophyll maximum (DCM, 75–150 m). Potential temperature and bottle salinity were also recorded for the upper 45 m. Mixed layer depth was calculated using

a potential density gradient threshold of 0.005 kg m^{-4} and a potential density offset of 0.125 kg m^{-3} from the surface (Karl and Lukas, 1996).

Statistical Analysis

Cross correlation analyses were conducted to determine the correlations between climate and geographic metrics, the relationship between seascape dynamics and *in situ* conditions at Station ALOHA, and the time scales or lags at which the correlation was strongest. Cross correlation analysis was also conducted to determine the effect of EKE on spatial mismatch between geographic metrics. Prior to analysis, monthly climatological means were calculated by removing outliers (exceeding ± 3 standard deviations), then missing *in situ* data were interpolated using a 3-month LOESS filter to minimize the effect of within-year data density on interannual trends. Then, anomalies for each time series were calculated by subtracting the monthly climatological mean, calculated from the smoothed data, and then smoothing with a 12-month LOESS filter prior to correlation analysis. Statistical significance of correlation coefficients were determined using a critical value which adjusted degrees of freedom to account for autocorrelation in covariance (Glover et al., 2011). Correlations that exceeded this value are considered significant ($p < 0.05$).

Trends over time were adjusted to account for the effect of climate oscillations. We conducted a PCA across the NPGO, PDO, and MEI indices; multiple linear regression was conducted using the PCA scores as predictors and individual seasonally-detrended anomalies as responses. Trends were then a result of a simple linear fit to the residuals of the multiple linear regression model.

RESULTS

Climate Variability

From 1985 to 2016, three to four cycles of the NPGO, MEI, and PDO were evident (Figure 2). In the early part of the record (1985–1998), the PDO and MEI were out of phase but moved into phase following the 1997–1998 El Niño and subsequent La Niña, remaining in phase for the rest of the data record ($r = 0.6, p < 0.001$). Throughout our study period, the NPGO was anticorrelated ($r = -0.5, p < 0.001$) with the other two indices, but also led the PDO and MEI by 5 and 8 months, respectively (Figure S2). Thus, any secular trend reported is that which remains after accounting for the effect of oscillations in the sign and magnitude of the climate indicators.

Expansion and Isolation Trends and Drivers

Patterns and trends among the different gyre geographic metrics varied and were associated with different climate forcing. The area of low-level chl *a* was dependent on algorithm, with the lower sensitivity of the OCX resulting in a larger expanse of oligotrophy (Figure 3A, Table 1). Large interannual oscillations were evident, with any linear trend being highly dependent on record length (Table S1). From 1998 to 2016, expansion of the area of low-level chl *a* occurred at a rate of $0.36\% \text{ year}^{-1}$

(Table 1). Seasonal and interannual oscillations as well as weak increases (0.5% per year) in the physical extent of the gyre were evident from the altimetry-based time series (Figure 3B, Table 1). Trends were weaker in data adjusted for steric sea-level changes than those unadjusted for absolute dynamic height (ADT_adj and ADT, respectively, Table S1). As with the extent of oligotrophy, presence or magnitude of a trend depended on the length of the time series, with no trend evident from 1998 to 2006 (Figure 3B, Table S1), despite the strong ENSO signal during that span. Because modeled and satellite seascapes were highly correlated and in phase for both indices (Figures S1B,C; expansion: $r = 0.64, p < 0.05$; isolation $r = 0.76, p < 0.05$), the data records were combined and a single index of expansion or isolation was used that spanned the entire data record (1985–2016). There was evidence of slight expansion of the subtropical seascape from 1985 to 2016 (Table 1). Isolation distance also varied from year to year, although aseasonal, within-year variability was higher relative to the other metrics (Figure 3D). A linear trend was evident from 1985 to 2016 (but not over a shorter duration), with isolation distance increasing by 0.9% per year (Table 1).

Gyre extent, defined by oligotrophic threshold chl *a*, was positively correlated to the MEI, with positive MEI preceding expansion of low-level chl *a* area by 6–12 months (Figure 4A). The areal extent of recirculation was positively correlated with the NPGO and strongly negatively correlated with the PDO and MEI (Figure 4B). Similar to the area of low-level chl *a*, the subtropical seascape was strongly correlated to the MEI and was also related to the PDO (Figure 4C), whereas the isolation of Station ALOHA within the subtropical gyre was positively correlated with the NPGO and negatively correlated with the MEI and PDO (Figure 4D). While covering a much larger area, areal extent of multivariate seascapes was weakly correlated to that of threshold chl *a* patterns, (Figure S3A: $r = 0.24, p < 0.05$); however, patterns preceded the chl-only index by approximately 7 months. Multivariate seascape expansion was anti-correlated to both the dynamic topography extent described above ($r = -0.48, p < 0.05$), and the distance of Station ALOHA to the edge of the subtropical seascape (Figure S3B: $r = -0.36, p < 0.05$). Isolation distance was positively correlated to gyre extent as measured by geostrophy ($r = 0.33, p < 0.05$), with isolation shifts preceding that of gyre extent also by 7 months. Isolation was not correlated to the low-level chl *a* metric.

The NPSG is most contracted in winter and at its greatest extent in September for both definitions of the gyre (Figures 5A,B). The northern winter boundary of the physical gyre exceeds that of low-level chl *a*, and the summer eastern boundary extends less than the low-level chl-a. However, on interannual scales, the physical extent and low-level chl *a*-based extent were anti-correlated, due to different climate forcing. The physical extent is strongly positively correlated with the NPGO, whereas the extent of low-level chl *a* is positively correlated with the PDO and MEI. Increased EKE resulted in expansion of the areal extent of oligotrophic-threshold chl *a*. The result is that off of the Kuroshio, the spatial mismatch between the two definitions is minimized with increased EKE between their boundaries (Figure 5C),

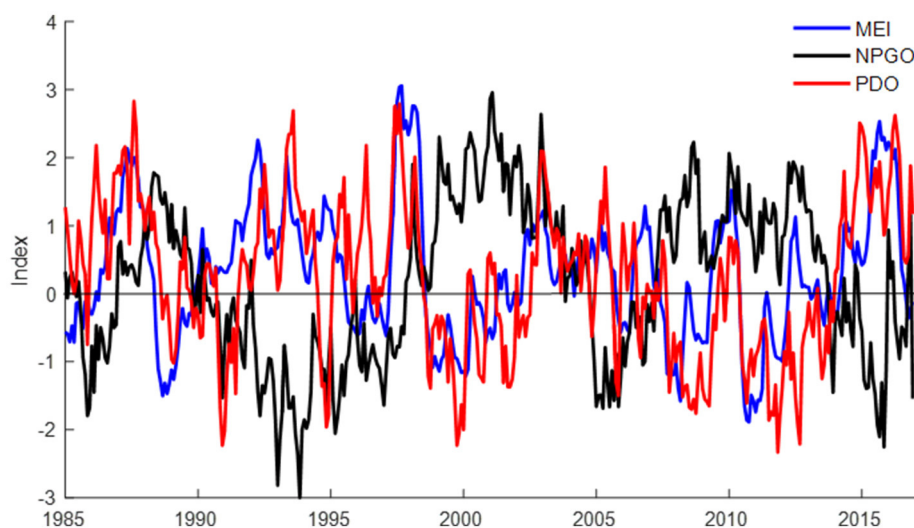


FIGURE 2 | Time series of climate indices including (a) the North Pacific Gyre Oscillation, NPGO; (b) the Multivariate ENSO Index, MEI; and (c) the Pacific Decadal Oscillation, PDO. Data sources are included in Methods. All series were smoothed using a 12-month LOESS filter.

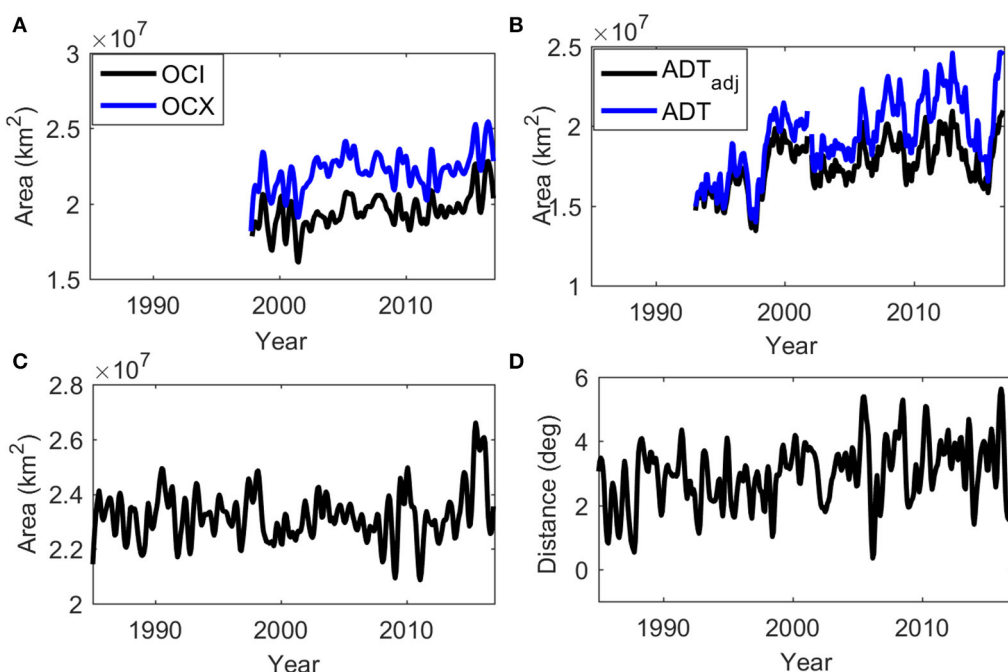


FIGURE 3 | Temporal trends of North Pacific subtropical gyre dynamic geography indices showing (A) areal extent calculated from oligotrophic threshold chl *a* across different satellite ocean color algorithms; (B) areal extent (expansion/contraction) calculated from satellite altimetry derived dynamic topography with and without adjustment for steric sea-level rise; (C) merged model and satellite seascape extent; (D) distance of Station ALOHA to the edge of the merged modeled and satellite subtropical seascape (isolation). All series were smoothed using a 12-month LOESS filter. Trends calculated over various durations are reported in **Table 1** and **Table S1**.

where instabilities associated with the Kuroshio extension appeared to blend the physical and chl *a*-based boundaries. On the eastern and southern edge, the spatial mismatch increases with increased EKE (**Figure 5D**), where expanded oligotrophy is associated with greater EKE, particularly in summer.

In Situ Trends

Local SST averaged over the upper 45 m at Station ALOHA exhibited strong oscillations in response to changing climate forcing over the data record, with warmer temperatures associated with positive ENSO and PDO and negative NPGO (**Figure 6A, Figure S4**). While there was a significant linear

TABLE 1 | Secular trends across geographic metrics, chl *a* algorithms, and *in situ* characteristics at Station ALOHA.

Algorithm	Span	Span mean	Trend (year ⁻¹)	Trend (SE)	% change year ⁻¹	R ²	p-Value
AREA METRICS (km²)							
ocx: chl <i>a</i> $\leq 0.07 \text{ mg m}^{-3}$	1998–2016	2.23E+007	4.87E+04	1.39E+04	0.220	0.05	<0.001
oci: chl <i>a</i> $\leq 0.07 \text{ mg m}^{-3}$	1998–2016	1.95E+007	7.00E+04	1.36E+04	0.360	0.11	<0.001
ADT_adj	1993–2016	1.76E+007	8.66E+04	1.11E+04	0.491	0.42	<0.001
ADT_adj	1998–2016	1.76E+007	8.48E+04	1.08E+04	0.481	0.27	<0.001
Subtropical Seascape	1985–2016	2.32E+007	1.64E+04	6.03E+03	0.071	0.02	<0.01
DISTANCE METRICS (km)							
Station ALOHA to SS edge	1985–2016	3.28E+02	3.20E+00	8.90E-01	0.970	0.04	<0.001
STATION ALOHA							
SST (°C)	1989–2016	24.8	0.013	0.004	0.052	0.04	<0.01
SSS (psu)	1989–2016	35.1	0.008	0.001	0.023	0.14	<0.001
MLD (surface offset, m)	1989–2016	58.7	0.29	0.13	0.494	0.02	0.02
MLD (gradient threshold, m)	1989–2016	32.5	0.14	0.11	0.431	0	0.2
[chl <i>a</i>]: 0–45 m (mg chl <i>a</i> m ⁻³)	1989–2016	0.09	0	0	0.000	0	0.72
[chl <i>a</i>]: 75–150 m (mg chl <i>a</i> m ⁻³)	1989–2016	0.17	0.001	0.0002	0.588	0.06	<0.001
NPP: 0–45 m (mg C m ⁻³ d ⁻¹)	1989–2016	6.07	0.053	0.01	0.873	0.08	<0.001
NPP: 75–150 m (mg C m ⁻³ d ⁻¹)	1989–2016	1.13	0.045	0.004	3.982	0.34	<0.001
NPP: Int to 150 m (mg C m ⁻² d ⁻¹)	1989–2016	513	5.63	0.85	1.097	0.18	<0.001

Italicized values denote no significant trend over the duration measured. Signatures of the NPGO, PDO, and MEI have been removed from each time series prior to analysis (see section Methods).

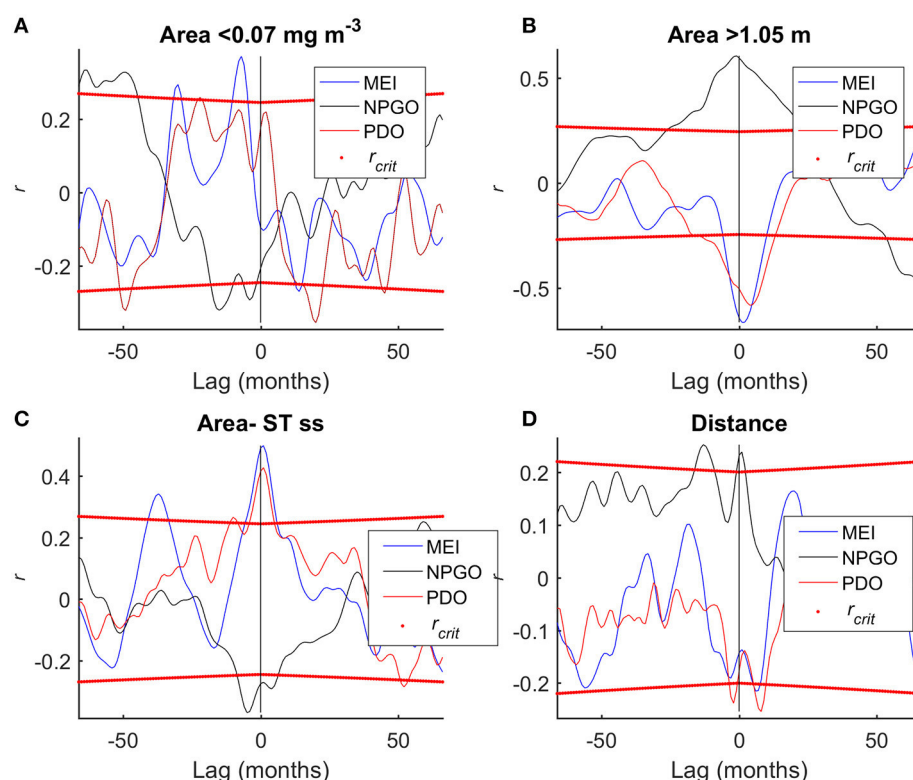


FIGURE 4 | Lagged correlations between climate indices and dynamic geography indices of the North Pacific Subtropical Gyre. Where lag is negative, climate index leads geographic metric; the converse is true for positive lags. Correlations are significant when they exceed the critical value (dotted red lines). **(A)** Gyre area defined by chl *a* $\leq 0.07 \text{ mg m}^{-3}$. **(B)** Gyre area defined by closing contour of dynamic height (1.05 m). **(C)** Gyre area defined by the extent of the multivariate subtropical seascape. **(D)** Distance from Station ALOHA to the edge of the subtropical seascape.

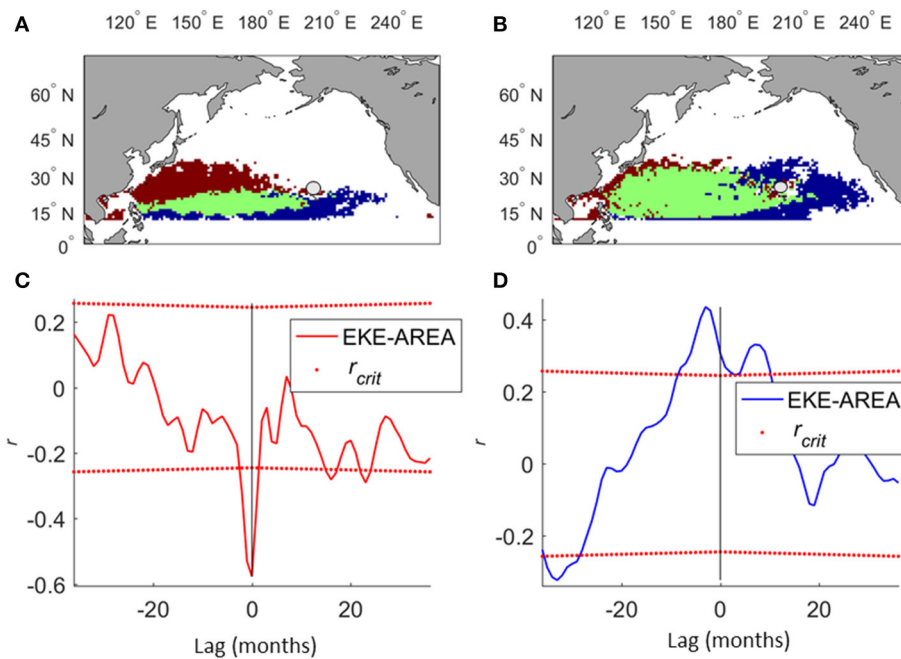


FIGURE 5 | Drivers of spatiotemporal differences in gyre extent based on dynamic height and oligotrophic threshold chl *a*. **(A)** Extent of gyre in February 2003 showing topographic (red) and pigment (blue)-based extents and region of overlap (green). **(B)** Same as **(A)**, but for September 2003. **(C)** Cross correlation of mean eddy kinetic energy (EKE) in region represented solely by the physical definition with areal extent of that region. **(D)** Same as **(C)**, but in extents solely represented by oligotrophic threshold chl *a*.

trend from 1989 to 2016 (**Table 1**: $0.010 \pm 0.004^{\circ}\text{C year}^{-1}$, $p < 0.01$), it was very weak ($R^2 = 0.04$). Sea surface salinity exhibited large oscillations in the opposite direction of SST and also a relatively strong increasing trend over the data record ($0.008 \pm 0.001 \text{ psu year}^{-1}$, $p < 0.001$, $R^2 = 0.18$; **Figure 6B**). Mixed layer depth had large interannual variability over the data record, but also oscillated in response to changing surface salinity and temperature. A weak linear increase was apparent over the data record for mixed layer calculated via the surface offset method ($0.29 \pm 0.13 \text{ m year}^{-1}$, $p = 0.02$, $R^2 = 0.02$; **Figure 6D**), although none was apparent with the mixed layer depth calculated via the gradient method (**Figure 6C**, **Table 1**).

With the exception of isolated events (e.g., early 2001), seasonal patterns of T-chl *a* in the surface and at depth were out of phase (**Figure 7A**). Concentrations in the light-limited euphotic zone were approximately double that of the surface, and also increased over the data record (**Table 1**: $0.001 \pm 0.0002 \text{ mg chl } a \text{ m}^{-3} \text{ year}^{-1}$, $p < 0.001$, $R^2 = 0.08$). No analogous trend was evident in surface chlorophyll.

NPP increased over the data record in both the surface and at depth (**Figure 7B**, **Table 1**). Mean rates in the surface were $\sim 4x$ higher than that in the 75–150 m depth bin (**Table 1**: $5.7 \text{ mg C m}^{-3} \text{ d}^{-1}$ vs. $1.2 \text{ mg C m}^{-3} \text{ d}^{-1}$). However, the relative rate of increase in NPP over time was stronger in the light limited euphotic zone vs. the surface (**Table 1**: surface $\sim 1\% \text{ year}^{-1}$, trend $= 0.053 \pm 0.010 \text{ mg C m}^{-3} \text{ d}^{-1} \text{ year}^{-1}$, $p < 0.001$, $R^2 = 0.09$; At depth $\sim 3\% \text{ year}^{-1}$, trend $= 0.045 \pm 0.004 \text{ mg C m}^{-3} \text{ d}^{-1} \text{ year}^{-1}$,

$p < 0.001$, $R^2 = 0.34$). Together, these trends contributed to a relatively strong linear increase in NPP integrated over 150 m (**Figure 7C**, $5.63 \pm 0.85 \text{ mg C m}^{-2} \text{ d}^{-1} \text{ year}^{-1}$, $p < 0.001$, $R^2 = 0.18$). Oscillations were also evident in both chl *a* and NPP time series.

Correlation of Seascape Geography With *in Situ* Physics and Biology

Increased mixed layer depth followed isolation of Station ALOHA (**Figure 8A**, $r = 0.32$, $p < 0.05$) and preceded a contracted subtropical seascape (**Figure 8B**, $r = -0.32$, $p < 0.05$) by ~ 6 months. Salinity was positively associated with isolation but at longer lags ($r = 0.28\text{--}0.32$, lags > 20 months) and negatively associated with, but preceding expansion of the subtropical seascape ($r = -0.35$, $p < 0.05$, ~ 1 year). SST was positively associated with subtropical seascape expansion (**Figure 8B**), but preceded expansion by ~ 1 year ($r = 0.3$, $p < 0.05$). These patterns generally followed what would be expected by the climate forcing of geography (**Figure 4**, **Figure S4**) with SST at Station ALOHA positively correlated with the PDO and MEI (and negatively with the NPGO), and surface salinity and mixed layer depth positively correlated with the NPGO (and negatively correlated with the PDO and MEI) (**Figure S4**). Time lags and wavelengths were much longer and broader when considering climate indices directly, rather than their geographic signatures.

Station ALOHA T chl *a* and NPP were also correlated to gyre geography following local physical forcing. Isolation was

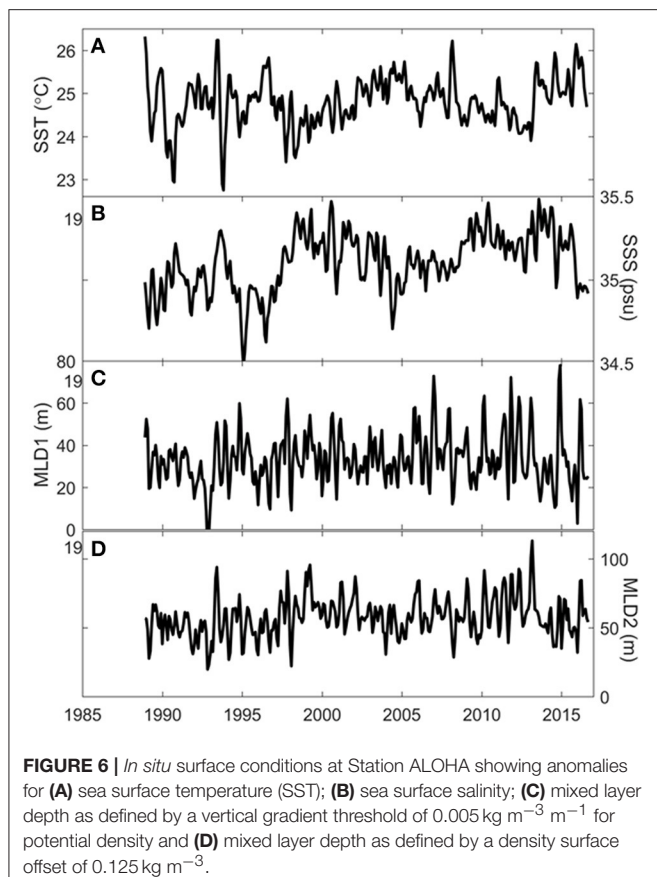


FIGURE 6 | *In situ* surface conditions at Station ALOHA showing anomalies for (A) sea surface temperature (SST); (B) sea surface salinity; (C) mixed layer depth as defined by a vertical gradient threshold of $0.005 \text{ kg m}^{-3} \text{ m}^{-1}$ for potential density and (D) mixed layer depth as defined by a density surface offset of 0.125 kg m^{-3} .

associated with increased chl *a* in the surface (Figure 8C, $r = 0.32$, $p < 0.05$), and increased surface and integrated NPP (Figure 8E, $r = 0.32$ to 0.4 , $p < 0.05$) followed isolation by ~ 5 months. Decreased Tchl *a* at depth was strongly associated with expansion of the subtropical seascape (Figure 8D: $r = -0.41$, $p < 0.05$) as was decreased NPP throughout the water column (Figure 8F: $r = -0.28$ to -0.39 , $p < 0.05$).

DISCUSSION

Where satellite metrics have suggested that oligotrophic systems such as the NPSG will expand in response to warming oceans (Behrenfeld et al., 2006; Polovina et al., 2008; Irwin and Oliver, 2009), analogous changes have not been evident at Station ALOHA (Corno et al., 2007) or the Bermuda Atlantic Time-series Station BATS in the subtropical North Atlantic (Lomas et al., 2010). This suggests that there may be physiological or structural reorganization not observed from space, uncharacterized spatiotemporal variability, or satellite sensor drift. We examined the geographic dynamics of the NPSG, the role of climate forcing on those dynamics, and the relationships between shifting gyre geography and local *in situ* conditions at the long-term time-series station, Station ALOHA over a 31-year data record. While weak secular trends in the expansion of different metrics of the subtropical

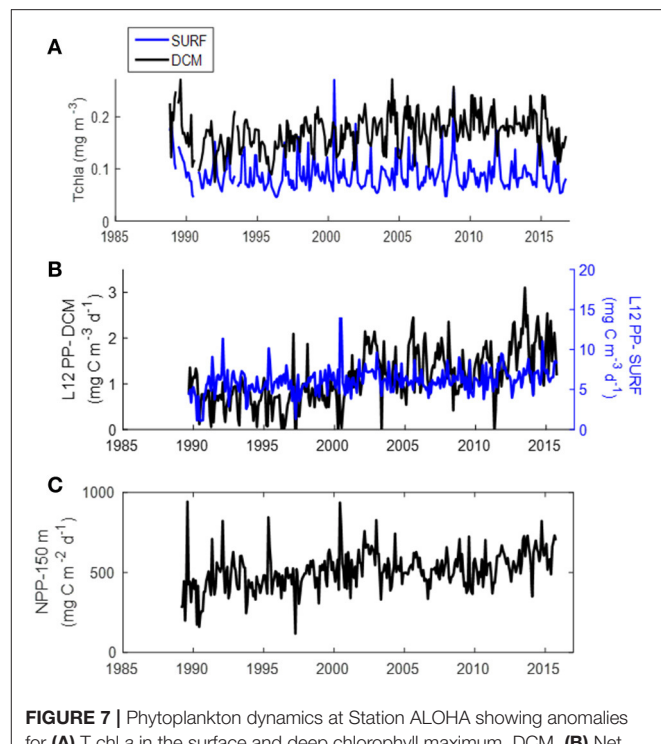


FIGURE 7 | Phytoplankton dynamics at Station ALOHA showing anomalies for (A) Tchl *a* in the surface and deep chlorophyll maximum, DCM, (B) Net primary productivity in the surface (0–45 m) and depth (75–150 m) as calculated from daytime incubations, and (C) vertically integrated NPP from 0 to 150 m.

gyre were evident, they were dominated by large oscillations, correlated with changes in ENSO and PDO conditions as well as the NPGO. With oscillations, we observe that *in situ* biophysical conditions at Station ALOHA are congruent to what would be predicted during periods of expanded oligotrophy via an expanded subtropical seascape including warmer SST and declines in Tchl *a* and NPP. We also observe that conditions at Station ALOHA shift prior to multivariate seascape expansion, suggesting that Station ALOHA may serve as a leading indicator for changes throughout the North Pacific subtropical region.

The location of Station ALOHA at the edge of the subtropics (this study) and other pivot points of climate forcing (Chavez et al., 2011; Messié and Chavez, 2011) may result in different climate effects depending on the interaction of multiple climate modes. During positive ENSO phases, water column stabilization restricts upward mixing of new nitrate and selects for organisms that can fix atmospheric nitrogen (Karl et al., 1995, 2001; Campbell et al., 1997). During positive PDO, the Aleutian Low is further south and leads to a southern anomaly in the transition zone chlorophyll front and potentially higher than average primary productivity in the subtropics (Chai et al., 2003). Positive NPGO periods are associated with more northward Aleutian Lows (Chavez et al., 2011) along with stronger North Pacific and California currents, higher pressure and deeper thermocline depths at the center of the subtropics (Di Lorenzo et al., 2008, 2009), potentially leading to decreased access to

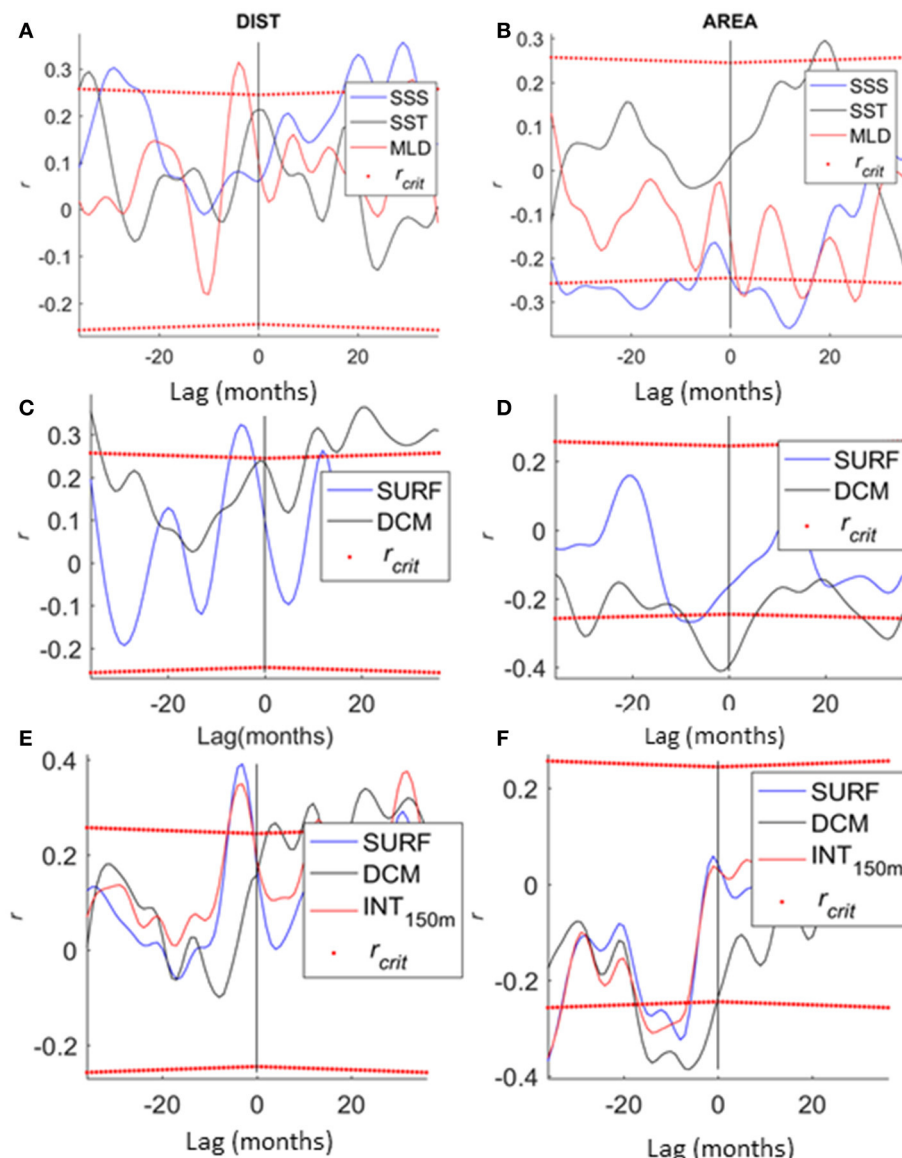


FIGURE 8 | Correlation between *in situ* biophysical variables at Station ALOHA and isolation of Station ALOHA (DIST) and expansion of subtropical seascape (AREA). **(A,B)** SST, mixed layer depth, and salinity; **(C,D)** Tchl a in the surface and DCM; **(E,F)** NPP in surface, DCM, and integrated over the upper 150 m. Geographic metrics lead biophysical variables when lag is negative.

deep nutrients in the interior of the gyre. However we found that positive phases of the NPGO were associated with increased mixed layer depth, salinity, and isolation of Station ALOHA which preceded increased T chl *a* and NPP. Conversely, the subtropical seascape (as well as the extent of oligotrophy defined solely by the threshold chl *a*) were associated with positive phases of the MEI and PDO, a shoaling and freshening mixed layer, and declines in T chl *a* and NPP at Station ALOHA. Thus while a stronger gyre may result in decreased access to nutrients at the center of the gyre (Di Lorenzo et al., 2008), the positive NPGO may result in increased access to nutrients at the edge. Furthermore, changes of biological and physical properties at

Station ALOHA tend to precede expansion by a few months. Thus, despite its location on the northeastern edge of the NPSG, or perhaps because of it, the time-series station provides an early indication of biogeographic conditions of the gyre as a whole.

The expansion of the topography-defined gyre positively correlated with the NPGO, and negatively correlated with MEI, PDO, and the gyre defined by the $0.07 \text{ mg chl } a \text{ m}^{-3}$ threshold. Isolation of Station ALOHA (the distance to the NE boundary of the most oligotrophic seascape) also was related to the NPGO (was positively correlated but led geostrophic expansion by 7 months) and exhibited a weak trend toward increased isolation

over the duration of the study. During positive NPGO conditions, transport through the North Pacific and California currents is stronger (Di Lorenzo et al., 2008), and meanders of the southern edge of the North Pacific Current-California current bifurcation may be reduced leading to the associated increase in isolation of Station ALOHA within the northeast corner of the subtropical seascape.

Eddy kinetic energy appears to expand the geographic signature of oligotrophy, resulting in a temporal mismatch between the gyre defined by low-level chl *a* and dynamic topography. While this suggests that the net effect of mesoscale processes on chl *a* (extent of oligotrophy) is negative (expansive), the observed effect of eddies on phytoplankton biomass and NPP near Station ALOHA are mixed. Upwelling within cyclonic eddies have also been purported to change community structure (Bidigare et al., 2003), primary and new production (Vaillancourt et al., 2003). Anticyclonic eddies can result in increased nitrogen fixation (Fong et al., 2008; Church et al., 2009) which is responsible for over 40% of the new/export production at HOT. Finally, regions between anticyclonic and cyclonic eddies have also been shown to have increased PP and particulate organic carbon flux (Guidi et al., 2012). Sea surface height variation in general, has been found to affect the location and species composition in the DCM, with a shallower DCM with higher abundance of larger eukaryotic phytoplankton occurring with lower SSH (Barone et al., in review). Future studies could use existing databases to investigate the relative frequency of eddies (e.g., Chelton et al., 2011) in the NPSG during different climate modes, and determine whether changes in frequency are accompanied by changes in nitrogen fixation, NPP, and export at Station ALOHA.

Secular increases in the gyre geographical extent are weak, but evident within all four geographic indices. Limited by the satellite record at the time of publication, Polovina et al. (2008) reported increases in the areal extent of oligotrophic threshold chl *a* in the North Pacific at a rate of 2.2% per year from 1998 to 2007. Irwin and Oliver (2009) reported general increases through time in the most oligotrophic provinces in their classification, with oscillatory behavior found across all oligotrophic provinces. Using a longer record and linear regression analyses, Signorini et al. (2015) found mostly secular declines in surface chl *a* over large, subjectively chosen regions, but also discussed the influence of mixed layer depth changes and subsequent photoacclimation on chl *a* in the subtropics. In our re-analysis of geographic trends in the North Pacific using the latest processing of MODIS and SeaWiFS, we observe ENSO- and PDO-influenced oscillations of areal extent of regions with chl *a* <0.07 mg m⁻³ over a weak secular trend (Figure 3A, Table 1); however, we derive much slower rates of expansion than previously reported. Reprocessing and subsequent lowering of blue water chl *a* concentrations in the early SeaWiFS record (<https://oceancolor.gsfc.nasa.gov/reprocessing/r2014/seawifs/>) may be one reason for this discrepancy in expansion rate (2–1.1%). However, the chl *a* algorithm used (a decline of 1.1–0.7% year⁻¹) and a data record length that could account for climate oscillations (a decline

from 0.7 to 0.4% year⁻¹) may contribute to a greater extent. Nevertheless, the gyre as defined by dynamic topography also appears to be expanding, and relatedly, increasing the isolation of Station ALOHA. Physical gyre expansion was fastest prior to 1998, but appeared to increase throughout the altimetry record even with adjustments made for steric sea level rise (e.g., Gille, 2014). Note that surface topography in our analysis has not been corrected for interannual variability in atmospheric pressure; for this reason our reported trends based on SSH must be viewed as preliminary. Finally, we see no secular trend, but strong oscillations and correlation with both ENSO and PDO were apparent with the extent of the multivariate subtropical seascape (Figures 3C, 4C), where chl *a* dynamics may have been balanced in the classification by SST and spatial light variability. The latter result is in agreement with Behrenfeld et al. (2016), who found large oscillations in surface chl *a* concentrations in the subtropical gyres after accounting for the effect of photoacclimation.

After accounting for climate oscillations in the *in situ* data record at Station ALOHA, we observed that SST, salinity, and mixed layer depth (but only as defined by the surface offset method) were weakly increasing over 1989–2016. Concomitant to geographic and physical trends, we also confirm the increase of primary production, as well as phytoplankton standing stock derived from chl *a* in the euphotic zone, throughout the data record at Station ALOHA, as previously reported by Corno et al. (2007) and Karl and Church (2017). It is unclear whether long-term trends in T chl *a* and NPP are associated with changes in nutrient inputs (Luo et al., 2012; Letelier et al., in preparation), community structure, and/or increased efficiency of photosynthesis, particularly in the DCM (Letelier et al., 2017).

While lags in how climate oscillations affect *in situ* conditions at Station ALOHA relative to the rest of the gyre may suggest better agreement with respect to expanding oligotrophy, the divergence of secular trends measured by satellite-based geography and *in situ* conditions at Station ALOHA point toward an alternative hypothesis. *In situ* PP in the surface appears to be balanced by loss on diurnal time scales (White et al., 2017), allowing no accumulation of biomass through time. In our study, we found that secular trends of phytoplankton appear to be stronger in the deeper light-limited region of the euphotic zone, below the optical depth that satellites can see. Increased NPP in the DCM is correlated with greater abundances of nanophytoplankton (White et al., 2015), which represent over 40% of the particulate carbon (Barone et al., 2015). However, the debate about what exactly ¹⁴C incubations measure (NPP, gross PP or something in between, e.g., Marra, 2009) is exacerbated when considering shifts in community structure, particularly toward increased dominance by nano- and picophytoplankton. Species with relatively high ratios of respiration to photosynthesis may tend to substantially overestimate net primary production, perhaps because a substantial percentage of the carbon respired by such species is old carbon (Pei and Laws, 2013). ¹⁴C also overestimates NPP at low growth rates, although the discrepancy is less in 12-h than in 24-h incubations (Pei and Laws, 2014). Certainly, careful intercomparison of incubation and bottle-free

methods (e.g., Quay et al., 2010; Juranek and Quay, 2013), optical assessments of size structure (White et al., 2015) and gross carbon accumulation (White et al., 2017) along with 1-D modeling (e.g., Luo et al., 2012) will be helpful to determine how long-term changes in physical and chemical parameters are affecting the ecosystem structure and function at Station ALOHA.

Our results also suggest that long-term satellite and 3-D modeling studies, particularly those that parameterize multiple species and currencies of production (e.g., Luo et al., 2012; Nicholson et al., 2014) are necessary to understand the spatial and temporal scales of physical forcing and ecological responses in the NPSG. We note that, although the 30+ year record may be sufficient to examine many oscillations, a modeling study determined that ~40 years was necessary to detect secular trends in the subtropics (Henson et al., 2010). However, the relationships between the geographic indicators and conditions at Station ALOHA revealed in this study may allow for future hypotheses to be tested, particularly those that relate to the role of mesoscale variability in modulating seasonal to interannual change and the role of Station ALOHA as an early indicator of gyre responses to climate oscillations.

CONCLUSION

Through the lens of pelagic seascapes ecology, we have quantified different geographic systems in the North Pacific that expand and contract on seasonal and interannual scales and have embedded long-term Eulerian *in situ* observations from Station ALOHA in a dynamic mosaic of the NPSG. Over a three-decade time-series, we were able to quantify subtle secular trends and strong oscillations in gyre-scale geographic patterns and *in situ* conditions at Station ALOHA. Due to a longer data record and improved sensitivity of satellite algorithms to low-level chl *a*, we observe secular trends that are weaker than previously reported, but evident in both physical and biological definitions of the gyre, physical changes at Station ALOHA, and changes in phytoplankton standing stock and NPP, primarily in the deeper euphotic zone. Finally, we observe that conditions at Station ALOHA shift analogously to strong interannual oscillations in gyre-scale oligotrophy as defined by multivariate seascapes, with shoaled mixed layer and declines in phytoplankton biomass and production occurring with an expanded subtropical seascapes.

REFERENCES

- Anouar, F., Badran, F., and Thiria, S. (1998). Probabilistic self-organizing map and radial basis function networks. *Neurocomputing* 20, 83–96. doi: 10.1016/S0925-2312(98)00026-5
- Barone, B., Bidigare, R. R., Church, M.J., Karl, D.M., Letelier, R.M., and White, A.E. (2015). Particle distributions and dynamics in the euphotic zone of the North Pacific Subtropical Gyre. *J. Geophys. Res. Oceans* 120, 3229–3247. doi: 10.1002/2015JC010774
- Behrenfeld, M. J., O’Malley, R. T., Boss, E. S., Westberry, T. K., Graff, J. R., Halsey, K. H., et al. (2016). Reevaluating ocean warming impacts on global phytoplankton. *Nat. Clim. Chang.* 6, 323–330. doi: 10.1038/nclimate2838

AUTHOR CONTRIBUTIONS

MK: Devised the original question with input from CD and RL, created the study design, and analyzed the data with input from SD; MC and DK: Contributed data and historical context to the manuscript. All authors contributed to the writing and editing of the manuscript.

ACKNOWLEDGMENTS

We acknowledge support from the National Science Foundation through the Center for Microbial Oceanography: Research and Education (C-MORE), an NSF Science and Technology Center (EF-0424599), and the Hawaii Ocean Time-series (OCE-1260164; MC and DK), and the National Aeronautics and Space Administration Ocean Biology and Biogeochemistry Program (NASA NNX14AM36G, SD and MK) and the Biodiversity and Ecological Forecasting Program (NNX14AP62A and 80NSSC18K0412, MK). Additional support was provided by the Gordon and Betty Moore Foundation (#3794; DK) and the Simons Foundation’s SCOPE project (#329104 ; DK).

SUPPLEMENTARY MATERIAL

The Supplementary Material for this article can be found online at: <https://www.frontiersin.org/articles/10.3389/fmars.2018.00130/full#supplementary-material>

Figure S1 | Seascapes determination of dynamic gyre geography. **(A)** Variance explained by satellite and model seascapes and the percent of pixels that have the same classification in space and time between satellite and modeled seascapes. **(B)** Cross-correlation of model and satellite time series of subtropical seascapes expansion. **(C)** Cross-correlation of model and satellite time series of isolation of Station ALOHA.

Figure S2 | Cross-correlation of MEI and PDO with NPGO.

Figure S3 | Cross-correlation of geographic indicators. **(A)** Areal extent of low level chl *a*, extent defined by geostrophy, and isolation distance of Station ALOHA in relation to variations in subtropical seascapes extent. **(B)** Areal extent of low level chl *a*, extent defined by geostrophy, and subtropical seascapes extent in relation to variations in the isolation distance of Station ALOHA within the subtropical seascapes.

Figure S4 | Cross correlation analysis of climate indices and *in situ* surface properties at station ALOHA.

Table S1 | Trends of subtropical expansion across geographic metrics, chl *a* algorithms, and time-series duration. Italicized values denote no significant trend over the duration measured. The effect of climate oscillations has not been removed.

- Behrenfeld, M. J., O’Malley, R., T., Siegel, D. A., McClain, C. R., Sarmiento, J. L., Feldman, G. C., et al. (2006). Climate-driven trends in contemporary ocean productivity. *Nature* 444, 752–755. doi: 10.1038/nature05317
- Bidigare, R. R., Benitez-Nelson, C., Leonard, C. L., Quay, P. D., Parsons, M. L., Foley, D. G., et al. (2003). Influence of a cyclonic eddy on microheterotroph biomass and carbon export in the lee of Hawaii. *Geophys. Res. Lett.* 30:1318. doi: 10.1029/2002GL01639
- Boyce, D. G., Dowd, M., Lewis, M. R., and Worm, B. (2014). Estimating global chlorophyll changes over the past century. *Prog. Oceanogr.* 122, 163–173. doi: 10.1016/j.pocean.2014.01.004
- Boyce, D. G., Lewis, M. R., and Worm, B. (2010). Global phytoplankton decline over the past century. *Nature*, 466, 591–596. doi: 10.1038/nature09268

- Boyce, D. G., Lewis, M. R., and Worm, B. (2011). Boyce et al. reply. *Nature*, 472, E8–E9. doi: 10.1038/nature09953
- Campbell, L., Liu, H., Nolla, H. A., and Vaulot, D. (1997). Annual variability of phytoplankton and bacteria in the subtropical North Pacific Ocean at Station ALOHA during the 1991–1994 ENSO event. *Deep Sea Res. Part I Oceanogr. Res. Pap.* 44, 167–192. doi: 10.1016/S0967-0637(96)00102-1
- Chai, F., Jiang, M., Barber, R., Dugdale, R., and Chao, Y. (2003). Interdecadal variation of the transition zone chlorophyll front: a physical-biological model simulation between 1960 and 1990. *J. Oceanogr.* 59, 461–475. doi: 10.1023/A:1025540632491
- Chavez, F. P., Messié, M., and Pennington, J. T. (2011). Marine primary production in relation to climate variability and change. *Ann. Rev. Mar. Sci.* 3, 227–260. doi: 10.1146/annurev.marine.010908.163917
- Chelton, D. B., Schlax, M. G., and Samelson, R. M. (2011). Global observations of nonlinear mesoscale eddies. *Prog. Oceanogr.* 91, 167–216. doi: 10.1016/j.pocean.2011.01.002
- Church, M. J., Mahaffey, C., Letelier, R. M., Lukas, R., Zehr, J. P., and Karl, D. M. (2009). Physical forcing of nitrogen fixation and diazotroph community structure in the North Pacific subtropical gyre. *Glob. Biogeochem. Cycles* 23:GB2020. doi: 10.1029/2008GB003418
- Corno, G., Karl, D. M., Church, M. J., Letelier, R. M., Lukas, R., Bidigare, R. R., et al. (2007). Impact of climate forcing on ecosystem processes in the North Pacific Subtropical Gyre. *J. Geophys. Res. Oceans* 112:C04021. doi: 10.1029/2006JC003730
- Di Lorenzo, E., Schneider, N., Cobb, K. M., Franks, P. J. S., Chhak, K., Miller, A. J., et al. (2008). North Pacific Gyre Oscillation links ocean climate and ecosystem change. *Geophys. Res. Lett.* 35:L08607. doi: 10.1029/2007GL032838
- Di Lorenzo, E., Fiechter, J., Schneider, N., Bracco, A., Miller, A. J., Franks, P. J. S., et al. (2009). Nutrient and salinity decadal variations in the central and eastern North Pacific. *Geophys. Res. Lett.* 36:L14601. doi: 10.1029/2009GL038261
- DiTullio, G. R., and Laws, E. A. (1991). Impact of an atmospheric-oceanic disturbance on phytoplankton community dynamics in the North Pacific Central Gyre. *Deep Sea Res. Part A Oceanogr. Res. Pap.* 38, 1305–1329. doi: 10.1016/0198-0149(91)90029-F
- Doney, S. C., Lima, I., Feely, R. A., Glover, D. M., Lindsay, K., Mahowald, N., et al. (2009). Mechanisms governing interannual variability in upper-ocean inorganic carbon system and air-sea CO₂ fluxes: physical climate and atmospheric dust. *Deep Sea Res. Part II Top. Stud. Oceanogr.* 56, 640–655. doi: 10.1016/j.dsr2.2008.12.006
- Dore, J. E., Lukas, R., Sadler, D. W., Church, M. J., and Karl, D. M. (2009). Physical and biogeochemical modulation of ocean acidification in the central North Pacific. *Proc. Natl. Acad. Sci. U.S.A.* 106, 12235–12240. doi: 10.1073/pnas.0906044106
- Emerson, S., Quay, P., Karl, D., Winn, C., Tupas, L., and Landry, M. (1997). Experimental determination of the organic carbon flux from open-ocean surface waters. *Nature* 389, 951–954. doi: 10.1038/40111
- Fong, A. A., Karl, D. M., Lukas, R., Letelier, R. M., Zehr, J. P., and Church, M. J. (2008). Nitrogen fixation in an anticyclonic eddy in the oligotrophic North Pacific Ocean. *ISME J.* 2, 663–676. doi: 10.1038/ismej.2008.22
- Franz, B. A. (2009). *Methods for Assessing the Quality and Consistency of Ocean Color Products*. NASA Goddard Space Flight Center, Ocean Biology Processing Group. Available online at: https://oceancolor.gsfc.nasa.gov/docs/methods/sensor_analysis_methods/
- Franz, B. A., Bailey, S. W., Werdell, P. J., and McClain, C. R. (2007). Sensor-independent approach to the vicarious calibration of satellite ocean color radiometry. *Appl. Opt.* 46:5068. doi: 10.1364/AO.46.005068
- Gille, S. T. (2014). Meridional displacement of the Antarctic Circumpolar Current. *Phil. Trans. R. Soc. A* 372:20130273. doi: 10.1098/rsta.2013.0273
- Glover, D.M., Jenkins, W.J., and Doney, S.C. (2011). *Modeling Methods for Marine Science*. Cambridge: Cambridge University Press.
- Guidi, L., Calil, P. H., Duhamel, S., Björkman, K. M., Doney, S. C., Jackson, G. A., et al. (2012). Does eddy-eddy interaction control surface phytoplankton distribution and carbon export in the North Pacific Subtropical Gyre? *J. Geophys. Res.* 117:G02024. doi: 10.1029/2012JG001984
- Hammond, M. L., Beaulieu, C., Sahu, S. K., and Henson, S. A. (2017). Assessing trends and uncertainties in satellite-era ocean chlorophyll using space-time modeling. *Glob. Biogeochem. Cycles* 31, 1103–1117. doi: 10.1002/2016GB005600
- Henson, S. A., Sarmiento, J. L., Dunne, J. P., Bopp, L., Lima, I., Doney, S. C., et al. (2010). Detection of anthropogenic climate change in satellite records of ocean chlorophyll and productivity. *Biogeosciences* 7, 621–640. doi: 10.5194/bg-7-621-2010
- Hu, C., Lee, Z., and Franz, B. (2012). Chlorophyll a algorithms for oligotrophic oceans: a novel approach based on three-band reflectance difference. *J. Geophys. Res. Oceans* 117:CO1011. doi: 10.1029/2011JC007395
- Irwin, A. J., and Oliver, M. J. (2009). Are ocean deserts getting larger? *Geophys. Res. Lett.* 36:L18609. doi: 10.1029/2009GL039883
- Juranek, L. W., and Quay, P. D. (2013). Using triple isotopes of dissolved oxygen to evaluate global marine productivity. *Ann. Rev. Mar. Sci.* 5, 503–524. doi: 10.1146/annurev-marine-121211-172430
- Karl, D. M. (2010). Oceanic ecosystem time-series programs: ten lessons learned. *Oceanography* 23, 104–125. doi: 10.5670/oceanog.2010.27
- Karl, D. M., Bidigare, R. R., and Letelier, R. M. (2001). Long-term changes in plankton community structure and productivity in the North Pacific Subtropical Gyre: the domain shift hypothesis. *Deep Sea Res. Part II Top. Stud. Oceanogr.* 48, 1449–1470. doi: 10.1016/S0967-0645(00)00149-1
- Karl, D. M., and Church, M. J. (2017). Ecosystem structure and dynamics in the North Pacific Subtropical Gyre: new views of an old ocean. *Ecosystems* 20, 433–457. doi: 10.1007/s10021-017-0117-0
- Karl, D. M., Letelier, R., Hebel, D., Tupas, L., Dore, J., Christian, J., et al. (1995). Ecosystem changes in the North Pacific subtropical gyre attributed to the 1991–92 El Niño. *Nature* 373, 230–234. doi: 10.1038/373230a0
- Karl, D. M., and Lukas, R. (1996). The Hawaii Ocean Time-series (HOT) program: background, rationale and field implementation. *Deep Sea Res. Part II Top. Stud. Oceanogr.* 43, 129–156. doi: 10.1016/0967-0645(96)00005-7
- Kavanaugh, M.T., Emerson, S. R., Lockwood, D. M., Quay, P.D., and Letelier, R. M. (2014a). Physicochemical and biological controls on primary and net community production across NE Pacific seascapes. *Limnol. Oceanogr.* 59, 2013–2027. doi: 10.4319/lo.2014.59.6.2013
- Kavanaugh, M. T., Hales, B., Saraceno, M., Spitz, Y. H., White, A. E., and Letelier, R. M. (2014b). Hierarchical and dynamic seascapes: a quantitative framework for scaling pelagic biogeochemistry and ecology. *Prog. Oceanogr.* 120, 291–304. doi: 10.1016/j.pocean.2013.10.013
- Kavanaugh, M. T., Oliver, M., Chavez, F., Letelier, R. M., Muller-Karger, F., and Doney, S. C. (2016). Seascapes as a new vernacular for ocean monitoring, management and conservation. *ICES J. Mar. Sci.* 73, 1839–1850. doi: 10.1093/icesjms/fsw086
- Letelier, R. M., Bidigare, R. R., Hebel, D. V., Ondrusek, M., Winn, C. D., and Karl, D. M. (1993). Temporal variability of phytoplankton community structure based on pigment analysis. *Limnol. Oceanogr.* 38, 1420–1437. doi: 10.4319/lo.1993.38.7.1420
- Letelier, R. M., Dore, J. E., Winn, C. D., and Karl, D. M. (1996). Seasonal and interannual variations in photosynthetic carbon assimilation at Station ALOHA. *Deep Sea Res. Part II Top. Stud. Oceanogr.* 43, 467–490. doi: 10.1016/0967-0645(96)00006-9
- Letelier, R. M., Karl, D. M., Abbott, M. R., Flament, P., Freilich, M., Lukas, R., et al. (2000). Role of late winter mesoscale events in the biogeochemical variability of the upper water column of the North Pacific Subtropical Gyre. *J. Geophys. Res. Oceans* 105, 28723–28739. doi: 10.1029/1999JC000306
- Letelier, R. M., White, A. E., Bidigare, R. R., Barone, B., Church, M. J., and Karl, D. M. (2017). Light absorption by phytoplankton in the North Pacific Subtropical Gyre. *Limnol. Oceanogr.* 62, 1526–1540. doi: 10.1002/lno.10515
- Levitus, S., Antonov, J. I., Boyer, T. P., Baranova, O. K., Garcia, H. E., Locarnini, R. A., et al. (2012). World ocean heat content and thermosteric sea level change (0–2000 m), 1955–2010. *Geophys. Res. Lett.* 39:L10603. doi: 10.1029/2012GL051106
- Li, B., Karl, D. M., Letelier, R. M., and Church, M. J. (2011). Size-dependent photosynthetic variability in the North Pacific Subtropical Gyre. *Mar. Ecol. Prog. Ser.* 440, 27–40. doi: 10.3354/meps09345
- Lomas, M. W., Steinberg, D. K., Dickey, T., Carlson, C. A., Nelson, N. B., Condon, R. H., et al. (2010). Increased ocean carbon export in the Sargasso Sea linked to climate variability is countered by its enhanced mesopelagic attenuation. *Biogeosciences* 7, 57–70. doi: 10.5194/bg-7-57-2010
- Luo, Y.-W., Ducklow, H. W., Friedrichs, M. A. M., Church, M. J., Karl, D. M., and Doney, S. C. (2012). Interannual variability of primary production and

- dissolved organic nitrogen storage in the North Pacific Subtropical Gyre. *J. Geophys. Res.* 117:G03019. doi: 10.1029/2011JG001830
- Mantua, N. J., Hare, S. R., Zhang, Y., Wallace, J. M., and Francis, R. C. (1997). A Pacific interdecadal climate oscillation with impacts on salmon production. *Bull. Am. Meteorol. Soc.* 78, 1069–1079. doi: 10.1175/1520-0477(1997)078<1069:APICOW>2.0.CO;2
- Marra, J. (2009). Net and gross productivity: weighing in with ^{14}C . *Aquat. Microbial. Ecol.* 56, 123–131. doi: 10.3354/ame01306
- Martin, J. H., Knauer, G. A., Karl, D. M., and Broenkow, W.W. (1987). VERTEX: carbon cycling in the northeast Pacific. *Deep Sea Res. Part A Oceanogr. Res. Pap.* 34, 267–285. doi: 10.1016/0198-0149(87)90086-0
- McCune, B., Grace, J. B., and Urban, D. L. (2002). *Analysis of Ecological Communities Vol. 28*. Gleneden Beach, OR: MjM software design.
- McQuatters-Gollop, A., Reid, P. C., Edwards, M., Burkhill, P. H., Castellani, C., Batten, S., et al. (2011). Is there a decline in marine phytoplankton? *Nature* 472, E6–E7. doi: 10.1038/nature09950
- Messié, M. and Chavez, F. P. (2011). Global modes of sea surface temperature variability in relation to regional climate indices. *J. Climate* 24, 4313–4330. doi: 10.1175/2011JCLI3941.1
- Moore, J. K., Lindsay, K., Doney, S. C., Long, M. C., and Misumi, K. (2013). Marine ecosystem dynamics and biogeochemical cycling in the Community Earth System Model CESM1(BGC). *Clim. J.* 26, 9291–9321. doi: 10.1175/JCLI-D-12-00566.1
- Nicholson, D., Stanley, R. H. and Doney, S. C. (2014). The triple oxygen isotope tracer of primary productivity in a dynamic ocean model. *Glob. Biogeochem. Cycles* 28, 538–552. doi: 10.1002/2013GB004704
- Oliver, M. J., and Irwin, A. J. (2008). Objective global ocean biogeographic provinces. *Geophys. Res. Lett.* 35:L15601. doi: 10.1029/2008GL034238
- Pei, S., and Laws, E. A. (2013). Does the ^{14}C method estimate net photosynthesis? Implications from batch and continuous culture studies of marine phytoplankton. *Deep Sea Res. Part I Oceanogr. Res. Pap.* 82, 1–9. doi: 10.1016/j.dsr.2013.07.011
- Pei, S., and Laws, E. A. (2014). Does the ^{14}C method estimate net photosynthesis? II. Implications from cyclostudies of marine phytoplankton. *Deep Sea Res. Part I Oceanogr. Res. Pap.* 91, 94–100. doi: 10.1016/j.dsr.2014.05.015
- Polovina, J. J., Howell, E. A., and Abecassis, M. (2008). Ocean's least productive waters are expanding. *Geophys. Res. Lett.* 35:L03618. doi: 10.1029/2007GL031745
- Quay, P. D., Peacock, C., Björkman, K., and Karl, D. M. (2010). Measuring primary production rates in the ocean: Enigmatic results between incubation and non-incubation methods at Station ALOHA, Global Biogeochem. Cycles 24:GB3014. doi: 10.1029/2009GB003665
- Saba, V. S., Friedrichs, M. A. M., Carr, M.-E., Antoine, D., Armstrong, R. A., Asanuma, I., et al. (2010). Challenges of modeling depth-integrated marine primary productivity over multiple decades : a case study at BATS and HOT. *Glob. Biogeochem. Cycles* 24:GB3020. doi: 10.1029/2009GB003655
- Sakamoto, C. M., Karl, D. M., Jannasch, H. W., Bidigare, R. R., Letelier, R. M., Walz, P. M., et al. (2004). Influence of Rossby waves on nutrient dynamics and the plankton community structure in the North Pacific subtropical gyre. *J. Geophys. Res. Oceans* 109:C05032. doi: 10.1029/2003JC001976
- Siegel, D.A., Behrenfeld, M. J., Maritorena, S., McClain, C. R., Antoine, D., Bailey, S. W., et al. (2013). Regional to global assessments of phytoplankton dynamics from the SeaWiFS mission. *Remote Sens. Environ.* 135, 77–91. doi: 10.1016/j.rse.2013.03.025
- Signorini, S. R., Franz, B. A., and McClain, C. R. (2015). Chlorophyll variability in the oligotrophic gyres: mechanisms, seasonality and trends. *Front. Mar. Sci.* 2:1. doi: 10.3389/fmars.2015.00001
- Signorini, S. R., and McClain, C. R. (2012). Subtropical gyre variability as seen from satellites. *Remote Sens. Lett.* 3, 471–479. doi: 10.1080/01431161.2011.625053
- Sverdrup, H. U., Johnson, M. W., and Fleming, R. H. (1942). *The Oceans, Their Physics, Chemistry, and General Biology. Vol. 1087*. New York, NY: Prentice-Hall.
- Vaillancourt, R. D., Marra, J., Seki, M. P., Parsons, M. L., and Bidigare, R. R. (2003). Impact of a cyclonic eddy on phytoplankton community structure and photosynthetic competency in the subtropical North Pacific Ocean. *Deep Sea Res. Part I Oceanogr. Res. Pap.* 50, 829–847. doi: 10.1016/S0967-0637(03)00059-1
- Venrick, E. L. (1995). “Scales of variability in a stable environment: phytoplankton in the central North Pacific,” in *Ecological Time Series*. eds T. M. Powell and J. H. Steele(Boston, MA: Springer).
- Venrick, E. L., McGowan, J. A., Cayan, D. R., and Hayward, T. L. (1987). Climate and chlorophyll a: long-term trends in the central North Pacific Ocean. *Science* 238, 70–72. doi: 10.1126/science.238.4823.70
- Ward, J. (1963). Hierarchical grouping to optimize an objective function. *J. Am. Stat. Assoc.* 58, 236–244. doi: 10.1080/01621459.1963.10500845
- White, A. E., Barone, B., Letelier, R. M., and Karl, D. M. (2017). Productivity diagnosed from the diel cycle of particulate carbon in the North Pacific Subtropical Gyre. *Geophys. Res. Lett.* 44, 3752–3760. doi: 10.1002/2016GL071607
- White, A. E., Letelier, R. M., Whitmire, A. L., Barone, B., Bidigare, R. R., Church, M. J., et al. (2015). Phenology of particle size distributions and primary productivity in the North Pacific subtropical gyre (Station ALOHA). *J. Geophys. Res. Oceans* 120, 7381–7399. doi: 10.1002/2015JC010897
- Wilson, C., and Adamec, D. (2001). Correlations between surface chlorophyll and sea surface height in the tropical Pacific during the 1997–1999 El Niño-Southern Oscillation event. *J. Geophys. Res. Oceans* 106, 31175–31188. doi: 10.1029/2000JC000724
- Winn, C. D., Campbell, L., Christian, J. R., Letelier, R. M., Hebel, D. V., Dore, J. E., et al. (1993). Seasonal variability in the phytoplankton community of the North Pacific Subtropical Gyre. *Glob. Biogeochem. Cycles* 9, 605–620. doi: 10.1029/95GB02149
- Wright, S. W., Jeffrey, S. W., Mantoura, R. F. C., Llewellyn, C. A., Bjørnland, T., and Repeta, D. (1991). Improved HPLC method for the analysis of chlorophylls and carotenoids from marine phytoplankton. *Mar. Ecol. Prog. Ser.* 77, 183–196.
- Wolter, K., and Timlin, M. S. (1993). “Monitoring ENSO in COADS with a seasonally adjusted principal component index,” in *Proceedings of the 17th Climate Diagnostics Workshop*, Vol. 5257 (Norman, OK).
- Zhang, Y., Wallace, J. M., and Battisti, D. S. (1997). ENSO-like interdecadal variability: 1900–93. *J. Clim.* 10, 1004–1020. doi: 10.1175/1520-0442(1997)010<1004:ELIV>2.0.CO;2

Conflict of Interest Statement: The authors declare that the research was conducted in the absence of any commercial or financial relationships that could be construed as a potential conflict of interest.

Copyright © 2018 Kavanaugh, Church, Davis, Karl, Letelier and Doney. This is an open-access article distributed under the terms of the Creative Commons Attribution License (CC BY). The use, distribution or reproduction in other forums is permitted, provided the original author(s) and the copyright owner are credited and that the original publication in this journal is cited, in accordance with accepted academic practice. No use, distribution or reproduction is permitted which does not comply with these terms.



Bacterial Succession on Sinking Particles in the Ocean's Interior

Erik A. Pelve¹, Kristina M. Fontanez^{2†} and Edward F. DeLong^{3*}

¹ Department of Cell and Molecular Biology—Molecular Evolution, Biomedical Center, Uppsala University, Uppsala, Sweden,

² Department of Civil and Environmental Engineering, Massachusetts Institute of Technology, Cambridge, MA, United States,

³ Daniel K. Inouye Center for Microbial Oceanography: Research and Education, Department of Oceanography, University of Hawaii at Manoa, Honolulu, HI, United States

OPEN ACCESS

Edited by:

Matthew J. Church,
University of Montana, United States

Reviewed by:

Frank Stewart,

Georgia Institute of Technology,

United States

Haiwei Luo,

Chinese University of Hong Kong,

China

*Correspondence:

Edward F. DeLong
edelong@hawaii.edu

†Present Address:

Kristina M. Fontanez,
Fluid-Screen, Inc., Cambridge, MA,
United States

Specialty section:

This article was submitted to
Aquatic Microbiology,
a section of the journal
Frontiers in Microbiology

Received: 29 August 2017

Accepted: 03 November 2017

Published: 24 November 2017

Citation:

Pelve EA, Fontanez KM and DeLong EF (2017) Bacterial Succession on Sinking Particles in the Ocean's Interior. *Front. Microbiol.* 8:2269.
doi: 10.3389/fmicb.2017.02269

Sinking particles formed in the photic zone and moving vertically through the water column are a main mechanism for nutrient transport to the deep ocean, and a key component of the biological carbon pump. The particles appear to be processed by a microbial community substantially different from the surrounding waters. Single cell genomics and metagenomics were employed to describe the succession of dominant bacterial groups during particle processing. Sinking particles were extracted from sediment traps at Station Aloha in the North Pacific Subtropical Gyre (NPSG) during two different trap deployments conducted in July and August 2012. The microbial communities in poisoned vs. live sediment traps differed significantly from one another, consistent with prior observations by Fontanez et al. (2015). Partial genomes from these communities were sequenced from cells belonging to the genus *Arcobacter* (commensalists potentially associated with protists such as Radiolaria), and *Vibrio campbellii* (a group previously reported to be associated with crustacea). These bacteria were found in the particle-associated communities at specific depths in both trap deployments, presumably due to their specific host-associations. Partial genomes were also sequenced from cells belonging to *Idiomarina* and *Kangiella* that were enriched in live traps over a broad depth range, that represented a motile copiotroph and a putatively non-motile algicidal saprophyte, respectively. Planktonic bacterial cells most likely caught in the wake of the particles belonging to *Actinomarina* and the SAR11 clade were also sequenced. Our results suggest that similar groups of eukaryote-associated bacteria are consistently found on sinking particles at different times, and that particle remineralization involves specific, reproducible bacterial succession events in oligotrophic ocean waters.

Keywords: marine bacteria, oligotrophic gyre, metagenomics, marine particles, sediment trap, biological pump, single cell genomics

INTRODUCTION

Sinking particles produced in the photic zone that transport nutrients to the deep ocean are an important sink for carbon dioxide from the atmosphere. The particles in the upper layers of the ocean are formed from a complex interplay between abiotic factors, eukaryotic cells, and phototrophic and heterotrophic bacteria. As the particles sink they are processed by a distinct community of microbes, and the nutrients released are made available to other trophic levels of the ecosystem through the microbial carbon pump (Jiao et al., 2010). Sinking particles in the ocean can be viewed as discrete loci that share some properties to island habitats, as isolated, discrete environments with different environmental conditions than are found in the surrounding water.

As such, they are hot spots for microbial activity and are important hubs in the food web, with anaerobic and aerobic metabolic micro-niches (Honjo et al., 2008).

Particles exist in the ocean in a range of forms, sizes, and compositions (Simon et al., 2002). Many remain in the photic zone until they are disaggregated, but some particles sink, mainly macroaggregates composed of algae, diatoms, dinoflagellates, fecal material, and minerals derived from eukaryotic shells and similar remains. Microbial communities on particles have sometimes been shown to be significantly different from that of the surrounding water (DeLong et al., 1993; Allen et al., 2013), but they are diverse and heterogeneous and are still not fully understood. For example, the identity and relative abundance of eukaryotes that produce particulate materials is still largely unknown, as is the specificity of their bacterial associations and depth distributions, and how species interactions may affect particle degradation. How initial microbial communities found on sinking particles might change during transformation of particulate organic material (POM) to dissolved organic material (DOM) also remains to be fully determined.

Methods typically used to separate different size fractions from one other can present challenges in identifying authentic particle-associated communities (Grossart, 2010). Additionally, microbial composition and degradation processes on sinking particles may differ in their degradation dynamics as compared to marine debris that are stationary in the water column (Honjo et al., 2008). Yet another consideration are the methods used to characterize microbial components on the sinking particles. PCR-based approaches that use functional or taxonomic indicator genes can provide an extensive fingerprint of the community composition, but are also vulnerable to well known biases. Shotgun metagenome sequencing has the potential to provide a more even description of the community, but requires larger sequencing effort, and may miss rare members of the community. Single cell genomics can provide partial genomes and more precise identification of gene origins, albeit with lower overall throughput. In this study, we sought to combine several approaches (single cell genomics and metagenomics) to overcome the individual shortcomings of either of these techniques used alone.

A recent study demonstrated that the initial microbial community on sinking particles in the oligotrophic North Pacific was dominated by bacterial groups associated with eukaryotes, while copiotrophic bacterial species dominated in sediment traps in which particle degradation occurred (Fontanez et al., 2015). Metagenomes from particles caught in sediment traps contained DNA from microbial communities distinct from the surrounding seawater. Poisoned traps containing a fixative that preserves the microbes and their nucleic acids as they enter the trap, were rich in sequences associated with eukaryotes, viruses, and bacteria (including the functions pathogenicity, anaerobic metabolism, and chitin degradation). Live traps, that allow the particle degrading community to enrich *in situ*, were rich in bacterial taxonomic and functional genes known to be involved in degradation of the DOM released during POM processing, as well as bacteria associated with eukaryotes.

In this study, we combined the metagenomes obtained from a previous report (Fontanez et al., 2015) with corresponding metagenomes collected on a different set of deployments and single cell genomes that represented six dominant bacterial genera found in the traps, to improve our understanding of the major microbial players associated with the initial and processed sinking particles in the oligotrophic North Pacific Subtropical Gyre (NPSG). Single cell genomes combine taxonomic marker genes with functional genes, allowing for specific predictions of ecological function. Based on earlier studies, we postulated that dominant bacterial genera found in the initial sinking community on particles (poisoned traps), would encode genes indicative of their association with eukaryotes. Similarly, we postulated that bacterial genera enriched in the “processed” community (live traps), would be enriched in genes coding for particle degradation, motility, chemotaxis, and DOM degradation. To test these hypotheses, we combined results from several different trap deployments, using both metagenomics, and single cell sequencing, to more completely describe the characteristics of microbes on sinking materials and in processed POM, and how they varied at different times and as a function of depth. Using the same data, we also tested the hypothesis that particle-associated bacteria are typically recruited onto sinking particles mainly in the photic zone, and are subsequently present on the particles throughout the water column at greater depths.

MATERIALS AND METHODS

Metagenomes collected from poisoned and live traps from the July HD5 cruise at station ALOHA in the NPSG ($22^{\circ}48.5'N$, $158^{\circ}3.02'W$) in 2012 were analyzed by Fontanez et al. (2015). In the current study, these metagenome data were combined with a different set of metagenomes collected in August of the same year in a separate set of trap deployments on cruise HD9, in addition to determination of single cell genomes collected from the sediment traps (this study).

Sampling

Sinking particles were collected during the 2012 HD5 and HD9 cruises. Two sets of free drifting sediment traps were placed at depths of 110, 150, 200, 300, and 500 m, both sets containing ~ 1.8 L of sterile filtered seawater ($0.2\ \mu\text{m}$), adjusted to a density of $1.05\ \text{g}/\text{cc}$ with NaCl (Figure 1). The poisoned traps contained the fixative RNAlater (Ambion, Carlsbad, CA, USA), designed to prevent biological degradation of material that enters the traps. A $335\ \mu\text{m}$ nylon screen (Nitex) was placed on top of the tubes to prevent larger zooplankton from entering the trap. The traps from the HD5 cruise were deployed in July 14 and recovered in July 26 2012 and the traps from the HD9 cruise were deployed in August 27 and recovered in September 12 2012 (see Fontanez et al., 2015 for methodological detail).

Sample Processing

About 500 mL of seawater from the top of each tube was removed to limit contaminating traces of the surrounding sea water. In the HD5 samples, particles in the $0.2\text{--}335\ \mu\text{m}$ fraction were collected on a Sterivex filters (EMD Millipore, Billerica, MA, USA). In the

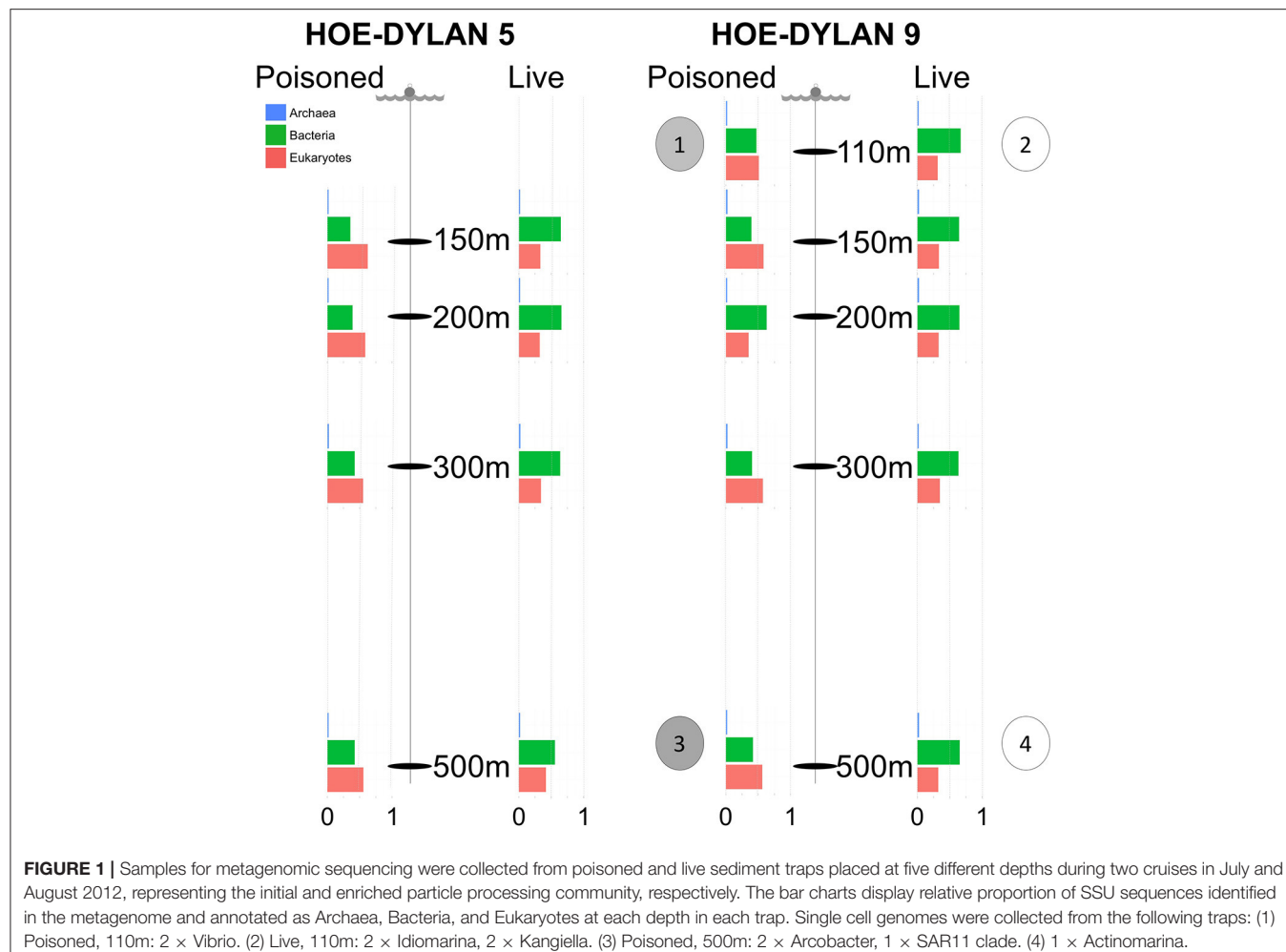


FIGURE 1 | Samples for metagenomic sequencing were collected from poisoned and live sediment traps placed at five different depths during two cruises in July and August 2012, representing the initial and enriched particle processing community, respectively. The bar charts display relative proportion of SSU sequences identified in the metagenome and annotated as Archaea, Bacteria, and Eukaryotes at each depth in each trap. Single cell genomes were collected from the following traps: (1) Poisoned, 110m: 2 × *Vibrio*. (2) Live, 110m: 2 × *Idiomarina*, 2 × *Kangiella*. (3) Poisoned, 500m: 2 × *Arcobacter*, 1 × SAR11 clade. (4) 1 × *Actinomarina*.

HD9 samples, particles were collected by serial filtration in two different size fractions, first in the 5.0–335 µm size fraction, and next in the 0.2–5.0 µm size fraction. After filtration, filters were stored in 1.5 mL RNAlater and frozen at –80°C (see Fontanez et al., 2015 for details). Samples for single cell analyses were collected from the bottom of live and poisoned sediment traps at 110 and 500 m. A total of 1.6 mL of the unfiltered sediment trap solution was added to 400 µL of 50% glycerol in 1X phosphate buffered saline, flash frozen, and stored at –80°C until single cell genome amplification at the Bigelow Single Cell Genomics Center.

Metagenomic Sequencing and Processing

DNA from the traps were purified and sequenced (as described in detail in the Supplemental information of Fontanez et al., 2015). In short, DNA was purified from filters with the Mobio Powerwater DNA Isolation kit (Mobio, Carlsbad, CA). Libraries were prepared using the Nextera XT DNA sample preparation protocol (Illumina, San Diego, CA, USA) and sequenced on an Illumina MiSeq instrument, with 10 dual indexed samples pooled for each sequencing run. Library quality and fragment size range were evaluated with a Bioanalyzer

2100 (Agilent Technologies, Santa Clara, CA, USA). All metagenomic data are available at NCBI under bioproject number PRJNA270248.

Single Cell Genomic Sequencing

Single cells were isolated through FACS flow cytometry at the Bigelow Single Cell Genomics Center (as described in Woyke et al., 2009). DNA was amplified with by multiple displacement amplification (MDA) and single amplified genomes (SAGs) were screened with PCR using primers targeting bacterial and archaeal 16S genes (27F:AGRGTTYGATYMTGGCTCAG/907R:CCGT CAATTCTTTRAGTT; Arc_344F:ACGGGGYGCAGCAG GCGCGA/Arc_915R:GTGCTCCCCGCCAATTCT). PCR products were Sanger sequenced using the BigDye 3.1 kit at the ABI 3730 DNA analyzer, and the sequences quality controlled with the software Sequencher (Sequencher® version 4.10.1 sequence analysis software, Gene Codes Corporation, Ann Arbor, MI, USA <http://www.genecodes.com>) and aligned to the SILVA 115 database using LAST (Zhang et al., 2000) with a cutoff of lastscore 50, *e*-value 0.01.

Ten SAGs were selected for whole genome sequencing. The selected SAGs were chosen to represent different trap conditions

and time points in particle progression. From the poisoned traps, two SAGs each were chosen belonging to the genera *Arcobacter* and *Vibrio*. Both were found to be significantly enriched in poisoned traps compared to the surrounding sea water, and both harbored genes that were highly enriched in the poisoned traps (Fontanez et al., 2015). Both genera are also known to include strains closely associated with eukaryotic cells of the kind that are suggested to be important for the early stages of particle processing. From the live traps, two SAGs each belonging to the genera *Idiomarina* and *Kangiella* were chosen. Both genera are enriched in live traps compared to poisoned traps and the surrounding sea water (Fontanez et al., 2015). *Idiomarina* is commonly enriched in mesocosms and *Kangiella* is related to the hydrocarbon degrader *Oceanospirillales*, which suggests an important function in the latter stages of particle processing. In addition, two SAGs were selected that did not represent dominant strains in the particle communities—one belonging to the SAR11 clade and one to the newly described genus *Actinomarina*. These SAGs were selected to shed light on their presence in the particles and to expand on the known genomic diversity of these groups.

For all sets of duplicate SAGs from the same genus, the pair of SAGs with the highest SSU nucleotide identity was chosen to allow for comparisons of closely related genomes. The selected SAGs were sequenced using Illumina NextEra and MiSeq. The libraries were quality controlled using Bioanalyzer 2100 (Agilent Technologies, Santa Clara, CA, USA).

Metagenomic Analysis

Reads from the two different size fractions (0.2–0.5 and 0.5–335 μm) from the HD9 cruise were pooled together and treated in aggregate, for comparison to the 0.2–335 μm samples from the HD5 cruise. The reads were trimmed and processed as described by Fontanez et al. (2015) and queried against the SILVA 123, Refseq64, and KEGG (September 2013) databases using LAST (0.1.0; Score penalty: 500; Initial match multiplicity (-m): 10; Zhang et al., 2000). Selective enrichment of Operational Taxonomic Units (OTUs) in metagenomes were analyzed using the R packages phyloseq (McMurdie and Holmes, 2013), vegan (Oksanen et al., 2016) and DESeq2 (Love et al., 2014). In DESeq2, the regularized log transformation was used to normalize the samples (blind = FALSE), taking into account different sample sizes. The complete dataset (sequences belonging to all domains of life) was used for normalization, comparable to what was described in Fontanez et al. (2015). Abundance plots of $2^{\wedge}(\text{transformed value})$ was created in the phyloseq R package, where principal coordinate analysis was used to ordinate the normalized sequences. The Vegan R package was used to detect significantly divergent clusters ($p < 0.05$) with the Adonis function. The DESeq2 package was used to statistically infer divergent groups based on taxonomic inference (using the Wald function) from the Silva and Refseq databases, as well as functional genes based on the KEGG database. Traps were compared in an experimental design where poisoned and live traps were compared over both cruises with traps at all depths used as biological replicates. Deep (300, 500 m) and Shallow traps (110, 150, and 200 m) were compared with traps from both cruises and both treatments as biological replicates. Cruises

were compared with traps of all depths and both treatments as biological replicates (Table S5). Significantly enriched OTUs were extracted at a p value of 0.01 (see Fontanez et al., 2015 for details.).

Single Cell Data Processing

Single cell datasets were analyzed on the Galaxy platform. The Illumina reads were filtered using trimomatic (Seed mismatches: 2; Palindrome clip threshold: 40; Sliding window size: 4 Average quality required: 15; Minimum quality leading/trailing bases: 5 Minimum length read: 45; Lohse et al., 2012). Paired reads were assembled using SPADES 3.0 with BWA-mediated MismatchCorrector (K-mers: 21,33,55; Bankevich et al., 2012). Assembly quality was assessed using QUAST (Gurevich et al., 2013) and completeness predicted using a set of 139 marker genes (Rinke et al., 2013). Scaffolds were annotated using PROKKA (transl_table: 11, Similarity e-value cut-off: 1e-06; Cuccuru et al., 2014; Seemann, 2014) and LAST (0.1.0; Score penalty: 500; Initial match multiplicity (-m): 10; Zhang et al., 2000) against the databases Refseq64 and KEGG (September 2013), and the carbohydrate-active enzymes database (CAZymes, October 2017; Lombard et al., 2014).

Related genes to the SAG SSU RNA genes predicted from PROKKA were identified in the SILVA 123 database. The sequences were filtered to 1,000 bp, clustered to 95% similarity with usearch (Edgar, 2010), aligned using linsi (with the parameters set to auto) in the MAFFT package (Katoh and Standley, 2013), cropped with BMGE (DNAPAM1:2; Criscuolo and Gribaldo, 2010), and a phylogenetic tree was produced with IQ-tree (fast bootstrapping, 1,000 replicates, model selected by the TEST algorithm and reported for each tree in Figure S4; Nguyen et al., 2015). The trees were refined in the software FigTree (<http://tree.bio.ed.ac.uk/software/figtree/>).

Average nucleotide identity and tetranucleotide frequency were used to determine relationship between the SAGs and reference genomes using the script pyani (<https://github.com/widdowquinn/pyani>). Shared genes between related genomes were determined using reciprocal best blast hit (60% similarity, e-value 1e-10). Shared genes between multiple genomes were defined from shared homologous orthoMCL groups (Chen et al., 2006). Metagenomic reads were recruited to the SAGs with blastn (cutoff: 200 bp, 90% sequence similarity) and used to estimate SAG abundance between depths, treatments, and cruises. Relative read recruitment as aspects of treatment, depth, and cruise were compared to each other with an ANOVA test, with the other samples as biological replicates in the same experimental design as described for the metagenome. Reads annotated to the same genus as the SAGs in the metagenomes of the same traps as where the SAGs were isolated were selected and gene orthology (on KO level) annotated. These annotations were compared to the annotations from the SAGs as well as corresponding annotations from the closest fully sequenced genome (to compensate for missing regions from the SAGs) to determine to which extent the SAGs represent their genera in the traps. Reference genomes: *Arcobacter nitrofigilis* (NC_014166); *Vibrio campbellii* BAA1116 (NC_009783; NC_009784; NC_009777); *Idiomarina loihensis* (NC_021286); *Kangiella koreensis* (NC_013166); *Actinomarina minuta* (KC811150); *Alpha proteobacteria* HIMB5 (NC_018643).

All single cell data are available at NCBI under bioproject number PRJNA270248 with the following nomenclature:

Uncultured Actinomarina	Actinomarina	HD9-500	m-PIT-SAG01—
Arcobacter1	Arcobacter	HD9-500	m-PIT-SAG02—
Arcobacter2	Arcobacter	HD9-500	m-PIT-SAG03—
Idiomarina1	Idiomarina	HD9-110	m-PIT-SAG04—
Idiomarina2	Idiomarina	HD9-110	m-PIT-SAG05—
Uncultured Kangiella HD9-110 m-PIT-SAG06—Kangiella1			
Uncultured Kangiella HD9-110 m-PIT-SAG07—Kangiella2			
SAR11clade	SAR11clade	HD9-500	m-PIT-SAG08—SAR11_clade
Uncultured Vibrio HD9-110 m-PIT-SAG09—Vibrio1			
Uncultured Vibrio HD9-110 m-PIT-SAG10—Vibrio2			

RESULTS

Single cell genomes from the HD9 cruise and metagenomes from the HD5 and HD9 cruises were sequenced and analyzed to enable comparisons of the microbial assemblages on sinking particles caught in poisoned and live sediment traps deployed in the NPSG ($22^{\circ}48.5\text{ N }158^{\circ}3.02\text{ W}$).

Samples

Metagenome samples were collected from traps placed at 150, 200, 300, and 500 m depth during two cruises (HD5 and HD9) in July and August 2012, as well as at 110 m for the second cruise (Figure 1, Table 1, Table S5). Two types of traps were deployed: (1) poisoned traps which contained filtered seawater adjusted to a density of 1.05 g/cc with brine solution, combined with a fixative to preserve nucleic acids of the initial community of the sequestered particles; and (2) live traps, containing only the brine solution that allowed living microbial communities to further process particles collected in the traps (see section Materials and Methods and Fontanez et al., 2015). Single cells were isolated and their genomes were sequenced from both live and poisoned traps from 110 to 500 m depth during the HD9 cruise.

Metagenomes

Previously reported observations for samples collected during the HD5 cruise (Fontanez et al., 2015) were compared to processed and analyzed samples from the HD9 cruise 1 month later. Specifically, the metagenomes in the poisoned and live traps displayed distinct differences in microbial assemblage compositions. This was evident in KEGG, Refseq, and Silva database annotations (Figures 1, 2, Table 2, Table S1, Figure S1). There were only slight differences between traps of the same treatment from different depths (i.e., shallow poisoned traps compared to deep poisoned traps and shallow live traps compared to deep live traps).

The possibility exists that differences between the HD5 and HD9 filtration methods (HD5, whole sample filtration, extraction, and sequencing, vs. HD9 serial filtration, extraction, and sequencing of two different size fractions separately, followed by *in silico* pooling of the two fractions) could introduce methodological differences in abundance estimates between the two different cruises. However, since very few differences were detected between the HD5 and HD9 results when the same sample treatments (poisoned or dead at the same depths) were compared, the different methods used did not appear to have compromised the overall results, at the level of resolution studied (see below).

Only a small number of OTUs were significantly different between the cruises (Table S1). Eukaryotes and viruses were more commonly observed and had higher relative abundance in poisoned traps compared to live traps (Figure 1). Bacteria were common in both sets of traps and relatively few sequences in any trap belonged to archaea. At a functional level, there were groups of genes involved in energy metabolism that appeared significantly enriched in deep, poisoned traps, including genes for carbon metabolism (K00177, K01846), a sulfite reductase (K00392), and genes involved in cofactor biosynthesis (K02188, K02190, K03404, K02293) (Figure S2). This might suggest specific life styles specifically enriched for growth among deep-dwelling eukaryotes and their associated bacteria.

Single Cell Genomes

Ninety single cells were isolated by flow cytometry at the Single Cell Genomics Center at the Bigelow Laboratory for Ocean Sciences. Their genomes were Multiple Displacement Amplified

TABLE 1 | Significantly enriched operational taxonomic units (OTUs) in the metagenomes (p value < 0.01).

Database	Domain	Poiss_vs_Live	Live_vs_Poiss	Deep_vs_Shallow	Shallow_vs_Deep	HD5_vs_HD9	HD9_vs_HD5
Refseq	Archaea	1	3	0	0	0	0
	Bacteria	31 (4)	213 (47)	8 (2)	4	0	5 (2)
	Eukaryotes	313 (205)	2	0	0	17	1
	Virus	32 (10)	1	0	0	0	0
Silva	Archaea	0	2 (2)	0	0	0	0
	Bacteria	3 (3)	28 (15)	1	0	0	2 (2)
	Eukaryotes	2 (1)	40 (36)	1	0	0	0
Kegg		3054 (2940)	347 (200)	19 (14)	2 (1)	0	2 (2)

Numbers in parenthesis indicate enriched OTUs with log₂-fold change > 2 .

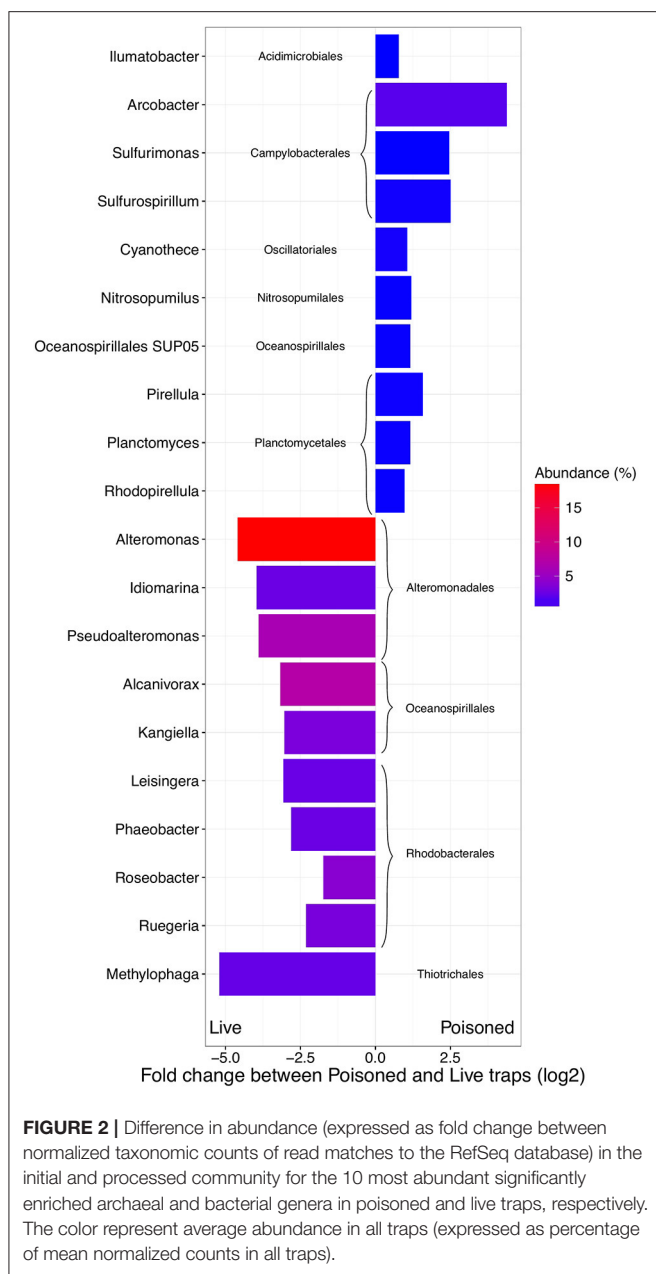


FIGURE 2 | Difference in abundance (expressed as fold change between normalized taxonomic counts of read matches to the RefSeq database) in the initial and processed community for the 10 most abundant significantly enriched archaeal and bacterial genera in poisoned and live traps, respectively. The color represent average abundance in all traps (expressed as percentage of mean normalized counts in all traps).

(MDA), followed by 16S ribosomal RNA gene amplification and sequencing (Figure S3). Ten cells of the most abundant genera were selected for partial genome sequencing (Table 2). From the 110 m live trap, two cells for Idiomarina and two cells for Kangiella were sequenced, and from the 500 m live trap one cell was chosen for Actinomarina. From the 110 m poisoned trap two cells were chosen for Vibrio, and for the 500 m poisoned trap two cells were chosen for Arcobacter and one cell for the SAR11 clade. All four pairs of SAGs from the same genus were closely related, with identical 16S rRNA gene sequences and high average nucleotide identity (>95%; Figure S5). Interestingly, all four of these genera were highlighted in analyses of microbes associated with export in the upper water column from the Tara

expedition, as being important for carbon export (Guidi et al., 2015). The genomes were analyzed for genetic features (Figure 3, Table 2), taxonomic signals (Figures S4–S6) and gene content (Figure 4; Table S2), as well as relative read recruitment from the metagenomes (Figure 5, Figure S7).

Initial Microbial Assemblages in the Poisoned Traps

The poisoned trap metagenomes represented cells on sinking particles that were immediately fixed by the preservative as they entered the trap. We refer material in the posoined traps, consisting of eukaryotes that make up the bulk of the particles and their associated bacteria as the “initial community.” Eukaryotes and associated viruses were more common in the initial community, than in the live traps (Figure 1). Many of the significantly more abundant bacteria in poisoned traps were either associated with eukaryotes (Arcobacter, Ilumatobacter, and Planctomyces) or potentially with the micro-niches specific to particles (Chroococcales, Sulfurimonas, and Oceanospirillales; Figure 2). The phototroph Cyanothecae was also identified, which is known to form aggregates and thus might have contributed to the particle formation. Ammonia oxidizing archaea and bacteria were significantly enriched in this fraction, despite low overall abundance in the traps.

Bacterial genes significantly enriched in the poisoned traps included components for sulfate reduction, cyanobacterial photosynthesis, and carbon metabolism, possibly carbon fixation by the reductive TCA cycle (Table S1c). There were genes for cell signaling, secretion and environmental information processing, and genes for uptake of zinc, manganese, biotin, and oligopeptides. Genes encoded by the Arcobacter and Vibrio SAGs were enriched primarily in the poisoned traps (Figure 4), where Arcobacter—but not Vibrio—were significantly enriched in the metagenomes on a genus marker gene level (Figure 2).

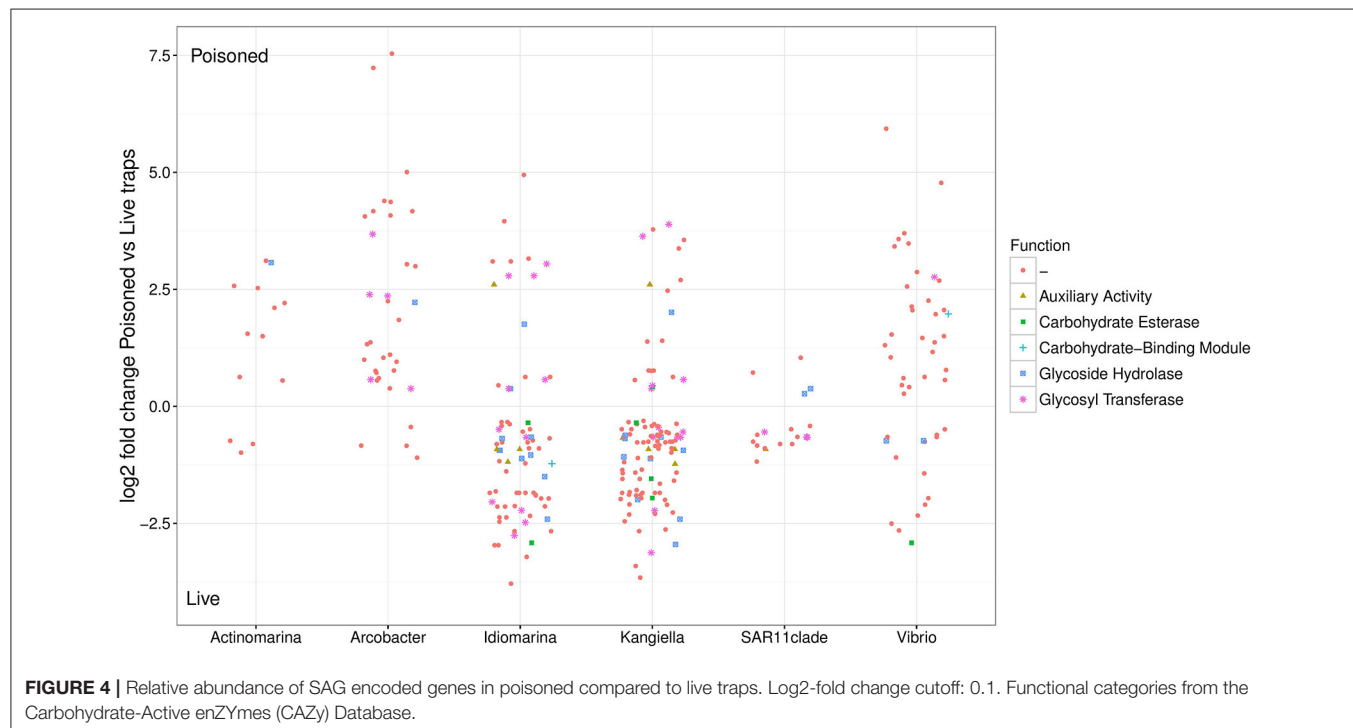
Arcobacter

Two closely related Arcobacter SAGs were isolated from the 500 m poisoned trap during the second cruise (HD9). Although Arcobacter is best known as an animal pathogen, the genus contains both animal associated and free-living pathogenic and non-pathogenic strains. It is known to form mutualistic relationships with the amoeboflagellate Breviatea (Colomban de Vargas et al., 2015; Hamann et al., 2016). Arcobacter representatives have also been found as part of the biofilm community on sunken wood where they have been suggested to mineralize sulfur and fix nitrogen (Kalenitchenko et al., 2016).

These SAGs cluster together with the marine strain *Arcobacter geojedonensis* (Choe et al., 2015), with a 94% 16S rRNA nucleotide identity to the closest related genome sequenced strain (Figures S4, S5). The highest number of genes were shared with the free-living strain *A. nitrofigilis*, but the level of genome synteny was low, with shared genes dispersed over the genome (Figure S6). The coding densities of the single cell genomes were not as high as those of related strains, which might suggest adaptation to higher nutrient availability

TABLE 2 | Assembly statistics of single cell genomes.

	Initial community				Processed community				Planktonic	
	Arcobacter1	Arcobacter2	Vibrio1	Vibrio2	Idiomarina1	Idiomarina2	Kangiella1	Kangiella2	Actinomarina	SAR11-clade
HD9 trap	500P	500P	110P	110P	110L	110L	110L	110L	500L	500P
Reads	693926	820791	898088	925567	821621	908546	828156	775789	729489	804475
Scaffolds	18	56	68	42	8	11	6	31	9	37
Total length	162008	397249	917768	1265-273	325153	597848	238196	1421-680	257233	361876
Largest scaffold	24156	56862	60299	167359	106931	163684	188967	240315	59530	28337
GC (%)	29.72	30.57	43.49	44.95	46.37	47.35	44.38	43.45	33.09	30.06
N50	15811	19010	26108	63133	72189	143629	188967	75140	41063	17212
L50	4	7	12	7	2	2	1	5	3	9
Estimated recovery (%)	3	20	6	33	8	20	13	61	22	30
Coding density (%)	78	86	79	84	94	94	90	90	96	91
Median intergenic length (bp)	89	36	114	94	19	16	63	60	2	3
rRNA	3	2	3	3	3	3	3	3	3	2
tRNA		14	14	29	4	8	10	21	13	11
tmRNA				1				1		
CDS	148	408	867	1211	334	581	244	1343	288	373
Hypothetical	44	41	68	62	80	29	239	32	251	237
CAZy genes		13	25	50	7	15	5	23	9	12
Novel genes			52	38		1		30	52	3

**FIGURE 4 |** Relative abundance of SAG encoded genes in poisoned compared to live traps. Log2-fold change cutoff: 0.1. Functional categories from the Carbohydrate-Active enZYmes (CAZy) Database.

(Figure 3, Table 2, Giovannoni et al., 2015). The GC content was relatively low (~30%).

Similar to known strains, the Arcobacter single cell genomes encoded genes for motility and chemotaxis (Table S2). The SAG

genes also included the glycerol transporter system *glpPQSTV* as well as the glycerol kinase gene *glpK*, which suggests their ability to use glycerol as a carbon source. The zinc transporter *znuABC* genes were also present in the SAG.

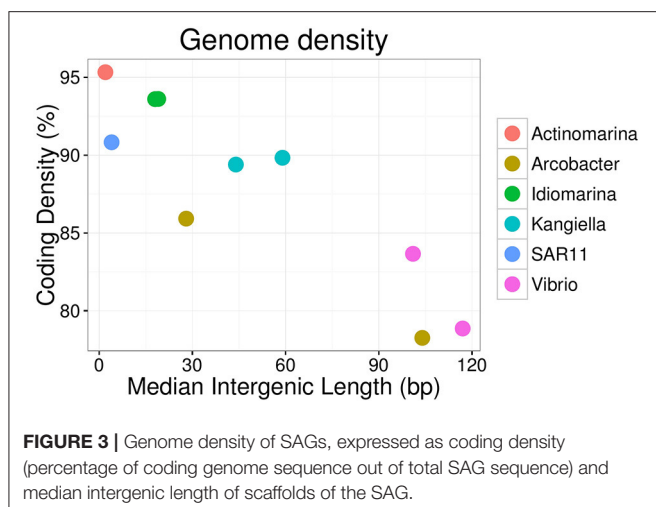


FIGURE 3 | Genome density of SAGs, expressed as coding density (percentage of coding genome sequence out of total SAG sequence) and median intergenic length of scaffolds of the SAG.

The Arcobacter cell encoded several glycoside hydrolases with a putative substrate range that included glucoses, mannoses, xyloses, and peptidoglycan (Table 3, Table S4). In contrast to the other SAGs, and despite their suggested importance in the initial community (Fontanez et al., 2015), the Arcobacter SAGs encoded no glycoside hydrolases specific for chitin, commonly found in eukaryotes including fungi, algae, and crustaceans. This could be a consequence of incomplete representation of the genomes, or it might suggest adaptation to different hosts. Two genes known to be induced in Arcobacter epibionts by the presence of the metazoan *Lenisia limosa* were identified—an Na^+/H^+ antiporter of the NhaD family and the 2-oxoglutarate carboxylase *cfa* (Table S2; Hamann et al., 2016). None of the virulence factors previously described for the pathogen *Arcobacter butzleri* (Douidah et al., 2012) were identified in the SAGs or in assembled contigs of the metagenomes, suggesting that the identified Arcobacter strain is likely a commensalist, rather than a pathogen.

Arcobacter taxonomic marker genes and reads recruited to the Arcobacter SAGs were almost exclusively found in the 500 m poisoned trap metagenomes, where the SAGs were isolated (Figure 5). This may correspond to the preferred habitat depth of a host eukaryote. A possible candidate for a communalistic partner was identified in two assembled metagenomic contigs containing marker genes related to unicellular protists belonging to the order Collodaria (Biard et al., 2015) that, similar to the Arcobacter SAGs, primarily recruited metagenomic reads from the deep traps (Table S3). This organism has been suggested to be associated with carbon export (Guidi et al., 2015).

Vibrio

The two Vibrio SAGs clustered with *V. campbellii* affiliated with the *Vibrio harveyi* clade (Figures S4, S5), some strains of which are pathogens of crustacea (Ruwandepika et al., 2010). The level of genome synteny and shared gene content between the SAGs and reference genomes was high, with the SAGs aligning well to large, discrete parts of both the *V. campbellii* chromosomes and the plasmid NC_009777 (Figure S6). The SAGs were reflective of large genomes typical of copiotrophic organisms, having

TABLE 3 | Glycoside Hydrolases identified in the SAGs annotated in the carbohydrate-active enzymes database (CAZymes).

Glycoside hydrolase family	Substrate	SAGs
GH130	1,6-mannans	Actinomarina, Idiomarina, Kangiella, Vibrio
GH76	1,6-mannans	Idiomarina, Kangiella, SAR11clade, Vibrio
GH109	Acetylgalactosamine	Kangiella, SAR11clade
GH2	Aminosugars	Kangiella, SAR11clade, Vibrio
GH20	Aminosugars	Vibrio
GH5	Cellulose	Actinomarina, Idiomarina
GH9	Cellulose	Vibrio
GH18	Chitin	Actinomarina, Idiomarina, Kangiella, SAR11clade, Vibrio
GH53	Galactans and arabinogalactans	Arcobacter, Idiomarina, Kangiella, Vibrio
GH72	Glucans and galactans	Arcobacter, Idiomarina, Kangiella, SAR11clade, Vibrio
GH16	Glucans and galactans	Arcobacter, Idiomarina, Kangiella, Vibrio
GH3	Glucose, arabinose, xylose	Actinomarina, Idiomarina, Kangiella, Vibrio
GH1	Glucose, galactose	Actinomarina, Arcobacter, Idiomarina, Vibrio
GH84	Hyaluronic Acid	Actinomarina, Idiomarina, Kangiella, SAR11clade, Vibrio
GH99	Mannoses	Actinomarina, Idiomarina, Kangiella, Vibrio
GH92	Mannoses	Arcobacter, Idiomarina, Kangiella, SAR11clade, Vibrio
GH38	Mannoses	Arcobacter, Vibrio
GH47	Mannoses	Kangiella
GH73	Peptidoglycan	Actinomarina, Arcobacter, Idiomarina, SAR11clade, Vibrio
GH23	Peptidoglycan	Arcobacter, Idiomarina, Kangiella, SAR11clade, Vibrio
GH103	Peptidoglycan	Idiomarina, Kangiella, SAR11clade
GH33	Sialic acid	Kangiella, SAR11clade, Vibrio
GH13	Starch	Actinomarina, Idiomarina, Kangiella, Vibrio
GH15	Starch	Idiomarina
GH31	Starch	Kangiella, Vibrio
GH32	Sucrose and fructose containing polymers	Kangiella, SAR11clade, Vibrio
GH107	Unknown	Kangiella
GH24	Unknown	Vibrio
GH10	Xylan	Arcobacter, Idiomarina
GH12	Xyloglucan	Kangiella, Vibrio
GH39	Xylose	Arcobacter, Idiomarina, Kangiella, Vibrio
GH77	α -amylase	Vibrio
GH65	α -glucosidic linkages	Arcobacter, Idiomarina, Vibrio

low coding density and sizable intergenic regions (Figure 3, Table 2). The SAGs encoded peptide transporters (*oppABCD* and *sapACD*) and sugar transporters (*potABCD*, *proVWX*), as well as transporters of molybdate (*modABC*), phosphate (*pstABCS*), and zinc (*znuABC*). Chitin specific glycoside hydrolases and chitin-binding protein *cbpD* were also present in the Vibrio SAGs, consistent with their potential association

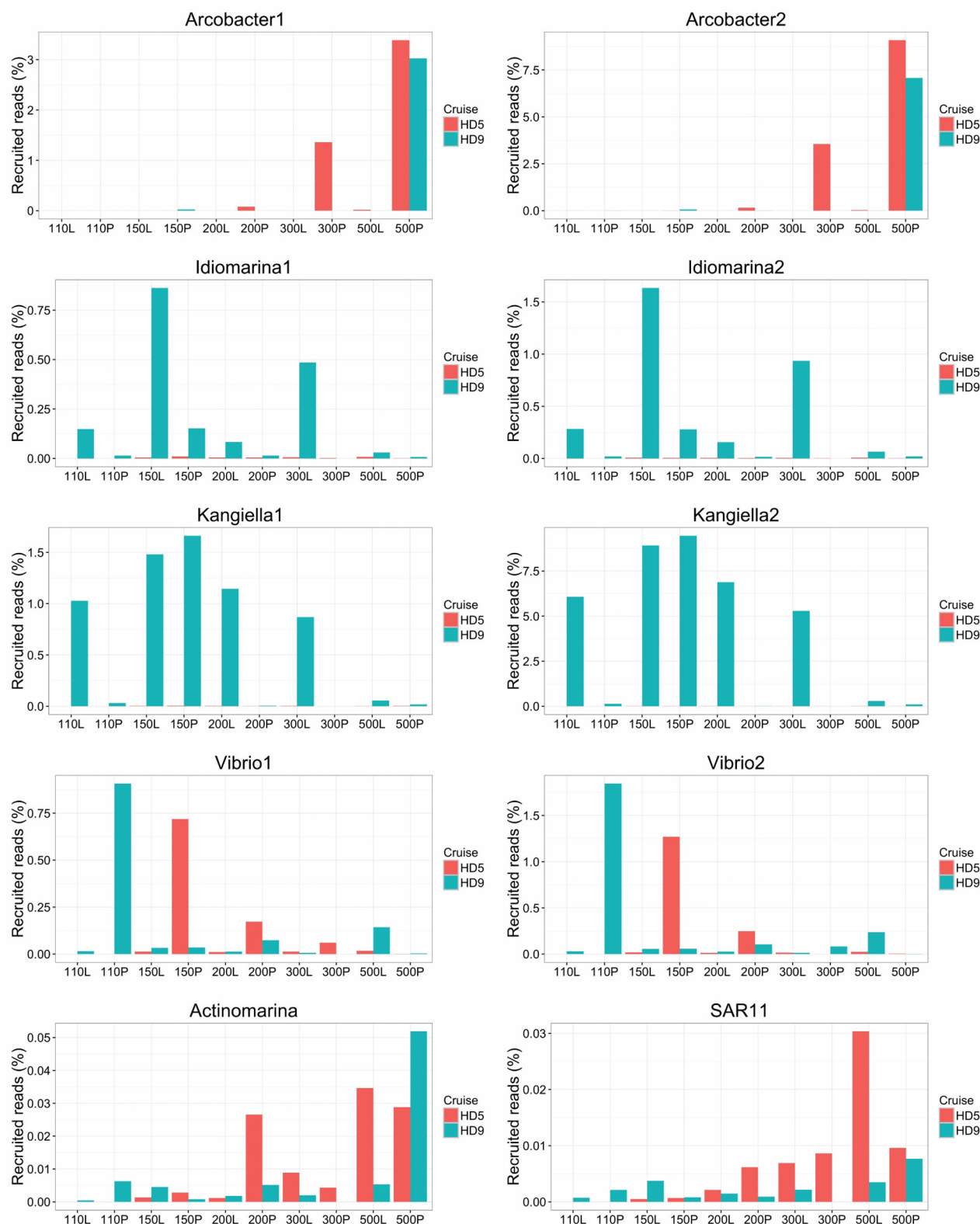


FIGURE 5 | Relative abundance of SAGs in the HD5 and HD9 traps. Percentage of blastn-recruited metagenomic bacterial reads with 99% identity and 200 bp cutoff. Percentage of recruited reads from poisoned and live traps were compared with ANOVA using traps of different depth and from different cruises as biological control. Deep and Shallow traps and traps from the two cruises, respectively, were compared in the same way. The Arcobacter SAGs were significantly divergent between traps of different treatment and depth and the kangiella traps were significantly divergent between traps of different cruises ($p < 0.05$).

with crustaceans. Other glycoside hydrolases with a predicted broad range for other substrates associated with eukaryotes (cellulose, starch, and xyloglucan), bacteria (peptidoglycan), and of general cellular origins (include glucose, mannose, and aminosugars; **Table 3**, Table S4) were also found. Components of the luminescence quorum sensing machinery (*luxOQRSU*) as well genes homologous to the *rtxA* toxin were present as well. In addition, the gene cysteine synthase (*cysK*), with a suggested role in biofilm formation, was also identified (Table S2; Singh et al., 2015).

The *Vibrio* SAGs recruited metagenomic reads mostly from the poisoned, shallow traps from which the SAGs were isolated (**Figure 5**). Although this trend was not statistically significant, it suggested a distribution limited by a eukaryotic host presence, most likely one of the arthropods that were found to be significantly enriched in poisoned traps (Table S1b). This pattern was only seen for reads recruited to the single cell genomes and not in the metagenomes on a taxonomic marker gene level, where *Vibrio* as a genus was not significantly enriched in any of the sediment traps (**Figure 2**, Table S1ab). This suggests that different *Vibrio* strains were present that were adapted to different ecological niches. This observation is obscured when all *Vibrio* sequence reads are treated cumulatively at the genus level, but can be seen at the higher resolution provided by the single cell genomes. In support of this observation, the diversity of metagenomic functional gene categories for *Vibrios* in the trap where the SAGs were isolated was larger than what was observed in both *Vibrio* SAGs along with the *V. campbellii* reference genome (**Figure 6**). In total, these observations suggested that there were multiple *Vibrio* strains present in the trap, with different sets of functional genes corresponding to different lifestyles.

Enriched Microbial Assemblages in the Live Traps

The live traps that contained only seawater (without fixative) were enriched in bacteria using nutrients released from the particles during degradation, that we refer to here as the “processed community.” Due to this enrichment, these traps had lower relative numbers of eukaryotes (and their associated viruses) compared to the initial community (**Figure 1**). The bacteria found here were dominated by known copiotrophic genera including *Alteromonas* and *Idiomarina*, their increased numbers resulting presumably from POM or DOM utilization (**Figure 2**). There were also presumptive hydrocarbon degraders *Alcanivorax* and *Methylophaga* that likely were enriched due to reduced carbon compounds associated with the particles. Live traps had fewer uniquely enriched gene suites than poisoned traps, corresponding probably to the lower relative abundance of eukaryotes and their associated microbial assemblages in these samples (**Figures 1, 2**). This was consistent with the greater amount of specifically enriched bacteria in processed traps, compared to poisoned traps (**Table 1**, Table S1ab). This likely reflects the smorgasbord of nutrients available for copiotrophic bacteria in the live traps as particles were processed. Enriched bacteria were present at high relative abundance, especially the

genus *Alteromonas* representing nearly one fifth of recovered sequences with similarity to homologs in the RefSeq database (**Figure 2**), likely reflecting a “bloom” caused by POM and DOM degradation and their accumulation in the live traps. Bacterial genes enriched in live traps included components of pathways for cellular interaction such as two-component systems for signal processing and antibiotics resistance and secretion (Table S1c). There were also genes for the sox sulfur oxidation system (K17224, K17226, K17227) and degradation of amino-acids, nucleotides, and aromatic compounds. Some of the identified iron transport genes were enriched in the live traps (K02014, K16091, K16088; Table S1c), reflecting specialized strategies for iron uptake. This provides further evidence that iron limitation may be strong selective agent for heterotrophic bacteria, as well as oxygenic phototrophs, in the ocean (Boiteau et al., 2016). Genes encoded by the *Idiomarina* and *Kangiella* SAGs were enriched primarily in the live traps (**Figure 4**), where they were significantly enriched also on a genus marker gene level (**Figure 2**).

Idiomarina

Idiomarina was first described as a deep-sea bacterium with particle-associated life style and protein metabolism as an important source of nutrients (Donachie et al., 2003; Hou et al., 2004), and representatives have since been found in other environments including shallow water and salterns (e.g., Poddar et al., 2014; León et al., 2015). Isolated *Idiomarina* strains are described as obligately aerobic and heterotrophic, which is generally consistent with the gene content found in the *Idiomarina* SAGs. The two *Idiomarina* SAGs had high similarity to described strains (99% 16S rRNA nucleotide identity), with a slightly larger genomic identity to the copiotrophic *I. loihensis* (Figures S4, S5). There was a high level of genome synteny, with the SAGs corresponding to large, discrete parts of the *I. loihensis* genome (Figure S6). The genomes were comparably dense, with short intergenic regions (**Figure 3**, **Table 2**). The trap-associated *Idiomarina* SAGs encoded a broad range of glycoside hydrolases, reflecting the DOM released during particle degradation, including putative substrates of both eukaryotic and bacterial origin (**Table 3**, Table S4). Similar to other *Idiomarina*, the genomes contained several genes for cell motility and chemotaxis, and also the transporters of phosphate (*pstABCs*) and iron(III) (*afuABC*) as well as the heme exporter *ccmABCD* which allows the cell to regulate the internal iron level (Table S2). The SAGs contained the secretion system *gspCDEFGHIJKL* as well as a Photoactive Yellow Protein (PYP) which has been suggested to be involved in depth adaptive biofilm formation (van Der Horst et al., 2009). However, none of the biofilm forming genes that were identified adjacent to the PYP gene in *I. loihensis* (Hou et al., 2004) were found in the SAGs, although some of them were present in six assembled contigs of the metagenomes, with highest coverage in the 150 m live trap from HD9 cruise where the *Idiomarina* SAGs were most common (Table S3). Some *Idiomarina* genotypes may also be degraders of high molecular weight DOM (McCarren et al., 2010). These findings suggest that *Idiomarina* in the ocean may associate with sinking particles initially via chemotaxis followed by biofilm

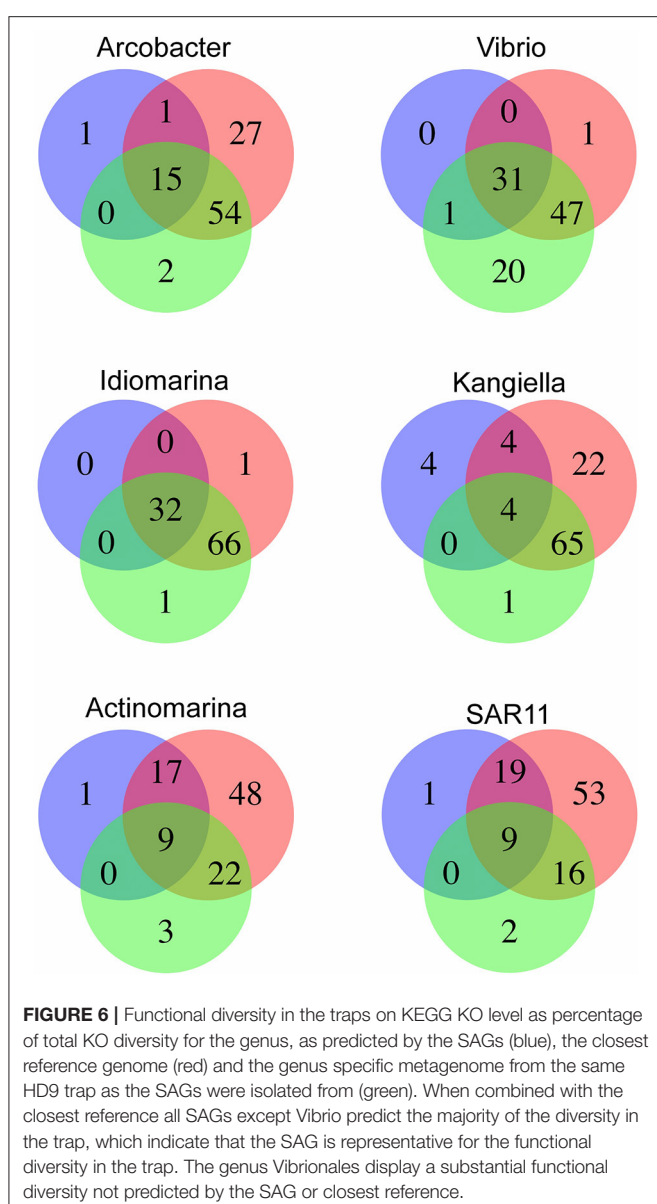


FIGURE 6 | Functional diversity in the traps on KEGG KO level as percentage of total KO diversity for the genus, as predicted by the SAGs (blue), the closest reference genome (red) and the genus specific metagenome from the same HD9 trap as the SAGs were isolated from (green). When combined with the closest reference all SAGs except Vibrio predict the majority of the diversity in the trap, which indicate that the SAG is representative for the functional diversity in the trap. The genus Vibrionales display a substantial functional diversity not predicted by the SAG or closest reference.

formation, and subsequently degrade DOM liberated from POM by other species.

Idiomarina marker genes in the metagenome were significantly enriched in live traps, and in traps from the HD9 cruise. A similar trend was seen by metagenomic reads recruited to the SAGs which were recruited mainly from live traps from most depths (except the deepest sampling point), with a higher fraction of reads recruited from the HD9 metagenomes compared to the HD5 metagenomes (Figure S7), although this trend was not statistically significant (Figure 5). Genes encoded by the Idiomarina SAGs on the other hand, did not show significant differences in abundance between cruises, suggesting a succession between different copiotrophic species with redundant function (Figure S7).

Kangiella

Kangiella are heterotrophic bacteria first isolated from tidal flats (Yoon et al., 2004). The two Kangiella SAGs form a sister clade to previously known species (Figures S4, S5), with a 96% 16S rRNA nucleotide identity to *K. koreensis* and large, discrete chunks of syntenic genomic regions (Figure S6). The SAGs were less dense than those of *Idiomarina*, with larger intergenic regions with a divergence between the two SAGs most likely explained by different genomic regions being recovered (Figure 3, Table 2). Similar to *Idiomarina*, the Kangiella SAGs contain multiple glycoside hydrolases with a broad substrate range (Table 3, Table S4). Kangiella are related to the hydrocarbon degrading Alcanivorax, but no such activity has been associated with Kangiella and no genes for hydrocarbon degradation have been identified. Kangiella has been reported to have the ability to degrade lignocellulose (Darjany et al., 2014) as well as algicidal activity (Shi et al., 2013), and there were genes annotated as toxins and antitoxins with potential algicidal activity in the SAGs, including the hemolycin *tlyC*. The Kangiella SAGs encode the peptide transporters *dppACDF*, the phosphate transporter *pstABCs* as well as the iron (III) transport protein *afuB* and the heme exporter *ccmABCD*. There were no genes for motility, either in the SAGs or in the genomes of related strains (Table S2), which is consistent with the non-motility of all known isolated Kangiella strains and the lack of motility genes in the reference genome (Han et al., 2009).

The Kangiella SAGs recruited metagenomic reads from most depths except the deepest sampling point, mostly from live but also from the 150 m poisoned trap (Figure 5). The Kangiella SAGs recruited significantly more reads from the HD9 than the HD5 traps. A similar pattern was seen in the metagenome where Kangiella taxonomic marker genes were significantly enriched in HD9 traps and live traps (Figure S2). The genes encoded by the Kangiella SAGs on an orthology level (KEGG), on the other hand are present in the metagenomes for both cruises with no significant difference in relative abundance (Figure S8, Table S1c). This suggests a succession between different species with redundant function between cruises, similar to what is hypothesized for *Idiomarina*.

These findings suggest a model for Kangiella's active role in particle degradation. The non-motile bacteria may be brought to the particles or hosts by Brownian motion and random encounter, and associate with them either as commensalists, or potentially as pathogens. They might then remain attached to sinking particles, accounting for their presence in both live and poisoned traps. As the particles degrade, the Kangiella might then proliferate growing on POM or released DOM.

Planktonic Microbial “Bycatch” in the Sediment Traps

Two of the SAGs (Actinomarina, SAR11 clade) had small predicted genome sizes and low abundance in the metagenome, which suggest planktonic life styles rather than direct association with the particles, and therefore their presence in the traps are thought to be caused by them being caught in the downdraft movement of the particles. Both these SAGs have small, compact

genomes which would be consistent with an oligotrophic rather than copiotrophic life style (**Figure 3**), although they did both contain multiple glycoside hydrolases which suggest at least partial adaption to the DOM released by degrading particles (**Table 3**, Table S4).

Actinomarina

The *Actinomarina* SAG was most closely related to single cell genomes isolated from marine environments with 99% 16S rRNA nucleotide identity (Figures S4, S5; Ghai et al., 2013), but no related strain has been cultivated nor complete reference genome yet published. The *Actinomarina* SAG coding density was high (**Figure 3**, **Table 2**) and included the amino acid transporter *livFGHKM*. The SAG also encoded a proteorhodopsin (PR) belonging to the MAC-cluster of previously described *Actinomarina* PRs, containing signature residues that suggest adaption to green light (Figure S9, Table S2, Fuhrman et al., 2008). The *Actinomarina* SAG recruited few reads in the metagenome but was slightly more common in deep traps (**Figure 5**).

SAR11 Clade

The SAR11 clade SAG that was sequenced shared high nucleotide identity with previously sequenced isolates (99% 16S rRNA nucleotide identity). The genome coding density was high (**Figure 3**, **Table 2**) and, similar to *Actinomarina*, encoded the *livFGHKM* amino acid transporter. The genome also contained genes for the sarcosine oxidase *soxABD* (Table S2), which has been noted to be upregulated under nitrogen limited conditions in related organisms (Smith et al., 2013). The SAG recruited few reads from the metagenomes, but appeared slightly more common in the deep traps (**Figure 5**).

Single Amplified Genomes as Models

The SAGs can serve as models of potential successional strategies that occur during sinking particle degradation. To estimate how representative they might be for trap microorganisms, the gene content of the SAGs was compared to that of the corresponding metagenomes. Genomic regions not recovered in the single cell genomes were compensated for by also comparing SAGs to their closest relative with a fully sequenced reference genome. The full genetic diversity of organisms that belong to the same genera as the SAGs in the samples were then estimated by isolating genera-specific reads from the metagenomes of the trap corresponding to the SAGs. The gene content of KEGG orthologous groups were predicted from these three datasets and compared (**Figure 6**).

Except for the *Vibrio* SAGs, most of the genes from the metagenome were also encoded by the SAGs, which suggest that there is low diversity of the genus in the trap and that the SAGs were reasonably representative of members of the trap bacterial community. The *Vibrio* genus on the other hand, displayed a greater diversity in the trap metagenomes than what was represented by the SAGs. The pathogenic life style suggested for the *Vibrio* SAGs might therefore not be the only ecological adaption for *Vibrio* in the traps, and further sampling would be required to obtain a larger genomic representation of *Vibrio* associated with sinking particles.

Depth Distributions of Microbes Captured by the Sediment Traps

When samples from different depths were compared, there were four genera of alpha and gammaproteobacteria significantly enriched in shallow compared to deep traps—*Acinetobacter*, *Ferrimonas*, *Maricaulis*, and *Pseudoalteromonas*. In deep traps, eight epsilonproteobacterial genera (mainly *Campylobacterales*) were enriched (Table S1ab). There was an overlap between groups enriched in deep and poisoned traps, contrasted to shallow and live, as well as an overlap between shallow and live traps (Figure S2). Interestingly, no such overlap was seen between groups enriched in deep and live traps, or shallow, and poisoned. Similarly, the deep, poisoned traps were enriched in Epsilonproteobacteria, mainly *Campylobacterales* (*Arcobacter*, *Nitratiruptor*, *Sulfuricurvum*, *Sulfurimonas*, and *Sulfurospirillum*) while the shallow, live traps were enriched in Alphaproteobacteria and Gammaproteobacteria (*Acinetobacter*, *Ferrimonas*, *Maricaulis*, and *Pseudoalteromonas*), suggesting a shift in either particle composition or bacterial recruitment as the particles move downwards in the water column. Only a small number of genes were significantly divergent in abundance between shallow and deep traps, including genes for aromatic degradation (K01821) and carbohydrate and nucleotide metabolism (K01846, K02293, K00619, K18284)—all of them enriched in deep traps (>300 m; Table S1c).

Difference between Cruises

Only five bacterial genera displayed differential representation on particles collected in the two different cruises. Four of them (*Brevundimonas*, *Herbaspirillum*, *Idiomarina*, and *Kangiella*; Table S1ab) were significantly enriched in the live traps as well as during the later cruise (HD9). In contrast, 16 of 18 Eukaryotic genera (Figure S2, Table S1ab), significantly enriched in the later cruise (HD9), were enriched in poisoned traps. This suggests a relatively stable bacterial system during the time frame of this study even as the eukaryotic community itself shifted.

DISCUSSION

Particles that sink to the dark ocean appear to be predominantly composed of eukaryotic biomass (Simon et al., 2002; Fontanez et al., 2015; Guidi et al., 2015). This may include the presence of fecal pellets, diatom aggregates, a variety of protists and their associated microflora, as well as non-organic components. Most recently, the Tara expedition has highlighted the association of both prokaryotes and viruses, as well as previously overlooked eukaryotic groups including Rhizaria, with carbon export and potentially sinking particles (Fontanez et al., 2015; Guidi et al., 2015).

Microbes attached to sinking particles in the upper water column have been suggested to be primarily recruited in the photic zone, so that particles collected at greater depths would be predicted to harbor microbes from photic zone, rather than in surrounding deep water. The recruitment of metagenomic reads to the SAGs appeared to be in general agreement at least for these upper mesopelagic samples, as we observed enrichment of

specific microbial communities in shallow live traps and deep poisoned traps, but no enrichment of specific groups in shallow poisoned traps or deep live traps.

In a simplified model the microbial assemblages on sinking particles may be affected mainly by recruitment in shallow water, and by microbes associated with depth-specific eukaryotes. The initial microbial assemblage of the shallow poisoned traps consisted of eukaryotic cells with their associated pathogens, predators, commensalists, and saprophytes (represented by *Vibrio* and *Kangiella*), as well as recruited motile copiotrophs (represented by *Idiomarina*). Correspondingly, the initial assemblage of the deep poisoned traps consisted of the same copiotrophs—recruited from the photic zone—but also along with a set of unique depth-specific eukaryotic associated microbes (represented by *Arcobacter*).

The above model may explain why no bacterial groups were specifically enriched in the live, deep traps. The particle-enriched assemblage in these traps was expected to be seeded by copiotrophs recruited in shallow depths, and therefore not be unique for either depth. In addition, bacteria enriched in the deep, poisoned trap appear associated with eukaryotes specifically adapted to these depths, as exemplified by *Arcobacter*, rather than having been transported from the photic zone.

Particles are hotspots for microbial life in the deep ocean, and the lifestyles represented by the trap associated microbial assemblage genes and genomes demonstrate some of their important adaptations to this environment. The *Arcobacter* and *Vibrio* SAG data seemed to indicate they were eukaryotic-associated and adapted to specific depths, most likely dictated by the preference of their host(s). *Arcobacter* was apparently a commensalist, and *Vibrio* either a commensalist or possibly a pathogen, with genes encoding both toxins, quorum sensing and chitinase. Both strains were present in both cruises in relatively high numbers in the initial community, but were rapidly outcompeted by generalist copiotrophs as the particles were processed. *Idiomarina* spp., appeared as copiotrophs present in live traps at several depths of the water column, potentially migrating to particles via chemotaxis. In contrast, *Kangiella* spp., were presumably non-motile and seemed to be present in both the initial as well as processed assemblages. They may possibly act as both as a non-specific pathogens (given their encoded toxins), and as saprophytes. The Actinomarina and SAR11 clade SAGs with small, dense genomes, were not significantly enriched by the presence of the particles generally consistent with their presumptive planktonic lifestyles.

REFERENCES

- Allen, A. E., Allen, L. Z., and McCrow, J. P. (2013). Lineage specific gene family enrichment at the microscale in marine systems. *Curr. Opin. Microbiol.* 16, 605–617. doi: 10.1016/j.mib.2013.10.001
- Bankevich, A., Nurk, S., Antipov, D., Gurevich, A. A., Dvorkin, M., Kulikov, A. S., et al. (2012). SPAdes: a new genome assembly algorithm and its applications to single-cell sequencing. *J. Comput. Biol.* 19, 455–477. doi: 10.1089/cmb.2012.0021
- Biard, T., Pillet, L., Decelle, J., Poirier, C., Suzuki, N., and Not, F. (2015). Towards an integrative morpho-molecular classification of the Collodaria

The combination of SAG and metagenome data we used proved useful for gaining a deeper perspective on microorganisms inhabiting and degrading sinking particles. The distributions and gene contents of the *Arcobacter*, *Idiomarina*, and *Kangiella* SAGs suggested some of their functional roles on particulates. Our findings corroborate and extend an earlier study, where the importance of eukaryotes for determining the initial microbial community of sinking particles was proposed (Fontanez et al., 2015). Specific ecological strategies for particle processing were indicated by single cell genomes of *Arcobacter*, *Vibrio*, *Idiomarina*, and *Kangiella*, furthering our knowledge of bacterial processes and succession on sinking particles in the open ocean.

AUTHOR CONTRIBUTIONS

EP, KF, and ED designed research. EP sequenced and analyzed single cell genomes and analyzed metagenomes. KF designed sediment traps and sequenced metagenomes as well as performed initial metagenomic analysis. EP, KF, and ED wrote the paper.

ACKNOWLEDGMENTS

We thank the captain and crew of the R/V Kilo Moana for their expert assistance at sea, Tara Clemente for assistance deploying and processing sediment traps, HOE-DYLAN chief scientist Sam Wilson, and Oscar Sosa for collecting some of the sediment trap samples. This work was supported by grants from the Simons Foundation (#329108 to ED), the Gordon and Betty Moore Foundation #3777 (to ED), a gift from the Agouron Institute (AI-M09.12.1) to ED, and National Science Foundation Science and Technology Center grant, Center for Microbial Oceanography, Research and Education EF0424599. KF was also supported by a NSF Postdoctoral Research Fellowship in Biology DBI-1202684. EP was supported by funds from the Swedish Research Council (grant 2012-6584). This work is a contribution of the Center for Microbial Oceanography: Research and Education (CMORE) and the Simons Collaboration on Ocean Processes and Ecology.

SUPPLEMENTARY MATERIAL

The Supplementary Material for this article can be found online at: <https://www.frontiersin.org/articles/10.3389/fmicb.2017.02269/full#supplementary-material>

(Polycystinea, Radiolaria). *Protist* 166, 374–388. doi: 10.1016/j.protis.2015.05.002

- Boiteau, R. M., Mende, D. R., Hawco, N. J., McIlvin, M. R., Fitzsimmons, J. N., Saito, M. A., et al. (2016). Siderophore-based microbial adaptations to iron scarcity across the eastern Pacific Ocean. *Proc. Natl. Acad. Sci. U.S.A.* 113, 14237–14242. doi: 10.1073/pnas.1608594113
- Chen, F., Mackey, A. J., Stoeckert, C. J., Roos, D. S. (2006). OrthoMCL-DB: querying a comprehensive multi-species collection of ortholog groups. *Nucleic Acids Res.* 34, D363–D368. doi: 10.1093/nar/gkj123

- Choe, H., Kim, S., Oh, J., Nasir, A., Kim, B. K., and Kim, K. M. (2015). Complete genome of *Kangiella geojeodonensis* KCTC 23420T, putative evidence for recent genome reduction in marine environments. *Mar. Genomics* 24, 215–217. doi: 10.1016/j.margen.2015.05.015
- Criscuolo, A., and Gribaldo, S. (2010). BMGE (Block Mapping and Gathering with Entropy): a new software for selection of phylogenetic informative regions from multiple sequence alignments. *BMC Evol. Biol.* 10:210. doi: 10.1186/1471-2148-10-210
- Cuccuru, G., Orsini, M., Pinna, A., Sbardellati, A., Soranzo, N., Travaglione, A., et al. (2014). Orione, a web-based framework for NGS analysis in microbiology. *Bioinformatics* 30, 1928–1929. doi: 10.1093/bioinformatics/btu135
- Darjany, L. E., Whitcraft, C. R., and Dillon, J. G. (2014). Lignocellulose-responsive bacteria in a southern California salt marsh identified by stable isotope probing. *Front. Microbiol.* 5:263. doi: 10.3389/fmicb.2014.00263
- de Vargas, C., Audic, S., Henry, N., Decelle, J., Mahe, F., Logares, R., et al. (2015). Eukaryotic plankton diversity in the sunlit ocean. *Science* 348:1261605. doi: 10.1126/science.1261605
- DeLong, E. F., Franks, D. G., and Alldredge, A. L. (1993). Phylogenetic diversity of aggregate-attached vs. free-living marine bacterial assemblages. *Limnol. Oceanogr.* 38, 924–934. doi: 10.4319/lo.1993.38.5.0924
- Donachie, S. P., Hou, S., Gregory, T. S., Malahoff, A., and Alam, M. (2003). *Idiomarina loihiensis* sp. nov., a halophilic γ -proteobacterium from the Lo'ihii submarine volcano, Hawai'i. *Int. J. Syst. Evol. Microbiol.* 53, 1873–1879. doi: 10.1099/ijss.0.02701-0
- Doudah, L., de Zutter, L., Baré, J., De Vos, P., Vandamme, P., Vandenberg, O., et al. (2012). Occurrence of putative virulence genes in Arcobacter species isolated from humans and animals. *J. Clin. Microbiol.* 50, 735–741. doi: 10.1128/JCM.05872-11
- Edgar, R. C. (2010). Search and clustering orders of magnitude faster than BLAST 26, 2460–2461. doi: 10.1093/bioinformatics/btq461
- Fontanez, K. M., Eppley, J. M., Samo, T. J., Karl, D. M., and DeLong, E. F. (2015). Microbial community structure and function on sinking particles in the North Pacific Subtropical Gyre. *Front. Microbiol.* 6:469. doi: 10.3389/fmicb.2015.00469
- Fuhrman, J. A., Schwalbach, M. S., and Stingl, U. (2008). Proteorhodopsins: an array of physiological roles? *Nat. Rev. Microbiol.* 6, 488–494. doi: 10.1038/nrmicro1893
- Ghai, R., Mizuno, C. M., Picazo, A., Camacho, A., and Rodriguez-Valera, F. (2013). Metagenomics uncovers a new group of low GC and ultra-small marine Actinobacteria. *Sci. Rep.* 3:2471. doi: 10.1038/srep02471
- Giovannoni, S. J., Tripp, H. J., Givan, S., Podar, M., Vergin, K. L., Baptista, D., et al. (2015). Genome streamlining in a cosmopolitan oceanic bacterium. *Science* 309, 1242–1245. doi: 10.1126/science.1114057
- Grossart, H. P. (2010). Ecological consequences of bacterioplankton lifestyles: changes in concepts are needed. *Environ. Microbiol. Rep.* 2, 706–714. doi: 10.1111/j.1758-2229.2010.00179.x
- Guidi, L., Chaffron, S., Bittner, L., Eveillard, D., Larhlimi, A., Roux, S., et al. (2015). Plankton networks driving carbon export in the oligotrophic ocean. *Nature* 532, 465–470. doi: 10.1038/nature16942
- Gurevich, A., Saveliev, V., Vyahhi, N., and Tesler, G. (2013). QUAST: Quality assessment tool for genome assemblies. *Bioinformatics* 29, 1072–1075. doi: 10.1093/bioinformatics/btt086
- Hamann, E., Gruber-Vodicka, H., Kleiner, M., Tegetmeyer, H. E., Riedel, D., Littmann, S., et al. (2016). Environmental Breviatea harbour mutualistic *Arcobacter epibionts*. *Nat. Adv.* 534, 254–258. doi: 10.1038/nature18297
- Han, C., Sikorski, J., Lapidus, A., Nolan, M., Glavina Del Rio, T., Tice, H., et al. (2009). Complete genome sequence of *Kangiella koreensis* type strain (SW-125). *Stand. Genomic Sci.* 1, 226–233. doi: 10.4056/sigs.36635
- Honjo, S., Manganini, S. J., Krishfield, R. A., and Francois, R. (2008). Particulate organic carbon fluxes to the ocean interior and factors controlling the biological pump: a synthesis of global sediment trap programs since 1983. *Prog. Oceanogr.* 76, 217–285. doi: 10.1016/j.pocean.2007.11.003
- Hou, S., Saw, J. H., Lee, K. S., Freitas, T. A., Belisle, C., Kawarabayasi, Y., et al. (2004). Genome sequence of the deep-sea gamma-proteobacterium *Idiomarina loihiensis* reveals amino acid fermentation as a source of carbon and energy. *Proc. Natl. Acad. Sci. U.S.A.* 101, 18036–18041. doi: 10.1073/pnas.0407638102
- Jiao, N., Herndl, G. J., Hansell, D. A., Benner, R., Kattner, G., Wilhelm, S. W., et al. (2010). Microbial production of recalcitrant dissolved organic matter: long-term carbon storage in the global ocean. *Nat. Rev. Microbiol.* 8, 593–599. doi: 10.1038/nrmicro2386
- Kalenitchenko, D., Dupraz, M., Le Bris, N., Petetin, C., Rose, C., West, N. J., et al. (2016). Ecological succession leads to chemosynthesis in mats colonizing wood in sea water. *ISME J.* 10, 2246–2258. doi: 10.1038/ismej.2016.12
- Katoh, K., and Standley, D. M. (2013). MAFFT multiple sequence alignment software version 7: improvements in performance and usability. *Mol. Biol. Evol.* 30, 772–780. doi: 10.1093/molbev/mst010
- León, M. J., Martínez-Checa, F., Ventosa, A., and Sánchez-Porro, C. (2015). *Idiomarina aquatica* sp. nov., a moderately halophilic bacterium isolated from salterns. *Int. J. Syst. Evol. Microbiol.* 65, 4595–4600. doi: 10.1099/ijsem.0.000619
- Lohse, M., Bolger, A. M., Nagel, A., Fernie, A. R., Lunn, J. E., Stitt, M., et al. (2012). RobiNA: A user-friendly, integrated software solution for RNA-Seq-based transcriptomics. *Nucleic Acids Res.* 40, 622–627. doi: 10.1093/nar/gks540
- Lombard, V., Golaconda Ramulu, H., Drula, E., Coutinho, P. M., and Henrissat, B. (2014). The carbohydrate-active enzymes database (CAZy) in 2013. *Nucleic Acids Res.* 42, 490–495. doi: 10.1093/nar/gkt1178
- Love, M. I., Huber, W., and Anders, S. (2014). Moderated estimation of fold change and dispersion for RNA-seq data with DESeq2. *Genome Biol.* 15:550. doi: 10.1186/s13059-014-0550-8
- McCarren, J., Becker, J. W., Repeta, D. J., Shi, Y., Young, C. R., Malmstrom, R. R., et al. (2010). Microbial community transcriptomes reveal microbes and metabolic pathways associated with dissolved organic matter turnover in the sea. *Proc. Natl. Acad. Sci. U.S.A.* 107, 16420–16427. doi: 10.1073/pnas.1010732107
- McMurdie, P. J., and Holmes, S. (2013). Phyloseq: An R Package for reproducible interactive analysis and graphics of microbiome census data. *PLoS ONE* 8:61217. doi: 10.1371/journal.pone.0061217
- Nguyen, L. T., Schmidt, H. A., Von Haeseler, A., and Minh, B. Q. (2015). IQ-TREE: a fast and effective stochastic algorithm for estimating maximum-likelihood phylogenies. *Mol. Biol. Evol.* 32, 268–274. doi: 10.1093/molbev/msu300
- Oksanen, J., Blanchet, F. G., Friendly, M., Kindt, R., Legendre, P., McGlinn, D., et al. (2016). *vegan: Community Ecology Package. R package version 2.4–1*. Available online at: <http://CRAN.R-project.org/package=vegan>
- Poddar, A., Lepcha, R. T., Mukherjee, D., Bhattacharyya, D., and Das, S. K. (2014). Comparative analysis of 16S rRNA signature sequences of the genus *Idiomarina* and *Idiomarina woeseli* sp. nov., a novel marine bacterium isolated from the Andaman Sea. *Res. Microbiol.* 165, 501–507. doi: 10.1016/j.resmic.2014.07.008
- Rinke, C., Schwientek, P., Sczyrba, A., Ivanova, N. N., Anderson, I. J., Cheng, J.-F., et al. (2013). Insights into the phylogeny and coding potential of microbial dark matter. *Nature* 499, 431–437. doi: 10.1038/nature12352
- Ruwandepika, H. A., Defoirdt, T., Bhowmick, P. P., Shekar, M., Bossier, P., and Karunasagar, I. (2010). Presence of typical and atypical virulence genes in *Vibrio* isolates belonging to the Harveyi clade. *J. Appl. Microbiol.* 109, 888–899. doi: 10.1111/j.1365-2672.2010.04715.x
- Seemann, T. (2014). Prokka: rapid prokaryotic genome annotation. *Bioinformatics* 30, 2068–2069. doi: 10.1093/bioinformatics/btu153
- Shi, R., Huang, H., Qi, Z., Hu, W., Tian, Z., and Dai, M. (2013). Algicidal activity against *Skeletonema costatum* by marine bacteria isolated from a high frequency harmful algal blooms area in southern Chinese coast. *World J. Microbiol. Biotechnol.* 29, 153–162. doi: 10.1007/s11274-012-1168-1
- Simon, M., Grossart, H. P., Schweitzer, B., and Ploug, H. (2002). Microbial ecology of organic aggregates in aquatic ecosystems. *Aquat. Microb. Ecol.* 28, 175–211. doi: 10.3354/ame028175
- Singh, P., Brooks, J. F., Ray, V. A., Mandel, M. J., and Visick, K. L. (2015). CysK plays a role in biofilm formation and colonization by *Vibrio fischeri*. *Appl. Environ. Microbiol.* 81, 5223–5234. doi: 10.1128/AEM.00157-15
- Smith, D. P., Thrash, J. C., Nicora, C. D., Lipton, M. S., Burnum-Johnson, K. E., Carini, P., et al. (2013). Proteomic and transcriptomic analysis of *candidatus pelagibacter ubique* describe the first P II -independent response to nitrogen limitation in a free-living alphaproteobacterium. *MBio* 4, 1–11. doi: 10.1128/mBio.00133-12
- van Der Horst, M. A., Stalcup, T. P., Kaledhonkar, S., Kumauchi, M., Hara, M., Xie, A., et al. (2009). Locked chromophore analogs reveal that photoactive yellow protein regulates biofilm formation in the deep sea bacterium *Idiomarina loihiensis*. *J. Am. Chem. Soc.* 131, 17443–17451. doi: 10.1021/ja9057103

- Woyke, T., Xie, G., Copeland, A., González, J. M., Han, C., Kiss, H., et al. (2009). Assembling the marine metagenome, one cell at a time. *PLoS ONE* 4:e5299. doi: 10.1371/journal.pone.0005299
- Yoon, J. H., Oh, T. K., and Park, Y. H. (2004). *Kangiella koreensis* gen. nov., sp. nov. and *Kangiella aquimarina* sp. nov., isolated from a tidal flat of the Yellow Sea in Korea. *Int. J. Syst. Evol. Microbiol.* 54, 1829–1835. doi: 10.1099/ijss.0.63156-0
- Zhang, Z., Schwartz, S., Wagner, L., and Miller, W. (2000). A greedy algorithm for aligning DNA sequences. *J. Comput. Biol.* 7, 203–214. doi: 10.1089/10665270050081478

Conflict of Interest Statement: The authors declare that the research was conducted in the absence of any commercial or financial relationships that could be construed as a potential conflict of interest.

Copyright © 2017 Pelve, Fontanez and DeLong. This is an open-access article distributed under the terms of the Creative Commons Attribution License (CC BY). The use, distribution or reproduction in other forums is permitted, provided the original author(s) or licensor are credited and that the original publication in this journal is cited, in accordance with accepted academic practice. No use, distribution or reproduction is permitted which does not comply with these terms.



Differential Responses of Eukaryotic Phytoplankton to Nitrogenous Nutrients in the North Pacific Subtropical Gyre

Yoshimi M. Rii^{1,2†}, **Robert R. Bidigare**^{2,3} and **Matthew J. Church**^{1,2*}

¹ Department of Oceanography, University of Hawaii at Mānoa, Honolulu, HI, United States, ² Daniel K. Inouye Center for Microbial Oceanography: Research and Education, University of Hawaii at Mānoa, Honolulu, HI, United States, ³ Hawaii Institute of Marine Biology, University of Hawaii at Mānoa, Kāne'ohe, HI, United States

OPEN ACCESS

Edited by:

Alison Buchan,
University of Tennessee, Knoxville,
United States

Reviewed by:

Jun Sun,
Tianjin University of Science and
Technology, China
Anne W. Thompson,
Portland State University,
United States

*Correspondence:

Matthew J. Church
matt.church@umontana.edu

†Present Address:

Yoshimi M. Rii,
Hawaii Institute of Marine Biology,
University of Hawaii at Mānoa,
Kāne'ohe, HI, United States
Matthew J. Church,
Flathead Lake Biological Station,
University of Montana, Polson, MT,
United States

Specialty section:

This article was submitted to
Aquatic Microbiology,
a section of the journal
Frontiers in Marine Science

Received: 31 October 2017

Accepted: 06 March 2018

Published: 21 March 2018

Citation:

Rii YM, Bidigare RR and Church MJ (2018) Differential Responses of Eukaryotic Phytoplankton to Nitrogenous Nutrients in the North Pacific Subtropical Gyre. *Front. Mar. Sci.* 5:92.
doi: 10.3389/fmars.2018.00092

Fixed inorganic nitrogen (N) is persistently scarce in the well-lit regions of the subtropical ocean gyres and its supply plays an important role in controlling phytoplankton productivity. In a series of experiments conducted in the North Pacific Subtropical Gyre (NPSG), we examined changes in primary productivity and eukaryotic phytoplankton community structure in response to additions of nitrate (NO_3^-), ammonium (NH_4^+), or urea in conjunction with phosphate and silicic acid. Overall, we observed large increases in rates of ^{14}C -primary productivity (~2- to 27-fold) and concentrations of chlorophyll a (~2- to 7-fold) following N addition. Much of the physiological response was due to larger (>3 μm) phytoplankton, whose contributions to primary productivity increased ~2-fold while picophytoplankton (0.2–3 μm) contributions decreased by a similar proportion. Five experiments, conducted in the spring, summer and winter, revealed apparent seasonally-dependent responses in phytoplankton community structure to N availability. During the summer, pennate diatoms increased significantly following N addition as evidenced by both photosynthetic pigment analyses and high-throughput sequencing of 18S rDNA. For example, following the addition of N substrates, concentrations of fucoxanthin (a diatom pigment biomarker) increased between 23- and 49-fold, and relative abundances of rRNA genes belonging to *Pseudo-nitzschia* increased from negligible (~0.3%) to 30–60% of the >3 μm phytoplankton assemblage. However, unlike the diatom-driven responses observed in the summer, experiments conducted in the spring and winter demonstrated large increases in concentrations of 19'-butanoyloxyfucoxanthin (a pelagophyte pigment biomarker) together with increases in the relative abundance of rRNA genes clustering among *Pelagomonas*. Overall, our findings revealed differences in the responses of major taxa during experiments conducted in different times of the year, with concomitant impacts on patterns of phytoplankton diversity. In addition, the overall responses in chlorophyll a, ^{14}C -primary production, and eukaryotic phytoplankton community composition appeared largely independent of the type of N substrate added. Our results highlight seasonal-scale differences on the role of N availability in shaping eukaryotic phytoplankton diversity in the surface waters of the oligotrophic NPSG.

Keywords: nitrogen, nitrate, ammonium, phytoplankton, eukaryotes, picoeukaryotes

INTRODUCTION

In oligotrophic marine ecosystems such as the North Pacific Subtropical Gyre (NPSG), less than 10% of organic matter produced is exported out of the euphotic zone as sinking particles, implying rapid organic matter turnover and nutrient remineralization (Karl et al., 1996). Such low organic matter export in these regions has been attributed to the restricted supply of inorganic nutrients such as nitrogen (N) and phosphorus (P) to the euphotic zone (Karl, 2002; Arrigo, 2005). Concentrations of nitrate + nitrite ($\text{N}+\text{N}$) and ammonium (NH_4^+) in the near-surface waters of the NPSG are typically <5 and $<50\text{ nM}$, respectively (Wada and Hattori, 1990; Karl et al., 2001). Hence, competition for limiting N could be central to structuring the productivity and diversity of planktonic communities in this ecosystem.

N availability in the euphotic zone of the NPSG varies on seasonal, event-, to interannual scales, exerting important control on plankton community succession, primary productivity, and particulate matter export in this oligotrophic habitat. Seasonal variability of nutrients in the euphotic zone is partly controlled by variations in the penetration of light. For example, the flux of light penetrating to the dimly lit regions of the euphotic zone varies seasonally, and as a result, nitrate (NO_3^-) concentrations accumulate during the winter (Letelier et al., 2004). The accumulated nutrients are subsequently consumed when the flux of light to the lower euphotic zone increases during the spring (Letelier et al., 2004). Additionally, episodic to seasonal-scale supply of NO_3^- to the lower euphotic zone can occur through convective mixing and displacement of isopycnal surfaces due to mesoscale processes such as eddies and planetary waves (Dandonneau et al., 2003; Sakamoto et al., 2004; Johnson et al., 2010). In addition, activities of N_2 -fixing microorganisms increase during the warm, stratified summer months (Church et al., 2009), increasing concentrations of dissolved organic N and NH_4^+ in the surface waters (Karl et al., 1992, 1997).

Although picoplanktonic cyanobacteria are dominant contributors to biomass and rates of gross primary production in oligotrophic ocean ecosystems (Campbell et al., 1994; Karl, 1999; Karl and Church, 2017), eukaryotic phytoplankton play central roles in controlling material export, net community production, and nutrient cycling in these ecosystems (Benitez-Nelson et al., 2007; Juranek et al., 2012; Alexander et al., 2015). In the NPSG, analyses of photosynthetic pigment concentrations and quantification of cell abundances (by both microscopy and flow cytometry) has revealed that major taxa of eukaryotic phytoplankton distributed throughout the upper ocean include diatoms, haptophytes, pelagophytes, and dinoflagellates (Bienfang and Szyper, 1981; Campbell and Vaulot, 1993; Venrick, 1997; Cortés et al., 2001). Moreover, distributions and abundances of these eukaryotic phytoplankton are temporally and spatially variable, fluctuating in response to physical and chemical changes to the upper ocean habitat. For example, sampling of two cyclonic eddies with varying rates of nutrient input (as a result of spin-up duration) in the oligotrophic waters southwest of the Hawaiian islands revealed disparities in major eukaryotic phytoplankton response within

each eddy, with subsequent consequences in food web structure and carbon export (Benitez-Nelson et al., 2007; Rii et al., 2008). Additionally, observations at Station ALOHA to the north of the Hawaiian islands have highlighted the important role of diatoms in regulating carbon export (Karl et al., 2012). Notably, peaks in diatom-driven export coincides with summertime periods when rates of N_2 fixation and biomass of N_2 -fixing cyanobacteria are elevated (Dore et al., 2008; Villareal et al., 2011; Karl et al., 2012).

Past studies have demonstrated preferential uptake of NH_4^+ relative to NO_3^- by phytoplankton, a finding hypothesized to reflect the energetic savings in assimilating reduced forms of N (e.g., Eppley et al., 1977; Dortch, 1990). However, various field-based studies have concluded that cyanobacteria and eukaryotic phytoplankton in the oligotrophic oceans may rely on different forms of N to support their growth (Fawcett et al., 2011; Shilova et al., 2017). Such results highlight the potential role for different forms of N in controlling time-varying phytoplankton community structure. To date, however, there is limited information available on how different taxa of phytoplankton respond to changes in the availability and form of N substrates.

In the current study, we experimentally examined responses in upper ocean primary productivity and eukaryotic phytoplankton community structure to N enrichments at Station ALOHA. In five separate experiments, natural seawater plankton communities were treated with additions of NO_3^- or NH_4^+ (or urea in one experiment) and sampled daily over a 120- to 144-hour period. We sought to determine which eukaryotic phytoplankton assemblages responded to the additions of nitrogenous substrates and over what time-scales, providing insight into how variations in the availability of nitrogenous nutrients contribute to variability in phytoplankton community structure and growth in the euphotic zone of oligotrophic subtropical gyres.

MATERIALS AND METHODS

Experimental Design

Experiments were conducted between July 2011 and April 2013 during five research cruises to Station ALOHA (22.75°N , 158°W), the well-characterized study site of the Hawaii Ocean Time-series (HOT) program (Karl and Lukas, 1996). Sampling occurred during HOT 233 (July 2011; “NvN1”), HOT 240 (March 2012; “NvN2”), HOE-DYLAN V (July 2012; “NvN3”), HOT 248 (December 2012; “N248”), and HOT 251 (April 2013; “NvN4”) aboard the R/V *Kilo Moana* (Table 1). Seawater was collected in 12-L polyvinylchloride bottles affixed to a 24-bottle rosette sampler equipped with a Sea-Bird 911+ conductivity, temperature, and pressure sensors. Nine 20-L polycarbonate carboys were filled with seawater from 25 m that was pre-filtered from the rosette sampler through a Nitex screen (mesh size $\sim 202\text{ }\mu\text{m}$) to exclude larger zooplankton. Three carboys received additions of NO_3^- (target $2.8\text{ }\mu\text{M}$ N final concentration as NaNO_3) and three carboys received additions of NH_4^+ (target $2.8\text{ }\mu\text{M}$ N final concentration as NH_4Cl). All carboys, including three “Control” carboys, received additions of phosphate (PO_4^{3-} ; target $\sim 0.2\text{ }\mu\text{M}$ P final concentration as KH_2PO_4) and silicic

TABLE 1 | Dates, cruise ID, duration, sea surface temperature (SST), mixed layer depth (MLD), and day length when each experiment was conducted.

Parameter	Experiment				
	NvN1	NvN2	NvN3	N248	NvN4
Dates	22–27 Jul 2011	27 Mar–1 Apr 2012	11–17 Jul 2012	7–13 Dec 2012	9–14 Apr 2013
Cruise ID	HOT 233	HOT 240	HD 5 [‡]	HOT 248	HOT 251
Exp. duration (h)	120	120	144	144	120
SST (°C)	25.3	23.0	24.8	24.8	22.7
MLD (m)	78 ± 9	36 ± 6	58 ± 13	92 ± 11	77 ± 28
Day length (hh:mm)*	13:11	12:14	13:23	10:50	12:20
PROPERTIES AT 25 m					
PAR (mol quanta m ⁻² d ⁻¹)	12.6	n/a	n/a	3.6	11.0
Chl <i>a</i> (ng L ⁻¹)	65.0	77.0	81.6	111.4	68.0
N+N (nM N)	3.0	4.2	2.0	3.5	4
PO ₄ ³⁻ (nM P)	90	89	60	91	70
Si(OH) ₄ (nM Si)	1,050	1,159	850	1,122	1,210
SAMPLES COLLECTED†					
Nutrients	+ [‡]	+	+	+	+
Chl <i>a</i> / Sz fx Chl <i>a</i>	+/-	-/-	+/-	-/+	++
Pigments / FCM	-/+	-/+	+/-	-/+	+/+
¹⁴ C-PP	-	+	+	+	+
DNA	+	+	+	+	+

Measurements of downwelling PAR and concentrations of chlorophyll *a* (Chl *a*), nitrate + nitrite (N+N), phosphate (PO₄³⁻), and silicic acid (Si(OH)₄) at 25 m are also shown. Samples collected for each experiment are also indicated.

n/a, not available.

*Day length obtained from www.solartopo.com.

†Nutrients = N+N, NH₄⁺, PO₄³⁻, and Si(OH)₄; Sz fx Chl *a* = Size-fractionated chlorophyll *a*; FCM = flow cytometric cell abundances; ¹⁴C-PP = ¹⁴C-primary production.

‡Symbols designate whether samples were collected ("+" or not collected ("−") for subsequent analyses during each experiment.

[‡]HOE-DYLAN V.

acid (Si(OH)₄; target 2.8 μM Si final concentration as Na₂SiO₃) to achieve a final N:P:Si stoichiometric ratio of 14:1:14 in the treatment carboys, similar to the stoichiometry of these nutrients in the sub-euphotic zone (~300 m) waters at Station ALOHA (**Table 2**). For the experiment conducted in December 2012 (N248), the setup was identical to that described above except 10-L carboys were used and three additional carboys were enriched with urea [target 2.8 μM N final concentration as CO(NH₂)₂]. All carboys were incubated for 120–144 h and subsampled at approximately daily timescales throughout the experiment (**Table 1**). All sampling was conducted before sunrise in order to allow primary productivity measurements to span the full photoperiod. Incubators used for the experiments were covered with blue Plexiglas filters shaded to 50% of the surface photosynthetic active radiation (PAR). Temperature and solar irradiance levels were monitored continuously throughout the experiment using a waterproof temperature/light logger (HOBO Pendant® UA-002-08). Accompanying physical and biogeochemical properties at the time of sampling for these experiments were obtained from the HOT program database (<http://hahana.soest.hawaii.edu/hot/hot-dogs/>).

Nutrient Analyses

Nutrient samples were collected at each time point in 125- or 500-mL acid-washed high density polyethylene (HDPE) bottles and frozen upright at −20°C until analyzed. Concentrations of

N+N, PO₄³⁻, and Si(OH)₄ were determined using a 3-channel, Bran+Luebbe AA III™ continuous segmented flow autoanalyzer (Armstrong et al., 1967; Bernhardt and Wilhelms, 1967; Atlas et al., 1971). Detection limits for the instrumental settings used, defined as the lowest resolvable concentrations for each analysis, were 58 nM N+N, 14 nM PO₄³⁻, and 13 nM Si(OH)₄. NH₄⁺ concentrations were determined on a hybrid SEAL AA III coupled with a 2 m liquid waveguide capillary detection cell with modified chemistry and an indo-phenol blue reaction (Li et al., 2005). The limit of detection for this method was 4 nM NH₄⁺.

¹⁴C-Based Rates of Primary Production

Rates of size-fractionated (0.2–3 μm and >3 μm) primary production were assessed based on the assimilation of ¹⁴C-bicarbonate into particulate organic matter (Steeman Nielsen, 1952). Seawater was collected into 30-mL polycarbonate centrifuge tubes (Nalgene™ Oak Ridge) before sunrise and spiked under subdued light with 70 μL of NaH¹⁴CO₃[−] (MP Biomedicals 1,7441H, stock concentration 2 mCi mL^{−1}) to a final activity of ~0.14 MBq mL^{−1}. The tubes were placed in white mesh bags in the same incubator as the experiment carboys over the full photoperiod (~12–14 h). After sundown, 25 μL aliquots from each sample were collected and stored in 20-mL glass scintillation vials containing 500 μL of β-phenylethylamine to determine the total activity of ¹⁴C added to each sample.

TABLE 2 | Concentrations and rates of consumption of N+N, NH₄⁺, PO₄³⁻, and Si(OH)₄ at initial time point (T₀) of experiments.

Experiment	Treatment	N+N		NH ₄ ⁺		PO ₄ ³⁻		Si(OH) ₄	
		T ₀ (nM)	Drawdown rate (nM d ⁻¹) / % of initial	T ₀ (nM)	Drawdown rate (nM d ⁻¹) / % of initial	T ₀ (nM)	Drawdown rate (nM d ⁻¹)	T ₀ (nM)	Drawdown rate (nM d ⁻¹)
NvN1 (July 2011)	Control	32 ± 3	–	nm	nm	269 ± 1	–	2,736 ± 6	–
	+NO ₃ ⁻	3,166 ± 11	528 / 83%	nm	nm	270 ± 0	30	2,833 ± 9	240
	+NH ₄ ⁺	45 ± 4	–	nm	nm	270 ± 0	34	2,737 ± 13	230
NvN2 (March 2012)	Control	46 ± 2	–	53 ± 1	–	143 ± 0	–	1,273 ± 2	–
	+NO ₃ ⁻	2,504 ± 1	140 / 28%	106 ± 1	–	273 ± 0	8*	2,520 ± 6	19
	+NH ₄ ⁺	39 ± 3	–	5,198 ± 21	887 / 85%*	289 ± 1	18*	2,469 ± 5	13
NvN3 (July 2012)	Control	24 ± 5	–	72 ± 1	–	128 ± 3	3	2,279 ± 7	–
	+NO ₃ ⁻	2,580 ± 2	164 / 32%	79 ± 0	–	148 ± 2	9*	2,276 ± 10	72
	+NH ₄ ⁺	17 ± 2	–	2,218 ± 14	142 / 32%	160 ± 2	2	2,281 ± 11	58
N248 (Dec 2012)	Control	71 ± 1	–	22 ± 0	–	190 ± 3	4	2,823 ± 11	38
	+NO ₃ ⁻	2,948 ± 21	108 / 18%	59 ± 0	–	141 ± 5	–	3,722 ± 5	–
	+NH ₄ ⁺	86 ± 3	–	2,975 ± 21	191 / 32%*	149 ± 0	–	2,459 ± 6	–
NvN4 (April 2013)	+Urea	292 ± 6	–	177 ± 2	18 / 50%	166 ± 3	–	4,066 ± 2	–
	Control	165 ± 10	–	23 ± 0	–	192 ± 2	0	2,472 ± 3	6
	+NO ₃ ⁻	2,753 ± 6	210 / 38%*	26 ± 3	–	193 ± 1	7*	2,482 ± 6	16*
	+NH ₄ ⁺	204 ± 8	–	2,685 ± 5	220 / 41%*	185 ± 1	4	2,487 ± 4	17*

Concentrations of urea were not measured.

Values shown are mean ± standard deviation of the triplicate bottles from each treatment. Drawdown rates were calculated as the total nutrient consumption divided by a 120 h (5 days) period. –: calculation not applicable due to nutrient concentrations being < detection limits or differences in concentrations being negligible. nm: not measured. *: significant difference in concentrations over time (one-way ANOVA, Kruskal-Wallis, and linear regression model against null hypothesis of slope = 0, $p < 0.05$).

The remaining sample volume (~25 mL) was serially vacuum-filtered, first onto 25 mm diameter, 3 μm pore size polycarbonate membranes (Millipore IsoporeTM), then onto 25 mm diameter, 0.2 μm pore size membranes (GE Osmonics polycarbonate track-etched). After filtration, each filter was placed in 20-mL glass scintillation vials, to which 1 mL of 2 M hydrochloric acid was added and vented for at least 24 h to remove adsorbed ¹⁴C-bicarbonate. Ten mL of Ultima Gold liquid scintillation cocktail was then added to each vial and placed in a liquid scintillation counter (Packard TRI-Carb 4640) for the determination of ¹⁴C activities. ¹⁴C-assimilation rates were calculated based on the resulting radioactivity of the filters, total added activity, and dissolved inorganic carbon concentrations derived from respective water depths at Station ALOHA (Letelier et al., 1996).

Photosynthetic Eukaryote Cell Abundance

Seawater samples (2 mL) for photosynthetic eukaryote cell abundance measurements were collected for each experiment into cryotubes (Corning) containing 30 μL of 16% paraformaldehyde (PFA, in water, Alfa Aesar 43,368) for a final concentration of 0.24% (w/v), kept for 15 m in the dark, flash-frozen in liquid nitrogen, and stored at –80°C until analyzed. Photosynthetic eukaryote cells were distinguished using a BD InfluxTM flow cytometer (80 μm nozzle tip) with the data acquisition software Spigot. Microspherical beads (1 μm Fluoresbrite, Polysciences) were included per sample for size reference during enumeration. Phytoplankton cells were triggered on forward scatter (FSC) and enumerated based on FSC, side scatter, chlorophyll-based red fluorescence (692

± 20 nm), and phycoerythrin-based orange fluorescence (585 ± 20 nm) on two lasers, 488 and 457 nm through separate pinholes. To determine photosynthetic eukaryote cell counts, cyanobacteria *Prochlorococcus* and *Synechococcus* cells were first identified based on red fluorescence signals against FSC, then further gated by side scatter and orange fluorescence (the two lasers were used to improve identification of *Prochlorococcus*). Photosynthetic eukaryote cells were then distinguished as those excluding the cyanobacteria and based on high red fluorescence and low orange fluorescence in reference to FSC. Cell counts were calculated using the data analysis software FlowJo 10.0.7.

Photosynthetic Pigments

For measurements of size-fractionated chlorophyll *a* (Chl *a*), 250 mL of seawater was collected in amber HDPE bottles and serially filtered using a peristaltic pump, first onto 25 mm diameter, 3 μm pore size polycarbonate membranes (Millipore IsoporeTM), then onto 25 mm diameter, GF/F (Whatman[®]) filters (nominal pore size ~0.7 μm). Though different filters were used for Chl *a* concentrations and ¹⁴C-primary production measurements, previous analyses at Station ALOHA indicate Chl *a* concentrations estimated using 0.2 μm polycarbonate and GF/F glass fiber filters are comparable (Viviani et al., 2015). After filtration, filters were immediately submerged in 5 mL of 100% acetone in glass culture tubes which were wrapped in aluminum foil, and stored at –20°C for pigment extraction. After 7 days, tubes containing the filters were warmed to room temperature, and Chl *a* concentrations in the extracts were quantified using

a Turner Designs 10-AU fluorometer (Strickland and Parsons, 1972).

For photosynthetic pigment analyses using high-performance liquid chromatography (HPLC), seawater (2 L) was collected into brown, narrow-mouthed HDPE bottles and subsequently filtered using a peristaltic pump onto 25 mm diameter, GF/F (Whatman®) filters. Filters were immediately flash-frozen in liquid nitrogen and stored at -80°C until analyzed. Photosynthetic pigments were extracted from the filters in 3 mL 100% acetone (HPLC grade) in culture tubes along with 50 μL canthaxanthin, an internal standard, and placed at 4°C for 24 h. Chlorophyll and carotenoid pigments were separated on a Varian 9012 HPLC system (Waters Spherisorb® 5 μm ODS-2 C₁₈ column with a corresponding guard cartridge and a Timberline column heater) and analyzed using SpectraSYSTEM Thermo Separation Products dual wavelength UV/VIS UV2000 and fluorescence FL2000 detectors (Wright et al., 1991; Bidigare et al., 2005). Pigment identifications were based on absorbance spectra, co-chromatography with standards, and relative retention time with a monovinyl Chl *a* standard and representative culture extracts, and Spectra-Physics WOW® software was used to calculate peak area.

DNA Extraction, PCR, and Sequence Analyses

Seawater samples (2 L) for subsequent extraction of planktonic DNA were collected into acid-washed low density polyethylene (LDPE) bottles and serially filtered using a peristaltic pump through 25 mm diameter, 3 μm pore size polycarbonate membranes (Millipore Isopore™), then onto 25 mm diameter, 0.2 μm pore size polyethersulfone membranes (Pall Supor®). After filtration, filters were placed in 1.5-mL microcentrifuge tubes, immediately flash-frozen in liquid nitrogen, and stored at -80°C until analyzed. DNA was extracted and purified using the QIAGEN DNeasy Plant Mini Kit including a bead-beating step (with 0.1 and 0.5 mm beads) and Proteinase K (360 mAU mL⁻¹ final activity, QIAGEN) for additional cell disruption and lysing (Paerl et al., 2008). Extracts were eluted in 200 μL of nuclease-free PCR grade water.

The V9 regions of eukaryote 18S rRNA genes were amplified using the PCR primer pairs 1391F (5'-GTACACACCGCCGT C-3'; *S. cerevisiae* NCBI GenBank Accession #U53879 position 1629–1644; Lane, 1991) and Euk Br (5'-TGATCCTTCTGCA GGTTCACCTAC-3'; *S. cerevisiae* NCBI GenBank Accession #U53879 position 1774–1797; Medlin et al., 1988; Amaral-Zettler et al., 2009) containing unique barcode indices. Each PCR reaction contained both primers (0.2 μM final concentration), 1X 5 PRIME HotMasterMix (Cat# 2200410), and \sim 5 ng of template DNA in a 25 μL reaction (Amaral-Zettler et al., 2009). The thermal cycling conditions consisted of an initial activation step at 94°C for 3 min, followed by 35 cycles of 45 s at 94°C , 60 s at 57°C , and 90 s at 72°C , ending with a final extension of 10 min at 72°C . The resulting PCR products (344 in total) were run on an agarose gel to verify product amplification, quantified, pooled (\sim 8 ng of each sample into a single tube), and purified using the MoBio UltraClean PCR Clean-Up Kit (Cat#

12500). The quality of the pooled PCR product was evaluated on a BioAnalyzer 2100 (Agilent). Sequencing was conducted (paired end, 300 cycles) on an Illumina MiSeq (University of Hawaii Core Functional Genomics Facility at the Hawaii Institute of Marine Biology), from which individual samples were demultiplexed using QIIME (Caporaso et al., 2012) and 12,193,511 total sequence reads were recovered. Paired-end sequencing reads were merged using PEAR (Zhang et al., 2014), quality filtered (reads trimmed to 100–150 bp in size, maximum expected error of 1%, no ambiguous bases allowed, and an average Phred quality threshold >34), and poor quality reads were removed from further analyses. *De novo* and reference-based chimeras were detected and removed using USEARCH v7.0.1090 (Edgar et al., 2011). Sequences were first clustered using UCLUST v1.2.22q (max accepts = 20, max rejects = 500) into operational taxonomic units (OTUs) based on the SILVA 119 (pre-clustered at 97% similarity threshold) database (Quast et al., 2012), clustered *de novo* at the 97% similarity threshold, and the centroid sequence within each OTU was selected as the representative sequence. Sequences that failed to align using PyNAST (minimum percent identification 0.75; Caporaso et al., 2010), singletons, and OTUs present in only one sample were removed. Taxonomy was assigned to representative sequences at 90% similarity with BLAST (max *E*-value at $1 \times e^{-30}$) based on the SILVA 119 database (pre-clustered at 97%). Bacteria, Archaea, and Metazoa sequences were removed, resulting in 5,820,084 sequence reads and 11,811 total OTUs. Of these, taxonomy was not assigned to 2,800 OTUs consistent with the stringent *E*-value used. OTUs with assigned taxonomy presumed to be photosynthetic, including Archaeplastida, Dinophyceae, Cryptophyceae, Haptophyta, Chlorarachniophyta, and Ochrophyta (Bacillariophyceae, Bolidophyceae, Chrysophyceae, Dictyochophyceae, Eustigmatophyceae, Pelagophyceae, and Raphidophyceae), were separated into a “phytoplankton-only” OTU table which was used for subsequent analyses. Final quality-filtered sequences were deposited in the Sequence Read Archive in NCBI under BioProject ID PRJNA357861 and Accession #SRP095616.

Statistical Analyses

Nutrient concentrations measured in each treatment and experiment were tested for normality using the Shapiro-Wilk Test (Royston, 1982) and quantile-quantile plots, and analysis of variance (ANOVA) tests were performed. Data not normally distributed were log-transformed and ANOVA or non-parametric Kruskal-Wallis tests (Hollander and Wolfe, 1973) were used to test for significant differences between distributions. One-way ANOVA and linear regression analyses were also used to test for significant differences in nutrient concentrations over the duration of the experiment (Faraway, 2002). Community analyses were performed in R 3.1.1. (R Core Development Team, 2014) with the R package *Vegan* (Oksanen et al., 2007) and graphical outputs were constructed with the package *ggplot2* (Wickham, 2009). Subsampling for calculations of alpha diversity was conducted with 150 reads. Differences in eukaryotic phytoplankton community composition and alpha diversity between experiments were statistically tested using

Mantel tests on Bray-Curtis derived dissimilarity matrices and paired *t*-tests on distribution of Shannon indices.

RESULTS

Station ALOHA Conditions at Initial Time Points

Two experiments were conducted during the summer (NvN1 in July 2011 and NvN3 in July 2012), two were performed during the spring months (NvN2 in March 2012 and NvN4 in April 2013), and one was conducted during the winter (N248 in December 2012; **Table 1**). At the time these experiments were conducted, sea surface temperatures (SST), mixed layer depths (MLD), and the flux of PAR and concentrations of N+N at 25 m were characteristic of the monthly HOT program climatology for Station ALOHA (**Figure 1**). During the summer sampling periods the near-surface waters were characterized by relatively warm temperatures (24.8–25.3°C), the MLD ranged between 58 and 78 m, and the flux of PAR at 25 m was 12.6 mol quanta $m^{-2} d^{-1}$ (**Table 1**, **Figure 1**). In comparison, during the spring experiments the upper ocean waters exhibited slightly lower temperatures (22.7–23.0°C), the MLD ranged between 36 and 77 m, and incident PAR at 25 m was 11 mol quanta $m^{-2} d^{-1}$. For the experiment conducted in December, the near-surface waters were 24.8°C, the MLD was relatively deep (averaging 92 m), and incident PAR at 25 m was ~3-fold lower than in spring or summer (3.6 mol quanta $m^{-2} d^{-1}$). Concentrations of Chl *a* at 25 m ranged 65–111 ng L^{-1} during the study, with no discernible seasonal pattern among the various experiments (**Table 1**). Similarly, concentrations of N+N at 25 m were consistently low (<5 nM N) throughout the year with no apparent seasonal-scale differences (**Figure 1D**, **Table 1**). Concentrations of PO_4^{3-} and $Si(OH)_4$ at 25 m also depicted no apparent seasonality, ranging 60–90 nM P and 0.8–1.2 μM Si, respectively (**Table 1**).

Nutrients, Primary Production, Chlorophyll *a*, and Cell Abundances Following N Additions

Concentrations of N+N, NH_4^+ , PO_4^{3-} , and $Si(OH)_4$ in the control incubations did not vary significantly over time in any of the experiments (one-way ANOVA and linear regression, $p > 0.05$; **Table 2**). The addition of either NO_3^- or NH_4^+ (final concentrations ranging ~2504–3166 nM N+N and 2218–5198 nM NH_4^+) with PO_4^{3-} and $Si(OH)_4$ resulted in significant consumption of added N substrates over time. Over the course of 120 h, 18–83% of the added NO_3^- was consumed in all experiments, resulting in rates of NO_3^- drawdown ranging between 108 and 528 nM N d^{-1} (**Table 2**). For the NH_4^+ treatments, 32–85% of the added NH_4^+ was consumed over the duration of the experiments, with rates of consumption ranging 142–887 nM N d^{-1} (one-way ANOVA and linear regression $p < 0.05$). For the experiment conducted in March 2012 (NvN2), the initial NH_4^+ concentration (5198 nM) was ~2x greater than the target NH_4^+ concentration as well as the initial NO_3^- concentration. The resulting rate of NH_4^+ consumption for March 2012 was greater for this treatment than in other

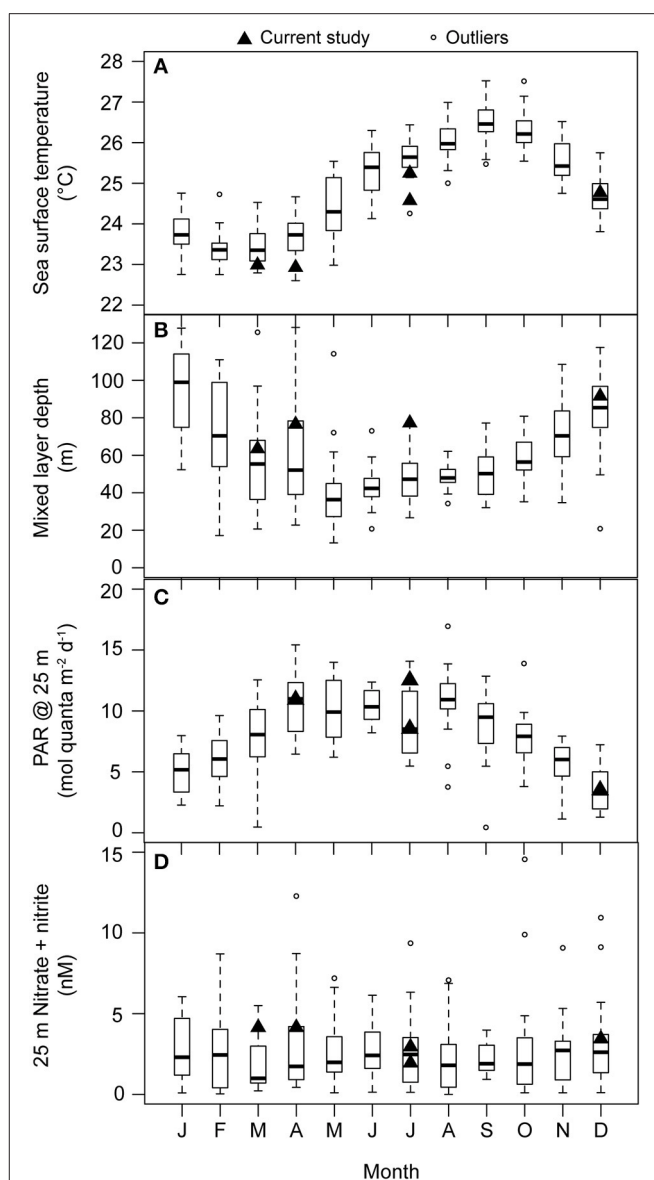


FIGURE 1 | Monthly-scale variability in (A) sea surface temperature (°C; 1988–2014), (B) mixed layer depth (m; 1988–2014), (C) daily integrated PAR at 25 m (mol quanta $m^{-2} d^{-1}$; 1998–2013), and (D) concentrations of N+N at 25 m (nM N; 1989–2013) at Station ALOHA. Measurements from the research cruises during which experiments for the current study were conducted are denoted with black triangles. For each boxplot: dark horizontal line indicates the median, the box boundaries represent the 25th and the 75th percentile, and the whiskers extend to the maximum and minimum (boundary \pm 1.5*interquartile range) of the selected observations. Outlier observations, considered to be beyond the maximum and minimum limits of the observations, are depicted as open circles.

treatments (**Table 2**). For both NO_3^- and NH_4^+ treatments, there was no significant change in $Si(OH)_4$ concentrations over the course of the experiments except during April 2013 (**Table 2**). PO_4^{3-} was consumed in the NO_3^- treatments at rates ranging 7–30 nM P d^{-1} (with the N:P of consumption being ~14–30), and at the rate of 2–34 nM P d^{-1} for the NH_4^+ treatments

(with the stoichiometry of N:P consumption being ~49–71). Urea (target concentration of ~2800 nM N) was also included as one of the treatments in an experiment conducted in December 2012; however, urea concentrations were not measured during the experiment so rates of consumption or production could not be evaluated.

Rates of ^{14}C -primary production and Chl *a* concentrations in the control incubations remained largely unchanged for the control carboys during the experiments conducted. Contributions of picophytoplankton (0.2–3 μm) to >0.2 μm ^{14}C -primary production at initial time points ranged 68–77% and rates of production in the >3 μm size fraction contributed 23–32% in all experiments except July 2012 (NvN3), when picophytoplankton were 43–60% of the initial ^{14}C -productivity and phytoplankton >3 μm comprised 40–57% of the production (Supplementary Table 1). Concentrations of Chl *a* remained stable in the control carboys of the experiments, with the majority (75–78%) of the total Chl *a* attributed to the picophytoplankton fraction (Supplementary Table 1). Photosynthetic eukaryote cell abundances were also relatively stable over time in the control incubations for all experiments except during July 2011 (NvN1), when cell abundances increased ~3-fold (Supplementary Table 1).

Rates of ^{14}C -primary production (sum of >3 μm and 0.2–3 μm filter size classes) in the NO_3^- and NH_4^+ treatments differed seasonally. During the experiment conducted in March 2012, ^{14}C -primary production increased ~17-fold in response to NO_3^- addition and 27-fold in response to NH_4^+ addition over 120 h, with contributions by the >3 μm fraction in the NO_3^- treatment comprising 75 ± 5% (mean of triplicate treatments) of the sum of two fractions, and rates of production by the >3 μm size class comprising 48 ± 14% (mean of triplicate treatments) of the sum of fractions in the NH_4^+ treatment (Supplementary Table 1). The ~1.6-fold greater response in the rate of ^{14}C -primary production in the NH_4^+ compared to NO_3^- addition may have resulted from the higher initial NH_4^+ concentration in this experiment (Table 2). During July 2012, rates of >0.2 μm ^{14}C -primary production increased ~21 and 15-fold in the NO_3^- and NH_4^+ treatments, respectively, with contributions by the >3 μm fraction increasing 2- and 1.5-fold for both treatments, respectively. Chl *a* concentrations during July 2012 also increased ~5-fold in NO_3^- treatments and ~3-fold in NH_4^+ treatments over 120 h. Approximately 2- to 4-fold increases in rates of >0.2 μm ^{14}C -primary production were observed for all N additions during December 2012 and April 2013, with a ~2-fold shift toward >3 μm organisms (Figure 2, Supplementary Table 1). Concentrations of Chl *a* increased modestly (~1.9 to 2.3-fold) during December 2012 in all N addition treatments, while ~3 to 4-fold increases in Chl *a* concentrations over 120 h were observed in both NO_3^- and NH_4^+ treatments during April 2013 (Figures 3A,B, Supplementary Table 1). For both the winter 2012 and spring 2013 experiments, moderate (~2 to 3-fold) increases in the contributions by the >3 μm size fraction to Chl *a* concentrations were observed. Cell abundances of photosynthetic eukaryotes increased ~3 to 5-fold in all N additions during all experiments, except for a ~12-fold increase in the NO_3^- treatment during July 2011 (Supplementary Table 1).

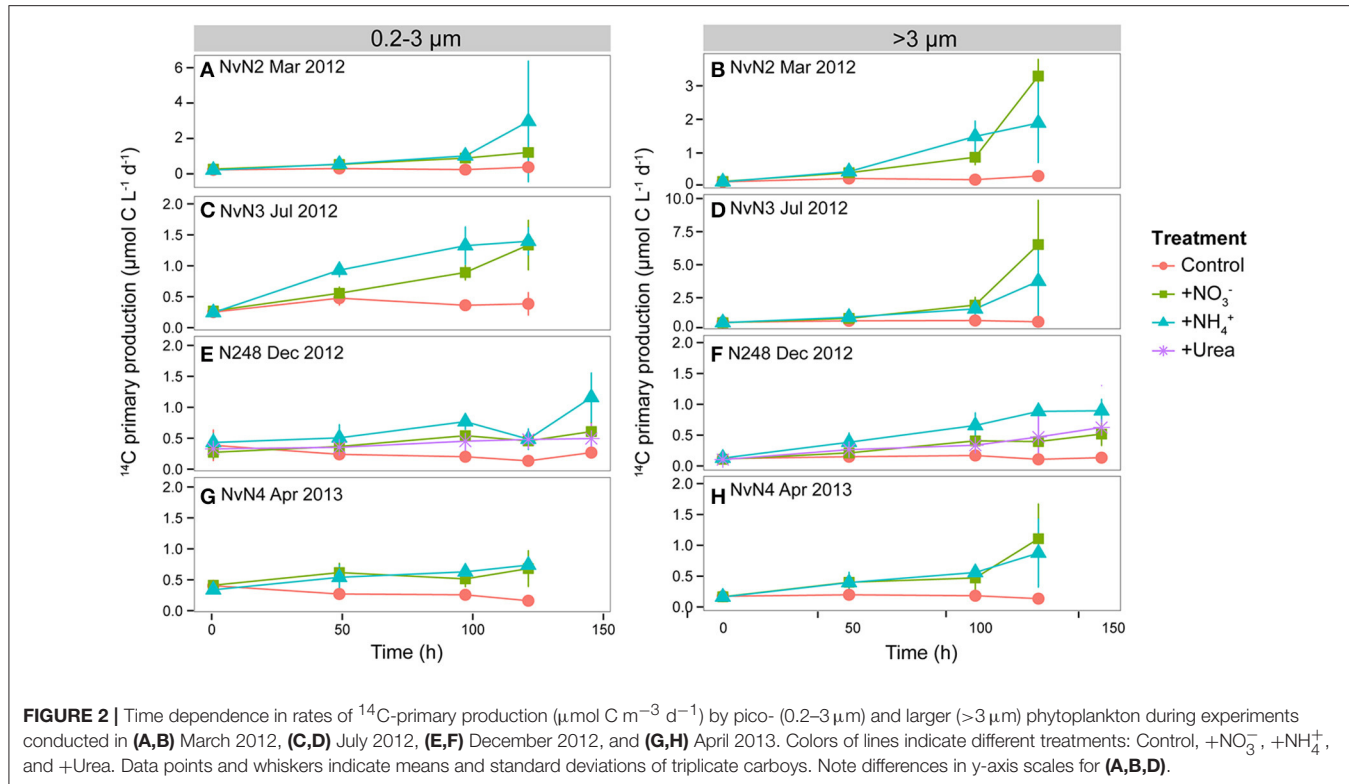
Changes in Eukaryotic Phytoplankton Community Composition

Photosynthetic Pigments

Photosynthetic pigments measured during the experiments conducted in July 2012 and April 2013 revealed variations in the timing and magnitude of the responses by different phytoplankton taxa to the various N additions (Figure 3). Initial concentrations of fucoxanthin, a pigment biomarker diagnostic of diatoms, were similar in both July (6.7 ng L⁻¹) and April (5.6 ng L⁻¹); however, large increases (49- and 23-fold increases in the NO_3^- and NH_4^+ treatments, respectively) were observed in July (Figure 3C) while modest increases (~9-fold increases in both NO_3^- and NH_4^+ treatments) were measured during April (Figure 3D). Pigments diagnostic of pelagophytes (19'-butanoyloxyfucoxanthin, or 19'-But) and prymnesiophytes (19'-hexanoyloxyfucoxanthin, or 19'-Hex) behaved differently than fucoxanthin. During July 2012, 19'-But and 19'-Hex increased 5- and 3-fold, respectively, by 96 h in both NO_3^- and NH_4^+ treatments, and decreased subsequently (Figures 3E,G). During the April experiment, both 19'-But and 19'-Hex reached maximum concentrations (11-fold and 6-fold increases, respectively) in the NO_3^- and NH_4^+ treatments after 48 h and remained elevated through the remainder of the experiment (Figures 3F,H). Concentrations of peridinin, a pigment biomarker for dinoflagellates, increased steadily throughout both July and April experiments (Figures 3I,J), with larger responses in the NH_4^+ treatments (increasing 7- to 9-fold in July and April, respectively, compared to 4- to 5-fold increases observed in the NO_3^- treatments) for both experiments.

18S rDNA Sequences

The V9 region of 18S rRNA genes was amplified and sequenced from size-fractionated samples collected during our experiments to assess possible time-varying changes in phytoplankton community structure following additions of nitrogenous substrates (Figure 4). Relative abundances of phytoplankton OTUs revealed differences in the initial composition of the eukaryotic picophytoplankton (0.2–3 μm) among the different experiments; in contrast, the initial community composition of larger (>3 μm) phytoplankton appeared very similar between experiments. Members of the Dinophyceae comprised 50–62% of the picophytoplankton 18S rRNA gene sequences during experiments conducted in the summer (July 2011 and 2012), with haptophytes and chrysophytes also relatively abundant (ranging ~11–16% and ~5–14%, respectively) in the picophytoplankton size fraction. In addition, phytoplankton belonging to the dictyochophytes, bolidophytes, and eustigmatophytes were present at low relative abundances in the picophytoplankton size fraction (Figure 4A). During the experiments conducted in the winter and spring months (March 2012, December 2012, and April 2013) relative abundances of dinoflagellates at the onset of experiments were lower (ranging 28–39% of picophytoplankton sequences) than observed during the summer experiments, with greater contributions by OTUs clustering among pelagophytes (7–21%), haptophytes (5–27%), chrysophytes (6–21%) and

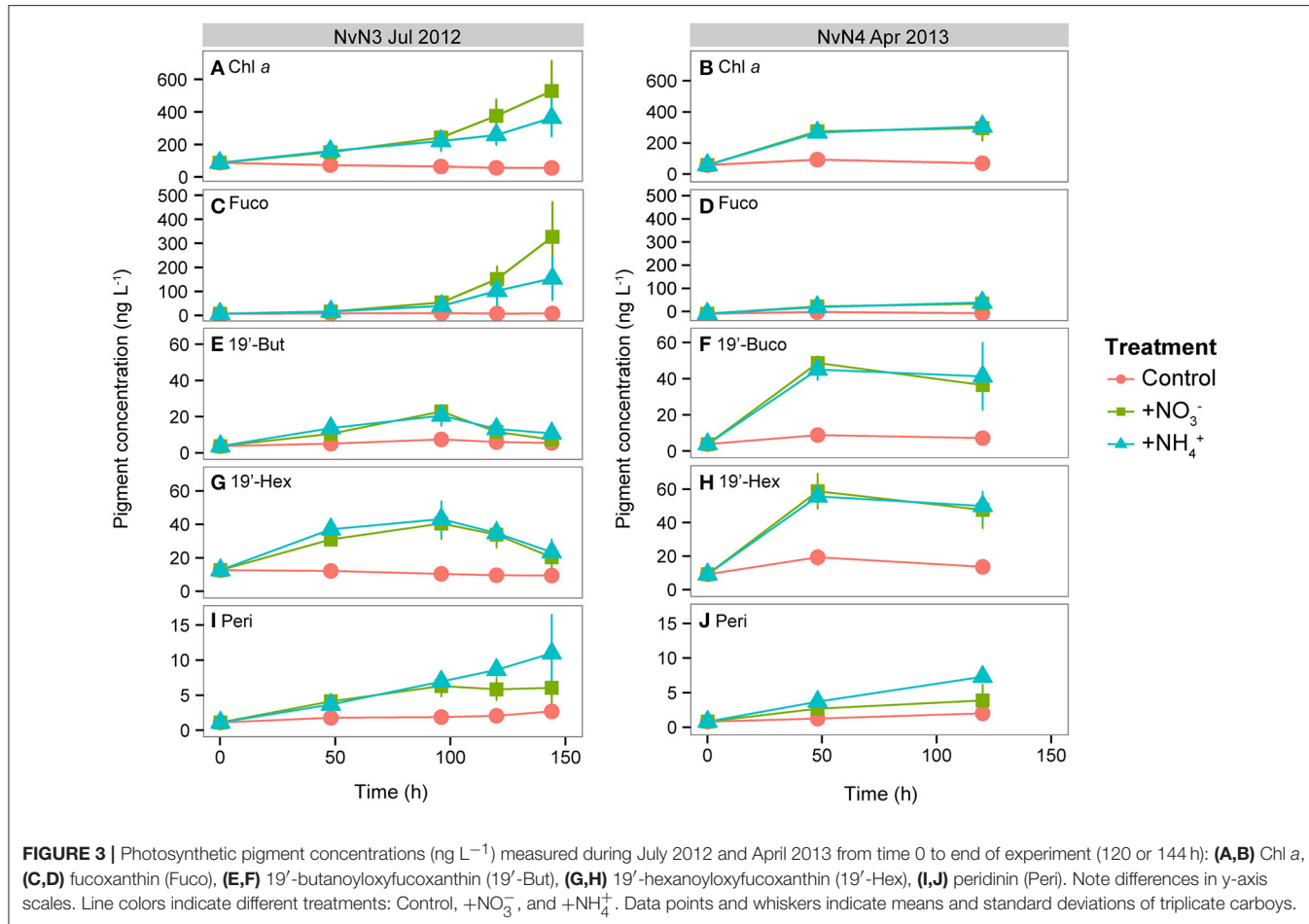


dictyochophytes (5–9%). During December 2012, members of the Rhodophyta and marine ochrophytes (MOCH) were also present (~10% of picophytoplankton 18S rRNA gene sequences). For the larger phytoplankton ($>3 \mu\text{m}$), a majority of the $>3 \mu\text{m}$ sequences in all experiments was comprised of dinoflagellates (~76–88% on average) and diatoms (~5–12% on average), with no discernible seasonal variability (Figure 4B). The taxonomic composition of the control carboys remained relatively constant for experiments in December 2012 and April 2013; however, taxa belonging to the Eustigmatophyceae and Bolidophyceae increased in the picophytoplankton fraction in July 2011 and 2012, respectively (Figure 4A), and members of the Bacillariophyceae increased in the $>3 \mu\text{m}$ size fraction in March 2011 and July 2012 (Figure 4B).

While changes in phytoplankton community composition were very similar in the various N treatments (NO_3^- , NH_4^+ , or urea), there were differences in the resulting phytoplankton responses to the additions of nitrogenous substrates depending on the time of year that the experiments were conducted. For the picophytoplankton, members of the Bacillariophyceae demonstrated the largest increases in relative abundances in the summer experiments (July 2011 and 2012), increasing from 0.8–1.4% at the onset of the experiments to ~38–59% of the picophytoplankton sequences by the end of the experiments. In contrast, for those experiments conducted in the winter and spring months (December, March, and April), members of the Pelagophyceae comprised ~7–21% of the picophytoplankton sequences at the onset of the experiments and increased to 34–39% following the additions of N by the end of the experiments,

while diatom composition remained fairly low (~0–1% at onset to ~5–14% at end; Figures 4A, 5). In the $>3 \mu\text{m}$ size fraction, various taxa of diatoms were the dominant responders to N additions during all experiments (30–60% of $>3 \mu\text{m}$ sequences), though the magnitude of response by diatoms was greatest during those experiments conducted in the summer (4–6% at onset of experiment to 57–60% of $>3 \mu\text{m}$ sequences at final time point) compared to the response observed during those experiments conducted in the spring and winter months (6–12% to 30–49% of $>3 \mu\text{m}$ sequences at final time point; Figures 4B, 5). In addition, the increase in the relative abundances of diatoms in the larger fraction during the summer was more rapid (occurring in the initial 48–96 h) compared to the responses observed in those experiments conducted in the spring and winter (Figure 4B).

Changes in the relative abundances of the five most abundant OTUs for both size fractions were examined for the NO_3^- and NH_4^+ treatments by comparing relative abundances at the beginning of each experiment to the results at the end of the experiments (Figure 5). Seasonal binning (winter, spring, and summer) of the experiments emphasized that the resulting trajectory of picophytoplankton community response appeared to depend on when the experiment was conducted. The dominant picophytoplankton at initial time points during the winter and spring included the pelagophyte *Pelagomonas* (averaging ~7% of picophytoplankton sequences in winter and ~19% in spring), dictyochophyte *Florenciella* (averaging ~8% of picophytoplankton sequences in winter and ~4% in spring), chrysophytes (averaging ~4–6% of picophytoplankton sequences in both winter and spring), and *Pfiesteria*-like dinoflagellates



(averaging $\sim 5\text{--}6\%$ of picophytoplankton sequences in both winter and spring). During the spring months, the haptophyte *Prymnesium* comprised $\sim 5\%$ of the picophytoplankton sequences, while members of the Raphidophyceae comprised $\sim 7\%$ of the picophytoplankton community during the winter experiment (Supplementary Table 2). In contrast, during those experiments conducted in the summer, all of the most abundant picophytoplankton OTUs at the beginning of the experiments clustered among the Dinophyceae, including OTUs classified as *Gymnodinium*, *Gyrodinium*, *Karldonium*, *Pfiesteria*-like, and *Azadinium*.

By the end of the experiments initiated in the winter and spring, *Pelagomonas* demonstrated the largest increases in relative abundances of picophytoplankton sequences, with smaller contributions by diatoms *Pseudo-nitzschia* and *Nitzschia*, dictyochophyte *Florenciella*, and Prasinophyceae Clade VII-A. In experiments conducted during the summer, diatoms *Pseudo-nitzschia*, *Nitzschia*, and *Minutocellus* demonstrated the largest increases in relative abundances of picophytoplankton (Supplementary Table 2, Figure 5). In the $>3\ \mu\text{m}$ fraction, the most dominant OTUs at the beginning of the experiments were members of the Dinophyceae irrespective of when the experiments were conducted (Supplementary Table 2, Figure 5).

Following the addition of N substrates, the relative contributions by these dinoflagellates decreased, with correspondingly large increases in relative abundances of OTUs closely related to the diatoms *Pseudo-nitzschia* and *Nitzschia* (Supplementary Table 2, Figure 5). Despite often being undetectable at the onset of the experiments, relative abundances of OTUs belonging to these diatom genera comprised ~ 20 to 60% of the $>3\ \mu\text{m}$ phytoplankton sequences during all seasons in the N addition treatments (Supplementary Table 2, Figure 5).

Alpha diversity (assessed by the Shannon Index) of the picoeukaryote phytoplankton communities decreased significantly following N additions compared to the control carboys for all experiments (paired *t*-test, $p < 0.05$; Figure 6). For the larger phytoplankton, the diversity of communities at the end of the experiments also decreased following N additions; however, the difference was significantly lower from that of the initial communities only during the summer (paired *t*-test, $p < 0.05$). Alpha diversity for both pico- and larger phytoplankton did not differ between the NO_3^- , NH_4^+ , and urea treatments amongst various seasons (paired *t*-test, $p > 0.1$; Figure 6). Significant differences (paired *t*-test, $p < 0.05$) were observed between the alpha diversity of both pico- and larger phytoplankton communities in the NO_3^- treatments,

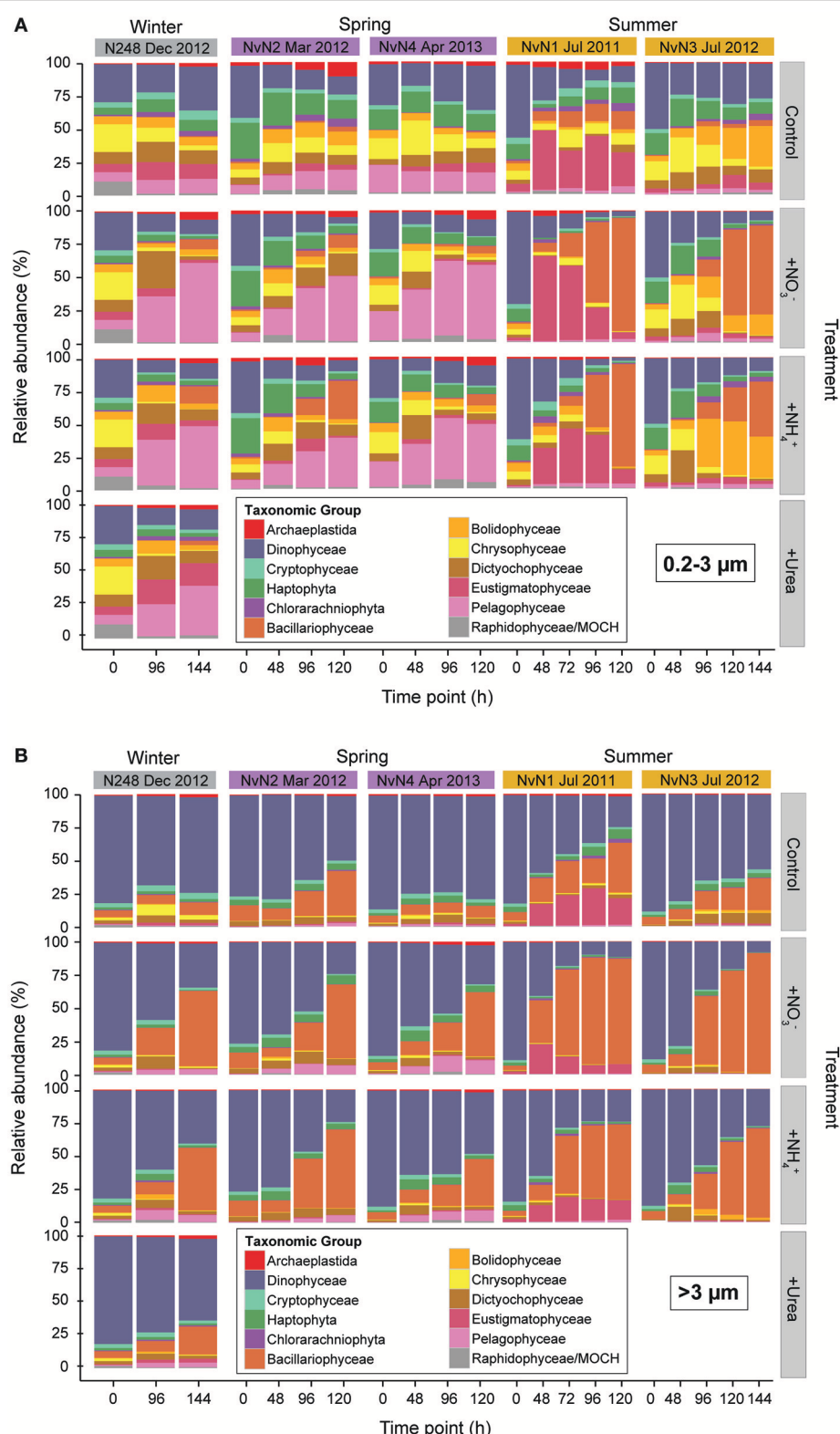


FIGURE 4 | Relative abundances (%) of (A) picophytoplankton and (B) $>3\text{ }\mu\text{m}$ phytoplankton taxa, binned by time point sampled per experiment conducted in different seasons. Columns indicate treatment mean (of triplicate carboys) relative abundances for different experiments and rows specify the different treatments: Control, $+\text{NO}_3^-$, $+\text{NH}_4^+$, and $+\text{Urea}$. Colors indicate various phytoplankton taxa.

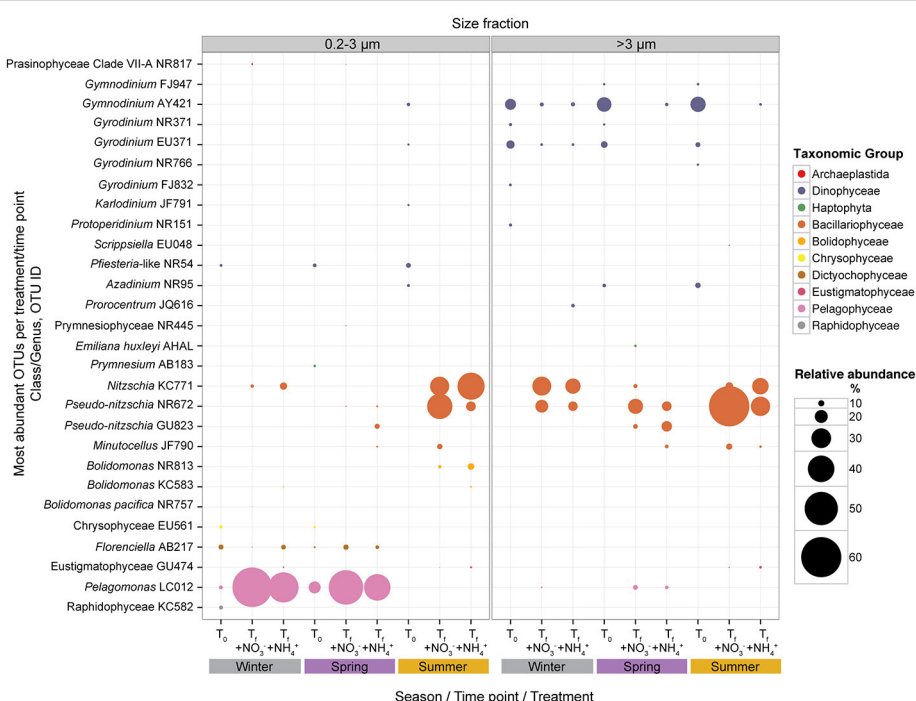


FIGURE 5 | Mean relative abundances (%) of the most abundant pico- and >3 μm phytoplankton at initial (T_0) time points and final (T_f) time points for $+\text{NO}_3^-$ and $+\text{NH}_4^+$ treatments; experiments binned by season (winter, spring, and summer). Mean relative abundances of phytoplankton taxa depicted using different colors and bubble sizes (size reflects relative abundance). Detailed information on the OTUs listed is listed in Supplementary Table 2.

between spring and summer. Higher Shannon index values were generally observed for both size fractions during the winter and spring compared to the summer experiments, regardless of treatment, likely reflecting the dominance of diatoms in the N amended treatments during the summer (**Figure 6**).

DISCUSSION

We conducted five experiments during the winter, spring, and summer months between July 2011 to April 2013 to examine the responses of the eukaryotic phytoplankton to additions of NO_3^- , NH_4^+ , or urea (along with PO_4^{3-} and $\text{Si}(\text{OH})_4$). We assessed how the addition of varying nitrogenous substrates influenced size-dependent responses in rates of primary production and concentrations of Chl *a*, and altered eukaryotic phytoplankton community structure based on changes in concentrations of photosynthetic pigments and analyses of 18S rDNA sequences. In three of the five experiments (July and December 2012, and April 2013), rates of NO_3^- and NH_4^+ drawdown were roughly equivalent between the N addition treatments. In addition, contributions of pico- and larger phytoplankton to ^{14}C -primary production and Chl *a* concentrations did not differ significantly based on the type of N substrates added, except for the experiment conducted in March 2012. In March 2012, we observed a ~27-fold increase in ^{14}C -primary

production from the initial timepoint to 120 h for the NH_4^+ treatment, concomitant with a greater response by diatoms in the pico-size fraction. This disparity in response from other experiments is likely due to the initial NH_4^+ concentration being $\sim 2x$ the target concentration as well as the initial NO_3^- concentration; despite the greater enrichment, $\sim 85\%$ of the NH_4^+ added was drawn down during this experiment. The different responses observed in this experiment may reflect a concentration-dependent response by the phytoplankton assemblage rather than reflecting a difference in the types of substrates added. Overall, results from these five experiments suggest that the oxidation state of the nitrogenous substrates that we selected (oxidized NO_3^- or reduced NH_4^+ and urea) did not play a major role in shaping rates of N drawdown or the resulting size class responses of phytoplankton biomass and productivity. In a series of experiments in the oligotrophic NPSG, Shilova et al. (2017) observed increases in rates of primary production and phytoplankton biomass, specifically by cyanobacteria *Prochlorococcus*, following the addition of urea. However, consistent with the findings from the present study, species composition and growth rates did not appear to be influenced by the type of N source added (Eppley et al., 1971) although previous studies comparing NO_3^- and NH_4^+ (Strickland et al., 1969; Eppley et al., 1971) and urea (Newell et al., 1967) demonstrated that elemental composition (C:N) and C:Chl ratio of phytoplankton changed depending on the form of N used for growth.

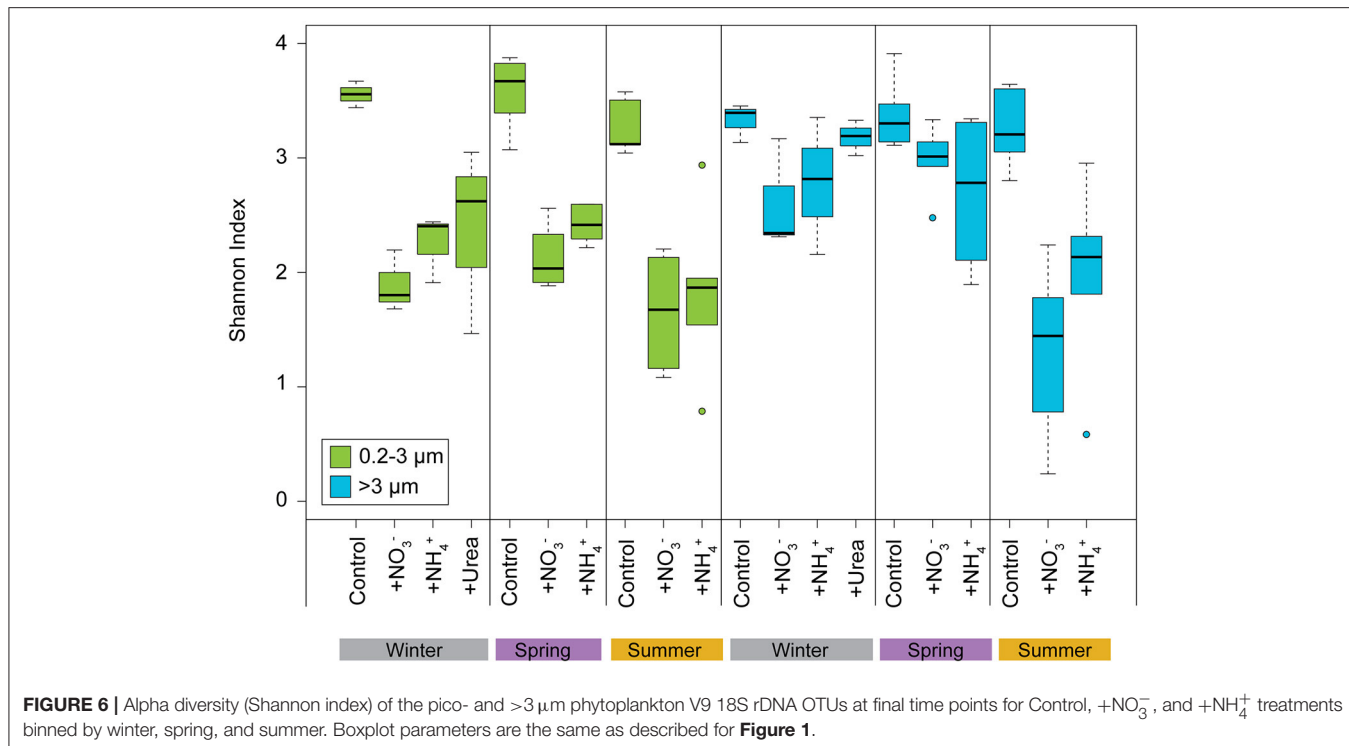


FIGURE 6 | Alpha diversity (Shannon index) of the pico- and >3 μm phytoplankton V9 18S rDNA OTUs at final time points for Control, +NO₃⁻, and +NH₄⁺ treatments binned by winter, spring, and summer. Boxplot parameters are the same as described for **Figure 1**.

Although our experiments were not designed to examine competition amongst phytoplankton for differing N substrates (e.g., through simultaneous additions of both NO₃⁻ and NH₄⁺ to the same treatment), our results do provide insight into taxa best poised to respond to relatively large changes in N availability in this ecosystem. Two of our observations, (1) that the timing and response of phytoplankton to both NO₃⁻ and NH₄⁺ were similar, and (2) that no significant changes were observed in our “control” carboys amended with only PO₄³⁻ and Si(OH)₄ (except for ~3-fold increase in photosynthetic eukaryote cell abundances during the July 2011 experiment), likely reflect the chronic N limitation of the oligotrophic upper ocean waters of the NPSG. In these well-lit upper ocean waters, phytoplankton production is consistently light-saturated (Li et al., 2011; White et al., 2015), while concentrations of inorganic N are proportionately much lower than required for growth (NO₃⁻:PO₄³⁻ ratios of the upper ocean <1). Our results suggest that energetic limitations likely do not restrict eukaryotic phytoplankton consumption of available N substrates in this habitat.

We observed moderate to large changes in the phytoplankton community response to N additions, shifting from a picophytoplankton-dominated community (43–77% picophytoplankton contribution to ¹⁴C-primary production and 86–91% contribution of picophytoplankton to Chl *a* by the end of experiments) to one with a greater contribution by the larger (>3 μm) phytoplankton (46–79% contribution to ¹⁴C-primary production and 19–45% contribution to Chl *a* by the end of experiments). Sequencing of 18S rDNA provided insight into the types of eukaryotic phytoplankton in these size classes. The larger (>3 μm) phytoplankton community was comprised

mainly of dinoflagellates at the onset of the experiment; however, following the addition of N substrates, diatom composition rapidly (within 5–6 days) expanded, contributing 30–60% of the >3 μm sequences. Intriguingly, we observed that relative abundances of various taxa of pennate diatoms were elevated in the 0.2–3 μm filter fraction following the addition of NH₄⁺ and NO₃⁻ during experiments conducted in the summer. Such cells might be expected to be larger than 3 μm; hence, it's unclear whether such results reflect time-varying differences in the sizes of these cells, poor trapping efficiency of these cells by the 3 μm filters, or potential breakage of cells during filtration with subsequent retention of fragmented cells by the 0.2 μm filter.

The diatom response was most significant during the experiments conducted in the summer, particularly in the NO₃⁻ treatment, where diatoms comprised ~90% of the >3 μm sequences at the end of the experiments. Such observations are consistent with those of Mahaffey et al. (2012), who observed greater responses (>~2-fold) in phytoplankton biomass following nutrient enrichment with deep-sea water during the summer months than in other times of the year. Consistent with microscopic observations at Station ALOHA (Venrick, 1993, 1999; Scharek et al., 1999), diatoms were present in low concentrations (<~1% of total sequences) at the onset of our experiments. The large response by diatoms following the addition of N likely partly reflects their physiological capacity to outcompete other phytoplankton for available N when concentrations of NO₃⁻ and NH₄⁺ are elevated (Eppley et al., 1969), and highlights potential N limitation of diatoms during summer periods. In addition, these results presumably reflect decoupling between diatom growth and removal processes

such as predation, parasitism, or viral lysis during the summer, permitting accumulation of pennate diatoms during this period. Thus, the diatom response to nitrogenous substrates observed during the experiments conducted in the summer suggests there are season-specific conditions at Station ALOHA, such as elevated incident light flux and warm upper ocean temperatures, that may favor diatom growth and allow them to outgrow or escape removal in order to accumulate biomass.

While diatoms were the dominant phytoplankton to respond to N additions in the $>3\text{ }\mu\text{m}$ fraction in all of the experiments, differential response between seasons was observed among the picophytoplankton. Diatoms were still the major responders to N additions in the picophytoplankton fraction during the summer; however, the pelagophyte *Pelagomonas* responded to additions of N substrates in the winter and spring. While such results may reflect that smaller, pennate diatoms are limited by some other nutrient (e.g., iron, vitamins) during the spring and winter months, our results highlight that other groups of picophytoplankton, in particular the pelagophytes, respond rapidly to N availability during these periods. Although pelagophytes comprised 0.8–1.4% of the picophytoplankton sequences at the onset of the summer experiments, they comprised a much larger fraction (6–21%) of the sequences at the onset of the winter and spring experiments. As pelagophytes are typically found in greatest abundances in the low-lit regions of the euphotic zone (i.e., Letelier et al., 1993; Bidigare and Ondrusek, 1996; Timmermans et al., 2005), the higher relative abundances of these organisms during the winter and spring months in the surface waters at Station ALOHA was somewhat surprising. We suspect that *Pelagomonas* may respond to periods when the mixed layer extends into the lower region of the euphotic zone (90–110 m), entraining organisms and nutrients typically found in the dimly lit regions of the euphotic zone into the well-lit upper ocean. As such, the survival of pelagophytes in the upper euphotic zone during this period of deeper mixing may reflect their flexible photophysiology (Dimier et al., 2009; Bidigare et al., 2014) compared to other phytoplankton, such as some diatoms, whose growth rates often decrease under fluctuating light conditions (van de Poll et al., 2007). Their success may also be due to their ability to acquire N through the increased supply of NO_3^- to the euphotic zone during periods of deeper mixing, as consistent with studies indicating elevated expression of NO_3^- transporter genes by *Pelagomonas* (DuPont et al., 2014). Moreover, there may be differences in selective removal processes in the upper vs. lower euphotic zone that specifically impact *Pelagomonas* or other competing organisms, resulting in the accumulation of *Pelagomonas* during this particular time of year. Hence, we suspect that the rapid response by pelagophytes (specifically *Pelagomonas*) during spring and winter resulted from the relatively elevated abundances of these organisms at the onset of the experiments, which may or may not reflect selective removal processes, as well as their ability to grow rapidly following the input of bioavailable N.

Examination of alpha diversity during our experiments revealed a differential response in the size structure of eukaryotic phytoplankton diversity with the addition of N substrates, indicating varying degrees of resource competition amongst

the different size classes. While the addition of N substrates induced “bloom”-like conditions in picophytoplankton (thereby significantly decreasing alpha diversity), addition of nitrogenous substrates induced growth in different taxa in the larger ($>3\text{ }\mu\text{m}$) phytoplankton throughout the year (e.g., alpha diversity of the N treatments remained similar to the controls), except in summer when diatoms dominated. This suggests that picophytoplankton diversity is more strongly influenced by competition for nutrients compared to the larger phytoplankton.

The proliferation of different taxa in our experiments during different times of the year presumably also reflects temporal variability in the strength of various top-down controls (predation, viruses, parasites). Our experiments excluded large grazers ($>202\text{ }\mu\text{m}$), presumably eliminating the influences of larger mesozooplankton as potential controls on phytoplankton diversity and community structure. However, microzooplankton and heterotrophic and mixotrophic protists can be significant grazers of phytoplankton biomass (>40% of Chl *a* per day) in the open ocean (Calbet and Landry, 2004). Though larger diatoms may be too big to be consumed efficiently by nano- and micro-predators (Frost, 1991; Cullen, 1995), smaller pennate diatoms (typically 2–15 μm in length) can be readily consumed by microzooplankton (Latasa et al., 1997). However, Latasa et al. (1997) observed that growth and grazing of diatoms and pelagophytes were uncoupled in the upper ocean, allowing net phytoplankton growth in the central equatorial Pacific. Thus, the rapid turnover of fast-growing species through active removal processes may maintain greater diversity (such as among the larger phytoplankton during the spring), despite the availability of nutrients (Longhurst, 1967; Timonin, 1969).

The apparent seasonally-dependent responses by the phytoplankton assemblage to N availability may provide insight into previously observed patterns in carbon export in the NPSG. In particular, Karl et al. (2012) describe diatom-driven summertime export of several bioelements to the deep sea (4000 m) at Station ALOHA. Based on 12-years of sediment-trap derived measurements of particulate matter flux, these authors highlight the role of diatom aggregation and sinking in regulating a large fraction of the annual export in this ecosystem; moreover, this seasonal event appears fueled by N supply via N_2 fixation (Karl et al., 2012). Other studies conducted in the NPSG further highlight diatom responses to nutrient availability. For example, analyses of particulate matter export from the upper ocean into the mesopelagic waters have revealed that nutrient supply via mesoscale eddies stimulates diatom growth and subsequent preferential settling of silica-enriched biomass (Benitez-Nelson et al., 2007). In our experiments, larger diatoms ($>3\text{ }\mu\text{m}$) consistently responded to the addition of N substrates, suggesting these organisms are poised for rapid growth following N input via N_2 fixation or vertical supply via mixing or mesoscale isopycnal uplift.

Interestingly, the initial eukaryotic phytoplankton communities (in the larger size class but also during the summer in the picophytoplankton size class) were dominated by members of the Dinophyceae. Autotrophic dinoflagellates such as *Gymnodinium* are reported to lack peridinin, while containing fucoxanthin-related carotenoids (Millie et al., 1993). Such

findings may explain why we observed high relative abundances of dinoflagellate OTUs in our study, while observations at Station ALOHA indicate low concentrations of peridinin (Letelier et al., 1993; Bidigare and Ondrusek, 1996). Alternatively, the dominance of dinoflagellates in 18S rDNA sequences may be due to high rRNA gene copy numbers previously described among the dinoflagellates (Zhu et al., 2005; Not et al., 2009; Medinger et al., 2010). Moreover, the primers targeting the region (V9) of the 18S rRNA gene amplified in the current study may preferentially amplify dinoflagellates (Stoeck et al., 2010), biasing the sequence results toward these organisms. A recent PCR-independent metatranscriptome approach found that dinoflagellates dominated (36–40%) the mapped eukaryote transcripts at Station ALOHA (Alexander et al., 2015), suggesting that dinoflagellates are indeed important contributors to phytoplankton biomass in this ecosystem. In the current study, despite their initial dominance, dinoflagellates did not respond significantly to additions of NO_3^- , NH_4^+ , or urea. Concentrations of peridinin increased gradually in the experiments where HPLC pigments were measured (in July 2012 and April 2013), but to a lesser extent than other measured pigments. Consistent with these results, additions of nutrient-enriched deep sea water to upper ocean plankton assemblages resulted in a minimal transcriptional response by dinoflagellates (Alexander et al., 2015). Such results, and those observed in the current study, may suggest that the dominant dinoflagellates at Station ALOHA are heterotrophic or mixotrophic, potentially decreasing their dependence on inorganic N substrates. Consistent with this hypothesis, several of the taxa that predominated at the beginning of our experiments are closely related to mixotrophic organisms, including dinoflagellates, haptophytes, chrysophytes, and dictyochophytes (Rothhaupt, 1996; Frias-Lopez et al., 2009; Liu et al., 2009). However, following N additions, many of these taxa decreased in relative abundance, with organisms not previously known to demonstrate mixotrophic growth (namely diatoms and pelagophytes) becoming increasing dominant. Such results provide support to the hypothesis that limiting nutrients are crucial to shaping plankton physiology, including promoting mixotrophic modes of nutrient acquisition (Zubkov and Tarran, 2008; Hartmann et al., 2012).

In summary, after addition of inorganic N substrates, we observed a general shift in the size structure of the phytoplankton community from a picophytoplankton-dominated one to a community dominated by larger ($>3\ \mu\text{m}$) phytoplankton. In our experiments, responses in ^{14}C -primary production and photosynthetic pigment biomass appeared independent of the type of N substrate added. However, resulting changes in the

picophytoplankton community composition appeared seasonally dependent, with diatoms dominating the response during the summer while pelagophytes responded most significantly in the winter and spring. Diatoms in the $>3\ \mu\text{m}$ size fraction appear to be poised for rapid net growth throughout the year, while smaller, pennate diatoms appeared best able to capitalize on added N during the summer months. The variability in the responses by phytoplankton may stem from differences in initial picophytoplankton populations or time-varying top-down controls, which likely vary with seasonal changes in mixed layer depth and light. Our findings provide insight into how abrupt changes in the availability of fixed N influence successional patterns in eukaryotic phytoplankton assemblages, and highlight those organisms poised for rapid net growth when fixed N is available.

AUTHOR CONTRIBUTIONS

YR and MC came up with the concept and design of experiments described in this paper. Experiments implementation and sample analyses were performed by YR, with input from MC and RB. Data analyses and manuscript write-up was conducted by YR and MC with input from RB.

ACKNOWLEDGMENTS

We thank the HOT program science team for the collection and analyses of some of the data used in this study. We would also like to acknowledge Donn Viviani and Brenner Wai for help with sample collection during the experiments. In addition, Brianne Maillot provided laboratory assistance, Susan Curless and Alexa Nelson contributed nutrient analyses, Markus Lindh assisted with R, and Edward DeLong enabled use of a computer server for the Illumina sequence analyses. We also appreciate the support of the captain and crew of R/V *Kilo Moana*. Support for this work derived from U.S. National Science Foundation (NSF) grants OCE-1241263 and OCE-1260164 (MC), the Center for Microbial Oceanography: Research and Education (C-MORE; EF-0424599), the Simons Collaboration on Ocean Processes and Ecology (SCOPE ID 329108, MC), and the University of Hawaii Denise B. Evans Research Fellowship in Oceanography (YR).

SUPPLEMENTARY MATERIAL

The Supplementary Material for this article can be found online at: <https://www.frontiersin.org/articles/10.3389/fmars.2018.00092/full#supplementary-material>

REFERENCES

- Alexander, H., Rouco, M., Haley, S. T., Wilson, S. T., Karl, D. M., and Dyhrman, S. T. (2015). Functional group-specific traits drive phytoplankton dynamics in the oligotrophic ocean. *Proc. Natl. Acad. Sci. U.S.A.* 112, E5972–E5979. doi: 10.1073/pnas.1518165112
- Amaral-Zettler, L. A., McCliment, E. A., Ducklow, H. W., and Huse, S. M. (2009). A method for studying protistan diversity using massively parallel sequencing of V9 hypervariable regions of small-subunit ribosomal RNA genes. *PLoS ONE* 4:e6372. doi: 10.1371/journal.pone.0006372
- Armstrong, F. A. J., Stearns, C. R., and Strickland, J. D. H. (1967). The measurement of upwelling and subsequent biological processes by means of the Technicon AutoAnalyzerTM and associated equipment. *Deep Sea Res.* 14, 381–389.
- Arrigo, K. R. (2005). Marine microorganisms and global nutrient cycles. *Nature* 437, 349–355. doi: 10.1038/nature04159

- Atlas, E. L., Hager, S. W., Gordon, L. I., and Park, P. K. (1971). *A Practical Manual for Use of the Technicon AutoanalyzerTM in Seawater Nutrient Analyses; Revised*. Technical Report 215, Ref. No. 71-22, Department of Oceanography, Oregon State University, 1–48.
- Benitez-Nelson, C. R., Bidigare, R. R., Dickey, T. D., Landry, M. R., Leonard, C. L., Brown, S. L., et al. (2007). Mesoscale eddies drive increased silica export in the subtropical Pacific Ocean. *Science* 316, 1017–1021. doi: 10.1126/science.1136221
- Bernhardt, H., and Wilhelms, A. (1967). “The continuous determination of low level iron, soluble phosphate and total phosphate with the AutoAnalyzer,” in *Technicon Symposium Vol. 1*, 386.
- Bidigare, R. R., Buttler, F. R., Christensen, S. J., Barone, B., Karl, D. M., and Wilson, S. T. (2014). Evaluation of the utility of xanthophyll cycle pigment dynamics for assessing upper ocean mixing processes at Station ALOHA. *J. Plankton Res.* 36, 1423–1433. doi: 10.1093/plankt/fbu069
- Bidigare, R. R., and Ondrusek, M. E. (1996). Spatial and temporal variability of phytoplankton pigment distributions in the central equatorial Pacific ocean. *Deep Sea Res. II* 43, 809–833. doi: 10.1016/0967-0645(96)0019-7
- Bidigare, R. R., van Heukelem, L., and Trees, C. C. (2005). “Analysis of algal pigments by high-performance liquid chromatography,” in *Algal Culturing Techniques*, ed R. A. Andersen (New York, NY: Academic Press), 327–345.
- Bienfang, P. K., and Szyper, J. P. (1981). Phytoplankton dynamics in the subtropical Pacific Ocean off Hawaii. *Deep Sea Res.* 28A, 981–1000. doi: 10.1016/0198-0149(81)90013-3
- Calbet, A., and Landry, M. R. (2004). Phytoplankton growth, microzooplankton grazing, and carbon cycling in marine systems. *Limnol. Oceanogr.* 49, 51–57. doi: 10.4319/lo.2004.49.1.0051
- Campbell, L., Nolla, H. A., and Vaulot, D. (1994). The importance of Prochlorococcus to community structure in the central North Pacific Ocean. *Limnol. Oceanogr.* 39, 954–961. doi: 10.4319/lo.1994.39.4.0954
- Campbell, L., and Vaulot, D. (1993). Photosynthetic picoplankton community structure in the subtropical North Pacific Ocean near Hawaii (station ALOHA). *Deep Sea Res. I* 40, 2043–2060. doi: 10.1016/0967-0637(93)90044-4
- Caporaso, J. G., Bittinger, K., Bushman, F. D., DeSantis, T. Z., Andersen, G. L., and Knight, R. (2010). PyNAST: a flexible tool for aligning sequences to a template alignment. *Bioinformatics* 26, 266–267. doi: 10.1093/bioinformatics/btp636
- Caporaso, J. G., Lauber, C. L., Walters, W. A., Berg-Lyons, D., Huntley, J., Fierer, N., et al. (2012). Ultra-high-throughput microbial community analysis on the Illumina HiSeq and MiSeq platforms. *ISME J.* 6, 1621–1624. doi: 10.1038/ismej.2012.8
- Church, M. J., Mahaffey, C., Letelier, R. M., Lukas, R., Zehr, J. P., and Karl, D. M. (2009). Physical forcing of nitrogen fixation and diazotroph community structure in the North Pacific subtropical gyre. *Glob. Biogeochem. Cycle* 23:GB2020. doi: 10.1029/2008GB003418
- Cortés, M. Y., Bollman, J., and Thierstein, H. R. (2001). Coccolithophore ecology at the HOT station ALOHA, Hawaii. *Deep Sea Res. II* 48, 1925–1956. doi: 10.1016/S0967-0645(00)00165-X
- Cullen, J. J. (1995). Status of the iron hypothesis after the open-ocean enrichment experiment. *Limnol. Oceanogr.* 47, 1336–1343. doi: 10.4319/lo.1995.40.7.1336
- Dandonneau, Y., Vega, A., Loisel, H., du Penhant, Y., and Menkes, C. (2003). Oceanic Rossby waves acting as a “hay rake” for ecosystem floating by-products. *Science* 302, 1548–1551. doi: 10.1126/science.1090729
- Dimier, C., Giovanni, S., Ferdinando, T., and Brunet, C. (2009). Comparative ecophysiology of the xanthophyll cycle in six marine phytoplanktonic species. *Protist* 160, 397–411. doi: 10.1016/j.protis.2009.03.001
- Dore, J. E., Letelier, R. M., Church, M. J., Lukas, R., and Karl, D. M. (2008). Summer phytoplankton blooms in the oligotrophic North Pacific subtropical gyre: historical perspective and recent observations. *Prog. Oceanogr.* 76, 2–38. doi: 10.1016/j.pocean.2007.10.002
- Dortch, Q. (1990). The interaction between ammonium and nitrate uptake in phytoplankton. *Mar. Ecol. Prog. Ser.* 61, 183–201. doi: 10.3354/meps061183
- Dupont, C. L., McCrow, J. P., Valas, R., Moustafa, A., Walworth, N., Goodenough, U., et al. (2014). Genomes and gene expression across light and productivity gradients in eastern subtropical Pacific microbial communities. *ISME J.* 9, 1076–1092. doi: 10.1038/ismej.2014.198
- Edgar, R. C., Haas, B. J., Clemente, J. C., Quince, C., and Knight, R. (2011). UCHIME improves sensitivity and speed of chimaera detection. *Bioinformatics* 27, 2194–2200. doi: 10.1093/bioinformatics/btr381
- Eppley, R. W., Carlucci, A. F., Holm-Hansen, O., Kiefer, D., McCarthy, J. J., Venrick, E., et al. (1971). Phytoplankton growth and composition in shipboard cultures supplied with nitrate, ammonium, or urea as the nitrogen source. *Limnol. Oceanogr.* 16, 741–751. doi: 10.4319/lo.1971.16.5.0741
- Eppley, R. W., Rogers, J. N., and McCarthy, J. J. (1969). Half-saturation constants for uptake of nitrate and ammonium by marine phytoplankton. *Limnol. Oceanogr.* 14, 912–920. doi: 10.4319/lo.1969.14.6.0912
- Eppley, R. W., Sharp, J. H., Renger, E. H., Perry, M. J., and Harrison, W. G. (1977). Nitrogen assimilation by phytoplankton and other microorganisms in the surface waters of the central North Pacific Ocean. *Mar. Biol.* 39, 111–120. doi: 10.1007/BF00386996
- Faraway, J. J. (2002). *Practical Regression and ANOVA Using R*. 128–129. Available online at: <http://cran.r-project.org/doc/contrib/Faraway-PRA.pdf>
- Fawcett, S. E., Lomas, M. W., Casey, J. R., Ward, B. B., and Sigman, D. M. (2011). Assimilation of upwelled nitrate by small eukaryotes in the Sargasso Sea. *Nat. Geosci.* 4, 717–722. doi: 10.1038/ngeo1265
- Frias-Lopez, J., Thompson, A., Waldbauer, J., and Chisholm, S. W. (2009). Use of stable isotope-labelled cells to identify active grazers of picocyanobacteria in ocean surface waters. *Environ. Microbiol.* 11, 512–525. doi: 10.1111/j.1462-2920.2008.01793.x
- Frost, B. W. (1991). The role of grazing in nutrient-rich areas of the open sea. *Limnol. Oceanogr.* 36, 1616–1630. doi: 10.4319/lo.1991.36.8.1616
- Hartmann, M., Grob, C., Tarhan, G. A., Martin, A. P., Burkhill, P. H., Scanlan, D. J., et al. (2012). Mixotrophic basis of Atlantic oligotrophic ecosystems. *Proc. Natl. Acad. Sci. U.S.A.* 109, 5756–5760. doi: 10.1073/pnas.1118179109
- Hollander, M., and Wolfe, D. A. (1973). *Nonparametric Statistical Procedures*. New York, NY: Wiley.
- Johnson, K. S., Riser, S. C., and Karl, D. M. (2010). Nitrate supply from deep to near-surface waters of the North Pacific subtropical gyre. *Nature* 465, 1062–1065. doi: 10.1038/nature09170
- Juranek, L. W., Quay, P. D., Feely, R. A., Lockwood, D., Karl, D. M., and Church, M. J. (2012). Biological production in the NE Pacific and its influence on air-sea CO₂ flux: evidence from dissolved oxygen isotopes and O₂/Ar. *J. Geophys. Res.* 117:C05022. doi: 10.1029/2011JC007450
- Karl, D. M. (1999). A sea of change: biogeochemical variability in the North Pacific subtropical gyre. *Ecosystems* 2, 181–214. doi: 10.1007/s100219900068
- Karl, D. M. (2002). Nutrient dynamics in the deep blue sea. *Trends Microbiol.* 10, 410–418. doi: 10.1016/S0966-842X(02)02430-7
- Karl, D. M., Björkman, K. M., Dore, J. E., and Fujieki, L. (2001). Ecological nitrogen-to-phosphorus stoichiometry at station ALOHA. *Deep Sea Res. II* 48, 1529–1566. doi: 10.1016/S0967-0645(00)00152-1
- Karl, D. M., Christian, J., Dore, J. E., Hebel, D. V., Letelier, R. M., Tupas, L. M., et al. (1996). Seasonal and interannual variability in primary production and particle flux at Station ALOHA. *Deep Sea Res. II* 43, 539–568. doi: 10.1016/0967-0645(96)00002-1
- Karl, D. M., and Church, M. J. (2017). Ecosystem structure and dynamics in the North pacific subtropical gyre: new views of an old ocean. *Ecosystems* 3, 433–457. doi: 10.1007/s10021-017-0117-0
- Karl, D. M., Church, M. J., Dore, J. E., Letelier, R. M., and Mahaffey, C. (2012). Predictable and efficient carbon sequestration in the North Pacific ocean supported by symbiotic nitrogen fixation. *Proc. Natl. Acad. Sci. U.S.A.* 109, 1842–1849. doi: 10.1073/pnas.1120312109
- Karl, D. M., Letelier, R., Hebel, D., Bird, D. F., and Winn, C. (1992). “Trichodesmium blooms and new nitrogen in the North Pacific gyre,” in *Marine Pelagic Cyanobacteria: Trichodesmium and Other Diazotrophs*, eds E. J. Carpenter and D. G. Capone (Dordrecht: Springer), 219–237.
- Karl, D. M., Letelier, R., Tupas, L., Dore, J. E., Christian, J., and Hebel, D. (1997). The role of nitrogen fixation in biogeochemical cycling in the subtropical North Pacific Ocean. *Nature* 388, 533–538. doi: 10.1038/41474
- Karl, D. M., and Lukas, R. (1996). The Hawaii Ocean Time-series (HOT) program: background, rationale and field implementation. *Deep Sea Res. II* 43, 129–156. doi: 10.1016/0967-0645(96)00005-7

- Lane, D. J. (1991). "16S / 23S sequencing," in *Nucleic Acid Technologies in Bacterial Systematics*, eds E. Stackebrandt and M. Goodfellow (New York, NY: Wiley), 115–175.
- Latasz, M., Landry, M. R., Schlüter, L., and Bidigare, R. R. (1997). Pigment-specific growth and grazing rates of phytoplankton in the central equatorial Pacific. *Limnol. Oceanogr.* 42, 289–298. doi: 10.4319/lo.1997.42.2.0289
- Letelier, R. M., Bidigare, R. R., Hebel, D. V., Ondrusek, M. E., Winn, C. D., and Karl, D. M. (1993). Temporal variability of phytoplankton community structure based on pigment analysis. *Limnol. Oceanogr.* 38, 1420–1437. doi: 10.4319/lo.1993.38.7.1420
- Letelier, R. M., Dore, J. E., Winn, C. D., and Karl, D. M. (1996). Seasonal and interannual variations in photosynthetic carbon assimilation at Station. *Deep Sea Res. II* 43, 467–490. doi: 10.1016/0967-0645(96)00006-9
- Letelier, R. M., Karl, D. M., Abbott, M. R., and Bidigare, R. R. (2004). Light driven seasonal patterns of chlorophyll and nitrate in the lower euphotic zone of the North Pacific subtropical gyre. *Limnol. Oceanogr.* 49, 508–519. doi: 10.4319/lo.2004.49.2.02058
- Li, B., Karl, D. M., Letelier, R. M., and Church, M. J. (2011). Size-dependent photosynthetic variability in the North Pacific subtropical gyre. *Mar. Ecol. Prog. Ser.* 440, 27–40. doi: 10.3354/meps09345
- Li, Q. P., Zhang, J.-Z., Millero, F. J., and Hansell, D. A. (2005). Continuous colorimetric determination of trace ammonium in seawater with a long-path liquid waveguide capillary cell. *Mar. Chem.* 96, 73–85. doi: 10.1016/j.marchem.2004.12.001
- Liu, H., Probert, I., Uitz, J., Claustré, H., Aris-Brosou, S., Frada, M., et al. (2009). Extreme diversity in noncalcifying haptophytes explains a major pigment paradox in open oceans. *Proc. Natl. Acad. Sci. U.S.A.* 106, 12803–12808. doi: 10.1073/pnas.0905841106
- Longhurst, A. R. (1967). Diversity and trophic structure of zooplankton communities in the California current. *Deep Sea Res.* 14, 393–408. doi: 10.1016/0011-7471(67)90047-2
- Mahaffey, C., Björkman, K. M., and Karl, D. M. (2012). Phytoplankton response to deep seawater nutrient addition in the North Pacific subtropical gyre. *Mar. Ecol. Prog. Ser.* 460, 13–34. doi: 10.3354/meps09699
- Medinger, R., Nolte, V., Pandey, R. V., Jost, S., Ottenwalder, B., Schlötterer, C., et al. (2010). Diversity in a hidden world: potential and limitation of next-generation sequencing for surveys of molecular diversity of eukaryotic microorganisms. *Mol. Ecol.* 19, 32–40. doi: 10.1111/j.1365-294X.2009.04478.x
- Medlin, L., Elwood, H. J., Stickel, S., and Sogin, M. L. (1988). The characterization of enzymatically amplified eukaryotic 16S-like rRNA-coding regions. *Gene* 71, 491–499. doi: 10.1016/0378-1119(88)90066-2
- Millie, D. F., Paerl, H. W., Hurley, J. P., and Kirkpatrick, G. J. (1993). Algal pigment determinations in aquatic ecosystems: analytical evaluations, applications and recommendations. *Curr. Top. Bot. Res.* 1, 1–13.
- Newell, B. S., Morgan, B., and Cundy, J. (1967). The determination of urea in seawater. *J. Mar. Res.* 25, 201–202.
- Not, F., del Campo, J., Balagué, V., de Vargas, C., and Massana, R. (2009). New insights into the diversity of marine picoeukaryotes. *PLoS ONE* 4:e7143. doi: 10.1371/journal.pone.0007143
- Oksanen, J., Blanchet, F. G., Kindt, R., Legendre, P., Minchin, P. R., O'Hara, R. B., et al. (2007). Package "vegan": Community Ecology Package. R package version 2.0-10. Available online at: <http://cran.r-project.org/web/packages/vegan/>
- Paerl, R. W., Foster, R. A., Jenkins, B. D., Montoya, J. P., and Zehr, J. P. (2008). Phylogenetic diversity of cyanobacterial narB genes from various marine habitats. *Environ. Microbiol.* 10, 3377–3387. doi: 10.1111/j.1462-2920.2008.01741.x
- Quast, C., Pruesse, E., Yilmaz, P., Gerken, J., Schweer, T., Yarza, P., et al. (2012). The SILVA ribosomal RNA gene database project: improved data processing and web-based tools. *Nucl. Acids Res.* 41, D590–D596. doi: 10.1093/nar/gks1219
- R Core Development Team. (2014). *R: A Language and Environment for Statistical Computing*. Vienna: R Foundation for Statistical Computing. Available online at: <https://cran.r-project.org>
- Rii, Y. M., Brown, S. L., Nencioli, F., Kuwahara, V., Dickey, T. D., Karl, D. M., et al. (2008). The transient oasis: nutrient-phytoplankton dynamics and particle export in Hawaiian lee cyclones. *Deep-Sea Res. II* 55, 1275–1290. doi: 10.1016/j.dsr2.2008.01.013
- Rothhaupt, K. O. (1996). Laboratory experiments with a mixotrophic chrysophyte and obligately phagotrophic and phototrophic competitors. *Ecology* 77, 716–724. doi: 10.2307/2265496
- Royston, J. P. (1982). An extension of Shapiro and Wilk's W test for normality to large samples. *Appl. Stat.* 31, 115–124. doi: 10.2307/2347973
- Sakamoto, C. M., Karl, D. M., Jannasch, H. W., Bidigare, R. R., Letelier, R. M., Walz, P. M., et al. (2004). Influence of Rossby waves on nutrient dynamics and the plankton community structure in the North Pacific subtropical gyre. *J. Geophys. Res.* 109:C05032. doi: 10.1029/2003JC001976
- Scharek, R., Latasa, M., Karl, D. M., and Bidigare, R. R. (1999). Temporal variations in diatom abundance and downward vertical flux in the oligotrophic North Pacific gyre. *Deep Sea Res. I* 46, 1051–1075. doi: 10.1016/S0967-0637(98)00102-2
- Shilova, I. N., Mills, M. M., Robidart, J. C., Turk-Kubo, K. A., Björkman, K. A., Kolber, Z., et al. (2017). Differential effects of nitrate, ammonium, and urea as N sources for microbial communities in the North Pacific Ocean. *Limnol. Oceanogr.* 62, 2550–2574. doi: 10.1002/lo.10590
- Steeman Nielsen, E. (1952). The use of radioactive carbon (14C) for measuring organic production in the sea. *J. Cons. Cons. Int. Explor. Mer* 18, 117–140. doi: 10.1093/icesjms/18.2.117
- Stoeck, T., Bass, D., Nebel, M., Christen, R., Jones, M. D., Breiner, H.-W., et al. (2010). Multiple marker parallel tag environmental DNA sequencing reveals a highly complex eukaryotic community in marine anoxic water. *Mol. Ecol.* 19, 21–31. doi: 10.1111/j.1365-294X.2009.04800.x
- Strickland, J. D. H., Holm-Hansen, O., Eppley, R. W., and Linn, R. J. (1969). The use of a deep tank in plankton ecology. *Limnol. Oceanogr.* 14, 23–34. doi: 10.4319/lo.1969.14.1.0023
- Strickland, J. D. H., and Parsons, T. R. (1972). *A Practical Handbook of Seawater Analysis*. Ottawa, ON: Fisheries Research Board of Canada Bulletin 167.
- Timmermans, K. R., Van der Wagt, B., Veldhuis, M. J. W., Maatman, A., and De Baar, H. J. W. (2005). Physiological responses of three species of marine pico-phytoplankton to ammonium, phosphate, iron and light limitation. *J. Sea. Res.* 53, 109–120. doi: 10.1016/j.seares.2004.05.003
- Timonin, A. G. (1969). Structure of pelagic associations – quantitative relationship between different trophic groups of plankton in frontal zones of tropical ocean. *Oceanology* 9, 686–694.
- van de Poll, W. H., Vissier, R. J. W., and Buma, A. G. J. (2007). Acclimation to a dynamic irradiance regime changes excessive irradiance sensitivity of *Emiliania huxleyi* and *Thalassiosira weissflogii*. *Limnol. Oceanogr.* 52, 1430–1438. doi: 10.4319/lo.2007.52.4.1430
- Venrick, E. L. (1993). Phytoplankton seasonality in the central North Pacific: the endless summer reconsidered. *Limnol. Oceanogr.* 38, 1135–1149. doi: 10.4319/lo.1993.38.6.1135
- Venrick, E. L. (1997). Comparison of the phytoplankton species composition and structure in the Climax area (1973–1985) with that of Station ALOHA (1994). *Limnol. Oceanogr.* 42, 1643–1648. doi: 10.4319/lo.1997.42.7.1643
- Venrick, E. L. (1999). Phytoplankton species structure in the central North Pacific 1973–1996: variability and persistence. *J. Plankton Res.* 21, 1029–1042. doi: 10.1093/plankt/21.6.1029
- Villareal, T. A., Adornato, L., Wilson, C., and Schoenbaechler, C. A. (2011). Summer blooms of diatom-diazotroph assemblages and surface chlorophyll in the North Pacific gyre: a disconnect. *J. Geophys. Res.* 116:C03001. doi: 10.1029/2010JC006268
- Viviani, D. A., Karl, D. M., and Church, M. J. (2015). Variability in photosynthetic production of dissolved and particulate organic carbon in the North Pacific subtropical gyre. *Front. Mar. Sci.* 2:763. doi: 10.3389/fmars.2015.00073
- Wada, E., and Hattori, A. (1990). *Nitrogen in the Sea: Forms, Abundance, and Rate Processes*. Boca Raton, FL: CRC Press.
- White, A. E., Letelier, R. M., Whitmire, A. L., Barone, B., Bidigare, R. R., Church, M. J., et al. (2015). Phenology of particle size distributions and primary productivity in the North Pacific subtropical gyre (Station

- ALOHA). *J. Geophys. Res. Oceans* 120, 7381–7399. doi: 10.1002/2015JC010897
- Wickham, H. (2009). *ggplot2: Elegant Graphics for Data Analysis*. New York, NY: Springer Science and Business Media.
- Wright, S. W., Jeffrey, S. W., Mantoura, R. F. C., Llewellyn, C. A., Bjornland, T., Repeta, D., et al. (1991). Improved HPLC method for the analysis of chlorophylls and carotenoids from marine phytoplankton. *Mar. Ecol. Prog. Ser.* 77, 183–196. doi: 10.3354/meps077183
- Zhang, J., Kobert, K., Flouri, T., and Stamatakis, A. (2014). PEAR: a fast and accurate Illumina Paired-End reAd mergeR. *Bioinformatics* 30, 614–620. doi: 10.1093/bioinformatics/btt593
- Zhu, F., Massana, R., Not, F., Marie, D., and Vaultot, D. (2005). Mapping of picoeucaryotes in marine ecosystems with quantitative PCR of the 18S rRNA gene. *FEMS Microbiol. Ecol.* 52, 79–92. doi: 10.1016/j.femsec.2004.10.006
- Zubkov, M. V., and Tarran, G. A. (2008). High bacterivory by the smallest phytoplankton in the North Atlantic Ocean. *Nature* 455, 224–226. doi: 10.1038/nature07236

Conflict of Interest Statement: The authors declare that the research was conducted in the absence of any commercial or financial relationships that could be construed as a potential conflict of interest.

Copyright © 2018 Rii, Bidigare and Church. This is an open-access article distributed under the terms of the Creative Commons Attribution License (CC BY). The use, distribution or reproduction in other forums is permitted, provided the original author(s) and the copyright owner are credited and that the original publication in this journal is cited, in accordance with accepted academic practice. No use, distribution or reproduction is permitted which does not comply with these terms.



Isolation and Characterization of Bacteria That Degrade Phosphonates in Marine Dissolved Organic Matter

Oscar A. Sosa^{1,2*}, Daniel J. Repeta³, Sara Ferrón^{1,2}, Jessica A. Bryant^{1,2}, Daniel R. Mende^{1,2}, David. M. Karl^{1,2} and Edward F. DeLong^{1,2*}

¹ Daniel K. Inouye Center for Microbial Oceanography: Research and Education, University of Hawaii, Honolulu, HI, United States, ² Department of Oceanography, School of Ocean and Earth Science and Technology, University of Hawaii, Honolulu, HI, United States, ³ Department of Marine Chemistry and Geochemistry, Woods Hole Oceanographic Institution, Woods Hole, MA, United States

OPEN ACCESS

Edited by:

Matthew J. Church,
University of Montana, United States

Reviewed by:

Ronald Benner,
University of South Carolina,
United States
Jason Michel Smith,
University of California,
Santa Barbara, United States

*Correspondence:

Edward F. DeLong
edelong@hawaii.edu
Oscar A. Sosa
ososa@hawaii.edu

Specialty section:

This article was submitted to
Aquatic Microbiology,
a section of the journal
Frontiers in Microbiology

Received: 18 June 2017

Accepted: 05 September 2017

Published: 26 September 2017

Citation:

Sosa OA, Repeta DJ, Ferrón S, Bryant JA, Mende DR, Karl DM and DeLong EF (2017) Isolation and Characterization of Bacteria That Degrade Phosphonates in Marine Dissolved Organic Matter. *Front. Microbiol.* 8:1786.
doi: 10.3389/fmicb.2017.01786

Semi-labile dissolved organic matter (DOM) accumulates in surface waters of the oligotrophic ocean gyres and turns over on seasonal to annual timescales. This reservoir of DOM represents an important source of carbon, energy, and nutrients to marine microbial communities but the identity of the microorganisms and the biochemical pathways underlying the cycling of DOM remain largely uncharacterized. In this study we describe bacteria isolated from the North Pacific Subtropical Gyre (NPSG) near Hawaii that are able to degrade phosphonates associated with high molecular weight dissolved organic matter (HMWDOM), which represents a large fraction of semi-labile DOM. We amended dilution-to-extinction cultures with HMWDOM collected from NPSG surface waters and with purified HMWDOM enriched with polysaccharides bearing alkylphosphonate esters. The HMWDOM-amended cultures were enriched in Roseobacter isolates closely related to *Sulfitobacter* and close relatives of hydrocarbon-degrading bacteria of the *Oceanospirillaceae* family, many of which encoded phosphonate degradation pathways. *Sulfitobacter* cultures encoding C-P lyase were able to catabolize methylphosphonate and 2-hydroxyethylphosphonate, as well as the esters of these phosphonates found in native HMWDOM polysaccharides to acquire phosphorus while producing methane and ethylene, respectively. Conversely, growth of these isolates on HMWDOM polysaccharides as carbon source did not support robust increases in cell yields, suggesting that the constituent carbohydrates in HMWDOM were not readily available to these individual isolates. We postulate that the complete remineralization of HMWDOM polysaccharides requires more complex microbial inter-species interactions. The degradation of phosphonate esters and other common substitutions in marine polysaccharides may be key steps in the turnover of marine DOM.

Keywords: bacterial degradation, dissolved organic matter (DOM), phosphonate metabolism, C-P lyase, methane, ethylene, oligotrophic conditions

INTRODUCTION

Microbial heterotrophs in the sunlit region of the ocean are thought to be highly dependent on labile dissolved organic matter (DOM) produced by photosynthetic microorganisms (Cole et al., 1988; Zweifel et al., 1993; Cherrier et al., 1996; Gasol et al., 1998; Kuipers et al., 2000). Recent studies of the transcriptional dynamics of microbial communities in marine surface waters also suggest that the metabolism of the dominant heterotrophic and photoheterotrophic bacterioplankton populations is synchronized to autotrophic processes (Ottesen et al., 2014; Aylward et al., 2015). Despite the tight coupling observed between autotrophic and heterotrophic processes, a fraction of DOM escapes immediate degradation and accumulates in surface waters, turning over slowly as a result of a hypothetical malfunctioning microbial loop wherein DOM cannot be consumed as quickly as it is produced (Thingstad et al., 1997). Some of this “semi-labile” DOM is also exported and degraded below the euphotic zone over seasonal to annual timescales (Hansell et al., 2002; Carlson et al., 2004, 2010), fueling deep sea microbial community respiration (Aristegui et al., 2005).

About one-third of the semi-labile DOM in marine surface waters is HMWDOM that can be collected by ultrafiltration. HMWDOM isolated from surface waters in the NPSG is rich in carbohydrates, approximately 50% of total carbon (C), and its carbohydrate content diminishes rapidly with depth in the upper ocean indicating these are actively consumed by microorganisms (Benner et al., 1992). The spectral properties of HMWDOM are notably similar across ocean basins and freshwater environments suggesting a widespread and common source of this material (Aluwihare et al., 1997; Repeta et al., 2002). HMWDOM carbohydrates consist largely of a family of acylated heteropolysaccharides that have a well conserved monosaccharide composition resembling algal structural polysaccharides (Aluwihare et al., 1997). The radiocarbon value of the monosaccharides from acid-labile carbohydrates in HMWDOM indicates this carbon pool turns over in <3 years (Repeta and Aluwihare, 2006), consistent with the residence time of semi-labile DOM (100–1000 days) estimated by ecosystem modeling approaches (Luo et al., 2010).

Polysaccharides in HMWDOM incorporate large amounts of nitrogen (N) and phosphorus (P) that serve as organic nutrients to support microbial growth. More than half of organic N in HMWDOM occurs as *N*-acetyl amino polysaccharides (Aluwihare et al., 1997, 2005), making this one of the largest N reservoirs in the ocean. HMWDOM polysaccharides also contain phosphate and alkylphosphonate esters, which represent approximately 80% and 20% of the total organic P, respectively (Repeta et al., 2016), and are likely a key source of P to microorganisms. Despite the detailed chemical characterization of HMWDOM, little is known about how microorganisms degrade and metabolize this pool of organic nutrients.

Phosphonates (organophosphorus compounds with a characteristic C-P bond) occur in HMWDOM throughout the water column and across ocean basins (Kolowith et al., 2001). The microbial cycling of HMWDOM polysaccharide

phosphonates, namely methylphosphonate (MPn) esters, has recently been shown to be a key pathway by which dissolved methane in the upper ocean reaches concentrations above equilibrium with the atmosphere (Repeta et al., 2016), a phenomenon known as the oceanic methane paradox (Kiene, 1991). Microcosm studies showed that microbial communities from surface waters in the NPSG metabolized MPn and 2-hydroxyethylphosphonate (2-HEP) esters in HMWDOM polysaccharides to obtain P, producing methane and ethylene, respectively, the dealkylation products of these phosphonates (Repeta et al., 2016). Furthermore, a *Pseudomonas stutzeri* bacterium isolated from HMWDOM-amended seawater was shown to employ the C-P lyase pathway (Metcalf and Wanner, 1993a,b; White and Metcalf, 2004) to breakdown the MPn and 2-HEP esters in HMWDOM polysaccharides in response to P-limitation (Repeta et al., 2016). These findings supported the role of HMWDOM as a key source of organic P to microbial communities and highlight its utility as a model substrate to study microbial DOM cycling.

In this study we identify and characterize populations of organisms from low primary productivity regions in the NPSG capable of degrading constituents of semi-labile DOM. Seawater samples collected at the bottom of the euphotic zone near the deep chlorophyll maximum (DCM) and from the upper mesopelagic zone were supplemented with HMWDOM isolated from surface water which stimulated the growth of select bacterial populations. The growth characteristics and predicted metabolic functions of the bacterial isolates identified provide information of the bio-availability and cycling of major chemical constituents of HMWDOM. Results of this study demonstrate that phosphonates associated with HMWDOM carbohydrates are readily available to bacteria but also suggest that inter-species microbial interactions are required to fully degrade these carbohydrates. Our observations also link widespread bacterial clades like Roseobacter to semi-labile DOM cycling and to the aerobic production of methane in the ocean.

MATERIALS AND METHODS

Collection and Characterization of HMWDOM and Purification of the Polysaccharide-Rich Fraction

HMWDOM with a nominal molecular weight >1 kDa was collected by ultrafiltration of Hawaii seawater pumped from offshore through a 20 m-depth intake pipe at the National Energy Laboratory Hawaii Authority in Kona, HI, United States in February, 2013. HMWDOM ultrafiltration, chromatographic purification of polysaccharide-rich fractions, and chemical and spectroscopic analyses were performed as described previously (Repeta et al., 2016). The P content of purified HMWDOM polysaccharides was determined by the total dissolved P method described by Karl and Björkman (2001) which is based on the high temperature wet persulfate oxidation method for seawater (Menzel and Corwin, 1965) followed by phosphate determination by the magnesium-induced

coprecipitation and standard Murphy-Riley molybdenum blue reaction.

Preparation of Dilution-to-Extinction Cultures Amended with HMWDOM

Seawater samples for culturing experiments were collected at the field site of the Hawaii Ocean Time-series program, Station ALOHA, a region representative of the general conditions of the NPSG (Karl and Lukas, 1996). Seawater from the DCM (95 m) and from the top of the mesopelagic zone (250 m) was sampled with 12 L Niskin bottles attached to a Sea-Bird CTD-rosette during the Hawaii Ocean Experiment Budget of Energy I cruise on March 23, 2014¹. The culturing strategy was based on a modified high-throughput dilution-to-extinction culturing method (Connon and Giovannoni, 2002) in which samples are amended with HMWDOM collected by ultrafiltration (Sosa et al., 2015). Total cell abundances in the seawater samples collected were measured at sea with an Influx flow cytometer (BD Biosciences, San Jose, CA, United States). Briefly, triplicate 1 mL sub-samples were fixed with 15 μ L of 16% paraformaldehyde for 10 min and stained with 5 μ L of a 200x solution of SYBR® Green I (Invitrogen, Carlsbad, CA, United States) for 20 min in darkness. Total cell concentrations from each sample were used to calculate the dilutions necessary to obtain a final concentration of 2–3 cells mL^{-1} for dilution-to-extinction. Seawater samples were diluted with sterile seawater from 125 m depth obtained by tangential flow filtration as described previously (Sosa et al., 2015). The seawater for this medium was collected at Station ALOHA during the Hawaii Ocean Time-series cruise no. 261 in March 2014 prior to the culturing experiments. The total organic carbon (TOC) content of this medium was 67 μM , as determined by high-temperature combustion using a V series Shimadzu TOC analyzer (Shimadzu Scientific Instruments, Columbia, MD, United States). Control dilution-to-extinction samples were prepared with this medium without HMWDOM additions (treatment I). To prepare dilution-to-extinction samples with HMWDOM (treatments II–IV), freeze-dried HMWDOM was first dissolved in ultrapure water and filter-sterilized through a 0.22 μm Supor membrane syringe filter (Pall Corp., Port Washington, NY, United States). Approximately 7–18 mg of HMWDOM (2–5 mg C) was subsequently added to 1 L dilution-to-extinction samples resulting in TOC concentrations ranging from 162 to 405 μM . Because the HMWDOM samples are rich in C relative to N and P, the medium was also amended with inorganic N (60 μM NaNO_3 and 4 μM NH_4Cl) and P (7 μM H_3PO_4). This approximated the final C, N, and P content of HMWDOM-amended media to that of marine bacterial biomass (C:N:P ~45:9:1; Goldman et al., 1987). Each dilution-to-extinction sample was inoculated into 720 wells (1 mL per well) in non-tissue culture treated 48-well cultivation plates (Corning, Inc., Corning, NY, United States). Sterile dilution medium, with and without HMWDOM, was also incubated in cultivation plates to evaluate the presence of microbial contamination in the base seawater medium and in HMWDOM. DCM samples were incubated at 26°C under a diurnal cycle

consisting of a 12 h period of continuous light ($30 \mu\text{mol m}^{-2} \text{s}^{-1}$ photons of photosynthetically active radiation) and a 12 h dark period. Mesopelagic samples were incubated at 25°C in darkness. All cultivation plates were incubated for 10–11 weeks before evaluating culture growth.

Growth Screen of Dilution-to-Extinction Cultures

To evaluate the effect of HMWDOM additions on the growth of dilution-to-extinction cultures, 100 μl were sub-sampled from each well to enumerate cells stained with SYBR® Green I on a GUAVA easyCyte PLUS flow cytometer (Millipore). Flow cytometry data were analyzed with the flowCore and prada R packages as described previously (Sosa et al., 2015). Wells with densities $>1 \times 10^4 \text{ cells mL}^{-1}$ were considered to test positive for growth. Cultures identified in positive wells were maintained by transferring samples into 10 mL of the same sterile dilution-to-extinction medium in which each was isolated, including the same concentration of HMWDOM and inorganic nutrients.

DNA Purification and Whole Genome Shotgun Sequencing

To obtain genomic DNA for whole genome shotgun sequencing, cultures that remained viable after transferring were grown in 100 mL of the same seawater medium used for dilution-to-extinction without added HMWDOM. Cells were harvested on 0.22 μm Supor membrane disc filters (Pall Corp.) and stored at -80°C in sucrose-based lysis buffer (40 mM EDTA, 50 mM Tris [pH 8.3], and 0.75 M sucrose). Cells were incubated in lysis buffer containing 2 mg mL^{-1} of lysozyme (Sigma-Aldrich, St. Louis, MO, United States) for 30 min at 37°C and subsequently with 0.8 mg mL^{-1} of proteinase K (Roche, Basel, Switzerland) and 1% SDS for 2 h at 55°C. DNA was purified from the lysate using a chemagic Magnetic Separation Module I (Perkin Elmer, Waltham, MA, United States). Purified DNA samples were quantified using the PicoGreen® assay (Invitrogen) and the DNA concentrations were normalized before sequencing. DNA samples were prepared for sequencing using a Nextera XT 96 DNA sample preparation kit (Illumina, San Diego, CA, United States) to obtain indexed paired-end libraries. Libraries were sequenced with a 2 × 300 nt paired-end MiSeq run (Illumina).

Genome Assembly and Annotation

For cultures with high quality Illumina data, paired-end reads were first assembled using MIRA version 4.9.3 (Chevreux et al., 1999) with options for removing remaining Illumina adapters, low quality stretches, phiX174 standard, as well as other common Illumina artifacts. This generated a very conservative assembly which was used to predict genes. As part of the MIRA assembly process, a set of cleaned/clipped reads was also generated. This set of clean reads was used as input to SPAdes version 3.5 (Bankevich et al., 2012) with default parameters and explored with different *k*-mer settings. The resulting contigs were annotated through NCBI's Prokaryotic Genome Annotation Pipeline (Tatusova et al., 2013).

¹<http://hahana.soest.hawaii.edu/hoebroe/hoebroe.html>

For the remaining cultures, FastQ files from the MiSeq run were imported into the CLC Genomics Workbench (CLC bio, Aarhus, Denmark). Reads were assembled into contigs using CLC's *de novo* assembler with automatic word and bubble sizes, a minimum contig length of 200, insertion and deletion costs set to 3, mismatch cost set to 2, length fraction set to 0.5, and the similarity fraction set to 0.8. These contigs were used to identify isolates with limited Illumina data.

Phylogenetic Placement of Cultures

For cultures with high-quality Illumina data, full-length small subunit (SSU) rRNA sequences were obtained from the annotated assemblies. For the remaining cultures, full-length or partial SSU rRNA sequences were extracted manually from contigs ≥ 1000 nt in length assembled in the CLC genomics workbench. To identify SSU rRNA sequences in these contigs, blastn was implemented in the CLC genomics workbench with default parameters (number of threads = 1, filter low complexity = yes, mask lower case = no, expectation value = 10, word size = 11, match = 2, mismatch = -3, gap costs: existence = 5 and extension = 2, and maximum number of hits = 100) using the SILVA 115 NR99 database. Complete and near full-length SSU rRNA genes identified in the assembled data were aligned using the SILVA Incremental Aligner (SINA) version 1.2.11 and classified with the least common ancestor method (Pruesse et al., 2012). The alignment was imported into ARB (Ludwig et al., 2004) and merged with the SILVA "All-Species Living Tree" (LTPs115) SSU reference tree (Muñoz et al., 2011). A total of 240 sequences including closely related reference sequences from SILVA were included for phylogenetic comparisons. The sequence alignment was filtered in ARB to exclude gaps, missing data, ambiguous nucleotide positions, and lower case positions. The filtered alignment contained 1172 comparable nucleotide positions across all sequences. Phylogenetic analysis was implemented using the Neighbor-Joining method (Saitou and Nei, 1987) with 1000-replicate bootstrap confidence limits (Felsenstein, 1985) in MEGA6 (Tamura et al., 2013). The evolutionary distances were computed using the Kimura 2-parameter method (Kimura, 1980) and are in the units of the number of base substitutions per site. The rate variation among sites was modeled with a gamma distribution (shape parameter = 2).

Functional Analysis of Coding DNA Sequences

We explored the functional annotations of protein coding DNA sequences (CDS) to assess the potential of our isolates to degrade known chemical constituents of HMWDOM, namely carbohydrates and phosphonates. To determine the potential of carbohydrate degradation, CDSs were annotated with the Carbohydrate-Active EnZyme (CAZy) database (Cantarel et al., 2009) using HMMER3.0 (Eddy, 2009) and hidden Markov models of CAZy signature domains (Yin et al., 2012). We compared the proportion of CDSs with predicted CAZy domains in each of the 55 assembled genomes to those of

well-known bacteria specialized in carbohydrate degradation. The analysis also targeted protein sequences associated with the C-P lyase pathway for alkylphosphonate degradation (Metcalf and Wanner, 1993a,b). BLASTp was employed to identify best matching C-P lyase pathway operons present in the genomes of HMWDOM isolates using as queries the protein sequences of C-P lyase pathway operons identified by Martínez et al. (2013) in the NPSG (Supplementary Table 1). In addition, the NCBI genome annotations of CDSs of these isolates were explored to identify additional proteins involved in phosphonate metabolism.

Gas Chromatography Analysis of Bacterial Cultures Amended with HMWDOM Polysaccharides or Phosphonates

Cultures of *Sulfitobacter* sp. HI0054 were amended with phosphonates or purified HMWDOM polysaccharides to test and measure the production of hydrocarbon gas products expected from dealkylation of phosphonates. *Sulfitobacter* cultures were pre-grown in seawater medium containing glycerol (0.2 mM C) and ammonium (0.8 mM). To force cells to take up phosphate present in natural seawater, P was not added to the medium. The medium was also supplemented with PRO99 medium trace metals (Moore et al., 2007) and with a vitamin cocktail based on the RMP medium for the cultivation of cyanobacteria (Supplementary Table 2). The culture was grown for 3 days at 25°C, stirred gently, and bubbled with filtered air to replenish oxygen. Subsequently, culture samples were aliquoted into 72 mL serum vials to prepare incubations with phosphonates or HMWDOM as follows: (1) control samples with no P added; (2) HMWDOM polysaccharides (27 $\mu\text{g mL}^{-1}$) containing approximately 855 μM C and 3.9 μM P; (3) methylphosphonate (MPn, 250 nM); (4) 2-hydroxyethylphosphonate (2-HEP, 250 nM); and (5) ethylphosphonate (EPn, 250 nM). Based on the C:P ratio of HMWDOM polysaccharides and the proportion of total P comprised of phosphonates (20%; Repeta et al., 2016), the HMWDOM amendment was estimated to contain ~ 780 nM phosphonates. Triplicate samples for each treatment were crimp-sealed with butyl/PTFE-faced plugs (Wheaton, Millville, NJ, United States) and aluminum collars and incubated at 25°C for 3 days.

Dissolved methane, ethylene, and ethane concentrations were measured by gas chromatography using a gas stripping and cryo-trap concentration method similar to that of Tilbrook and Karl (1995), and described in Repeta et al. (2016). Dissolved gases were purged from a known volume of culture with ultra high purity helium. The volume of sample purged, determined by weight, was approximately 50 mL. During the gas stripping procedure, the gas stream passed through Drierite® and Ascarite® columns to remove water vapor and carbon dioxide, and then the gases were concentrated in a 80–100 mesh Porapak-Q® trap cooled in liquid N₂. Once the gas extraction was completed (12 min), the trap was heated with boiling water and the concentrated gases were released and injected into the gas

chromatograph (model 7980A, Agilent Technologies, Inc., Santa Clara, CA, United States). The gases were separated in a GS-CarbonPLOT capillary column ($30\text{ m} \times 0.320\text{ mm I.D.}$, $3.0\text{ }\mu\text{M}$; Agilent Technologies, Inc.) and analyzed with a flame ionization detector (FID). The FID was calibrated by injecting different size loops of a gas mixture standard containing 10 ppm of methane, ethylene, and ethane in pure N₂ (Scott-Marrin, Inc., Riverside, CA, United States). The loops were injected into the purging chamber and concentrated into the Porapak-Q® trap following the same procedure as for the seawater samples.

Environmental Representation of C-P Lyase in the NPSG

Metagenomic coverage of SSU rRNA gene sequences of bacteria isolated from HMWDOM-amended treatments encoding C-P lyase was used to estimate their abundance throughout the water column at Station ALOHA. The metagenomes interrogated were obtained from seawater samples collected during 12 Hawaii Ocean Time-series cruises between August 2010 and December 2011 and correspond to the datasets comprising the ALOHA gene catalog (Mende et al., 2017). The SSU rRNA sequences of the bacterial isolates were assigned to operational taxonomic units (OTUs) by first combining them with a collection of sequences from the SILVA database representing OTUs (97% sequence identity) developed for QIIME (Caporaso et al., 2010; Quast et al., 2013; SILVA release 128). The combined sequences were then clustered into OTUs (97% sequence identity) using vsearch (Rognes et al., 2016) and a representative sequence from each OTU was selected. The normalized abundances of OTUs representing our isolates were estimated by mapping SSU rRNA gene fragments extracted from Station ALOHA shotgun metagenomes to the OTU reference sequences using bowtie2 (Langmead and Salzberg, 2012). Fragments were assigned to the OTU with the best alignment provided there was greater than 97% sequence identity over at least 70 bps. The number of gene fragments mapping to these OTUs was then divided by the total number of mapped fragments.

The ALOHA gene catalog (Mende et al., 2017) further provides normalized abundances for each gene and functional group as estimates of copy number per average genome size for each metagenome. To estimate the abundance of C-P lyase pathway genes at Station ALOHA, the individual genes in the C-P lyase operons of the HMWDOM isolates were first assigned to eggNOG orthologous groups (OG) (Huerta-Cepas et al., 2016) (PhnG: COG3624, PhnH: COG3625, PhnI: COG3626, PhnJ: COG3627, PhnK: COG4107, PhnL: COG4778, PhnM: COG3454, PhnN: ENOG4111MI2 and COG3709). Subsequently, the abundances of these OGs were obtained from the ALOHA gene catalog and mean abundances were plotted by sampling depth to explore the importance of this pathway throughout the water column. Differences in mean abundances between depths were evaluated using a Tukey multiple comparisons method adjusted for multiplicity (Bonferroni correction) implemented with R package multcomp.

HMWDOM Dose Growth Response Tests

To determine if HMWDOM supported increased cell yields of bacterial isolates relative to unamended seawater, we grew cultures with increasing concentrations of HMWDOM or purified HMWDOM polysaccharides. Sterile seawater media used for dilution-to-extinction (including the same inorganic nutrient additions) was amended with PRO99 trace metals (Moore et al., 2007) and a vitamin cocktail based on the RMP medium for the cultivation of cyanobacteria (Supplementary Table 2). In this experiment, cultures of two representative isolates were supplemented with 20, 40, or 60 $\mu\text{g mL}^{-1}$ of HMWDOM polysaccharides. In a second experiment, additional cultures were amended with 7.2, 14.4, or 21.6 $\mu\text{g mL}^{-1}$ of HMWDOM or with 14.4 or 28.8 $\mu\text{g mL}^{-1}$ of purified HMWDOM polysaccharides. The control media consisted of seawater without HMWDOM amendments. All tests were conducted in triplicate. Samples were inoculated with cultures maintained in seawater media without HMWDOM amendments at 25°C in darkness. Growth was measured over the course of a week as total SYBR® Green I-stained cells on a GUAVA easyCyte PLUS (Millipore) flow cytometer. To evaluate if HMWDOM treatments had a significant positive effect on growth, the average cell yields over stationary phase were compared between HMWDOM treatments and unamended seawater using a one-tailed Dunnett test implemented in R with package multcomp.

Carbon Substrate Utilization Profiles of Bacterial Isolates

To characterize the types of carbon compounds metabolized by bacterial isolates, representative isolates were assayed for increased cell yields in Biolog multi-carbon plates (PM1 and PM2A) containing a total of 190 different organic compounds (Biolog, Hayward, CA, United States). The exact formulation of Biolog plates is proprietary but is similar to the recipes published by Bochner et al. (2001) which utilize 25 mM carbon compound concentrations and 2 and 5 mM inorganic P and N concentrations, respectively. In our experiments, each compound was dissolved in 100 μL of sterile water and treated as a 10,000-fold concentrated stock. The seawater medium was also amended with PRO99 trace metals and RMP medium vitamins (Supplementary Table 2). Bacterial cultures were grown in 48-well cultivation plates (Corning, Inc.). The Biolog compounds were added to a final one-fold concentration. Samples were incubated for 3–7 days at 26°C. To determine which compounds supported growth, cell concentrations were obtained by flow cytometry several times during the incubation period from 100 μl sub-samples stained with SYBR® Green I.

The cell yields at each time point were analyzed using a modified outlier identifier method (Leys et al., 2013) which relies on the median absolute deviation (MAD) to determine upper (median + $2 \times \text{MAD}$) and lower (median - $2 \times \text{MAD}$) confidence intervals of the data. MAD was implemented in R with function MAD and default options. Substrates deemed to support growth had cell yields greater than the upper MAD-based thresholds. In addition, the relative growth effect of each Biolog compound was evaluated by

normalizing the cell yield by the median cell yield across all test compounds (190 total) and log₂-transforming this ratio to produce a doubling scale (log₂ fold-change). MAD-based positive growth agreed well with cell yields resulting in a log₂ fold change >1 and negative growth with log₂ fold-change <-1. The median was selected to analyze the data and normalize cell yields because its value closely approximated the cell yields in cultures with no Biolog carbon substrate added and because most test substrates did not result in considerable growth.

RESULTS

Elemental and Chemical Composition of HMWDOM

HMWDOM collected from Hawaii surface waters was composed of 30% carbon by weight. The polysaccharide chromatographic fraction was composed of 38–40% carbon by weight. The C:N ratio of these samples were similar, 12.6 and 12.9, respectively. HMWDOM polysaccharides were composed of 0.47% P by weight with a C:P ratio of 220. ³¹P-NMR analysis indicated the polysaccharide fraction consisted of phosphonate (20% total P), phosphate (70% of total P) and pyrophosphate (10% of total P) esters as reported previously (Repeta et al., 2016). The chromatographic separation procedure removed organic constituents consistent with the chemical spectra of humic substances and produced fractions consisting of ≥90% polysaccharides.

HMWDOM Amendments and Recovery of Cultures

Mean (\pm standard deviation, $n = 3$) cell abundances in DCM and mesopelagic seawater samples used for dilution-to-extinction culturing were $5.0 \times 10^5 \pm 1.4 \times 10^4$ cells mL⁻¹ and $1.1 \times 10^5 \pm 2.6 \times 10^3$ cells mL⁻¹, respectively. These cell densities are characteristic of the NPSG near Station ALOHA (Campbell et al., 1997). HMWDOM amendments to dilution-to-extinction cultures increased the total organic carbon (TOC) concentration of the cultivation media 3–7 times (230–472 μ M) over the TOC of the control medium (67 μ M) and the TOC values typically measured in surface waters at Station ALOHA (Supplementary Table 3).

The distribution of cell densities in dilution-to-extinction samples and the number of wells that tested positive for growth in each control sample or HMWDOM treatment during the flow cytometry screen are presented in Supplementary Table 4. The difference in the proportion of positive wells recovered from DCM samples was not significant between treatments, $X^2(3, N = 30) = 2.27, p > 0.05$. In contrast, there was a significant difference in the number of positive wells recovered between treatments in mesopelagic samples, $X^2(3, N = 84) = 32.95, p < 0.05$. Notably, HMWDOM amendments to mesopelagic samples (treatments II–IV, Figure 1) recovered 2–8 times more positive wells than the control experiment (treatment I, Figure 1). A total of 74 cultures out of 114 positive wells, 16 from the DCM

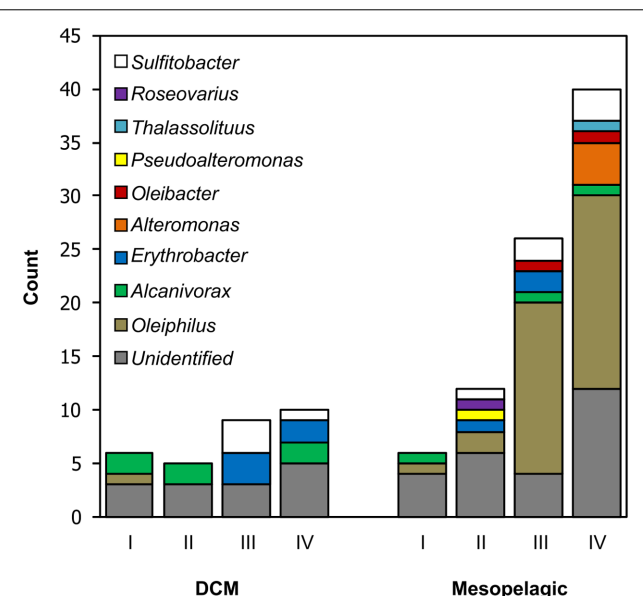


FIGURE 1 | Number and identity of bacterial isolates obtained in dilution-to-extinction culturing experiments. Column I represents control samples lacking HMWDOM amendments and columns II–IV indicate samples with HMWDOM amendments: treatment II: 7.2 mg L⁻¹; treatment III: 18 mg L⁻¹; treatment IV: 7.2 mg L⁻¹ (purified HMWDOM polysaccharides). The column height indicates the number of isolates that were viable and sub-cultured and the column color code indicates the SSU rRNA gene-based identification of isolates. Unidentified samples were positive wells that did not remain viable after sub-culturing and could not be sequenced. The total column height indicates the number of positive wells (>1 × 10⁴ cells mL⁻¹) originally detected in the flow cytometry growth screen.

and 58 from the mesopelagic, remained viable after subsequent transfers to HMWDOM-amended media and were grown for whole genome shotgun sequencing.

Genome Assemblies and Phylogeny of Cultures

Whole genome shotgun sequencing generated Illumina data for all 74 cultures of which 55 resulted in high-quality assemblies. The raw Illumina data was deposited in the NCBI sequence read archive under BioProject PRJNA305749 and is available under accessions SRX2766079–SRX2766152. The annotated assemblies were deposited in the DNA Data Bank of Japan, the European Nucleotide Archive, and GenBank and are available under accessions LWEI00000000–LWGK00000000. Individual isolate identifications, accession numbers, genome assembly metrics, and gene composition are summarized in Supplementary Tables 5 and 6.

Small subunit rRNA sequences of all 74 cultures fell under the classification of gammaproteobacteria (Supplementary Figure 1) or alphaproteobacteria (Supplementary Figure 2). The identity of SSU rRNA sequences in the SILVA database (119) best matching our bacterial isolates is presented in Supplementary Table 7. In addition to full-length SSU rRNA sequences, several partial SSU rRNA sequences were identified in the genome assemblies. In all but two of these assemblies, the partial sequences were 99–100%

similar to the full-length SSU rRNA sequences (Supplementary Table 5).

The number of isolates from each bacterial clade identified in the different treatments is summarized in **Figure 1**. The most common bacterial group isolated was closely related to the gammaproteobacterium *Oleiphilus messinensis* (Golyshin et al., 2002), enriched particularly in treatments III and IV in mesopelagic samples. The Roseobacter subclade *Sulfitobacter* was the second most common group in both DCM and mesopelagic samples amended with HMWDOM. Similarly, the *Erythrobacter* isolates were present in samples from both depths and only in treatments with HMWDOM. In turn, the *Alteromonas* isolates only occurred in mesopelagic samples amended with HMWDOM polysaccharides (treatment IV). In contrast, the *Alcanivorax* isolates were identified in all treatments and in samples from both depths, including unamended samples (treatment I). The remaining isolates were present in at least one HMWDOM treatment and were absent from the control treatment (I).

Phosphonate Degradation Pathways in Bacterial Isolates

Surveying the functional assignments of CDSs revealed the presence of complete C-P lyase pathway operons in 10 out of 55 genomes analyzed. *Sulfitobacter* sps. HI0021, HI0027, HI0054, HI0076, and HI0082, as well as *Roseovarius* sp. HI0049 encoded C-P lyase operons (**Figure 2B**) that were most similar to the *Rhodobacteraceae* operon B3TF_MPn_2 identified by Martínez et al. (2013) in surface waters near Hawaii (Supplementary Table 1). The *Roseovarius* sp. HI0049 draft genome encoded all predicted C-P lyase genes required for phosphonate degradation and additional putative auxiliary functions. These genes included a tetR family transcriptional regulator, phosphonate ABC transporters *phnCDE1E2*, a putative chloramphenicol acetyltransferase matching the transferase in the B3TF_MPn2 cluster, and a homolog of *phnM1* (contig LWFA01002944), *phnFGHIJK* (contig LWFA01001941) and

predicted protein homologs to *phnM*, *rcsF* (a phosphoesterase perhaps analogous to *phnF*; Martínez et al., 2013), and *phnNL* (contig LWFA01002897). The C-P lyase operons of *Sulfitobacter* isolates HI0021 (contig LWEP01000037), HI0027 (contig LWER01000183), *Sulfitobacter* sp. HI0054 (contig LWFD01000024), HI0076 (contig LWFQ01000564), and of HI0082 (contig LWFW01000191) were highly similar to the B3TF_MPn_2 operon but lacked a copy of *phnM1*. Also lacking in all but *Sulfitobacter* sp. HI0054 was a putative transferase located between *phnE2* and *phnM1* in the *Rhodobacterales* B3TF_MPn_2 cluster. Four phylogenetically similar *Oleiphilus* isolates (HI0009, HI0066, HI0067, and HI0125, Supplementary Figure 1) also encoded putative C-P lyase pathway operons. The putative C-P lyase operons of the *Oleiphilus* isolates shared 29–52% nucleotide sequence identity to gammaproteobacterium IMCC1989 B3TF_MPn_1 operon identified by Martínez et al. (2013) and contained all the genes in the *P. stutzeri* HI00D01 C-P lyase operon (**Figure 2A**). The C-P lyase gene clusters of isolates HI0009 and HI0066 were predicted to comprise of *phnFDCEGHJKLMNP* (**Figure 2C**). The two additional *Oleiphilus* isolates (HI0067 and HI0125) encoded all these genes but the assemblies could not resolve them together in the same contig.

In addition to C-P lyase, these same *Oleiphilus* isolates encoded genes bearing high similarity to *phnW* and *phnX*, which encode 2-aminoethylphosphonate:pyruvate aminotransferase and phosphonoacetaldehyde hydrolase, respectively. The former converts 2-aminoethylphosphonate into phosphonoacetaldehyde and alanine and the latter cleaves phosphonoacetaldehyde into acetaldehyde and phosphate (Quinn et al., 2007). *Pseudoalteromonas shioyasakiensis* HI0053 and *Thalassolitus* sp. HI0120 also carry genes annotated as *phnW* and *phnX*. *Roseovarius* sp. HI0049 carries gene *phnY*, which encodes phosphonoacetaldehyde dehydrogenase, an enzyme that mediates the formation of phosphonoacetate (Agarwal et al., 2014).

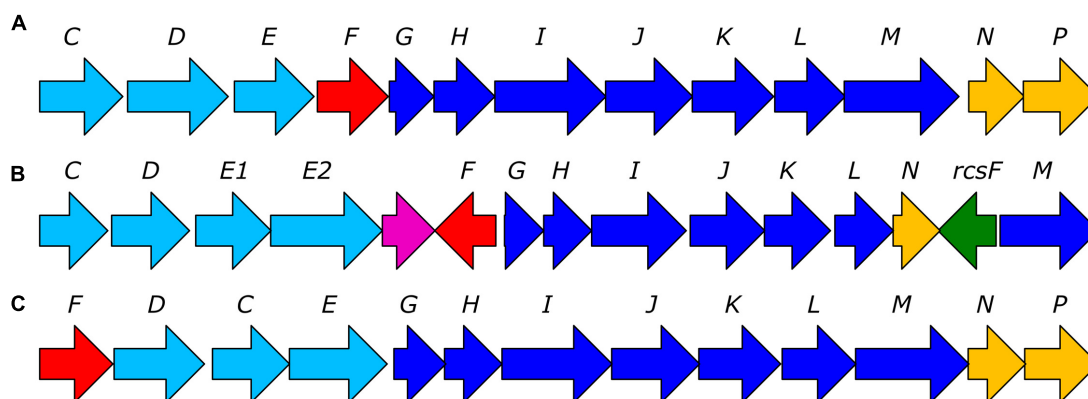


FIGURE 2 | Representative bacterial C-P lyase operons identified in HMWDOM enriched bacterial isolates. **(A)** The C-P lyase operon of *Pseudomonas stutzeri* HI00D01 (Repeta et al., 2016). **(B)** The C-P lyase operon of *Sulfitobacter* sp. HI0054. **(C)** A hypothetical C-P lyase operon identified in *Oleiphilus* sp. HI0066. The arrow color indicates genes involved in phosphonate transport (light blue), transcriptional regulation (red), catalytic functions (blue), auxiliary functions (yellow), and undetermined functions (green and violet).

TABLE 1 | Hydrocarbon gas production and cell yields of *Sulfitobacter* sp. HI0054 cultures amended with HMWDOM polysaccharides or phosphonates.

Treatment	Methane (nM)	Ethylene (nM)	Ethane (nM)	Cells mL ⁻¹
No phosphorus	-0.2 ± 0.0	0.1 ± 0.0	0.0 ± 0.0	2.6E+07 (3%)
HMWDOM polysaccharides	6.0 ± 0.1	11.1 ± 0.0	0.1 ± 0.0	3.9E+07 (8%)
Methylphosphonate	217.9 ± 3.2	0.1 ± 0.0	0.0 ± 0.0	3.9E+07 (3%)
2-Hydroxyethylphosphonate	-0.1 ± 0.1	232.9 ± 0.0	0.0 ± 0.0	3.5E+07 (3%)
Ethylphosphonate	-0.2 ± 0.0	0.1 ± 0.0	217.6 ± 4.6	3.8E+07 (5%)

Indicated are the mean and standard deviations of the final gas concentrations in the samples minus the gas concentration in the media at the beginning of the incubation. Also indicated are the cell concentrations (mean and coefficient of variation) of the samples at the end of the incubation.

Degradation of Phosphonates Associated with HMWDOM Polysaccharides

The ability of *Sulfitobacter* sp. HI0054 to degrade alkylphosphonates and phosphonates associated with HMWDOM polysaccharides was tested using batch cultures incubated in gas tight vials. Culture samples amended with MPn, 2-HEP, or ethylphosphonate (EPn) accumulated dissolved methane, ethylene, and ethane, respectively (Table 1). Based on the average gas concentrations measured in these cultures, an estimated 87–93% of the total phosphonate added (250 nM) was degraded during the incubation period. *Sulfitobacter* cultures grown with HMWDOM polysaccharides as sole P source produced methane and ethylene and reached cell yields comparable to samples amended with alkylphosphonates (Table 1).

Abundance of HMWDOM-Enriched Bacterial Isolates and of C-P Lyase Pathway Genes in the NPSG

A survey of the metagenomic ALOHA gene catalog representative of the open ocean near Hawaii (Mende et al., 2017) revealed the presence of C-P lyase pathway genes throughout the water column, on average 1 copy in every 300–400 genomes (Figure 3A). C-P lyase pathway genes encoding catalytic functions peaked at 125 and 200 m depths, respectively. At these depths roughly 1 in every 200 genomes (0.5%) encoded a C-P lyase gene. The mean abundance at 125 m depth was only significantly different from the abundance at 500 m (Bonferroni adjusted $p = 0.01625$). Mean C-P lyase abundance at 200 m depth was significantly different from the abundances at 25, 75, 500, and 770 m depths (Bonferroni adjusted $p < 0.05$). The sample to sample variability of C-P lyase gene abundance was also greatest at 125 and 200 m depths relative to other depths sampled (Figure 3A).

The abundance estimates of OTUs representative of our bacterial isolates, including those encoding C-P lyase gene operons, are presented in Supplementary Table 8. The OTUs representative of our bacterial isolates comprised on average 0.08% of the community throughout the water column and never exceeded 1%. The *Sulfitobacter* isolates with C-P lyase were mapped to two different rRNA OTUs. One included *Sulfitobacter* sps. HI0021, HI0027, and HI0054 and contributed approximately to 0.005% of the community in the upper 125

m of the water column and 0.01% below 200 m (Figure 3C). The remaining *Sulfitobacter* isolates with C-P lyase (HI0076 and HI0082) mapped to another OTU that made up on average 0.23% of the community throughout the water column (Supplementary Table 8). The *Oleiphilus* isolates encoding a C-P lyase-like operon (Figure 2C) were also found in two OTUs. The OTU that included *Oleiphilus* sp. HI0067 comprised an average of 0.13% of the community throughout the water column, and showed a marked increase in abundance below 200 m (Figure 3D). The second OTU including the C-P lyase-containing *Oleiphilus* isolates had an estimated abundance close to 0.007% consistently throughout the water column.

Isolate Growth Response to HMWDOM

Two representative isolates, *Sulfitobacter* sp. HI0054 and *Oleiphilus* sp. HI0066, were grown in a seawater medium supplemented with trace metals and vitamins and with different concentrations of HMWDOM polysaccharides. Both isolates showed small increases in cell concentrations in media amended with HMWDOM polysaccharide relative to unamended seawater (Figure 4). In the case of *Sulfitobacter* sp. HI0054, HMWDOM additions of 40 and 60 $\mu\text{g mL}^{-1}$ increased cell yields by $5.0\text{--}9.5 \times 10^4$ cells mL^{-1} relative to unamended seawater (Bonferroni-adjusted $p = [0.0063, 0.0008]$). For *Oleiphilus* sp. HI0066 cultures, HMWDOM additions of 40 and 60 $\mu\text{g mL}^{-1}$ stimulated cell growth by 2×10^3 to 1.7×10^4 cells mL^{-1} over unamended seawater (Bonferroni-adjusted $p = [0.0368, 0.0009]$). HMWDOM additions of 20 $\mu\text{g mL}^{-1}$ were not sufficient to induce significant increases in cell yields (Bonferroni-adjusted $p > 0.05$). *P. shioyasakiensis* HI0053, *Erythrobacter* sp. HI0063 (not shown), *Erythrobacter* sp. HI0077, and *Oleibacter* sp. HI0113 *Alcanivorax* sp. HI0096, *Alteromonas* sp. HI0090 and three additional *Alteromonas* isolates (HI0092, HI0107, and HI0109, not shown) were also grown with up to 28.8 $\mu\text{g mL}^{-1}$ of HMWDOM but none had a discernible growth response to the amendment (Supplementary Figure 3).

Carbon Substrate Utilization Profiles of Isolates

The growth screen and outlier test indicated that isolates closely related to known hydrocarbon degraders, including *Alcanivorax*, *Oleiphilus*, *Oleibacter*, *Thalassolituus*, and *Oleiphilus*, had a strong preference for fatty acids and hydrocarbon-containing compounds, and indicated they can also metabolize low

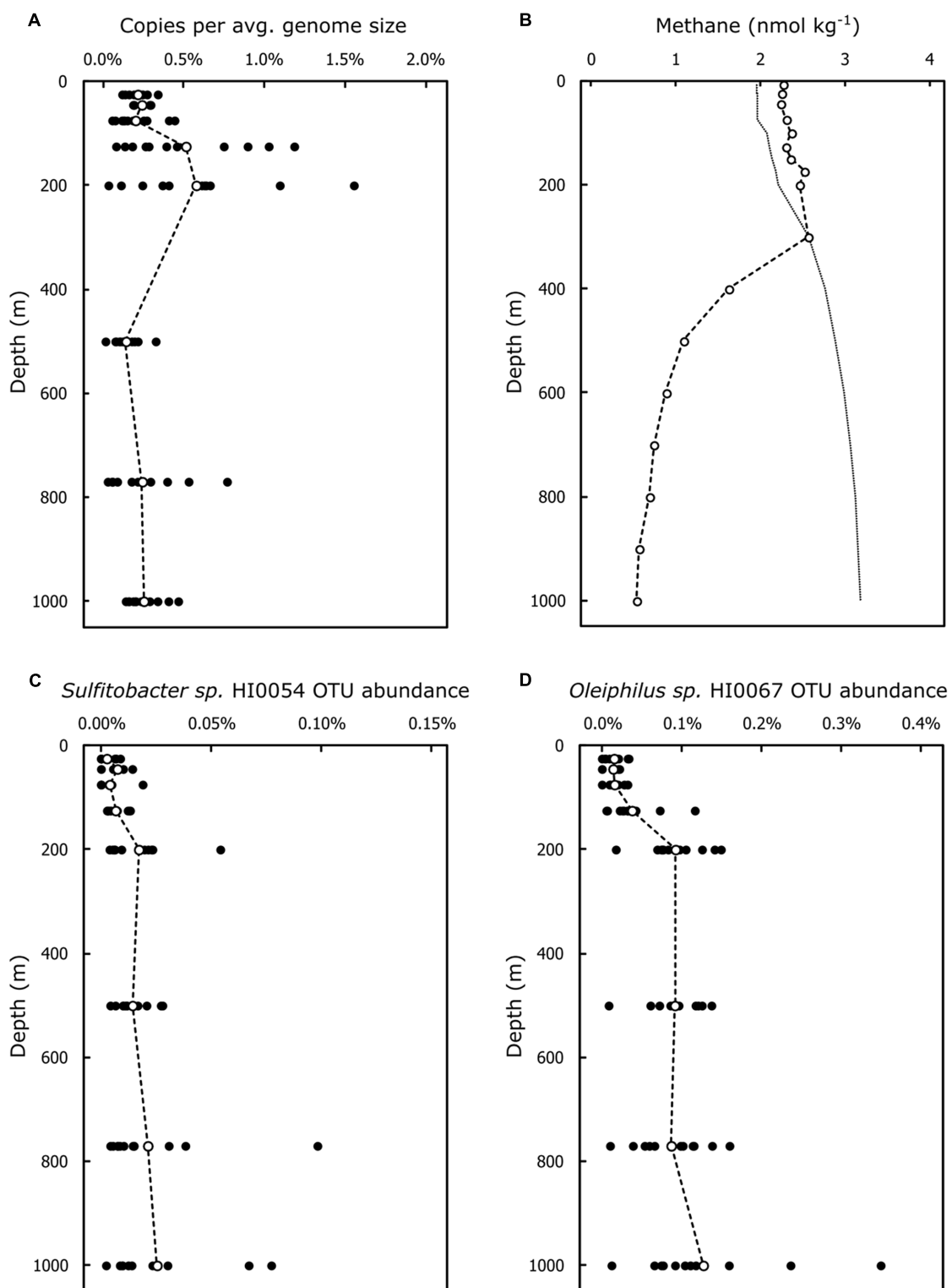


FIGURE 3 | Abundance of the C-P lyase pathway genes and of OTUs representative of HMWDOM enriched bacterial isolates encoding C-P lyase at Station ALOHA. **(A)** The average copy number of C-P lyase pathways genes with catalytic functions normalized to average genome size. **(B)** Typical depth profile of methane concentrations in the water column at Station ALOHA. Indicated are the average methane concentrations in samples collected during Spring 2013 (Hawaii Ocean Time-series cruises 249–251). The predicted methane concentrations in equilibrium with the atmosphere are indicated by the dotted line. **(C)** OTU proportional abundance of SSU rRNA sequences representative of *Sulfitobacter* sp. HI0054. **(D)** OTU proportional abundance of SSU rRNA sequences representative of *Oleiphilus* sp. HI0067. Closed circles represent abundances for individual samples. Open circles indicate the mean abundances for all samples at a given depth.

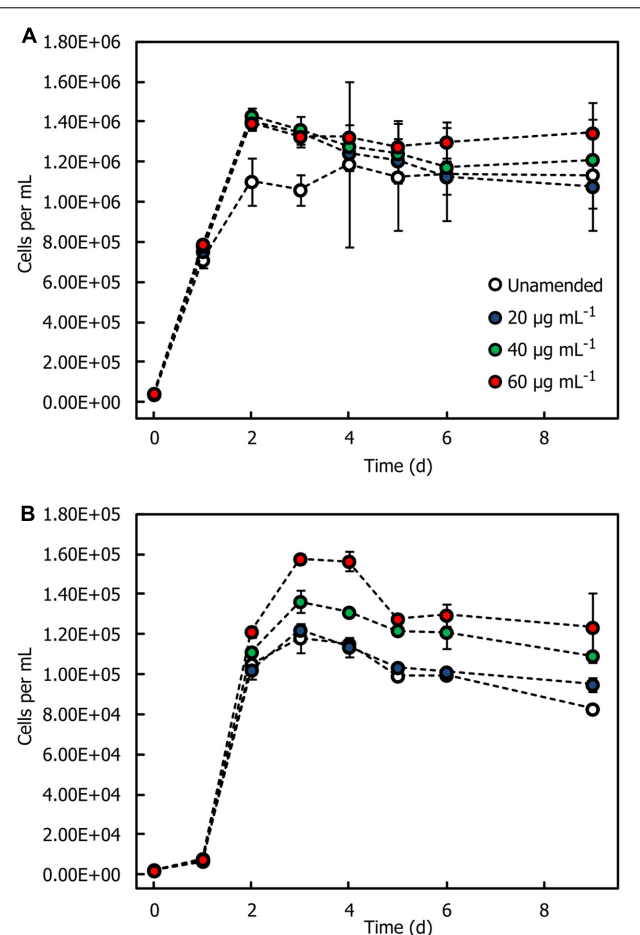


FIGURE 4 | Growth response of bacterial isolates in seawater amended with HMWDOM polysaccharides. **(A)** *Sulfitobacter* sp. HI0054. **(B)** *Oleiphilus* sp. HI0066. Treatments correspond to cultures grown in unamended seawater that had been enriched in nutrients, vitamins and trace metals, and seawater amended with 20, 40, and 60 µg mL⁻¹ of HMWDOM polysaccharides, respectively. The plot indicates the mean cell count of triplicate cultures. Error bars represent one standard deviation.

molecular weight (LMW) compounds including acetate and a few carbohydrates (Supplementary Figure 4). Growth of the *Erythrobacter* isolate tested was also stimulated by hydrocarbon-based compounds (Supplementary Figure 4). *Sulfitobacter* sp. HI0054 showed a strong preference for α-amino acids, non-proteinogenic amino acids, and other LMW carbonyl compounds (Supplementary Figure 5). In turn, *P. shioyasakiensis* HI0053 could metabolize simple sugars and polysaccharides, nucleosides, several amino acids, fatty acids, and several other LMW carbonyl compounds (Supplementary Figure 6).

Representation of Carbohydrate-Degrading Functions in HMWDOM-Enriched Isolates

The number of predicted genes with CAZy domains encoded by HMWDOM-enriched bacterial isolates and model

TABLE 2 | The number of predicted carbohydrate-active (CAZy) enzymes in representative bacterial isolates.

Taxon	CBM	CE	GH	PL	CDS
<i>Saccharophagus degradans</i> *	136	15	130	33	4008
<i>Teredinibacter turnerae</i> *	117	22	101	5	4690
<i>Cellvibrio japonicus</i> *	93	19	122	14	3790
<i>Roseovarius</i> sp. HI0049	0	28	30	0	5661
<i>P. shioyasakiensis</i> HI0053	6	38	53	1	5114
<i>Oleibacter</i> sp. HI0075	0	32	14	0	4668
<i>Thalassolituus</i> sp. HI0120	2	35	17	2	4424
<i>Alcanivorax</i> ssp.	0 (0)	33 (8)	13 (3)	1 (1)	3985 (783)
<i>Erythrobacter</i> ssp.	1 (1)	24 (6)	17 (4)	1 (1)	3206 (602)
<i>Sulfitobacter</i> ssp.	1 (0)	20 (3)	21 (2)	0 (1)	3947 (244)
<i>Oleiphilus</i> ssp.	3 (1)	28 (6)	13 (4)	1 (1)	3981 (588)

*Data from Yang et al., 2009

CDS, coding DNA sequences

The number of predicted CAZy genes of bacterial isolates was compared to those of cultured bacteria with known adaptations to degrade complex polysaccharides*. For isolates of the same genus, the means and standard deviations of CAZy genes are indicated. CAZy enzyme families: CBM, carbohydrate-binding modules; CE, carbohydrate esterases; GH, glycoside hydrolases; PL, polysaccharide lyases.

carbohydrate-degrading bacteria is presented in Table 2. The analysis focused on identifying CAZy genes with predicted carbohydrate-binding modules (CBM), carbohydrate esterases (CE), glycoside hydrolases (GH), and polysaccharide lyases (PL). In comparison to *Saccharophagus degradans* (Weiner et al., 2008), *Teredinibacter turnerae* (Yang et al., 2009), and *Cellvibrio japonicus* (DeBoy et al., 2008), which encode an unusually large number of carbohydrate-processing enzymes (6–8% of CDS), only 1–2% of the CDSs of the HMWDOM-enriched isolates were predicted to encode CAZy domains. Genes with CE domains accounted for most of the CDSs in these isolates and were comparable to the number of CEs in model carbohydrate-degrading bacteria. The rest of the CAZy families comprised less than 1% of CDSs in the bacterial genomes analyzed.

DISCUSSION

Our cultivation experiments were motivated by previous work that identified bacterial isolates capable of growth using organic carbon obtained from natural HMWDOM from marine surface waters characteristic of semi-labile DOM (Sosa et al., 2015). We hypothesized that microbial communities inhabiting oligotrophic regions characterized by low primary productivity would harbor bacterial populations adapted to degrade HMWDOM substrates to support their growth.

To this end, we targeted organisms from the lower euphotic zone near the DCM and the upper mesopelagic zone. The DCM at Station ALOHA is situated below the surface mixed layer and coincides roughly with the depth of 1% surface photosynthetically available radiation (Letelier et al., 2004; Laws et al., 2014). At this depth, *Prochlorococcus* makes up approximately 30% of the microbial community and dominates

the photosynthetic biomass (Campbell et al., 1997) but primary production rates are three to four times lower than in the surface (Karl and Church, 2014). In turn, in the mesopelagic region where light levels no longer support photosynthesis, the decline of DOC with depth reflects the net biological remineralization of semi-labile DOM (Kaiser and Benner, 2012). Thus, we expected to isolate microorganisms adapted to degrade HMWDOM from both depths, but also expected a lower number of isolates from the DCM since the prevalence of *Prochlorococcus* cells and other photosynthetic organisms at this depth precludes the isolation of other types of organisms by the dilution-to-extinction method.

We found that amending dilution-to-extinction cultures with HMWDOM had a positive effect on the recovery of bacterial isolates. As expected, this effect was greater in mesopelagic samples and was mostly attributed to the enrichment of *Oleiphilus* isolates, 37 of the 58 cultures in these samples (**Figure 1**). In addition, several isolates related to *Sulfitobacter* and *Erythrobacter* were recovered from HMWDOM-amended samples from both depths, suggesting these organisms participate in HMWDOM cycling throughout the lower euphotic zone and mesopelagic region.

HMWDOM as a Source of Organic Carbon Growth Substrates

Despite the positive effect HMWDOM had on the recovery of dilution-to-extinction cultures, growing these isolates with increasing concentrations of HMWDOM or purified HMWDOM polysaccharides did not stimulate a concomitant response in cell yields (Supplementary Figure 3). *Oleiphilus* and *Sulfitobacter* had the clearest growth response to HMWDOM polysaccharides (**Figure 4**) but the growth difference with respect to unamended media was minimal. Based on previous estimates of bacterial cellular mass (Cermak et al., 2016), a 50% carbon content, and a growth efficiency of 0.5, <1% of the total carbon added as HMWDOM could account for this growth and therefore could represent trace amounts of labile substrates that are co-isolated with HMWDOM polysaccharides (LMW compounds, proteins, etc.) or carbon contamination introduced from sample collection and processing.

This lack of growth on HMWDOM was unexpected and contrasts with the growth response of HMWDOM-enriched OM43 clade methylotrophic bacteria which could reach cell concentrations of up to 6×10^6 cells mL⁻¹ with similar HMWDOM amendments (Sosa et al., 2015). Gifford et al. (2016) found that OM43 clade methylotroph strain NB0046 upregulates expression of the methylcitrate cycle, a pathway that characteristically metabolizes propionyl-CoA, when grown in the presence of HMWDOM polysaccharides. This result suggested that compounds associated with HMWDOM polysaccharides were available to these methylotrophs. Whether the fraction of organic carbon in HMWDOM is more limited to our isolates or the specific carbon demands of these isolates and the OM43 clade methylotrophs differ significantly, our results indicate that HMWDOM is a poor

source of organic carbon growth substrates to the organisms we investigated.

The overall low representation of genes encoding carbohydrate-degrading functions in our bacterial isolates relative to well-known carbohydrate-degrading bacteria (**Table 2**) and their preference for non-carbohydrate growth substrates (Supplementary Figures 4, 5) is consistent with their minimal response to HMWDOM. Interestingly, however, many of the HMWDOM-enriched isolates had a similar number of predicted CEs as model carbohydrate-degrading bacteria. These enzymes catalyze the removal of ester-based substitutions (de-O or de-N-acylation) in carbohydrates and thereby facilitate the breakdown of polysaccharides by GHs (Cantarel et al., 2009). This result is consistent with the prevalence of acetyl ester substitutions characteristic of HMWDOM polysaccharides (Aluwihare et al., 1997, 2005) and may indicate that a small fraction of organic carbon in HMWDOM polysaccharides was available to these organisms.

Bioavailability of Phosphonates in HMWDOM Polysaccharides

The capability to degrade phosphonates is widespread in the marine environment (Villarreal-Chiu et al., 2012). The largest known pools of phosphonates in the marine environment are phosphonates in HMWDOM (Kolowith et al., 2001; Repeta et al., 2016), methylphosphonates derived from marine *Thaumarchaeota* (Metcalf et al., 2012), and phosphonates produced by the cyanobacterium *Trichodesmium* (Dyrman et al., 2009) and by marine invertebrates (Hilderbrand, 1983). In the NPSG, Martínez et al. (2013) identified bacterial populations related to *Vibrio nigripulchritudo* ATCC27043, the gammaproteobacterium IMCC1989, and the *Rhodobacterales* that express C-P lyase upon phosphate limitation to degrade alkylphosphonates. Furthermore, Repeta et al. (2016) showed that the native microbial community from surface waters in the NPSG and pure cultures of a *P. stutzeri* bacterium encoding C-P lyase can utilize alkylphosphonate esters in HMWDOM polysaccharides to obtain P.

The presence of phosphonate degradation pathways in our HMWDOM-enriched isolates suggested these bacteria might also degrade phosphonate esters in HMWDOM polysaccharides and thus contribute to the production of methane and other hydrocarbons in the ocean. As expected, P-limited cultures of *Sulfitobacter* sp. HI0054 grown with HMWDOM polysaccharides as sole P source produced methane and ethylene (**Table 1**), consistent with the degradation of MPn and 2-HEP esters in HMWDOM (Repeta et al., 2016). The total yield of methane and ethylene (17 nM) in *Sulfitobacter* cultures grown with HMWDOM polysaccharides was 2.2% of the estimated concentration of phosphonates added (780 nM P). These yields are similar to the methane and ethylene produced by P-limited *P. stutzeri* cultures grown with HMWDOM polysaccharides (Repeta et al., 2016).

Previous determinations of the flux of methane to the atmosphere in the NPSG (Holmes et al., 2000) indicate that

a minimum methane production rate of $1.7 \mu\text{mol m}^{-2} \text{d}^{-1}$ is necessary to maintain the steady state concentrations observed in the upper 300 m of the water column. Repeta et al. (2016) estimated that a daily turnover of 0.25% of the MPn inventory would be sufficient to support this flux. This translates to an average MPn degradation rate of $\sim 5.8 \times 10^{-3} \text{ nmol L}^{-1} \text{ d}^{-1}$. The MPn in HMWDOM polysaccharides available to *Sulfitobacter* cultures supported a methane production rate of approximately $2 \text{ nmol L}^{-1} \text{ d}^{-1}$, well in excess of this estimate. It is important to note that *Sulfitobacter* growth was stimulated by a concentration of labile organic C (0.2 mM) that may not occur in the environment. Assuming that the MPn degraded per mol of C provided to these cultures ($3 \times 10^{-5} \text{ mol MPn per mol C}$) is representative of the natural system, $<200 \text{ nmol C L}^{-1} \text{ d}^{-1}$ would be sufficient to support the MPn degradation rates necessary to sustain methane supersaturation in the upper ocean. In comparison, heterotrophic production rates in the ocean range from $136.5 \text{ nmol C L}^{-1} \text{ d}^{-1}$ in surface waters (0–200 m depths) to $24.4 \text{ nmol C L}^{-1} \text{ d}^{-1}$ in the mesopelagic region (200–1000 m depths; Arístegui et al., 2009).

Previous studies at Station ALOHA indicate C-P lyase and other phosphonate degradation pathways are prevalent among *Rhodobacterales* populations (Martínez et al., 2010, 2013). The abundance estimates of OTUs representative of the HMWDOM-enriched Roseobacter isolates encoding C-P lyase, including *Sulfitobacter* and *Roseovarius*, were only a small proportion of the microbial community at Station ALOHA, up to 0.24% or 1 out of every ~ 400 organisms (Supplementary Table 8). However, C-P lyase appears to be more broadly distributed in members of the Roseobacter clade. Out of 54 Roseobacter genomes searchable in the Roseobase², 38 encode proteins highly similar to the C-P lyase pathway catalytic proteins of *Sulfitobacter* sp. HI0054 (PhnI, 77–95% amino acid identity; PhnJ, 83–93%; PhnK, 85–99%; and PhnL, 71–97%). Assuming that members of this clade generally encode C-P lyase, they may account for most of the C-P lyase identified at Station ALOHA (1 copy in every 300–400 average genomes). Presumably, a much higher diversity of bacteria known to encode C-P lyase (Villarreal-Chiu et al., 2012), including our *Oleiphilus* isolates and more abundant clades such as SAR11 (Carini et al., 2014) that were not captured by our culturing experiments, contribute to this signal. Our findings nevertheless further associate members of the Roseobacter clade with phosphonate cycling and with the aerobic production of methane in the ocean.

Given that *Sulfitobacter* cultures grown with HMWDOM polysaccharides reached similar cell densities as cultures amended with alkylphosphonates (Table 1), it is possible that *Sulfitobacter* utilized additional forms of organic P available in HMWDOM polysaccharides. Phosphonates comprise only 20% of the total P in HMWDOM polysaccharides. Assuming the average methane, ethylene, and ethane yields in MPn, 2-HEP, and EPn treatments, respectively ($\sim 223 \text{ nM}$), approximates the P demand of these cultures, about 200 nM P was obtained from phosphate esters and diesters or other P

compounds in HMWDOM polysaccharides. This assumes also that the cellular C:P ratio of these cultures did not change.

Owing to the phosphate-dependent regulation of C-P lyase by the Pho regulon (Chen et al., 1990; Metcalf and Wanner, 1993a), we postulate that the hydrolysis of the ester bond between phosphonates and HMWDOM polysaccharides is mediated by enzymes similar to alkaline phosphatase (APase). The *P. stutzeri* strain HI00D01 used by Repeta et al. (2016) encodes an APase of the PhoD family (KZX59646.1). *Sulfitobacter* sp. HI0054 also encodes a PhoD-like APase (KZY51209.1) and a related enzyme (KZY52437.1) annotated as a phosphonate monoester hydrolase (PEH). This PEH was present in the genomes of 7 of the 8 *Sulfitobacter* isolates with annotated genomes, including all those containing C-P lyase. PEH has been characterized in *Burkholderia caryophilli* PG2982 (Dotson et al., 1996) and in *Rhizobium leguminosarum* (Jonas et al., 2008) as having high substrate specificity to phosphonate monoesters and phosphodiesters, the two major P functional groups in HMWDOM. The PEH of *Sulfitobacter* sp. HI0054 shared 31 and 34% amino acid sequence similarity with the PEH of *R. leguminosarum* and *B. caryophilli*, respectively. The isolation of these phosphonate degraders will allow us to explore the role of marine APases in the degradation of HMWDOM phosphonates and other HMWDOP substrates.

Links between Methane, Phosphonate Degradation, and Polysaccharide Cycling in the NPSG

In the NPSG, methane is typically supersaturated with respect to equilibrium concentrations with the atmosphere in the upper 300 m (Figure 3B; Tilbrook and Karl, 1995; Holmes et al., 2000). Luo et al. (2011) reported that C-P lyase is mostly present in surface waters ($<70 \text{ m}$) in the NPSG and is unlikely to occur below depths $>130 \text{ m}$. However, our metagenomic analysis at Station ALOHA identified C-P lyase pathway genes in all samples between the surface and 1000 m depths (Figure 3A). We also detected the highest abundance and variability of C-P lyase in the lower euphotic zone and upper mesopelagic region (Figure 3A). Our observations were in agreement with the abundance estimates of *phnI* and *phnJ* reported by Martínez et al. (2010) of $<1\%$ of organisms in samples between the surface and 500 m at Station ALOHA. It is possible that the detection of C-P lyase genes by Luo et al. (2011) was limited by the amount of metagenomic sequence data available ($\sim 64 \text{ Mbps}$ compared to 456 Gbp in the ALOHA gene catalog).

While the profile of dissolved methane with depth merely reflects steady state concentrations, the presence of C-P lyase in mesopelagic isolates and the increase in C-P lyase pathway genes at these depths are a strong indication that phosphonate cycling is important up to at least 200–300 m. The proportions of phosphonates and phosphate esters in HMWDOP remain relatively stable throughout surface, mesopelagic, and bathypelagic waters in the Pacific Ocean (Clark et al., 1998),

²<http://www.roseobase.org>

indicating these two P pools cycle at similar rates. These observations are consistent with the utilization of phosphonates in HMWDOM polysaccharides and the presence of C-P lyase throughout the water column, suggesting that MPn is not only an important source of methane in the upper ocean but may be a source of methane to the deep sea as well.

The preferential utilization of DOP in phosphate-replete environments like the mesopelagic zone suggests that organisms degrade organic P compounds for reasons other than to acquire phosphate (Karl and Björkman, 2015). Increased APase activity in the mesopelagic waters relative to surface waters, for example, has been associated with the bacterial degradation of DOP to obtain not only P but also C for energy and growth (Hoppe and Ullrich, 1999). One hypothesis that may explain the occurrence of C-P lyase in phosphate-replete depths in the ocean is that phosphonate substitutions in HMWDOM polysaccharides make these inaccessible to enzymes that break down carbohydrates. This protection would be a natural function of phosphonates in cells. Selection for phosphonate-degrading bacteria and for C-P lyase at these depths may therefore be driven by the need of the microbial community to access the chemical energy stored in phosphonate-bounded carbohydrates. Additionally, some phosphonate degraders may be localized on sinking particles as suggested by del Valle and Karl (2014) and would therefore be transported from the surface to the deep sea. Deeper in the mesopelagic region, the decline of methane concentrations from 300 to 1000 m depths (Figure 3B) and the enrichment of ¹³C-methane with depth (Holmes et al., 2000) suggests that methane-oxidizing organisms may benefit from the degradation of MPn stored in HMWDOM polysaccharides. Thus, C-P lyase would be valuable for the community at these depths as well.

CONCLUSION

This study investigated the potential of HMWDOM to serve as a source of carbon and phosphorus to marine bacteria inhabiting the open ocean environment. HMWDOM appears to be a poor source of carbon for monocultures of the bacteria we isolated. Organic phosphorus compounds in HMWDOM, however, like the alkylphosphonates metabolized by *Sulfitobacter* cultures, do seem more readily available and likely represent an important source of P to marine bacteria. Our findings, combined with previous observations, add support to the role of MPn stored in HMWDOM as a key methanogenic substrate in the aerobic ocean. The lack of growth response we observed in bacterial cultures supplemented with HMWDOM possibly reflects the semi-labile nature of this material and the complex microbial processing and inter-species interactions that may be required to mediate its turnover. It is also possible that some of the more abundant bacterial clades in the oligotrophic ocean contribute significantly to the degradation of semi-labile DOM, but our culturing conditions could not support

these. Due to the high representation of phosphonate-degrading bacteria in our samples, we postulate that the degradation of phosphonate ester substitutions in HMWDOM polysaccharides is a key biochemical step in the turnover of semi-labile DOM. The metabolic properties of the isolates obtained in this study will be explored further to investigate the degradation pathways of semi-labile DOM and marine phosphonates.

AUTHOR CONTRIBUTIONS

OS, DR, DK, and ED designed research. OS performed research. OS and SF performed gas analysis. JB and DM provided metagenomic analyses. DR isolated and processed the HMWDOM. OS, DR, DK, and ED wrote the paper with contributions from all authors.

FUNDING

Financial support for this work was provided by the National Science Foundation Center for Microbial Oceanography: Research and Education (award #EF0424599 to DK and ED), the National Science Foundation HOT program (OCE-1260164 to M. J. Church and DK), the Gordon and Betty Moore Foundation (grants #492.01 and #3777 to ED, #3298 to DR, and #3794 to DK), and the Simons Foundation (award ID 329108 to DK, DR, and ED). Additional support was provided by the Agouron Institute through a fellowship to OS.

ACKNOWLEDGMENTS

We thank the Hawaii Ocean Time-series (HOT) and the crew and captain of the R/V Kilo Moana during HOT cruise no. 261 and the Center for Microbial Oceanography: Research and Education's cruise *Hawaii Ocean Experiment – Budget of Energy I* for successful transiting and research at Station ALOHA. We thank Anna Romano for assistance with Illumina sequencing and John Eppley and Torben Nielsen for help with genome assemblies. Thanks also to Samuel Wilson for lending his expertise in gas chromatography of trace gases and for sharing analysis of water column profiles of methane from Station ALOHA. Thanks to Karin Björkman and Rhea Foreman for determination of total P content of HMWDOM samples. Culturing and genomics aspects of this research were contributed from the Sosa (2015) dissertation.

SUPPLEMENTARY MATERIAL

The Supplementary Material for this article can be found online at: <http://journal.frontiersin.org/article/10.3389/fmicb.2017.01786/full#supplementary-material>

REFERENCES

- Agarwal, V., Peck, S. C., Chen, J., Borisova, S. A., Chekan, J. R., van der Donk, W. A., et al. (2014). Structure and function of phosphonoacetaldehyde dehydrogenase: the missing link in phosphonoacetate formation. *J. Chem. Biol.* 21, 125–135. doi: 10.1016/j.chembiol.2013.11.006
- Aluwihare, L. I., Repeta, D. J., and Chen, R. F. (1997). A major biopolymeric component to dissolved organic carbon in surface sea water. *Nature* 387, 166–169. doi: 10.1038/387166a0
- Aluwihare, L. I., Repeta, D. J., Pantoja, S., and Johnson, C. G. (2005). Two chemically distinct pools of organic N accumulate in the ocean. *Science* 308, 1007–1010. doi: 10.1126/science.1108925
- Arístegui, J., Agustí, S., Middelburg, J. J., and Duarte, C. M. (2005). “Respiration in the mesopelagic and bathypelagic zones of the oceans,” in *Respiration in Aquatic Ecosystems*, eds P. del Giorgio and P. Williams (New York, NY: Oxford University Press), 181–205. doi: 10.1093/acprof:oso/9780198527084.001.0001
- Arístegui, J., Gasol, J. M., Duarte, C. M., and Herndl, G. J. (2009). Microbial oceanography of the dark ocean’s pelagic realm. *Limnol. Oceanogr.* 54, 1501–1529. doi: 10.4319/lo.2009.54.5.1501
- Aylward, F. O., Eppley, J. M., Smith, J. M., Chavez, F. P., Scholin, C. A., and DeLong, E. F. (2015). Microbial community transcriptional networks are conserved in three domains at ocean basin scales. *Proc. Natl. Acad. Sci. U.S.A.* 112, 5443–5448. doi: 10.1073/pnas.1502883112
- Bankovich, A., Nurk, S., Antipov, D., Gurevich, A. A., Dvorkin, M., Kulikov, A. S., et al. (2012). SPAdes: a new genome assembly algorithm and its applications to single-cell sequencing. *J. Comp. Biol.* 19, 455–477. doi: 10.1089/cmb.2012.0021
- Benner, R. I., Pakulski, J. D., McCarthy, M., Hedges, J. I., and Hatcher, P. G. (1992). Bulk chemical characteristics of dissolved organic matter in the ocean. *Science* 255, 1561–1564. doi: 10.1126/science.255.5051.1561
- Bochner, B. R., Gadzinski, P., and Panomitros, E. (2001). Phenotype microarrays for high-throughput phenotypic testing and assay of gene function. *Genome Res.* 11, 1246–1255. doi: 10.1101/gr.186501
- Campbell, L., Liu, H., Nolla, H. A., and Vaulot, D. (1997). Annual variability of phytoplankton and bacteria in the subtropical North Pacific Ocean at Station ALOHA during the 1991–1994 ENSO event. *Deep Sea Res. I* 44, 167–192. doi: 10.1016/S0967-0637(96)00102-1
- Cantarel, B. I., Coutinho, P. M., Rancurel, C., Bernard, T., Lombard, V., and Henrissat, B. (2009). The Carbohydrate-Active EnZymes database (CAZy): an expert resource for glycogenomics. *Nucleic Acids Res.* 37, 233–238. doi: 10.1093/nar/gkn663
- Caporaso, J. G., Kuczynski, J., Stombaugh, J., Bittinger, K., Bushman, F. D., Costello, E. K., et al. (2010). QIIME allows analysis of high-throughput community sequencing data. *Nat. Methods* 7, 335–336. doi: 10.1038/nmeth.f.303
- Carini, P., White, A. E., Campbell, E. O., and Giovannoni, S. J. (2014). Methane production by phosphate-starved SAR11 chemoheterotrophic marine bacteria. *Nat. Commun.* 5:436. doi: 10.1038/ncomms5346
- Carlson, C. A., Giovannoni, S. J., Hansell, D. A., Goldberg, S. J., Parsons, R., and Vergin, K. (2004). Interactions among dissolved organic carbon, microbial processes, and community structure in the mesopelagic one of the northwestern Sargasso Sea. *Limnol. Oceanogr.* 49, 1073–1083. doi: 10.2307/3597658
- Carlson, C. A., Hansell, D. A., Nelson, N. B., Siegel, D. A., Smethie, W. M., Khatiwala, S., et al. (2010). Dissolved organic carbon export and subsequent remineralization in the mesopelagic and bathypelagic realms of the North Atlantic basin. *Deep Sea Res. II* 57, 1433–1445. doi: 10.1016/j.dsr2.2010.02.013
- Cermak, N., Becker, J. W., Knudsen, S. M., Chisholm, S. W., Manalis, S. R., and Polz, M. F. (2016). Direct single-cell biomass estimates for marine bacteria via Archimedes’ principle. *ISME J.* 11, 825–828. doi: 10.1038/ismej.2016.161
- Chen, C. M., Ye, Q. Z., Zhu, Z. M., Wanner, B. L., and Walsh, C. T. (1990). Molecular biology of carbonP bond cleavage. Cloning and sequencing of the phn (psiD) genes involved in alkylphosphonate uptake and C-P lyase activity in *Escherichia coli*. *B. J. Biol. Chem.* 265, 4461–4471.
- Cherrier, J., Bauer, J. E., and Druffel, E. R. M. (1996). Utilization and turnover of labile dissolved organic matter by bacterial heterotrophs in eastern North Pacific surface waters. *Mar. Ecol. Prog. Ser.* 139, 267–279. doi: 10.3354/meps139267
- Chevreux, B., Wetter, T., and Suhai, S. (1999). “Genome sequence assembly using trace signals and additional sequence information,” in *Proceedings of the German Conference on Bioinformatics: Computer Science and Biology*, ed. E. Wingender (Braunschweig: GBF-Braunschweig), 45–56.
- Clark, L. L., Ingall, E. D., and Benner, R. (1998). Marine phosphorus is selectively remineralized. *Nature* 393:426. doi: 10.1038/30881
- Cole, J., Findlay, S., and Pace, M. (1988). Bacterial production in fresh and saltwater ecosystems: a cross-system overview. *Mar. Ecol. Prog. Ser.* 43, 1–10. doi: 10.3354/meps043001
- Connon, S. A., and Giovannoni, S. J. (2002). High-throughput methods for culturing microorganisms in very-low nutrient media yield diverse new marine isolates. *Appl. Environ. Microbiol.* 68, 3878–3885. doi: 10.1128/AEM.68.8.3878-3885.2002
- DeBoy, R. T., Mongodin, E. F., Fouts, D. E., Tailford, L. E., Khouri, H., Emerson, J. B., et al. (2008). Insights into plant cell wall degradation from the genome sequence of the soil bacterium *Celvibrio japonicus*. *J. Bacteriol.* 190, 5455–5463. doi: 10.1128/JB.01701-07
- del Valle, D. A., and Karl, D. M. (2014). Aerobic production of methane from dissolved water-column methylphosphonate and sinking particles in the North Pacific Subtropical Gyre. *Aquat. Microb. Ecol.* 73, 93–105. doi: 10.3354/ame01714
- Dotson, S. B., Smith, C. E., Ling, C. S., Barry, G. F., and Kishore, G. (1996). Identification, characterization, and cloning of a phosphonate monoester hydrolase from *Burkholderia caryophilli* PG2982*. *J. Biol. Chem.* 271, 25754–25761. doi: 10.1074/jbc.271.42.25754
- Dyrhman, S. T., Benitez-Nelson, C. R., Orchard, E. D., Haley, S. T., and Pellechia, P. J. (2009). A microbial source of phosphonates in oligotrophic marine systems. *Nat. Geosci.* 2, 696–699. doi: 10.1038/ngeo639
- Eddy, S. R. (2009). A new generation of homology search tools based on probabilistic inference. *Genome Inform.* 23, 205–211. doi: 10.1142/9781848165632_0019
- Felsenstein, J. (1985). Confidence limits on phylogenies: an approach using the bootstrap. *Evolution* 39, 783–791. doi: 10.2307/2408678
- Gasol, J. M., Doval, M. D., Pinhassi, J., Calderón-Paz, J. I., Guixa-Boixareu, N., Vaqué, D., et al. (1998). Diel variations in bacterial heterotrophic activity and growth in the northwestern Mediterranean Sea. *Mar. Ecol. Prog. Ser.* 164, 107–124. doi: 10.3354/meps164107
- Gifford, S. M., Becker, J. W., Sosa, O. A., Repeta, D. J., and DeLong, E. F. (2016). Quantitative transcriptomics reveals the growth- and nutrient-dependent response of a streamlined marine methylotroph to methanol and naturally occurring dissolved organic matter. *mBio* 7:e01279-16. doi: 10.1128/mBio.01279-16
- Goldman, J. C., Caron, D. A., and Dennett, M. R. (1987). Regulation of gross growth efficiency and ammonium regeneration in bacteria by substrate C:N ratio. *Limnol. Oceanogr.* 32, 1239–1252. doi: 10.4319/lo.1987.32.6.1239
- Golyshin, P. N., Chernikova, T. N., Abraham, W. R., Lünsdorf, H., Timmis, K. N., and Yakimov, M. M. (2002). Oleophilaceae fam. nov., to include *Oleiphilus messinensis* gen. nov., sp. nov., a novel marine bacterium that obligately utilizes hydrocarbons. *Int. J. Syst. Evol. Microbiol.* 52, 901–911. doi: 10.1099/00207713-52-3-901
- Hansell, D. A., Carlson, C. A., and Suzuki, Y. (2002). Dissolved organic carbon export with North Pacific Intermediate Water formation. *Glob. Biogeochem. Cycles* 16, 7–1. doi: 10.1029/2000GB001361
- Hilderbrand, R. L. (1983). *The Role of Phosphonates in Living Systems*. Boca Raton, FL: CRC Press Inc.
- Holmes, M. E., Sansone, F. J., Rust, T. M., and Popp, B. N. (2000). Methane production, consumption, and air-sea gas exchange in the open ocean: An evaluation based on carbon isotopic ratios. *Global Biochem. Cycles* 14, 1–10. doi: 10.1029/1999GB001209
- Hoppe, H.-G., and Ullrich, S. (1999). Profiles of ectoenzymes in the Indian Ocean: phenomena of phosphatase activity in the mesopelagic zone. *Aquat. Microb. Ecol.* 19, 139–148. doi: 10.3354/ame019139
- Huerta-Cepas, J., Szklarczyk, D., Forslund, K., Cook, H., Heller, D., Walter, M. C., et al. (2016). eggNOG 4.5: a hierarchical orthology framework with improved functional annotations for eukaryotic, prokaryotic and viral sequences. *Nucleic Acids Res.* 44, D286–D293. doi: 10.1093/nar/gkv1248
- Jonas, S., Loo, B. V., Hyvönen, M., and Hollfelder, F. (2008). A new member of the alkaline phosphatase superfamily with a formylglycine nucleophile: structural and kinetic characterisation of a phosphonate

- monoester hydrolase/phosphodiesterase from *Rhizobium leguminosarum*. *J. Mol. Biol.* 384, 120–136. doi: 10.1016/j.jmb.2008.08.072
- Kaiser, K., and Benner, R. (2012). Organic matter transformations in the upper mesopelagic zone of the North Pacific: chemical composition and linkages to microbial community structure. *J. Geophys. Res.* 117:C01023. doi: 10.1029/2011JC007141
- Karl, D. M., and Björkman, K. M. (2001). “Phosphorus cycle in seawater: dissolved and particulate pool inventories and selected phosphorus fluxes,” in *Methods in Microbiology (Marine Microbiology)*, Vol. 30, ed. J. H. Paul (San Diego, CA: Academic Press), 239–270.
- Karl, D. M., and Björkman, K. M. (2015). “Dynamics of dissolved organic phosphorus,” in *Biogeochemistry of Marine Dissolved Organic Matter*, eds D. A. Hansell and C. A. Carlson (San Diego, CA: Academic Press), 233–334. doi: 10.1016/B978-0-12-405940-5.00005-4
- Karl, D. M., and Church, M. J. (2014). Microbial oceanography and the Hawaii Ocean Time-series program. *Nat. Rev. Microbiol.* 12, 699–713. doi: 10.1038/nrmicro3333
- Karl, D. M., and Lukas, R. (1996). The Hawaii Ocean Time-series (HOT) program: background, rationale and field implementation. *Deep Sea Res. II* 43, 129–156. doi: 10.1016/0967-0645(96)00005-7
- Kiene, R. P. (1991). “Production and consumption of methane in aquatic systems,” in *Microbial Production and Consumption of Greenhouse Gases: Methane, Nitrogen Oxides, and Halomethanes*, eds J. E. Rogers and W. B. Whitman (Washington, DC: American Society for Microbiology), 111–146.
- Kimura, M. (1980). A simple method for estimating evolutionary rates of base substitutions through comparative studies of nucleotide sequences. *J. Mol. Evol.* 16, 111–120. doi: 10.1007/BF01731581
- Kolowith, L. C., Ingall, E. D., and Benner, R. (2001). Composition and cycling of marine organic phosphorus. *Limnol. Oceanogr.* 46, 309–320. doi: 10.4319/lo.2001.46.2.0309
- Kuipers, B., Van Noort, G. J., Vosjan, J., and Herndl, G. J. (2000). Diel periodicity of bacterioplankton in the euphotic zone of the subtropical Atlantic Ocean. *Mar. Ecol. Prog. Ser.* 201, 13–25. doi: 10.3354/meps201013
- Langmead, B., and Salzberg, S. (2012). Fast gapped-read alignment with Bowtie 2. *Nat. Methods* 9, 357–359. doi: 10.1038/nmeth.1923
- Laws, E. A., Letelier, R. M., and Karl, D. M. (2014). Estimating the compensation irradiance in the ocean: the importance of accounting for non-photosynthetic uptake of inorganic carbon. *Deep Sea Res. I* 93, 35–40. doi: 10.1016/j.dsr.2014.07.011
- Letelier, R. M., Karl, D. M., Abbott, M. R., and Bidigare, R. R. (2004). Light driven seasonal patterns of chlorophyll and nitrate in the lower euphotic zone of the North Pacific Subtropical Gyre. *Limnol. Oceanogr.* 49, 508–519. doi: 10.4319/lo.2004.49.2.0508
- Leys, C., Ley, C., Klein, O., Bernard, P., and Licata, L. (2013). Detecting outliers: do not use standard deviation around the mean, use absolute deviation around the median. *J. Exp. Soc. Psychol.* 49, 764–766. doi: 10.1016/j.jesp.2013.03.013
- Ludwig, W., Strunk, O., Westram, R., Richter, L., Meier, H., Yadhukumar, et al. (2004). ARB: a software environment for sequence data. *Nucleic Acids Res.* 32, 1363–1371. doi: 10.1093/nar/gkh293
- Luo, H., Zhang, H., Long, R. A., and Benner, R. (2011). Depth distribution of alkaline phosphatase and phosphonate utilization genes in the North Pacific Subtropical Gyre. *Aquat. Microb. Ecol.* 62, 61–69. doi: 10.3354/ame01458
- Luo, Y. W., Friedrichs, M. A. M., Doney, S. C., Church, M. J., and Ducklow, H. W. (2010). Oceanic heterotrophic bacterial nutrition by semilabile DOM as revealed by data assimilative modeling. *Aquat. Microb. Ecol.* 60, 273–287. doi: 10.3354/ame01427
- Martínez, A., Tyson, G. W., and DeLong, E. F. (2010). Widespread known and novel phosphonate utilization pathways in marine bacteria revealed by functional screening and metagenomic analyses. *Environ. Microbiol.* 12, 222–238. doi: 10.1111/j.1462-2920.2009.02062.x
- Martínez, A., Ventouras, L. A., Wilson, S. T., Karl, D. M., and DeLong, E. F. (2013). Metatranscriptomic and functional metagenomic analysis of methylphosphonate utilization by marine bacteria. *Front. Microbiol.* 4:340. doi: 10.3389/fmicb.2013.00340
- Mende, D. R., Bryant, J. A., Aylward, F. O., Eppley, J. M., Nielsen, T., Karl, M., et al. (2017). Environmental drivers of a microbial genomic transition zone in the ocean’s interior. *Nat. Microbiol. Adv.* doi: 10.1038/s41564-017-0008-3 [Epub ahead of print].
- Menzel, D. W., and Corwin, N. (1965). The measurement of total phosphorus in seawater based on the liberation of organically bound fractions by persulfate oxidation. *Limnol. Oceanogr.* 10, 280–282. doi: 10.4319/lo.1965.10.2.0280
- Metcalf, W. W., Griffin, B. M., Cicchillo, R. M., Gao, J., Chandra Janga, S., Cooke, H. A., et al. (2012). Synthesis of methylphosphonic acid by marine microbes: a source for methane in the aerobic ocean. *Science* 337, 1104–1107. doi: 10.1126/science.1219875
- Metcalf, W. W., and Wanner, B. L. (1993a). Evidence for a fourteen-gene, *phnC* to *phnP* contig for phosphonate metabolism in *Escherichia coli*. *Gene* 129, 27–32. doi: 10.1016/0378-1119(93)90692-V
- Metcalf, W. W., and Wanner, B. L. (1993b). Mutational analysis of an *Escherichia coli* fourteen-gene operon for phosphonate degradation, using TnphoA’ elements. *J. Bacteriol.* 175, 3430–3442.
- Moore, L. R., Coe, A., Zinser, E. R., Saito, M. A., Sullivan, M. B., Lindell, D., et al. (2007). Culturing the marine cyanobacterium *Prochlorococcus*. *Limnol. Oceanogr. Methods* 5, 353–362. doi: 10.4319/lom.2007.5.353
- Munoz, R., Yarza, P., Ludwig, W., Euzéby, J., Amann, R., Schleifer, K.-H., et al. (2011). Release LTPs104 of the all-species living tree. *Syst. Appl. Microbiol.* 34, 169–170. doi: 10.1016/j.syapm.2011.03.001
- Ottesen, E. A., Young, C. R., Gifford, S. M., Eppley, J. M., Marin, R., Schuster, S. C., et al. (2014). Ocean microbes. Multispecies diel transcriptional oscillations in open ocean heterotrophic bacterial assemblages. *Science* 345, 207–212. doi: 10.1126/science.1252476
- Pruess, E., Peplies, J., and Glockner, F. O. (2012). SINA: accurate high-throughput multiple sequence alignment of ribosomal RNA genes. *Bioinformatics* 28, 1823–1829. doi: 10.1093/bioinformatics/bts252
- Quast, C., Pruesse, E., Yilmaz, P., Gerken, J., Schweer, T., Yarza, P., et al. (2013). The SILVA ribosomal RNA gene database project: improved data processing and web-based tools. *Nucleic Acids Res.* 41, D590–D596. doi: 10.1093/nar/gks1219
- Quinn, J. P., Kulakova, A. N., Cooley, N. A., and McGrath, J. W. (2007). New ways to break an old bond: the bacterial carbon–P hydrolases and their role in biogeochemical P cycling. *Environ. Microbiol.* 9, 2392–2400. doi: 10.1111/j.1462-2920.2007.01397.x
- Repeta, D. J., and Aluwihare, L. I. (2006). Radiocarbon analysis of neutral sugars in high-molecular-weight dissolved organic carbon: implications for organic carbon cycling. *Limnol. Oceanogr.* 51, 1045–1053. doi: 10.4319/lo.2006.51.2.1045
- Repeta, D. J., Ferrón, S., Sosa, O. A., DeLong, E. F., and Karl, D. M. (2016). Marine methane paradox explained by bacterial degradation of dissolved organic matter. *Nat. Geosci.* 9, 884–887. doi: 10.1038/ngeo2837
- Repeta, D. J., Quan, T. M., Aluwihare, L. I., and Accardi, A. M. (2002). Chemical characterization of high molecular weight dissolved organic matter in fresh and marine waters. *Geochim. Cosmochim. Acta* 66, 955–962. doi: 10.1016/S0016-7037(01)00830-4
- Rognes, T., Flouri, T., Nichols, B., Quince, C., and Mahé, F. (2016). VSEARCH: a versatile open source tool for metagenomics. *PeerJ* 4:e2584. doi: 10.7717/peerj.2584
- Saitou, N., and Nei, M. (1987). The neighbor-joining method: a new method for reconstructing phylogenetic trees. *Mol. Biol. Evol.* 4, 406–425.
- Sosa, O. A. (2015). *Microbial Cycling of Marine High Molecular Weight Dissolved Organic Matter*. Available at: <http://hdl.handle.net/1721.1/104332>
- Sosa, O. A., Gifford, S. M., Repeta, D. J., and DeLong, E. F. (2015). High molecular weight dissolved organic matter enrichment selects for methylotrophs in dilution to extinction cultures. *ISME J.* 9, 2725–2739. doi: 10.1038/ismej.2015.68
- Tamura, K., Stecher, G., Peterson, D., Filipski, A., and Kumar, S. (2013). MEGA6: molecular evolutionary genetics analysis version 6.0. *Mol. Biol. Evol.* 30, 2725–2729. doi: 10.1093/molbev/mst197
- Tatusova, T., DiCuccio, M., Badretdin, A., Chetvernin, V., Ciuffo, S., and Li, W. (2013). “Prokaryotic genome annotation pipeline,” in *The NCBI Handbook*, 2nd Edn, eds J. Beck, D. Benson, J. Coleman, M. Hoeppner, M. Johnson, D. Maglott, et al. (Bethesda, MD: National Center for Biotechnology Information).
- Thingstad, T. F., Hagström, A., and Rassoulzadegan, F. (1997). Accumulation of degradable DOC in surface waters: is it caused by a malfunctioning microbial loop? *Limnol. Oceanogr.* 42, 398–404. doi: 10.4319/lo.1997.42.2.0398

- Tilbrook, B. D., and Karl, D. M. (1995). Methane sources, distributions and sinks from California coastal waters to the oligotrophic North Pacific gyre. *Mar. Chem.* 49, 51–64. doi: 10.1016/0304-4203(94)00058-L
- Villarreal-Chiu, J. F., Quinn, J. P., and McGrath, J. W. (2012). The genes and enzymes of phosphonate metabolism by bacteria, and their distribution in the marine environment. *Front. Microbiol.* 3:19. doi: 10.3389/fmicb.2012.00019
- Weiner, R. M., Taylor, L. E., Henrissat, B., Hauser, L., Land, M., Coutinho, P. M., et al. (2008). Complete genome sequence of the complex carbohydrate-degrading marine bacterium, *Saccharophagus degradans* strain 2-40T. *PLOS Genet.* 4:e1000087. doi: 10.1371/journal.pgen.1000087
- White, A. K., and Metcalf, W. W. (2004). Two C-P lyase operons in *Pseudomonas stutzeri* and their roles in the oxidation of phosphonates, phosphite, and hypophosphite. *J. Bacteriol.* 186, 4730–4739. doi: 10.1128/JB.186.14.4730-4739.2004
- Yang, J. C., Madupu, R., Durkin, A. S., Ekborg, N. A., Pedamallu, C. S., Hostetler, J. B., et al. (2009). The complete genome of *Teredinibacter turnerae* T7901: an intracellular endosymbiont of marine wood-boring bivalves (shipworms). *PLOS ONE* 4:e6085. doi: 10.1371/journal.pone.0006085
- Yin, Y., Mao, X., Yang, J., Chen, X., Mao, F., and Xu, Y. (2012). dbCAN: a web resource for automated carbohydrate-active enzyme annotation. *Nucleic Acids Res.* 40, W445–W451. doi: 10.1093/nar/gks479
- Zweifel, U. L., Norrman, B., and Hagström, Å. (1993). Consumption of dissolved organic carbon by marine bacteria and demand for inorganic nutrients. *Mar. Ecol. Prog. Ser.* 101, 23–32. doi: 10.3354/meps101023

Conflict of Interest Statement: The authors declare that the research was conducted in the absence of any commercial or financial relationships that could be construed as a potential conflict of interest.

Copyright © 2017 Sosa, Repeta, Ferrón, Bryant, Mende, Karl and DeLong. This is an open-access article distributed under the terms of the Creative Commons Attribution License (CC BY). The use, distribution or reproduction in other forums is permitted, provided the original author(s) or licensor are credited and that the original publication in this journal is cited, in accordance with accepted academic practice. No use, distribution or reproduction is permitted which does not comply with these terms.



In Situ Diazotroph Population Dynamics Under Different Resource Ratios in the North Pacific Subtropical Gyre

Kendra A. Turk-Kubo^{1*}, Paige Connell², David Caron², Mary E. Hogan¹, Hanna M. Farnelid^{1,3} and Jonathan P. Zehr¹

¹ Department of Ocean Sciences, University of California, Santa Cruz, Santa Cruz, CA, United States, ² Department of Biological Sciences, University of Southern California, Los Angeles, CA, United States, ³ Centre for Ecology and Evolution in Microbial Model Systems, Linnaeus University, Kalmar, Sweden

OPEN ACCESS

Edited by:

Samuel Wilson,
University of Hawaii at Manoa,
United States

Reviewed by:

Mar Benavides,
Institut de Recherche pour le
Développement (IRD), France
Tom Bibby,
University of Southampton,
United Kingdom

*Correspondence:

Kendra A. Turk-Kubo
ktk@ucsc.edu

Specialty section:

This article was submitted to
Aquatic Microbiology,
a section of the journal
Frontiers in Microbiology

Received: 26 April 2018

Accepted: 28 June 2018

Published: 25 July 2018

Citation:

Turk-Kubo KA, Connell P, Caron D, Hogan ME, Farnelid HM and Zehr JP (2018) In Situ Diazotroph Population Dynamics Under Different Resource Ratios in the North Pacific Subtropical Gyre. *Front. Microbiol.* 9:1616.
doi: 10.3389/fmicb.2018.01616

Major advances in understanding the diversity, distribution, and activity of marine N₂-fixing microorganisms (diazotrophs) have been made in the past decades, however, large gaps in knowledge remain about the environmental controls on growth and mortality rates. In order to measure diazotroph net growth rates and microzooplankton grazing rates on diazotrophs, nutrient perturbation experiments and dilution grazing experiments were conducted using free-floating *in situ* incubation arrays in the vicinity of Station ALOHA in March 2016. Net growth rates for targeted diazotroph taxa as well as *Prochlorococcus*, *Synechococcus* and photosynthetic picoeukaryotes were determined under high (H) and low (L) nitrate:phosphate (NP) ratio conditions at four depths in the photic zone (25, 45, 75, and 100 m) using quantitative PCR and flow cytometry. Changes in the prokaryote community composition in response to HNP and LNP treatments were characterized using 16S rRNA variable region tag sequencing. Microzooplankton grazing rates on diazotrophs were measured using a modified dilution technique at two depths in the photic zone (15 and 125 m). Net growth rates for most of the targeted diazotrophs after 48 h were not stimulated as expected by LNP conditions, rather enhanced growth rates were often measured in HNP treatments. Interestingly, net growth rates of the uncultivated prymnesiophyte symbiont UCYN-A1 were stimulated in HNP treatments at 75 and 100 m, suggesting that N used for growth was acquired through continuing to fix N₂ in the presence of nitrate. Net growth rates for UCYN-A1, UCYN-C, *Crocospaera* sp. (UCYN-B) and the diatom symbiont *Richelia* (associated with *Rhizosolenia*) were uniformly high at 45 m (up to $1.6 \pm 0.5 \text{ d}^{-1}$), implying that all were growing optimally at the onset of the experiment at that depth. Differences in microzooplankton grazing rates on UCYN-A1 and UCYN-C in 15 m waters indicate that the grazer assemblage preyed preferentially on UCYN-A1. Deeper in the water column (125 m), both diazotrophs were grazed at substantial rates, suggesting grazing pressure may increase with depth in the photic zone. Constraining *in situ* diazotroph growth and mortality rates are important steps for improving parameterization for diazotrophs in global ecosystem models.

Keywords: diazotroph, growth rates, mortality rates, *in situ* incubations, dilution technique, *nifH*, qPCR

INTRODUCTION

Our knowledge of the patterns of marine microbial biodiversity and functional activities has rapidly expanded (Sunagawa et al., 2015; Carradec et al., 2018) with the application of ‘omic’-based techniques. Spatial patterns, however, are ultimately a function of growth and mortality rates of individual taxa, which are processes that are difficult to measure in natural populations. This is especially true for microorganisms responsible for biological nitrogen (N_2) fixation (diazotrophs) in the marine environment because, despite their importance, they are present at low abundances and many lineages do not have cultivated representatives. Thus, it is not well understood how shifts in the availability of critical nutrients drive changes in the growth (and mortality) of natural populations of diazotrophs.

Marine diazotrophs are diverse, comprised of both phototrophic and heterotrophic Bacteria and Archaea. They vary greatly in morphology and physiology and are expected to have different optimal growth conditions and mortality factors. The filamentous colonial diazotroph *Trichodesmium* and the heterocyst-forming symbionts of diatoms (diatom-diazotroph associations, or DDAs) have long been recognized as important N_2 -fixers. These groups are distributed globally through tropical and subtropical regions, and are a major source of new N in temperate, oligotrophic regions (Villareal, 1992; Capone et al., 2005). Multiple lineages of unicellular N_2 -fixing cyanobacteria are also globally distributed (Moisander et al., 2010; Luo et al., 2012) and are a quantitatively important source of new N (Montoya et al., 2004). This is especially true in the oligotrophic North Pacific subtropical gyre (NPSG) (Dore et al., 2002; Church et al., 2009).

The free-living cyanobacterial diazotroph *Crocospaera* (UCYN-B) occasionally “blooms” in the NPSG, but arguably the more important unicellular diazotroph in this region is the uncultivated cyanobacteria group A (UCYN-A), which are present year-round in the NPSG. They reach peak abundances in the spring-early summer months and are comprised of diverse sublineages (Thompson et al., 2014; Farnelid et al., 2016; Turk-Kubo et al., 2017). Two of these sublineages, UCYN-A1 and UCYN-A2 are known to live in symbiosis with a prymnesiophyte algae (Thompson et al., 2012; Thompson et al., 2014). Both UCYN-A1 and UCYN-A2 have greatly reduced genomes, having lost important cyanobacterial metabolic capabilities including oxygenic photosynthesis and carbon fixation (Tripp et al., 2010; Bombar et al., 2014). These symbiotic associations are capable of high cellular rates of N_2 fixation (Martinez-Perez et al., 2016), presumably supported by the transfer of carbon from the host in exchange for reduced N from UCYN-A (Thompson et al., 2012).

Other unicellular cyanobacteria that have been reported include the unicellular cyanobacterial group C (UCYN-C; Foster et al., 2007), which includes some cultivated isolates (Taniuchi et al., 2012), however, little is known about their distribution or importance in the NPSG. *Trichodesmium* and several DDA lineages are also found in the NPSG (Letelier and Karl, 1996; Church et al., 2005a,b, 2009; Sohm et al., 2011b). *Richelia* spp. associated with *Rhizosolenia* (Het-1) and *Hemiaulus* (Het-2), are found in the NPSG and the latter has been identified

as the diazotroph that contributes to vertical export following summer blooms (Karl et al., 2012). Diverse non-cyanobacterial diazotrophs have been reported in the NPSG (Bombar et al., 2013; Gradoville et al., 2017), but their distributions and activities, as well as their quantitative significance to biological N_2 fixation, are not well understood (Turk-Kubo et al., 2014; Bombar et al., 2016; Moisander et al., 2017).

Controls on the N_2 fixation activity and distribution patterns of diazotrophs involve the interplay between the availability of nutrients needed for growth and activity and their ability to compete for these (often limiting) nutrients. Diazotrophic phytoplankton have a competitive advantage over non-diazotrophic phytoplankton when N is limiting, due to their ability to access gaseous N_2 . However, there are various costs associated with fixing N_2 , including a high cellular demand for Fe and the energy required to protect against inhibition of the oxygen-sensitive nitrogenase enzyme in aerobic environments, which are thought to result in a competitive disadvantage over non-diazotrophic phytoplankton when N is available. Under non-Fe limited conditions, diazotrophic phytoplankton are thought to be outcompeted by non-diazotrophic phytoplankton for the limited P at high N:P ratios (Schade et al., 2005). Thus the known biogeography of diazotrophs, at the basin scale, can be best predicted by models that consider the supply ratios of Fe:N and P:N (Ward et al., 2013).

It has been widely assumed that marine N_2 fixation is inhibited by the presence of nitrate, however, recent discoveries of diazotrophs and measurements of N_2 fixation rates in nitrate-replete marine environments such as coastal systems (Mulholland et al., 2012; Thompson et al., 2014), regions with seasonal upwelling (Sohm et al., 2011a; Moreira-Coello et al., 2017), mesopelagic waters (Hammersley et al., 2011; Benavides et al., 2018), the Bering (Shiozaki et al., 2017) and Chukchi Seas (Shiozaki et al., 2018) in the Arctic, the Great Belt (Bentzon-Tilia et al., 2015) and oxygen minimum zones (Fernandez et al., 2011), suggests that the influence of DIN availability on diazotroph biogeography and N_2 fixation is not well-understood. The assumption that DIN inhibits N_2 fixation is based on several lines of evidence including the competitive disadvantage faced by diazotrophs due to the energetic tradeoff between N_2 fixation versus nitrate assimilation (Falkowski, 1997), early observations of *Trichodesmium* only in N-depleted surface waters of the oligotrophic ocean (Capone et al., 1997), and direct measurements of nitrate and/or ammonia inhibition of N_2 fixation in culture experiments (e.g., Mulholland and Capone, 1999; Holl and Montoya, 2005). However, there is increasing evidence that the presence of DIN alone may not exclude diazotroph activity and N_2 fixation. In culture, evidence is emerging that short-term exposure to nitrate may not inhibit growth or N_2 fixation in the unicellular diazotroph *Crocospaera* (Dekaezemacker and Bonnet, 2011) and that N_2 fixation in *Trichodesmium* is not inhibited at nitrate concentrations typically found in surface waters (Knapp, 2012). Furthermore, the ratio of available N to P may play a critical role, as reduced cellular N_2 fixation rates at high nitrate concentrations can be offset by increased abundances when P is available in *Trichodesmium* (Knapp et al., 2012). Additionally, continuing to invest in N_2

fixation in the presence of DIN has been hypothesized as a unconventional strategy to balance redox states (Zehr and Bombar, 2015; Bombar et al., 2016 and references therein).

Cyanobacterial diazotroph net growth rates are a balance between taxa-specific requirements for growth (temperature, light, nutrients), and the ability to compete for limiting nutrients and avoid mortality (grazing and viral lysis). Each of these terms is challenging to evaluate in natural populations, thus predictive models rely heavily on culture-derived information, which is heavily biased toward *Trichodesmium*, to parameterize the N₂-fixing functional group (Dutkiewicz et al., 2009). Few direct measurements of diazotroph net growth rates have been made in natural populations. Net growth rates of UCYN-A1, *Crocospaera*, and the gammaproteobacteria γ -24774A11 have been reported to be stimulated by P, Fe+P, and to a lesser extent carbon additions in the South Pacific Ocean (Moisander et al., 2011). However, increases in diazotroph abundances (growth) or the transcription of the *nifH* gene (a proxy for N₂-fixing activity) are not always observed upon addition of P (Zehr et al., 2007; Turk-Kubo et al., 2012; Krupke et al., 2015; Barcelose Ramos et al., 2017). Turk-Kubo et al. (2015) observed fluctuations in net growth in mesocosms sampled for 23 days, underscoring that this is a dynamic process in which the top-down controls such as grazing and viral lysis are likely to be important factors.

Very little is known about diazotroph mortality in the marine environment. Grazing and viral lysis are assumed to be important factors affecting net growth rates and standing stocks, yet both are difficult to quantify. There have been a number of studies documenting the grazing of different copepod species on *Trichodesmium* (O'Neil et al., 1996; O'Neil, 1998), UCYN-A (Scavotto et al., 2015; Conroy et al., 2017), UCYN-B (Conroy et al., 2017), UCYN-C (Hunt et al., 2016) and *Richelia* associated with both *Rhizosolenia* (Het-1) and *Hemiaulus* (Het-2) (Hunt et al., 2016; Conroy et al., 2017), through direct observation or detection in full-gut copepods. Collectively, these studies indicate that direct transfer of diazotroph derived N to mesozooplankton (>200 μm) is potentially an important factor in marine food webs.

There are few direct observations of microzooplankton (<200 μm) grazing on diazotrophs, despite their prominent role as primary consumers in the oligotrophic open ocean (Schmoker et al., 2013). A recent study measured microzooplankton grazing rates on *Crocospaera* during a summertime *Crocospaera* bloom in the NPSG and concluded that grazing and viral lysis were likely controlling their abundances, rather than bottom-up factors (Wilson et al., 2017). Wilson et al. (2017) used a modification of the dilution technique developed by Landry and Hassett (1982) and flow cytometry to measure growth rates. This technique has been widely used to measure microzooplankton grazing rates on pico- and nanoplankton communities (0.2–2 μm and 2–20 μm size classes, respectively) in the ocean, and the underlying assumptions and limitations have been discussed in detail elsewhere (Landry et al., 1995; Schmoker et al., 2013). Growth and mortality rates of the entire phytoplankton community can be calculated using changes in chl *a* during the incubation, however, this approach can also be used to measure these parameters on individual taxa such as *Prochlorococcus* and

Synechococcus (Chen et al., 2009), as well as *Crocospaera* (Wilson et al., 2017).

In order to measure how shifts in the available nutrients influence the growth of natural diazotroph populations, free-floating *in situ* incubation arrays, originally described in Böttjer et al. (2017), were used to investigate net growth rates of phototrophic picoplankton and diazotrophic taxa as a function of depth and N:P ratio. In addition, microzooplankton grazing rates on diazotrophs were measured using a modified dilution method (Landry et al., 1995), at two depths in the photic zone (15 and 125 m) using a combination of *in situ* floating arrays and deckboard incubations. Diazotroph net growth rates were often stimulated by HNP conditions, which was an unexpected result, and the depth at which HNP conditions were favorable was taxa-dependent. Microzooplankton grazing pressure on the two most abundant diazotrophs, UCYN-A1 and UCYN-C, increased with depth, which was consistent with the pattern observed for the total phytoplankton community.

MATERIALS AND METHODS

Experimental Incubations

Five experiments were conducted as part of this study. Changes in diazotroph growth rates in response to shifts in available nutrient resource ratios were measured in growth experiment 1 (G1). Two experiments, grazing dilution experiment 1 (GR1) and 2 (GR2), were conducted to measure microzooplankton grazing rates on specific diazotrophic taxa, using a modified dilution technique amended with N, P and Fe (Landry et al., 1995). In parallel to the GR1 and GR2 experiments, smaller scale dilution experiments (GR1-N and GR2-N) amended only with P and Fe were conducted, based on the assumption that the addition of N substrates may inhibit diazotroph growth.

All experiments were conducted in the core of an anticyclonic eddy situated to the east of Station ALOHA in the NPSG between March 24 and 28, 2016 from aboard the R/V Kilo Moana (cruise no. KM1605). Seawater from the appropriate depths was collected for all experiments using a rosette of Niskin bottles coupled to a SeaBird CTD detector. Handling of water for each experiment type differed, and is detailed in sections below, however, all experiments were conducted in small (2.3 or 4 L) bottles, which have been recently shown to bias against large (20–200 μm) diazotrophic taxa (Follett et al., 2018). Experiments G1 and GR2 were incubated at fixed depths as part of a free-drifting array approach based on Böttjer et al. (2017), that makes it possible to incubate at *in situ* temperatures and irradiances. GR1, GR1-N, and GR2-N were incubated in simulated *in situ* light and temperature conditions in an on-deck incubator. Dates, experimental details and environmental parameters specific to each experiment are detailed in Table 1.

Diazotroph Net Growth Rate Incubations (G1)

Seawater collected from 25, 45, 75, and 100 m was dispensed directly from the Niskin bottles into 4 L polycarbonate bottles, taking measures to randomize the filling of the bottles. The polycarbonate bottles were acid-washed with trace metal clean

TABLE 1 | Growth (G1) and grazing rate (GR1, GR2) experiment details.

	GR1	GR1-N	G1	GR2	GR2-N
Date	March 24–25, 2016	March 24–25, 2016	March 25–27, 2016	March 27–28, 2016	March 27–28, 2016
Lat	22°23.799' N	22°23.799' N	22°23.997' N	22°33.276' N	22°33.276' N
Long	156°35.817' W	156°35.817' W	156°35.741' W	156°33.190' W	156°33.190' W
Experiment type	Grazing (5 pt. dilution)	Grazing (-N; 3 pt. dilution)	Growth rates (HNP vs. LNP)	Grazing (4 pt. dilution)	Grazing (-N; 2 pt. dilution)
% dilution levels	20,40,60,80,100	20,60,100	na	20,40,80,100	60,100
Incubation method	Deckboard	Deckboard	In situ array	In situ array	Deckboard
Depth(s) (m)	15	15	25, 45, 75, 100	15, 125	15
Incubation period (h)	24	24	48	24	24
MLD (m)	53 m	53 m	87 m	65 m	65 m
DCM (m)	140 m	140 m	140 m	140 m	140 m
Nitrocline (m)	125 m	125 m	125 m	125 m	125 m

MLD, mix layer depth; DCM, deep chlorophyll maximum; na, not applicable.

HCl prior to each experiment, however, these incubations are not considered trace metal clean. No pre-filtration to remove grazers was used, so measured growth rates determined from changes in cell abundances over the length of the incubation incorporate cell death, and are therefore net growth rates.

Replicate bottles from each depth were amended with either NaNO₃ (high N:P HNP) or KH₂PO₄ (low N:P; LNP) for final concentrations of 2 and 0.5 μM, respectively. All incubation bottles, including the controls (C), received FeCl₃ at a final concentration of 10 nM. Fe was added to ensure that the response of the diazotrophic community was to changes in the N:P ratio under non-Fe limiting conditions, as Fe is generally not considered to limit primary production at Station ALOHA (Boyle et al., 2005). Water was collected around 2 a.m. and the 4 L bottles were kept in the dark until the array was deployed before dawn. T₀ samples were immediately subsampled for phototrophic picoplankton cell counts using flow cytometry, nutrients, chl *a* and DNA. The G1 array was incubated *in situ* for 48 h, with bottles floating at the depths from which the water was originally sampled. The array deployment and recovery occurred at dawn, to minimize manipulating the communities in daylight. All bottles were kept in the dark until they were subsampled.

Incubations to Measure Microzooplankton Grazing Rates on Diazotrophs (GR1 and GR2)

For the dilution experiments GR1 and GR2, seawater from the appropriate depth was transferred into acid-washed 23 L polycarbonate carboys, which were then gently combined into a 50 L carboy to ensure homogeneity between treatments. Filtered seawater (FSW) for diluent was prepared by filtering experimental seawater through a Pall 0.2 μm Acropak 1550 Capsule Filter with Supor Membrane (Pall Corp, Port Washington, NY, United States), and was stored at room temperature in the dark while the experiment was setup. FSW was combined with whole sea water (WSW) in 2.3 L incubation bottles at ratios described below for each experiment and in Table 1. The bottles were amended with N, P and Fe at final concentrations of 2.0 μM NO₃⁻, 0.2 μM NH₄⁺, 0.5 μM PO₄³⁻, and 0.1 μM Fe. For each

experiment, a control set of triplicate bottles containing 100% WSW were not nutrient-amended in order to determine net growth rates during the incubation period. T₀ samples were taken from the 50 L carboy and immediately subsampled for chl *a* and DNA. All dilution experiments were initiated at night, to minimize photoadaptation or light shock.

GR1 consisted of five dilution levels, 20, 40, 60, 80, and 100% WSW. In parallel with GR1, a smaller-scale dilution experiment (GR1-N) was conducted that consisted of three dilution levels (20, 60, and 100% WSW) in triplicate 1.2 L bottles. Triplicate 1.2 L bottles containing 100% WSW were not amended with nutrients as noted above. The remaining bottles were amended with only P and Fe at final concentrations of 0.5 μM PO₄³⁻, and 0.1 μM Fe. All bottles (GR1 and GR1-N) were incubated for 24 h in simulated *in situ* light and temperature conditions in an on-deck incubator with a continuous flow of surface seawater to simulate conditions at 15 m. At T₂₄, all bottles were subsampled for chl *a* and DNA.

GR2 consisted of four dilution levels at each depth, 20, 40, 80, and 100% WSW. Incubation bottles were deployed on the *in situ* incubation array at 15 and 125 m and incubated for 24 h. As with GR1, a smaller-scale dilution experiment (GR2-N) was conducted in parallel with GR2, but only with 15 m water. GR2-N consisted of two dilution levels (60 and 100% WSW) in triplicate 1.2 L bottles. Nutrient amendments and WSW control bottles were consistent with GR2-N described above. The GR2-N bottles were incubated as described above for GR1-N. At T₂₄, all bottles were subsampled for chl *a* and DNA.

Quantifying Diazotroph Abundances Using Quantitative PCR and Calculating Net Growth and Mortality Rates

Samples for DNA extraction were gently filtered using peristaltic pumps through Sterivex filters (Millipore) for growth rate experiments or 0.2 μm pore-size 25 mm diameter Supor filters (Pall Corp, Port Washington, NY, United States) in sterile swinnex holders (Millipore) for grazing experiments. Sterivex filters were immediately sealed, and Supor filters were transferred into 2.0 mL bead beating tubes filled with 0.1 and

0.5 mm sterile glass beads. Filters were flash frozen in liquid nitrogen and stored at -80°C until extraction. Just prior to DNA extraction, the sterivex cartridges were broken and the filters were transferred into the bead beating tubes described above.

DNA was extracted using a protocol chosen for high quality recovery of DNA from algal cells. Details of this protocol are described in Moisander et al. (2008). Briefly, cells were disrupted using freeze-thaw, bead beating, and proteinase K digestion steps prior to a Qiacube[®] (Qiagen) automated on-column DNA extraction and clean-up protocol using DNeasy kit (Qiagen) components. Concentration and quality of purified DNA were measured using a NanoDrop (Thermo Scientific, Waltham, MA, United States). Extracted DNA was stored at -20°C until use.

Abundances of nine diazotrophic taxa were determined using quantitative PCR (qPCR) assays based on Taqman[®] chemistry. Primers and probes targeting the following diazotrophic taxa were used: unicellular cyanobacterial group A1 (UCYN-A1; Church et al., 2005a), unicellular cyanobacterial group A2/A3 (UCYN-A2/A3; Thompson et al., 2014), *Crocospaera* (UCYN-B; Moisander et al., 2010), *Cyanothece*-like organisms (UCYN-C; Foster et al., 2007), *Trichodesmium* spp. (Church et al., 2005a), *Richelia* associated with *Rhizosolenia* (Het-1; Church et al., 2005b), *Richelia* associated with *Hemialnus* (Het-2; Foster et al., 2007), *Calothrix* associated with *Chaetoceros* (Foster et al., 2007), and a gammaproteobacterial group (γ -24774A11; Moisander et al., 2008). All nine taxa were quantified in G1, but only the most abundant taxa present in the water at the time of the experimental work (UCYN-A1 and UCYN-C) were quantified in the grazing rate experiments.

Details of qPCR standard generation, plate design, thermocycling parameters, inhibition tests, determination of the limit of detection (LOD) and quantification (LOQ), as well as abundance calculations are described in Goebel et al. (2010). The LOD and LOQ for G1 and GR1 were 13 and 100 *nifH* copies L^{-1} , respectively. The LOD and LOQ for GR2 were between 33–50 and 267–400 *nifH* copies L^{-1} , respectively.

Net growth rates from G1 were calculated as in Turk-Kubo et al. (2015) using the equation $k = 2.303 \cdot [\log_{10}(N_{t_2}/N_{t_1})]/(t_2-t_1)$ where N_x = abundance at time x (t_x), and assuming that there is a single *nifH* copy per cell. It should be noted that there is evidence of multiple genome copies in natural populations of *Trichodesmium* (Sargent et al., 2016), and little is known about genome copy numbers in natural populations of other diazotroph taxa. Therefore, growth rates based on qPCR may be impacted if the number of genome copies is variable across time in a given population. However, based on the strong linear relationship between cell counts L^{-1} and *nifH* copies L^{-1} across variable sampling times reported by Sargent et al. (2016), the number of genome copies appears to be consistent, at least for *Trichodesmium*.

Net growth rates in G1 were determined for UCYN-A1, UCYN-B, UCYN-C in all depths and treatments, but only in surface waters for Het-1 (25 and 45 m) and Het-2 (25 m), due to low abundances for these latter taxa lower in the water column. UCYN-A2/A3, *Trichodesmium*, Het-3 and

γ -24774A11 were often detectable, but abundances were too low for establishing reliable rates (detected, not quantified; DNQs). Comparisons between treatments and the controls were made using one way analysis of variance, followed by testing independent variables with a pairwise *t*-test in R (R Development Core Team, 2012).

Mortality rates (m) on individual diazotroph taxa in GR1, GR1-N, GR2, and GR2-N were calculated using the slope of Model I linear regressions of qPCR-based diazotroph apparent growth rates in each nutrient-amended dilution vs. the dilution level, using the established convention that a negative slope indicated positive grazing pressure (Landry and Hassett, 1982). Nutrient enriched growth rates (μ_n) of each prey were determined using the *y*-intercept of the regression of nutrient-amended treatments, which represents a theoretical scenario where all grazing pressure is removed from the incubations. Intrinsic (unenriched) growth rates (μ_0) were calculated from the nutrient-enriched intrinsic growth rates, corrected for differences in growth rates between amended and unamended treatments of 100% WSW (Landry et al., 1995). Mortality rates are reported only when the linear regressions were significant ($p \leq 0.05$), otherwise they are reported as non-significant (ns).

Phototrophic Picoplankton Community Composition and Net Growth Rates in G1

Subsamples (2 mL) for the enumeration of *Prochlorococcus*, *Synechococcus* and photosynthetic picoeukaryotes (PPEs) were collected from G1 at times T_0 and T_{48} and immediately fixed with electron microscopy grade gluteraldehyde (Electron Microscopy Sciences, Hatfield, PA) for a final gluteraldehyde concentration of 0.25% v/v. Samples were fixed in the dark for 15 min, then flash frozen in liquid nitrogen and stored at -80°C until processing. Cells were enumerated using a BD Influx cell sorter with a 488 nm Sapphire laser (Coherent, Santa Clara, CA, United States). Large particles were removed from samples prior to counting using a CellTrics[®] filter with 30 μm mesh (Partec, Swedesboro, NJ, United States). *Synechococcus* cells were identified based on their phycoerythrin signal (orange fluorescence), and non-phycoerythrin containing cells (*Prochlorococcus* and PPEs) were identified using chl *a* fluorescence (red fluorescence) and forward scatter (FSC; a proxy for cell size). Data was triggered on the FSC channel, events were counted for 10 min, and data was processed using FlowJo v10.0.7 (Tree Star, Inc., Ashland, OR, United States). Net growth rates (G1) were calculated from abundances as described above.

Measuring Shifts in Microbial Community Composition During G1 Using 16S rRNA Gene Tag Sequencing

Bacterial community composition was characterized using the V3/V4 hypervariable region of the 16S-rRNA gene. Universal primers targeting Bacteria, Bakt_341F and Bakt_805R (Herlemann et al., 2011) were modified with common sequence linkers (Moonsamy et al., 2013) to facilitate library preparation

and sample barcoding. PCR amplifications were carried out in triplicate reactions for each sample, using reaction conditions and thermocycling parameters detailed in Shilova et al. (2017). Libraries were prepared at the DNA Services Facility at the University of Illinois, Chicago, using the targeted amplicon sequencing approach described in Green et al. (2015). Paired-end reads were sequenced using Illumina MiSeq technology at the W.M. Keck Center for Comparative and Functional Genomics at the University of Illinois at Urbana-Champaign. De-multiplexed raw paired-end reads were merged using PEAR (Zhang et al., 2014). QIIME (Caporaso et al., 2010) was used for quality filtering (phred score of 20), de novo chimera removal, operational taxonomic unit (OTU) determination (97% nucleotide similarity) using the usearch6.1 clustering method (Edgar, 2010), and assigning the taxonomy of representative sequences using the Silva reference database release 104 (Quast et al., 2013)¹. Raw reads were deposited in the Sequence Read Archive at National Center for Biotechnology Information² under BioSample Project ID PRJNA453423.

Community composition data was analyzed using the R package Phyloseq (McMurdie and Holmes, 2013). Data was subsampled using the following criteria: (i) removing OTUs not seen more than 100 times; and (ii) transforming to an equal sampling depth of 15,400 sequences; (iii) subsample for the top 20 most abundant OTUs. Ecological distances between samples based on community composition was determined using Jaccard and Bray–Curtis ecological indices on subsampled data and Principal coordinate analysis (PCoA) was performed on the resulting distance matrices, to visualize the dissimilarity between samples and community composition.

Chlorophyll a and Nutrient Sample Collection and Processing

For chl *a* concentrations from G1, between 250 and 500 mL of seawater was gently filtered under vacuum onto GF/F filters (Whatman®, Buckinghamshire, United Kingdom) and measured using the non-acidified protocol originally described in Welschmeyer (1994) using a Turner 10-AU fluorometer (San Jose, CA, United States).

Nutrient samples from the water column [nitrate + nitrite and inorganic phosphate (PO_4^{3-})] were collected and analyzed consistent with the Hawaii Ocean Time (HOT) Series Program³ at the University of Hawaii, Manoa.

RESULTS

Initial Environmental Conditions and Microbial Community Composition

All three experiments, G1, GR1, and GR2, were conducted during spring 2016 in the NPSG with water collected at the center

of an anticyclonic eddy characterized by enhanced chlorophyll located 60 km north of Molokai (22.5° N and 156.5° W). The eddy appeared to be decreasing in strength at the time of sampling, with low and variable currents at the center. The mixed layer depth and depth of the deep chlorophyll maximum (DCM) were apparent at 87 and 140 m, respectively (Table 1). Nitrate + nitrite concentrations were very low in the top 100 m of the water column at $2.8 \pm 3.2 \text{ nM}$, while PO_4^{3-} concentrations were $0.11 \pm 0.01 \mu\text{M}$. *Prochlorococcus* abundances at G1 T₀ were $7.2 \times 10^4 \pm 6.9 \times 10^3 \text{ cells mL}^{-1}$ at 25 m and increased slightly to $9.6 \times 10^4 \pm 5.2 \times 10^2 \text{ cells mL}^{-1}$ at 100 m; *Synechococcus* and photosynthetic picoeukaryote (PPE) abundances were consistent throughout the top 100 m at $7.5 \times 10^2 \pm 4.8 \times 10^1 \text{ cells mL}^{-1}$ and $1.5 \times 10^3 \pm 4.7 \times 10^2 \text{ cells mL}^{-1}$, respectively. The most abundant diazotrophs were unicellular cyanobacterial phylotypes UCYN-A1 and UCYN-C, which had maximum abundances of 4.7×10^4 and $1.2 \times 10^4 \text{ nifH copies L}^{-1}$, respectively. All other targeted diazotrophs were detected in the water column, but at much lower abundances than UCYN-A1 and UCYN-C (Figure 1), including the large (20–200 μm) diazotrophic taxa (*Trichodesmium* and DDAs), which is consistent with known annual patterns in their abundances (Church et al., 2009). However, it cannot be ruled out that these abundances are underestimated given a recent report that small bottle incubations may bias against the larger diazotrophs, presumably due to heterogeneity in these populations resulting from buoyancy and vertical migration (Follett et al., 2018).

Net Growth Rates in Photosynthetic Microbial Populations Exhibited Taxa- and Depth-Specific Responses to Different Nutrient Ratios

The responses of the major photosynthetic populations, *Prochlorococcus*, *Synechococcus*, and PPEs to HNP and LNP conditions during G1 were characterized using net growth rates derived from FCM-based cell counts (Figures 2A–D) as well as changes in chl *a* concentrations (as a proxy for photosynthetic biomass; Figures 2E–H). Over the course of the experiment, chl *a* content increased in all treatments and at all depths except at 100 m, where T₀ and T₄₈ chl *a* concentrations were similar (Figures 2E–H). Significant ($p \leq 0.01$) increases in chl *a* content with respect to control concentrations were measured only in the HNP treatment at 25 m (an approximately 2-fold increase; Figure 2E).

Increases in chl *a* concentrations in the 25 m HNP treatment may be due to a significant ($p \leq 0.05$) stimulation of biomass from the PPE population compared to T₄₈ controls (Figure 2A). This was the only depth and treatment where the PPE population had higher net growth rates than the controls, indicating that the PPE population was N-limited in surface waters. *Synechococcus* growth rates were highest in the LNP treatment at 25 m, implying that these populations were P-limited at the initiation of the experiment, despite ambient PO_4^{3-} concentration of $0.11 \pm 0.01 \mu\text{M}$ in the top 100 m of the water column (Figure 2A). In contrast, *Prochlorococcus* growth rates were

¹www.arb-silva.de/download/arb-files

²<http://www.ncbi.nlm.nih.gov/sra>

³<http://hahana.soest.hawaii.edu/hot/>

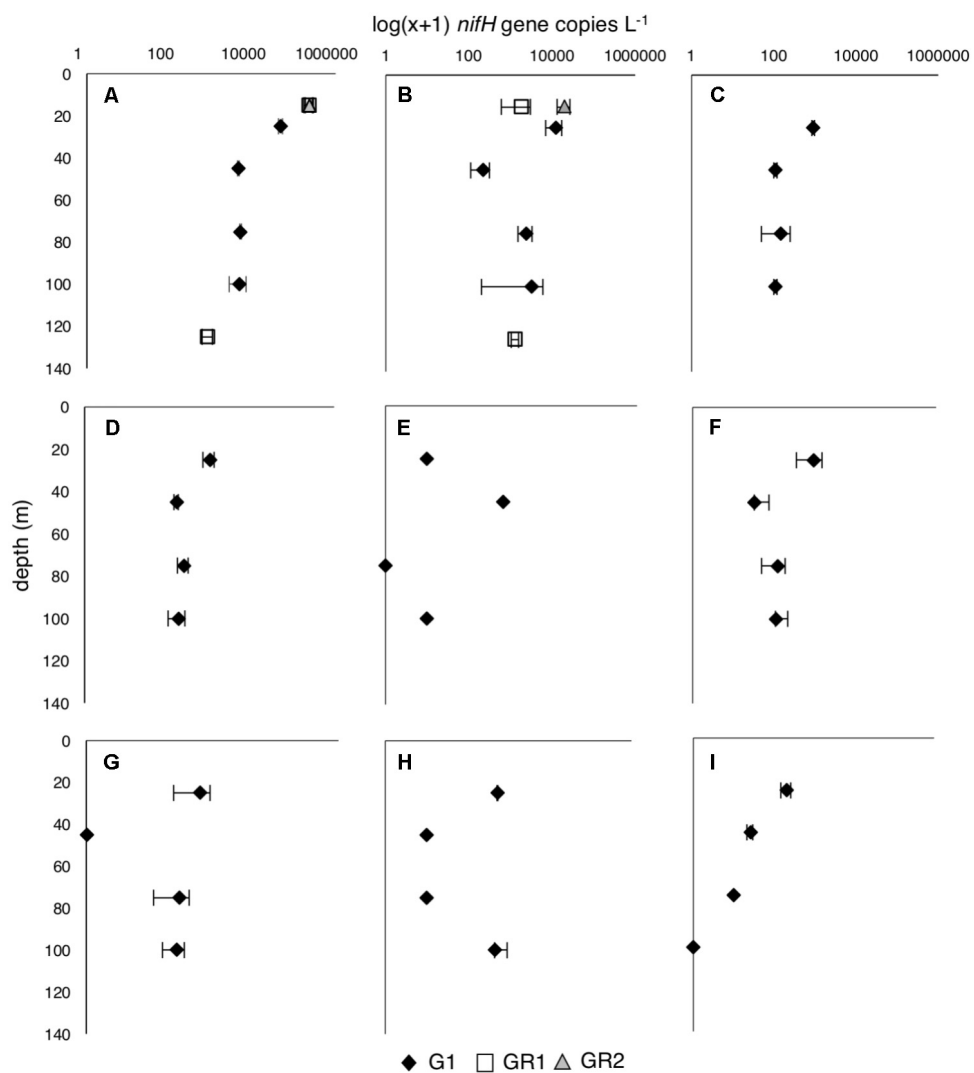


FIGURE 1 | Diazotroph abundances [$\log(x+1)$ *nifH* copies L^{-1}] throughout the water column at the beginning of growth rate (G1) and dilution grazing rate (GR1 and GR2) experiments. **(A)** UCYN-A1, **(B)** UCYN-C, **(C)** UCYN-A3, **(D)** UCYN-B, **(E)** *Trichodesmium*, **(F)** Het-1; **(G)** Het-2; **(H)** Het-3; **(I)** γ -24774A11. Only the most abundant diazotrophs, UCYN-A1 and UCYN-C, were measured for GR1 and GR2. Error bars are replicate incubations.

significantly ($p \leq 0.05$) stimulated only in HNP treatments at 45 m (Figure 2B).

Diazotroph Net Growth Rates Exhibit Taxa- and Depth-Specific Responses to Different Nutrient Ratios (G1)

Despite relatively stable abundances throughout the top 100 m (Figure 1), individual diazotrophic taxa exhibited depth-dependent responses to changes in nutrient ratio (Figure 3 and Supplementary Table S1). In surface waters (25 m), all of the diazotrophs had negative growth rates in the control treatment (Figures 3A,E,I,M,O). In 25 m HNP treatments, UCYN-B and UCYN-C had positive and enhanced growth rates (with respect to the control treatment) of $0.25 \pm 0.07 d^{-1}$ (Figure 3E) and $0.27 \pm 0.10 d^{-1}$ (Figure 3I), respectively; other groups had

negative or close to zero growth rates. The only diazotroph that had enhanced growth rates in the LNP treatment at this depth was Het-2 at $0.24 \pm 0.10 d^{-1}$ (Figure 3O).

Surprisingly, the most abundant diazotrophs, UCYN-A1, UCYN-B, UCYN-C and Het-1 had high net growth rates across all controls and treatments at 45 m (Figures 3B,F,J,N), despite all having peak abundances at 25 m (Figure 1). UCYN-A1 and UCYN-B growth rates were uniformly high and insensitive to nutrient additions ($1.32 \pm 0.02 d^{-1}$ and $1.39 \pm 0.08 d^{-1}$, respectively; Figures 3B,F), suggesting that these taxa were growing optimally at this depth at the start of the experiment, and growth was not inhibited or enhanced by experimental treatments. In contrast, both UCYN-C and Het-1 growth rates were slightly enhanced in LNP treatments (Figures 3J,N). UCYN-C growth rates in the control ($2.11 \pm 0.24 d^{-1}$) were less than those measured in LNP treatments ($2.71 \pm 0.26 d^{-1}$), and

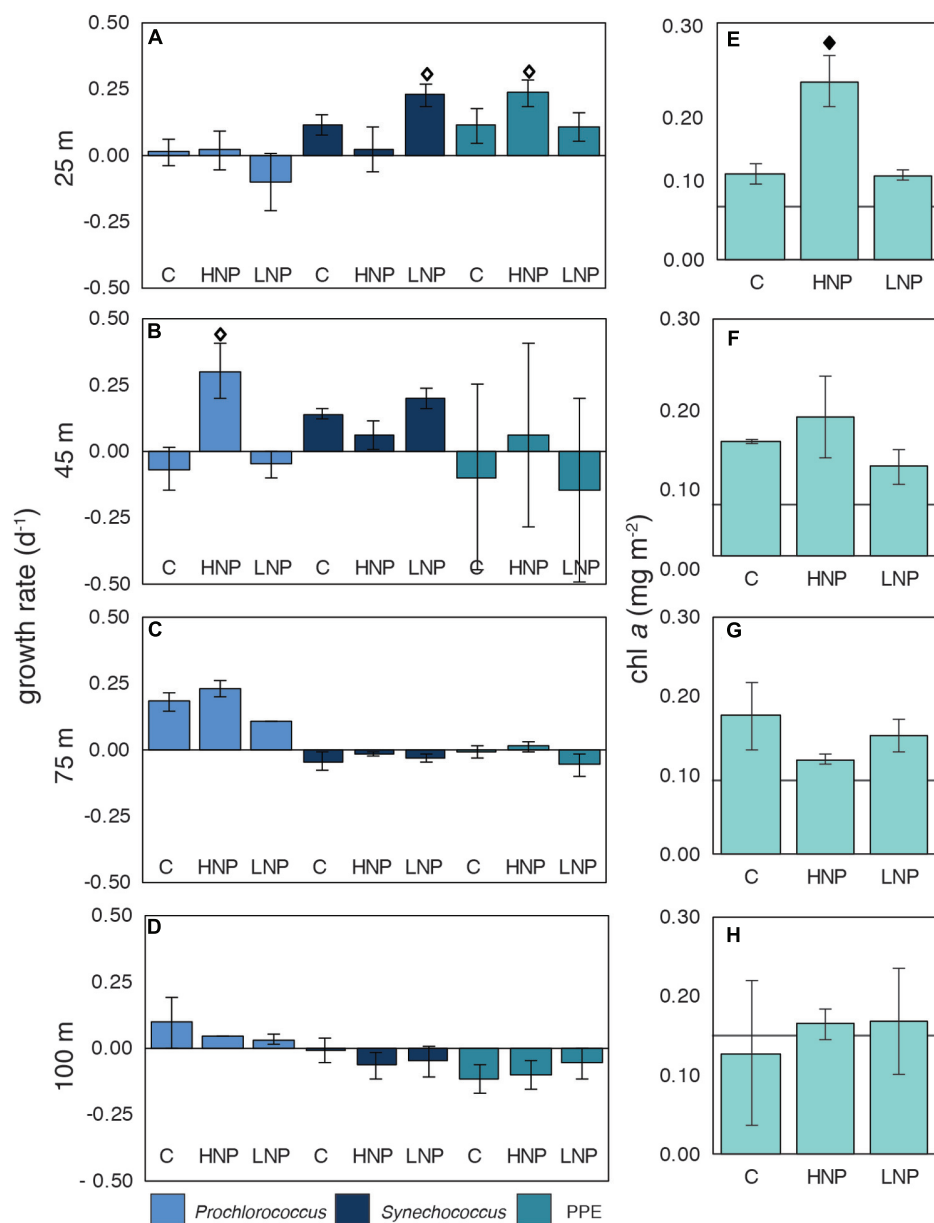


FIGURE 2 | Net growth rates of photosynthetic microbial populations (A–D) and biomass changes (chl a ; E–H) at four depths [25 (A,E), 45 (B,F), 75 (C,G) and 100 m (D,H)] in the photic zone during experiment G1. chl a concentrations at T_0 are indicated with a line. Error bars are replicate standard deviations. Statistically significant differences between control and treatment are indicated with a solid diamond ($p \leq 0.01$) or an open diamond ($p \leq 0.05$). C, control; HNP, high N:P treatment; LNP, low N:P treatment; PPE, photosynthetic picoeukaryote.

the same was true for Het-1 (control $1.42 \pm 0.17\ d^{-1}$ vs. LNP $1.74 \pm 0.11\ d^{-1}$). These results suggest UCYN-C and Het-1 have a competitive advantage in the N-limited conditions at this depth.

Deeper in the water column (75 and 100 m incubations), net growth rates could only be determined for the unicellular taxa. There was no significant difference in net growth rates between control and LNP/HNP treatments at these depths for UCYN-B and UCYN-C (Figures 3G,H,K,L). However, UCYN-A1 net growth rates were significantly stimulated ($p \leq 0.05$), with respect to control incubations, under HNP conditions at 75 m

($0.63 \pm 0.05\ d^{-1}$; Figure 3C) and 100 m ($0.70 \pm 0.08\ d^{-1}$; Figure 3D).

Shifts in Prokaryote Microbial Community Composition During G1

16S rRNA gene variable region amplicon tag sequencing was used to determine whether there were significant changes in microbial community composition. *Prochlorococcus* (21.8–51.3% of sequences per sample) and SAR11 (10.0–16.6% of sequences per sample) dominated the prokaryote community throughout

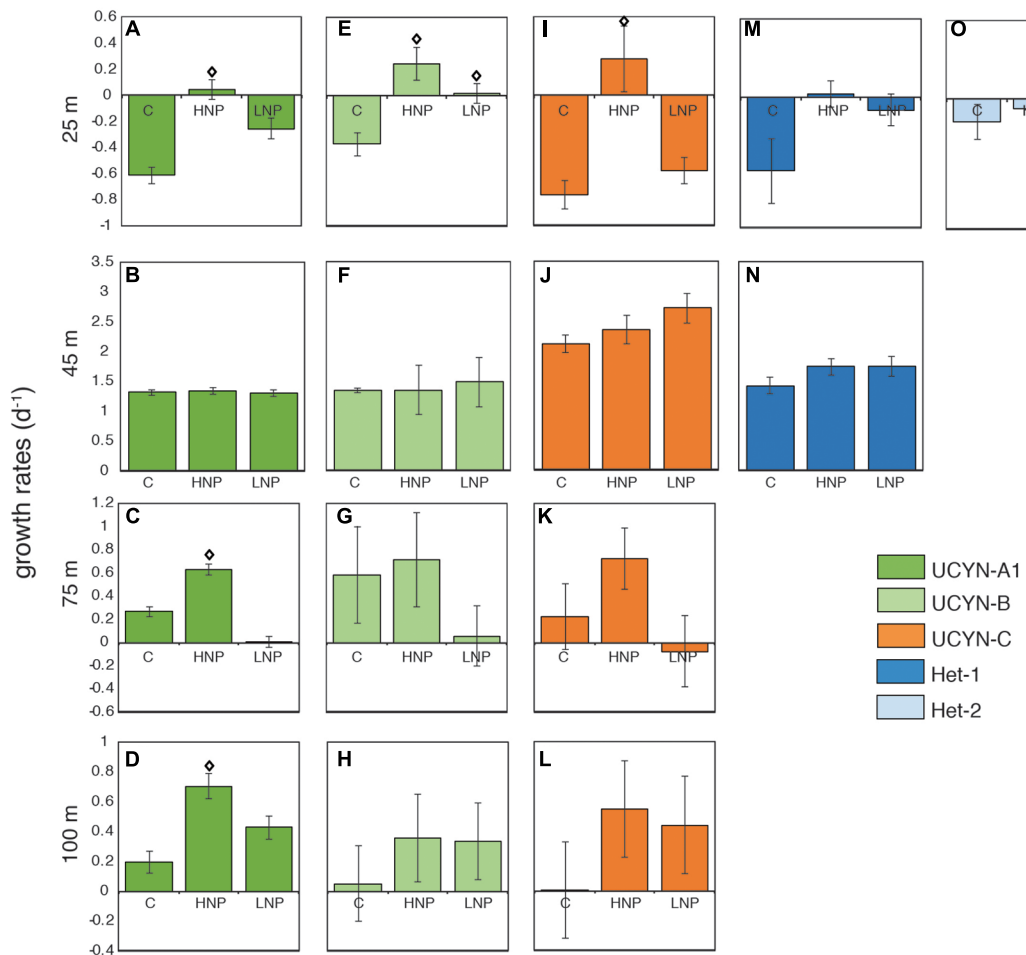


FIGURE 3 | Diazotroph net growth rates throughout the photic zone during experiment G1 at 25 m (A,E,I,M,O), 45 m (B,F,J,N), 75 m (C,G,K), and 100 m (D,H,L). Error bars are replicate standard deviations. Statistically significant differences between control and treatment are indicated with an open diamond ($p \leq 0.05$). C, control; HNP, high N:P treatments; LNP, low N:P treatment.

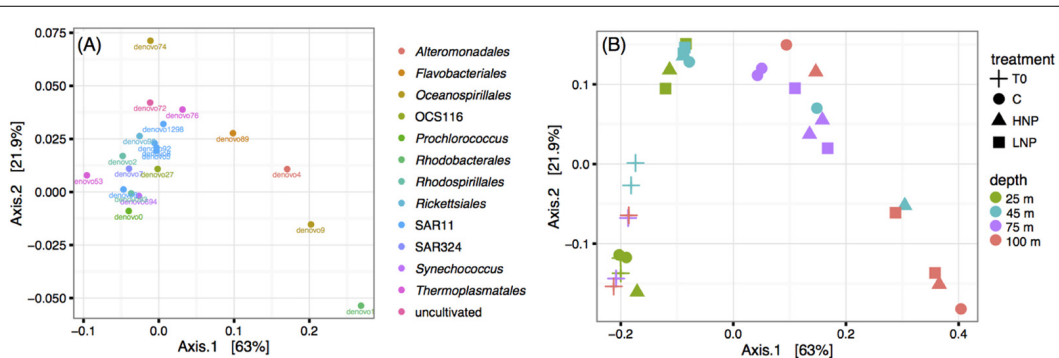


FIGURE 4 | Principal coordinate analysis using the Jaccard ecological index to determine dissimilarity between samples based on microbial community composition. Data was transformed to equal sampling depth and OTUs were defined at 97% nucleotide similarity. The 20 most abundant OTUs (A) and community composition of each experimental bottle (B). C, control; HNP, high N:P treatments; LNP, low N:P treatment.

the experiment (Supplementary Table S2). T₀ samples showed that there was a relatively constant microbial community within the top 100 m (Figure 4A), consistent with the presence of a

deep mixed layer at the time of the experiment. Furthermore, there were no large shifts in relative abundances of these taxa in response to HNP and LNP treatments, including

Prochlorococcus at 45 m, indicating that although cell numbers increased, the relative proportion of *Prochlorococcus* to other microbes (mainly SAR11) remained stable. Even at the finest taxonomic resolution, *Prochlorococcus* oligotypes (Eren et al., 2013) were also consistent across depths and treatments (data not shown).

There were minor changes in community composition between T₀ and T₄₈ at 75 and 100 m depths, but not between experimental treatments (Figure 4B). Ordination analysis using the Jaccard ecological index indicated that community shifts were driven by increases in relative abundances of the following four taxa in all treatments: *Rhodobacterales* (denovo1), *Alteromonadales* (denovo4), *Oceanospirillales* (denovo9), and *Flavobacteriales* (denovo89) (Figure 4A). These taxa are frequently found in associations and on particles and are known to respond quickly to incubation conditions (Fontanez et al., 2015). It is important to note that treatments often did not cluster together, indicating that changes in nutrient ratios did not drive any consistent patterns; T₄₈ samples clustered according to depth (Figure 4B). Furthermore, there was not a correlation between relative abundances and diazotroph net growth rates in samples where a diazotroph had differential responses to HNP/LNP treatments, e.g., UCYN-A1 at 75 or 100 m.

Microzooplankton Grazing Pressure on UCYN-A1 and UCYN-C Was Highest Near the Deep Chlorophyll Maximum

During GR2, grazing rates on the bulk phytoplankton community, based on changes in chl *a*, indicated that there was no detectable grazing pressure in surface waters (Figure 5A), while grazing pressure was significant near the DCM (125 m; Figure 5B). The measured mortality rate (*m*) on the bulk phytoplankton community at 125 m was 0.60 d⁻¹, which is higher than the mean rate for this region (0.29 d⁻¹) reported in Schmoker et al. (2013). Enriched (μ_n) and intrinsic (μ_0) growth rates at 15 m were 0.66 and 0.24 d⁻¹, respectively, indicating that the addition of nutrients stimulated phytoplankton growth rates in surface waters. The community seemed less responsive to added nutrients at 125 m, with μ_n and μ_0 of 0.59 and 0.62 d⁻¹, respectively.

Patterns of grazing mortality specifically for UCYN-A1 and UCYN-C were consistent with the depth-dependent patterns observed for the phytoplankton community. In GR1, no significant grazing pressure was measured at 15 m for either diazotroph taxa, however, variable mortality rates on UCYN-A1, and UCYN-C were measured during GR2 (Figure 6). In GR2, grazing rates on UCYN-A1 were lower at the surface (15 m; 0.24 d⁻¹) than deeper in the photic zone (125 m; 1.00 d⁻¹; Figure 6). UCYN-C did not seem to have significant grazing pressure at 15 m, while at 125 m, mortality rates were high (1.75 d⁻¹). Enrichment with nutrients did appear to stimulate UCYN-A1 growth rates at 15 m, with enriched (μ_n) and intrinsic (μ_0) growth rates of 0.16 and -0.13 d⁻¹, respectively. However, this was not the case for samples collected deeper in the water column for either taxa. Grazing rates for other diazotrophs were not measured due to their low abundances in T₀ samples.

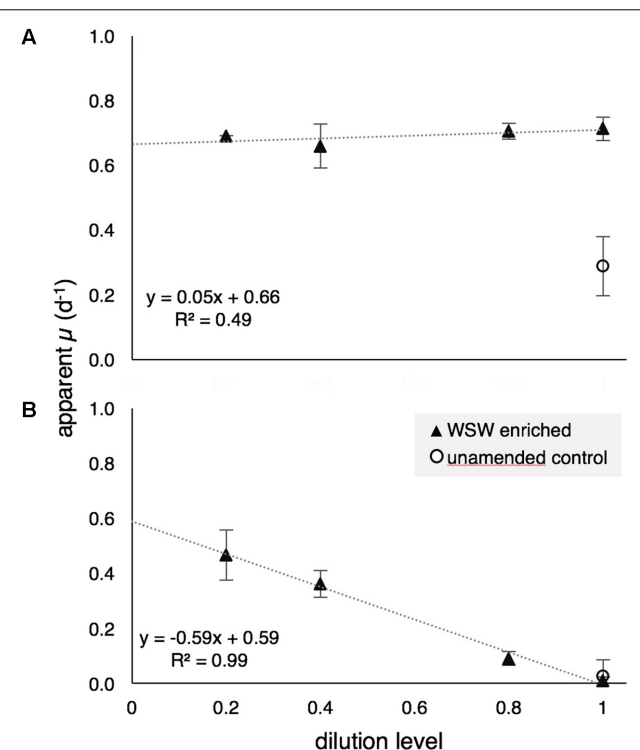


FIGURE 5 | Apparent growth rates (μ) of the bulk photosynthetic community (based on chl *a*) at 15 m (A) and 125 m (B) during modified dilution rate experiments GR2. Positive grazing mortality (*m*) at 125 m is evidenced by the negative slope of the model I linear regression. WSW, whole sea water.

Together, the chl *a*-based phytoplankton mortality rates and qPCR-based diazotroph mortality rates indicated that grazing pressure was less intense near the surface than deeper in the water column.

Grazing dilution incubations with water from 15 m were conducted during GR1 and GR2, using a nutrient addition that did not include additional fixed N (GR1-N and GR2-N), as the presence of N has been shown to inhibit diazotroph growth in cultures (e.g., Holl and Montoya, 2005). Mortality rates on UCYN-A1 in GR2-N and GR1-N were higher than in the typical modified dilution rate experiments at 1.25 and 0.69 d⁻¹, respectively (Figure 6). In these experiments, enriched growth rates for UCYN-A1 were positive with μ_n ranging between 0.28 and 0.82 d⁻¹. No significant mortality rates were measured for UCYN-C in these experiments. These findings are inconsistent with growth rates measured in G1 where growth rates at 25 m were negative in response to P additions (LNP treatment).

DISCUSSION

Diazotrophs Are Capable of High *in Situ* Growth Rates

Early culture-based studies suggested that diazotrophs should have slower growth rates than their non-diazotrophic

TABLE 2 | Compilation of diazotroph growth rates measured *in situ*, along with selected culture-based measurement.

Diazotroph	Maximum net growth rate d^{-1}	Method	Location	Experimental Conditions or <i>In situ</i>	Reference
UCYN-A ^a	0.4	^{13}C	Station ALOHA	<i>In situ</i>	Thompson et al., 2012
UCYN-A ^a	0.5	^{13}C	North Atlantic	<i>In situ</i>	Krupke et al., 2015
UCYN-A ^a	0.8	cell size, modeled	North Pacific	<i>In situ</i>	Goebel et al., 2008
UCYN-A (small) ^a	0.6 ^c	^{13}C	North Atlantic	<i>In situ</i>	Martinez-Perez et al., 2016
UCYN-A (large) ^b	1.1 ^c	^{13}C	North Atlantic	<i>In situ</i>	Martinez-Perez et al., 2016
UCYN-A1	1.3	qPCR	NPSG	HNP treatment; 45 m	<i>This study</i>
UCYN-A1	1.3	qPCR	NPSG	LNP treatment; 45 m	<i>This study</i>
UCYN-A1	1.3	qPCR	NPSG	C treatment; 45 m	<i>This study</i>
UCYN-A1	0.2	qPCR	South Pacific	Fe and P-Fe treatments	Moisander et al., 2011
UCYN-A1	0.7	qPCR	Southwest Pacific	P treatment	Turk-Kubo et al., 2015
UCYN-A2	1.7	qPCR	Southwest Pacific	P treatment	Turk-Kubo et al., 2015
UCYN-B	1.5	qPCR	NPSG	LNP treatment; 45 m	<i>This study</i>
UCYN-B	1.3	qPCR	NPSG	HNP treatment; 45 m	<i>This study</i>
UCYN-B	1.3	qPCR	NPSG	C treatment; 45 m	<i>This study</i>
UCYN-B	0.6	qPCR	South Pacific	Fe and P-Fe treatments	Moisander et al., 2011
UCYN-B	1.4	qPCR	Southwest Pacific	P treatment	Turk-Kubo et al., 2015
UCYN-B	0.6	FCM	NPSG	<i>In situ</i>	Wilson et al., 2017
UCYN-C	2.7	qPCR	NPSG	LNP treatment; 45 m	<i>This study</i>
UCYN-C	2.4	qPCR	NPSG	HNP treatment; 45 m	<i>This study</i>
UCYN-C	2.1	qPCR	NPSG	C treatment; 45 m	<i>This study</i>
UCYN-C	2.2	qPCR	Southwest Pacific	P treatment	Turk-Kubo et al., 2015
<i>Richelia</i> in <i>Rhizosolenia</i> (Het-1)	1.3	qPCR	Southwest Pacific	P treatment	Turk-Kubo et al., 2015
<i>Richelia</i> in <i>Rhizosolenia</i> (Het-1)	1.7	qPCR	NPSG	LNP conditions; 45 m	<i>This study</i>
<i>Richelia</i> in <i>Rhizosolenia</i> (Het-1)	1.7	qPCR	NPSG	HNP treatment; 45 m	<i>This study</i>
<i>Richelia</i> in <i>Rhizosolenia</i> (Het-1)	1.4	qPCR	NPSG	C treatment; 45 m	<i>This study</i>
<i>Richelia</i> in <i>Hemiaulus</i> (Het-2)	2.2	qPCR	Southwest Pacific	P treatment	Turk-Kubo et al., 2015
<i>Richelia</i> in <i>Hemiaulus</i> (Het-2)	0.2	qPCR	NPSG	LNP treatment; 25 m	<i>This study</i>
<i>Richelia</i> in <i>Hemiaulus</i> (Het-2)	0.6	^{15}N	North Pacific	<i>In situ</i>	Foster et al., 2011
<i>Calothrix</i> in <i>Chaetoceros</i> (Het-3)	1.1	qPCR	Southwest Pacific	P treatment	Turk-Kubo et al., 2015
<i>Trichodesmium</i>	0.1	^{13}C	North Atlantic	<i>In situ</i>	Martinez-Perez et al., 2016
Selected growth rates for cultivated isolates					
<i>Cyanothece</i> . sp ATCC 51142	1.92	Culture	na	na	Vu et al., 2012
UCYN-C TW3	0.84	Culture	na	na	Taniuchi et al., 2012
<i>Cyanothece</i> . sp ATCC 51142	2.4	Culture	na	na	Reddy et al., 1993
<i>Crocospheara watsonii</i> WH8501	0.49	Culture	na	na	Goebel et al., 2008
<i>Trichodesmium erythraeum</i> IMS101	0.51	Culture	na	na	Goebel et al., 2008
<i>Richelia</i> in <i>Rhizosolenia</i>	0.67	Culture	na	na	Villareal, 1989; Villareal, 1990

Maximum rates from each study are reported and negative rates (when reported) are not included. NPSG, North Pacific Subtropical Gyre; ^{13}C , measuring the incorporation of $^{13}\text{CO}_2$ using nanoSIMS; qPCR, quantitative PCR; FCM, flow cytometry. ^aAssumed by the authors of this study to be UCYN-A1 based on size and sample location.

^bAssumed by the authors of this study to be UCYN-A3 based on size and sample location. ^cEstimated from Figure 3 in Martinez-Perez et al. (2016).

counterparts in natural populations (Fu and Bell, 2003; Falcon et al., 2004; LaRoche and Breitbarth, 2005). However, this assumption was challenged when Moisander et al. (2011) reported net growth rates from field populations of *Crocospheara* in the South Pacific, which were higher than culture-based growth rate measurements (Table 2). *In situ* net growth rates were also unexpectedly high during a perturbation mesocosm study in the southwestern lagoon of New Caledonia (Turk-Kubo et al., 2015), where maximum net growth rates for unicellular and heterocyst-forming diazotrophs were as high as 2.2 d^{-1} (Table 2).

The maximum net growth rate measured for UCYN-A1 in this study, 1.3 d^{-1} , is higher than reported in the North Atlantic (0.19 d^{-1} ; Moisander et al., 2011) and in the South Pacific (0.73 d^{-1} ; Turk-Kubo et al., 2015) (Table 2). These previously reported net growth rates were from experimental manipulations of surface waters amended with P [or P and P + Fe, in the case of Moisander et al. (2011)], conditions which are generally thought to favor diazotrophs. Interestingly, net growth rates of UCYN-A1 were uniformly high in samples from 45 m, independent of treatment (1.3 d^{-1}), even though peak abundances of UCYN-A1 were measured at 25 m (Figure 1).

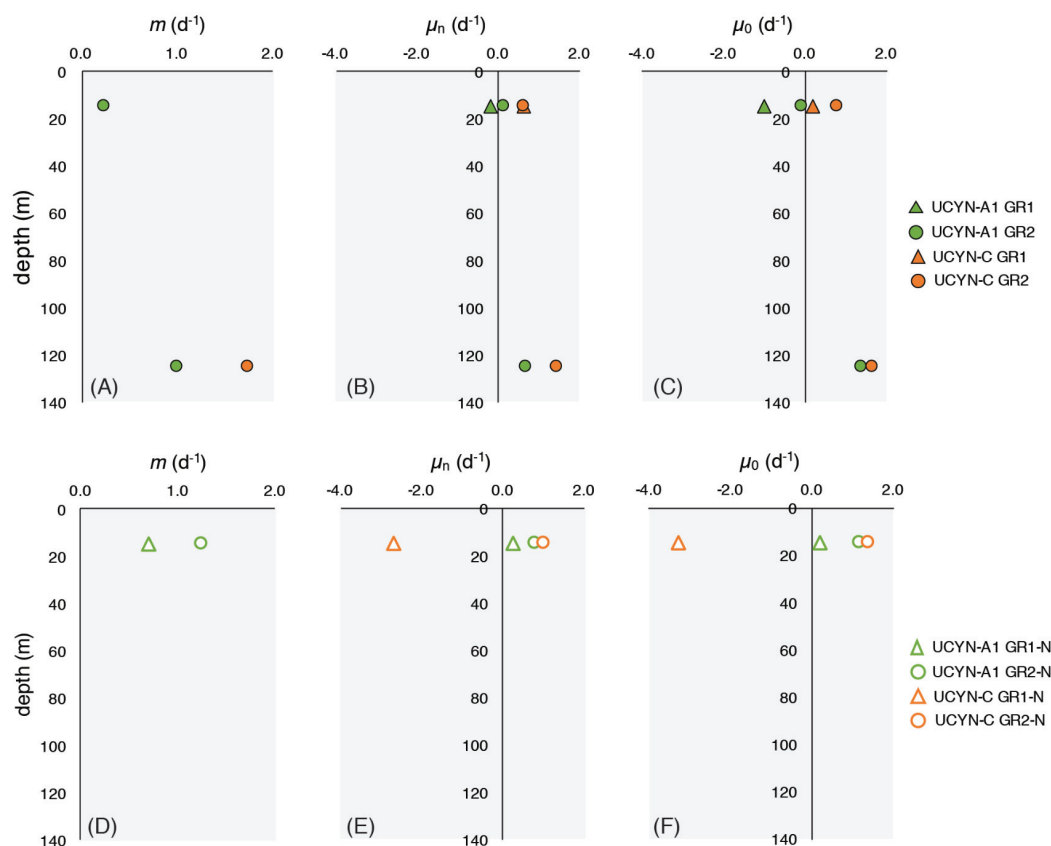


FIGURE 6 | Microzooplankton grazing rates on UCYN-A1 and UCYN-C during modified dilution grazing rate incubations GR1 and GR2 **(A–C)** and GR1-N and GR2-N **(D–F)**. Mortality rates (m) are reported only when $p \leq 0.05$. UCYN-A1 mortality rates in GR1 were non-significant. UCYN-C mortality rates were non-significant at 15 m for all experiments m , grazing mortality rate; μ_n , enriched growth rate; μ_0 , intrinsic growth rate.

Maximum net growth rates for UCYN-B (1.5 d^{-1}), UCYN-C (2.7 d^{-1}), Het-1 (1.7 d^{-1}) and Het-2 (0.2 d^{-1}) were comparable to rates measured in a P-perturbation experiment in the New Caledonia lagoon (Turk-Kubo et al., 2015). As with UCYN-A1, maximum net growth rates were measured exclusively in the samples collected at 45 m, and were high across all treatments. This was not observed in the growth rates for *Prochlorococcus*, *Synechococcus* or the PPEs (Figure 2). These findings imply that all diazotrophic taxa were either growing at optimal maximum rates at the start of the incubation, and maintained these rates throughout the 48 h incubation, or that the combination of light, temperature and Fe was optimal for all taxa at this depth (10 nM Fe was added to all incubation bottles, including controls). These results are surprising given that peak abundances for all diazotrophs were measured at 25 m depth, as well as the physiological differences among diazotrophs and the evidence that there is niche partitioning throughout the water column (Moisander et al., 2010). Results from the grazing rate experiments clearly show that grazing pressure increases with depth, which may explain why peak abundances were found at 25 m, but the highest net growth rates were found at 45 m. Preliminary growth rate experiments conducted in July 2015 yielded very similar results, with net

growth rates of the most abundant diazotrophs being high in control, HNP and LNP treatments at a single depth (see Supplementary Figure S1). Further research, and perhaps different tools for measuring growth rates in natural populations, are needed to determine the environmental factors behind this observation.

There have been relatively few measurements of *in situ* diazotroph growth rates, but when reported, they are often from nutrient perturbation experiments, where nutrient limitation may have been alleviated (Table 2). Due to this, along with differences in experimental design and measurement of growth rates, it is difficult to compare rates across studies, and between *in situ* and culture-based studies. However, results obtained in this and other recent studies together indicate that diazotrophs are capable of high net growth rates *in situ* over relatively short time periods, even in the presence of competition and mortality (grazing/viral lysis), which underscores the gaps in our understanding of their physiology and cellular requirements. In global ecological models, diazotroph growth rates are typically parameterized using $1/2$ the maximum growth rate of a comparably sized non-diazotroph, to compensate for the energetic costs of fixing N₂ (Dutkiewicz et al., 2009). Direct comparisons between

large diazotrophs (*Trichodesmium*, DDAs) and their non-diazotrophic counterparts cannot be drawn from this study, but growth rates measured for the smaller, non-symbiotic diazotrophs (*Crocospaera* and UCYN-C) are comparable to, and in many cases higher, than rates measured for *Synechococcus* (Figure 2).

Diazotrophs Can Grow in Nitrate-Replete Conditions

Diazotrophs are predicted to be unable to coexist with non-diazotrophs at high N:P ratios under equilibrium conditions when Fe is not limiting (Schade et al., 2005). This is based on resource ratio theory (Dutkiewicz et al., 2009 and references therein), which uses basic physiological requirements for a specific phytoplankton taxa to define the minimum concentration of a given nutrient needed for survival. Thus, under the conditions in the HNP treatments of this study, non-diazotrophs would be expected to outcompete diazotrophs for available P ($0.11 \pm 0.01 \mu\text{M}$ at the beginning of the experiment). However, findings from this study indicate that diazotrophic taxa can compete for nutrients on relatively short temporal scales (48 h) under conditions thought to favor “velocity adapted” organisms capable of responding quickly to pulses of nutrients, such as diatoms (Sommer, 1984).

These findings may be explained in part due to growth possibly being uncoupled from the energetically demanding process of N_2 fixation in HNP conditions, as some taxa can assimilate nitrate directly from the environment for growth (Agawin et al., 2007; Großkopf and LaRoche, 2012), or live in symbiosis with eukaryotic phytoplankton (diatoms, haptophytes) presumed to assimilate nitrate. The accessibility of a fixed N source has been shown to be a requirement for the initiation of N_2 fixation in free-living soil diazotrophs, given the upfront investment a cell must make to generate N-containing cellular components (Norman and Friesen, 2017), thus the ability to acquire and utilize diverse sources of DIN and DON may also be a critical strategy for marine diazotrophs.

Further research is needed to verify the N source(s) used for growth by each diazotroph taxa under these conditions, and whether N_2 fixation continues in nitrate-replete conditions. We cannot speculate about whether growth in these experiments was supported by increased N_2 fixation or nitrate. However, there is growing evidence that N_2 fixation *in situ* may not be as sensitive to DIN as previously thought (Knapp, 2012), especially when P concentrations are not limiting (Knapp et al., 2012). Meyer et al. (2016) recently reported that N_2 fixation rates remained reasonably constant over an 8-day period and a broad range of nitrate concentrations in the Eastern Tropical North Atlantic, indicating that the presumably DDA-dominated diazotroph community (Het-1) could fix N_2 in N replete conditions. Active N_2 fixation has been measured in a variety of N-replete environments including high latitude Arctic waters (Shiozaki et al., 2017, 2018), and upwelling regions (Sohm et al., 2011a; Moreira-Coello et al., 2017).

UCYN-A1 lacks the genetic ability to directly assimilate nitrate (Tripp et al., 2010), so the observation that UCYN-A1 grows in the presence of nitrate deeper in the water column implies that when nitrate is available to the host, the symbiont either continues to fix N_2 or obtains reduced N from its host to support growth. Although there have been several recent studies that have measured the response of UCYN-A1 to nutrient amendments (Moisander et al., 2011; Turk-Kubo et al., 2012; Krupke et al., 2015), it has been uncommon to include N species among the suite of nutrients added, since N_2 fixation is understood to be either P or Fe limited (or P/Fe co-limited) in oligotrophic waters (Mills et al., 2004; Moore et al., 2009). However, two recent studies conducted in the Subtropical North Atlantic did include N addition as a treatment. Langlois et al. (2012) reported increased UCYN-A *nifH*-based abundances (ca. an order of magnitude) after the addition of ammonium nitrate to surface waters in one of the three experiments conducted in this region, indicating that the association was able to grow in N-replete conditions. However, despite greatly increased abundances of UCYN-A, no stimulation of bulk N_2 fixation rates were measured in their N amended treatment. Without data on cell-specific N_2 fixation rates it is unclear whether UCYN-A stopped fixing N_2 in this incubation. However, Krupke et al. (2015) reported no reduction in cell-specific N_2 fixation rates or *nifH* transcript production after the addition of $2 \mu\text{M}$ ammonium nitrate to UCYN-A populations in the North Atlantic suggesting that UCYN-A continues to fix N_2 even when reduced N is available to the association.

It has been speculated that UCYN-A1 may reach peak abundances in oligotrophic waters with elevated nutrient conditions coinciding with entrainment of nutrient-rich waters from vertical mixing in the South Pacific Ocean (Moisander et al., 2010). At Station ALOHA, UCYN-A1 abundances peak in spring months when light intensity increases and the mixed layer begins to shoal, entraining nutrient-rich waters into the sunlit surface waters. However, it is unclear which component(s) of the deep nutrient pool are responsible for leading to peak UCYN-A abundances. Furthermore, Henke et al. (2018) found that UCYN-A1 peak abundances coincided with slightly elevated *in situ* nitrate concentrations in a time series conducted in the New Caledonia Lagoon. Results from this study may provide some insight into these observations, given that UCYN-A1 growth rates responded positively to the introduction of nitrate deeper in the water column. It is unclear why this was not the case for the samples collected at shallower depths, where more light energy was available for the prymnesiophyte host, and where the PPE population did have increased growth rates in the HNP treatment (Figure 2A), but active grazing on UCYN-A1 in surface waters may have depressed net growth rates. These findings underscore the likely tradeoff between conditions optimal for photosynthesis, N_2 fixation and availability of nutrients, and provide valuable insight to this enigmatic symbiosis which may help explain its niche preferences for deeper waters (closer to the nutricline than other diazotrophs), and occurrences in colder, sometimes N-replete environments.

UCYN-B and UCYN-C, unicellular diazotrophs that may be free-living or living in aggregates (Sohm et al., 2011b; Bonnet et al., 2016), had similar responses across treatments and depths in the present study. As with UCYN-A1, their growth rates were stimulated by HNP conditions, but only at the surface (25 m), implying that light or a nutrient other than N was limiting growth in the HNP treatments deeper in the water column. Microzooplankton grazing pressure on UCYN-C was greatest near the DCM, and it is possible that the same may be true for UCYN-B. Positive growth rates in HNP conditions for UCYN-B are not unexpected given that *Crocospaera* growth and N₂ fixation are insensitive to nitrate concentrations in culture (Großkopf and LaRoche, 2012). The same is assumed to be true for UCYN-C in the NPSG, as *Cyanothecae* isolates belonging to this group can grow on nitrate (Agawin et al., 2007). However, the qPCR assay used in this study does target a cluster that contains uncultivated marine sequence types, as well as the endosymbiont of the freshwater diatom *Rhopalodia gibba*. Therefore, without knowing with better certainty the source organism in the NPSG, the ability of the organisms targeted with the UCYN-C assay to assimilate nitrate remains speculative.

Stimulated growth rates in LNP treatments, conditions expected to favor diazotrophs due to N-limitation, were only measured for Het-2 at 25 m and UCYN-C and Het-1 at 45 m (**Figures 3O,J,N**). Notably, Het-2 was found only at the surface and did not have positive net growth rates in HNP treatments, unlike Het-1 (45 m). Both Het-1 and Het-2 lack the genetic capability to assimilate nitrate (Hilton et al., 2013; Hilton, 2014). The observation that Het-2 does not increase in abundance when its host is in an environment with replete nitrate availability, implies a different ecological strategy than the Het-1 symbiosis. Results from these incubations suggest that the Het-2 symbiosis has a competitive advantage in surface waters under LNP conditions in the NPSG.

Microzooplankton Actively Graze on Diazotrophs

Very little is known about mortality processes for diazotrophs in the oligotrophic marine environment. To the best of our knowledge, this is the first report of the measurement of *in situ* microzooplankton grazing on UCYN-A1 and UCYN-C. Interestingly, these data suggest that the rate of microzooplankton grazing differed depending on the location in the water column and the grazed diazotroph taxa (**Figure 6**). UCYN-A1 experienced significant grazing pressure at the surface (GR2; $m = 0.20 \text{ d}^{-1}$) that exceeded measured growth rates. UCYN-C was not grazed at the surface, yet UCYN-A1 and UCYN-C were present at similar abundances at this depth (**Figure 1**). These findings imply that the grazer assemblage preyed preferentially on UCYN-A1 in surface waters. Different mortality rates measured for co-occurring photosynthetic populations (*Prochlorococcus*, *Synechococcus*, and PPEs) have been previously reported (Chen et al., 2009), and this situation appears to also be true

for diazotrophs. Numerous factors contribute to preferential feeding of microzooplankton including prey size, cell surface properties, viral infection, nutrient composition, and the release of dissolved substances (Jürgens and Massana, 2008; Chrzanowski and Foster, 2014). However, cell size is generally a dominant factor determining the suitability of prey to microzooplankton consumers. UCYN-A1 lives in association with a prymnesiophyte, while UCYN-C occurs as free-living solitary cells. Thus, we speculate that differences in the size of the host-symbiont association of UCYN-A1 and the solitary cells of UCYN-C may explain the preferential grazing by the consumer assemblages on UCYN-A1 in surface waters. Size dependent grazing relationships would implicate microzooplanktonic protists (20–200 μm in size) as their consumers. This size category is dominated by ciliates, dinoflagellates and a variety of rhizarian taxa at Station ALOHA (Pasulka et al., 2013; Hu et al., unpublished data from the present study).

Interestingly, deeper in the water column, both diazotrophs were grazed at substantial rates (**Figure 6**), and there was general agreement between depth trends in the chl *a*-based grazing rates, which provide bulk microzooplankton grazing rates on the phytoplankton community, and qPCR-based grazing rates on diazotrophic taxa (**Table 2** and **Figure 4**). The mortality rate for UCYN-C at 125 m was the highest measured (1.75 d^{-1}), and greater than both intrinsic and enriched growth rates for this cyanobacterial group. Additionally, in contrast to results from surface waters, the grazing rate on UCYN-A1 (1.00 d^{-1}) was lower than the grazing rate for UCYN-C at this depth, and was also lower than its intrinsic growth rate (1.36 d^{-1}), indicating that grazing pressure was not controlling UCYN-A1 abundances deeper in the water column. It is not clear if these depth-related differences in grazing pressure reflected differences in the feeding activities of the grazer community between the two depths, differences in the taxonomic composition of the consumer community, or both. General depression of grazing activity near the ocean surface might be inferred from the lower mortality rates observed for chl *a*-based measurements and the results for UCYN-C, but mortality of UCYN-A1 in surface waters was substantial in most cases. Moreover, previous work at station ALOHA (Pasulka et al., 2013) and molecular diversity studies conducted during the present study (Hu et al., unpublished; Connell et al., unpublished) have documented substantive changes in absolute and relative abundances of the various consumer taxa between surface waters and the lower euphotic zone (i.e., commensurate with the depths sampling in this study). Therefore, taxonomic composition and feeding behavior may both contribute to the depth-related differences in cyanobacterial mortality rates observed in this study.

More measurements are needed at finer depth resolution throughout the photic zone, and in different seasons (typically characterized by different dominant diazotrophic taxa) to better constrain microzooplankton grazing pressure on diazotroph populations, and to identify their consumers. However, our experiments verify that it is possible to use the dilution method

technique to investigate mortality of diazotrophic taxa, when their abundances are high enough to remain above detection limits when diluted.

CONCLUSION

Diazotroph growth and mortality rates are critical variables for global ecosystem models. The high energetic cost associated with the ability to fix N₂ is typically offset in model parameterizations by assuming lower growth rates of diazotrophs relative to non-diazotrophic counterparts, as well as higher requirements for intracellular N:P and Fe:P ratios (e.g., Monteiro et al., 2010, 2011). Collectively, these assumptions are based on the tradeoffs of an organism which is never N-limited and the high energetic cost of N₂ fixation. However, these assumptions are based primarily on *Trichodesmium* data and observations, and are validated by very few *in situ* measurements, particularly for unicellular diazotrophs. Furthermore, estimates of grazing on diazotrophs have been based on a simple interaction between predator and prey based on size (Monteiro et al., 2010) and sometimes palatability (Dutkiewicz et al., 2009). For these reasons, direct measurements of growth rates and microzooplankton grazing rates on diazotrophs are valuable, especially considering that for many of the important diazotroph groups, we are unable to define these terms using culture-based experiments.

The *in situ* growth rate experiment (G1) yielded several surprising results. In general, *in situ* net growth rates measured were high, often comparable to or greater than culture-based measurements (when comparisons can be made). LNP treatments, which were anticipated to provide diazotrophs with a competitive advantage, were not always the favorable conditions for growth at a given depth. Net growth rates for most diazotroph taxa appeared to be stimulated in the HNP treatments. More research is needed to determine whether the N needed for growth under these conditions was supported by assimilation of nitrate, or N₂ fixation, acknowledging that the answer to this question is likely taxa-specific. However, these results suggest that the availability of DIN may be favorable on short time scales for natural populations of diazotrophs.

This is the first study to directly measure microzooplankton grazing rates on UCYN-A1 and UCYN-C. Future studies should focus on identifying the potential consumers of these minute diazotrophs, as well as using dilution grazing experiments to constrain mortality at higher spatial and temporal resolution. However, together with previously reported observations of copepod grazing on diazotrophs (O’Neil et al., 1996; O’Neil, 1998; Hunt et al., 2016; Conroy et al., 2017), these findings provide further indication that diazotroph derived N is, in some cases, directly transferred to higher trophic levels through grazing.

In summary, the high *in situ* net growth rates reported here, the competitive ability of some taxa in N-replete conditions, and measurement of depth-dependent microzooplankton grazing

on diazotrophs, provide new insight into their ecological roles, and indicate that current parameterizations for this functional group in global ecosystem models may need reevaluation.

AUTHOR CONTRIBUTIONS

KT-K, HF, and JZ designed the growth rate experiment. PC, DC, KT-K, and JZ designed the grazing experiments. MH, KT-K, PC, and DC executed the experiments at sea. KT-K processed all samples for molecular and flow cytometry analysis, with help from MH. PC and DC processed chlorophyll samples from the grazing experiments. KT-K analyzed the data sets, with input from PC and DC on grazing rate experimental data. KT-K wrote the manuscript with input from all authors.

FUNDING

This work was supported by grants from The Simons Foundation (SCOPE Award ID 329108, JZ and Award ID P49802, DC) and the National Science Foundation (OCE-1559165). HF was supported by the Swedish Research Council VR 637-2013-7502.

ACKNOWLEDGMENTS

We gratefully acknowledge Brittany Stewart (UCSC), Corrine Gibble (UCSC), Kendra Negrey (UCSC), Britt Henke (UCSC), and Alyssa G. Gellene (USC) for shipboard assistance and help processing samples, the Hawaii Ocean Time (HOT) Series and Simons Collaboration on Ocean Processes and Ecology (SCOPE) staff and crew, and Stefan Green and his staff at the DNA Services Facility and the University of Illinois, Chicago for NGS consultation.

SUPPLEMENTARY MATERIAL

The Supplementary Material for this article can be found online at: <https://www.frontiersin.org/articles/10.3389/fmicb.2018.01616/full#supplementary-material>

FIGURE S1 | Results from growth rate experiments conducted in the vicinity of Station ALOHA in July 2015. Experiments were conducted and samples were processed as described for G1, but with water from a single depth (25 m) incubated in deck board incubators with *in situ* simulated light and temperature. The incubation was conducted during a *Crocospheara* bloom described in detail in Wilson et al., 2017, but other diazotroph taxa were present (**A**). Differential responses in net growth rates to HNP and LNP conditions were not seen for any of the phototrophic phytoplankton groups (**B**). Diazotroph growth rates for the dominant diazotrophs (**C–H**) were uniformly high across all treatments and the controls, similar to the results from G1 at 45 m.

TABLE S1 | Growth rate data used in **Figure 5**.

TABLE S2 | OTU table, which includes taxonomy strings for each OTU for 16S rRNA data from G1.

REFERENCES

- Agawin, N. S. R., Rabouille, S., Veldhuis, M. J. W., Servatius, L., Hol, S., Van Overzee, H. M. J., et al. (2007). Competition and facilitation between unicellular nitrogen-fixing cyanobacteria and non-nitrogen-fixing phytoplankton species. *Limnol. Oceanogr.* 52, 2233–2248. doi: 10.4319/lo.2007.52.5.2233
- Barcelos Ramos, J., Schulz, K. G., Voss, M., Narciso, Á., Müller, M. N., Reis, F. V., et al. (2017). Nutrient-specific responses of a phytoplankton community: a case study of the north Atlantic gyre, azores. *J. Plankton Res.* 39, 744–761. doi: 10.1093/plankt/fbx025
- Benavides, M., Shoemaker, K. M., Moisander, P. H., Niggemann, J., Dittmar, T., Duhamel, S., et al. (2018). Aphotic N₂ fixation along an oligotrophic to ultraoligotrophic transect in the western tropical south Pacific ocean. *Biogeosciences* 15, 3107–3119. doi: 10.5194/bg-15-3107-2018
- Bentzon-Tilia, M., Traving, S. J., Mantikci, M., Knudsen-Leerbeck, H., Hansen, J. L. S., Markager, S., et al. (2015). Significant N₂ fixation by heterotrophs, photoheterotrophs and heterocystous cyanobacteria in two temperate estuaries. *ISME J.* 9, 273–285. doi: 10.1038/ismej.2014.119
- Bombar, D., Heller, P., Sanchez-Baracaldo, P., Carter, B. J., and Zehr, J. P. (2014). Comparative genomics reveals surprising divergence of two closely related strains of uncultivated UCYN-A cyanobacteria. *ISME J.* 8, 2530–2542. doi: 10.1038/ismej.2014.167
- Bombar, D., Paerl, R. W., and Riemann, L. (2016). Marine non-cyanobacterial diazotrophs: moving beyond molecular detection. *Trends Microbiol.* 24, 916–927. doi: 10.1016/j.tim.2016.07.002
- Bombar, D., Turk-Kubo, K. A., Robidart, J. C., Carter, B. J., and Zehr, J. P. (2013). Non-cyanobacterial *nifH* phylotypes in the North Pacific Subtropical Gyre detected by flow-cytometry cell sorting. *Environ. Microbiol. Rep.* 5, 705–715. doi: 10.1111/1758-2229.12070
- Bonnet, S., Berthelot, H., Turk-Kubo, K., Fawcett, S., Rahav, E., Lhelguen, S., et al. (2016). Dynamics of N₂ fixation and fate of diazotroph-derived nitrogen in a low-nutrient, low-chlorophyll ecosystem: results from the VAHINE mesocosm experiment (New Caledonia). *Biogeosciences* 13, 2653–2673. doi: 10.5194/bg-13-2653-2016
- Böttjer, D., Dore, J. E., Karl, D. M., Letelier, R. M., Mahaffey, C., Wilson, S. T., et al. (2017). Temporal variability of nitrogen fixation and particulate nitrogen export at station ALOHA. *Limnol. Oceanogr.* 62, 200–216. doi: 10.1002/lo.10386
- Boyle, E. A., Bergquist, B. A., Kayser, R. A., and Mahowald, N. (2005). Iron, manganese, and lead at hawaii ocean time-series station ALOHA: temporal variability and an intermediate water hydrothermal plume. *Geochim. Cosmochim. Acta* 69, 933–952. doi: 10.1016/j.gca.2004.07.034
- Capone, D., Zehr, J., Paerl, H., and Bergman, B. (1997). *Trichodesmium*, a globally significant marine cyanobacterium. *Science* 276, 1221–1229 doi: 10.1126/science.276.5316.1221
- Capone, D. G., Burns, J. A., Montoya, J. P., Subramaniam, A., Mahaffey, C., Gunderson, T., et al. (2005). Nitrogen fixation by *Trichodesmium* spp: an important source of new nitrogen to the tropical and subtropical north Atlantic ocean. *Global Biogeochem. Cycles* 19:GB2024. doi: 10.1029/2004GB002331
- Caporaso, J. G., Kuczynski, J., Stombaugh, J., Bittinger, K., Bushman, F. D., Costello, E. K., et al. (2010). QIIME allows analysis of high-throughput community sequencing data. *Nat. Methods* 7, 335–336. doi: 10.1038/nmeth.f.303
- Carradec, Q., Pelletier, E., Da Silva, C., Alberti, A., Seeleuthner, Y., Blanc-Mathieu, R., et al. (2018). A global ocean atlas of eukaryotic genes. *Nat. Commun.* 9:373. doi: 10.1038/s41467-017-02342-1
- Chen, B., Liu, H., Landry, M. R., Dai, M., Huang, B., and Sune, J. (2009). Close coupling between phytoplankton growth and microzooplankton grazing in the western south China sea. *Limnol. Oceanogr.* 54, 1084–1097. doi: 10.4319/lo.2009.54.4.1084
- Chrzanowski, T. H., and Foster, B. L. (2014). Prey element stoichiometry controls ecological fitness of the flagellate *ochromonas danica*. *Aquat. Microb. Ecol.* 71, 257–269. doi: 10.3354/ame01680
- Church, M., Jenkins, B., Karl, D., and Zehr, J. (2005a). Vertical distributions of nitrogen-fixing phylotypes at Stn ALOHA in the oligotrophic north Pacific Ocean. *Aquat. Microb. Ecol.* 38, 3–14. doi: 10.3354/ame038003
- Church, M., Short, C., Jenkins, B., Karl, D., and Zehr, J. (2005b). Temporal patterns of nitrogenase gene (*nifH*) expression in the oligotrophic north pacific ocean. *Appl. Environ. Microbiol.* 71, 5362–5370. doi: 10.1128/AEM.71.9.5362-5370.2005
- Church, M. J., Mahaffey, C., Letelier, R. M., Lukas, R., Zehr, J. P., and Karl, D. M. (2009). Physical forcing of nitrogen fixation and diazotroph community structure in the north Pacific subtropical gyre. *Global Biogeochem. Cycles* 23:GB2020. doi: 10.1029/2008GB003418
- Conroy, B. J., Steinberg, D. K., Song, B., Kalmbach, A., Carpenter, E. J., and Foster, R. A. (2017). Mesozooplankton graze on cyanobacteria in the amazon river plume and western tropical north Atlantic. *Front. Microbiol.* 8:1436. doi: 10.3389/fmicb.2017.01436
- Dekaezemacker, J., and Bonnet, S. (2011). Sensitivity of N₂ fixation to combined nitrogen forms (NO₃⁻ and NH₄⁺) in two strains of the marine diazotroph *Crocospaera watsonii* (Cyanobacteria). *Mar. Ecol. Prog. Ser.* 438, 33–46. doi: 10.3389/fmicb.2012.00374
- Dore, J. E., Brum, J. R., Tupas, L. M., and Karl, D. M. (2002). Seasonal and interannual variability in sources of nitrogen supporting export in the oligotrophic subtropical north Pacific Ocean. *Limnol. Oceanogr.* 47, 1595–1607. doi: 10.4319/lo.2002.47.6.1595
- Dutkiewicz, S., Follows, M. J., and Bragg, J. G. (2009). Modeling the coupling of ocean ecology and biogeochemistry. *Global Biogeochem. Cycles* 23:GB4017. doi: 10.1029/2008GB003405
- Edgar, R. C. (2010). Search and clustering orders of magnitude faster than BLAST. *Bioinformatics* 26, 2460–2461. doi: 10.1093/bioinformatics/btq461
- Eren, A. M., Maignien, L., Sul, W. J., Murphy, L. G., Grim, S. L., Morrison, H. G., et al. (2013). Oligotyping: differentiating between closely related microbial taxa using 16S rRNA gene data. *Methods Ecol. Evol.* 4, 1111–1119. doi: 10.1111/2041-210X.12114
- Falcon, L., Carpenter, E., Cipriano, F., Bergman, B., and Capone, D. (2004). N₂ fixation by unicellular bacterioplankton from the Atlantic and Pacific Oceans: phylogeny and in situ rates. *Appl. Environ. Microbiol.* 70, 765–770. doi: 10.1128/AEM.70.2.765-770.2004
- Falkowski, P. (1997). Evolution of the nitrogen cycle and its influence on the biological sequestration of CO₂ in the ocean. *Nature* 387, 272–275. doi: 10.1038/387272a0
- Farnelid, H., Turk-Kubo, K., Munoz-Marín, M. D., and Zehr, J. P. (2016). New insights into the ecology of the globally significant uncultured nitrogen-fixing symbiont UCYN-A. *Aquat. Microb. Ecol.* 77, 125–138. doi: 10.3354/ame01794
- Fernandez, C., Farias, L., and Ulloa, O. (2011). Nitrogen fixation in denitrified marine waters. *PLoS ONE* 6:e20539. doi: 10.1371/journal.pone.0020539
- Follett, C. L., White, A. E., Wilson, S. T., and Follows, M. J. (2018). Nitrogen fixation rates diagnosed from diurnal changes in elemental stoichiometry. *Limnol. Oceanogr.* doi: 10.1002/lo.10815 [Epub ahead of print].
- Fontanez, K. M., Eppley, J. M., Samo, T. J., Karl, D. M., and Delong, E. F. (2015). Microbial community structure and function on sinking particles in the north Pacific subtropical gyre. *Front. Microbiol.* 6:469. doi: 10.3389/fmicb.2015.00469
- Foster, R. A., Kuypers, M. M. M., Vagner, T., Paerl, R. W., Musat, N., and Zehr, J. P. (2011). Nitrogen fixation and transfer in open ocean diatom-cyanobacterial symbioses. *ISME J.* 5, 1484–1493. doi: 10.1038/ismej.2011.26
- Foster, R. A., Subramaniam, A., Mahaffey, C., Carpenter, E. J., Capone, D. G., and Zehr, J. P. (2007). Influence of the Amazon River plume on distributions of free-living and symbiotic cyanobacteria in the western tropical north Atlantic ocean. *Limnol. Oceanogr.* 52, 517–532. doi: 10.4319/lo.2007.52.2.0517
- Fu, F. X., and Bell, P. R. F. (2003). Growth, N₂ fixation and photosynthesis in a cyanobacterium, *Trichodesmium* sp., under Fe stress. *Biotechnol. Lett.* 25, 645–649. doi: 10.1023/A:1023068232375
- Goebel, N. L., Edwards, C. A., Carter, B. J., Achilles, K. M., Church, M. J., and Zehr, J. P. (2008). Growth and carbon content of three different sized diazotrophic cyanobacteria observed in the subtropical North Pacific. *J. Phycol.* 44, 1212–1220. doi: 10.1111/j.1529-8817.2008.00581
- Goebel, N. L., Turk, K. A., Achilles, K. M., Paerl, R. W., Hewson, I., Morrison, A. E., et al. (2010). Abundance and distribution of major groups of diazotrophic cyanobacteria and their potential contribution to N₂ fixation in the tropical Atlantic Ocean. *Environ. Microbiol.* 12, 3272–3289. doi: 10.1111/j.1462-2920.2010.02303.x
- Gradoville, M. R., Bombar, D., Crump, B. C., Letelier, R. M., Zehr, J. P., and White, A. E. (2017). Diversity and activity of nitrogen-fixing communities across ocean basins. *Limnol. Oceanogr.* 62, 1895–1909. doi: 10.1002/lo.10542

- Green, S. J., Venkatraman, R., and Naqib, A. (2015). Deconstructing the polymerase chain reaction: understanding and correcting bias associated with primer degeneracies and primer-template mismatches. *PLoS ONE* 10:e0128122. doi: 10.1371/journal.pone.0128122
- Großkopf, T., and LaRoche, J. (2012). Direct and indirect costs of dinitrogen fixation in *Crocospaera watsonii* WH8501 and possible implications for the nitrogen cycle. *Front. Microbiol.* 3:236. doi: 10.3389/fmicb.2012.00236
- Hamersley, M. R., Turk, K. A., Leinweber, A., Gruber, N., Zehr, J. P., and Gunderson, T. et al. (2011). Nitrogen fixation within the water column associated with two hypoxic basins in the southern California bight. *Aquat. Microb. Ecol.* 63, 193–205. doi: 10.3354/ame01494
- Henke, B. A., Turk-Kubo, K. A., Bonnet, S., and Zehr, J. P. (2018). Distributions and Abundances of sublineages of the N2-Fixing cyanobacterium *Candidatus Atelocyanobacterium thalassa* (UCYN-A) in the new caledonian coral lagoon. *Front. Microbiol.* 9:554. doi: 10.3389/fmicb.2018.00554
- Herlemann, D. P., Labrenz, M., Jürgens, K., Bertilsson, S., Wanek, J. J., and Andersson, A. F. (2011). Transitions in bacterial communities along the 2000 km salinity gradient of the Baltic sea. *ISME J.* 5, 1571–1579. doi: 10.1038/ismej.2011.41
- Hilton, J. A. (2014). *Ecology and Evolution of Diatom-Associated Cyanobacteria Through Genetic Analyses*. Santa Cruz, CA: University of California.
- Hilton, J. A., Foster, R. A., Tripp, H. J., Carter, B. J., Zehr, J. P., and Villareal, T. A. (2013). Genomic deletions disrupt nitrogen metabolism pathways of a cyanobacterial diatom symbiont. *Nat. Commun.* 4:1767. doi: 10.1038/ncomms2748
- Holl, C. M., and Montoya, J. P. (2005). Interactions between nitrate uptake and nitrogen fixation in continuous cultures of the marine diazotroph, *Trichodesmium* (cyanobacteria). *J. Phycol.* 41, 1178–1183. doi: 10.1111/j.1529-8817.2005.00146.x
- Hunt, B. P., Conroy, B. J., and Foster, R. A. (2016). Contribution and pathways of diazotroph-derived nitrogen to zooplankton during the VAHINE mesocosm experiment in the oligotrophic new caledonia lagoon. *Biogeosciences* 13, 3131–3135. doi: 10.5194/bg-13-3131-2016
- Jürgens, K., and Massana, R. (2008). “Protistan grazing on marine bacterioplankton,” in *Microbial Ecology of the Oceans*, 2nd Edn, ed. J. M. Gasol and D. L. Kirchman (Hoboken, NY: John Wiley & Sons), 383–441. doi: 10.1002/9780470281840.ch11
- Karl, D. M., Church, M. J., Dore, J. E., Letelier, R. M., and Mahaffey, C. (2012). Predictable and efficient carbon sequestration in the north Pacific Ocean supported by symbiotic nitrogen fixation. *Proc. Natl. Acad. Sci.* 109, 1842–1849. doi: 10.1073/pnas.1120312109
- Knapp, A. (2012). The sensitivity of marine N2 fixation to dissolved inorganic nitrogen. *Front. Microbiol.* 3:374. doi: 10.3389/fmicb.2012.00374
- Knapp, A. N., Dekaezemacker, J., Bonnet, S., Sohm, J. A., and Capone, D. G. (2012). Sensitivity of *Trichodesmium erythraeum* and *Crocospaera watsonii* abundance and N2 fixation rates to varying NO₃- and PO₄³⁻ concentrations in batch cultures. *Aquat. Microb. Ecol.* 66, 223–236. doi: 10.3354/ame01577
- Krupke, A., Mohr, W., Laroche, J., Fuchs, B. M., Amann, R. I., and Kuyper, M. M. (2015). The effect of nutrients on carbon and nitrogen fixation by the UCYN-A-haptophyte symbiosis. *ISME J.* 9, 1635–1647. doi: 10.1038/ismej.2014.253
- Landry, M., Kirshtein, J., and Constantinou, J. (1995). A refined dilution technique for measuring the community grazing impact of microzooplankton, with experimental tests in the central equatorial Pacific. *Mar. Ecol. Prog. Ser.* 120, 53–63. doi: 10.3354/meps120053
- Landry, M. R., and Hassett, R. P. (1982). Estimating the grazing impact of marine micro-zooplankton. *Mar. Biol.* 67, 283–288. doi: 10.1007/bf00397668
- Langlois, R. J., Mills, M. M., Ridame, C., Croot, P., and Laroche, J. (2012). Diazotrophic bacteria respond to Saharan dust additions. *Mar. Ecol. Prog. Ser.* 470, 1–14. doi: 10.3354/meps10109
- LaRoche, J., and Breitbarth, E. (2005). Importance of the diazotrophs as a source of new nitrogen in the ocean. *J. Sea Res.* 53, 67–91. doi: 10.1038/ismej.2014.71
- Letelier, R. M., and Karl, D. M. (1996). Role of *Trichodesmium* spp. in the productivity of the subtropical north Pacific Ocean. *Mar. Ecol. Prog. Ser.* 133, 263–273. doi: 10.3354/meps133263
- Luo, Y. W., Doney, S. C., Anderson, L. A., Benavides, M., Berman-Frank, I., Bode, A., et al. (2012). Database of diazotrophs in global ocean: abundance, biomass and nitrogen fixation rates. *Earth Syst. Sci. Data* 4, 47–73. doi: 10.5194/essd-4-47-2012
- Martinez-Perez, C., Mohr, W., Loscher, C. R., Dekaezemacker, J., Littmann, S., Yilmaz, P., et al. (2016). The small unicellular diazotrophic symbiont, UCYN-A, is a key player in the marine nitrogen cycle. *Nat. Microbiol.* 1:16163. doi: 10.1038/nmicrobiol.2016.163
- Meyer, J., Löscher, C., Neulinger, S., Reichel, A., Loginova, A., Borchard, C., et al. (2016). Changing nutrient stoichiometry affects phytoplankton production, DOP accumulation and dinitrogen fixation—a mesocosm experiment in the eastern tropical north Atlantic. *Biogeosciences* 13, 781–794. doi: 10.5194/bg-13-781-2016
- McMurdie, P. J., and Holmes, S. (2013). phyloseq: an R package for reproducible interactive analysis and graphics of microbiome census data. *PloS ONE* 8:e61217. doi: 10.1371/journal.pone.0061217
- Mills, M., Ridame, C., Davey, M., Roche, J. L., and Geider, R. (2004). Iron and phosphorus co-limit nitrogen fixation in the eastern tropical north Atlantic. *Nature* 429, 292–294. doi: 10.1038/nature02550
- Moisander, P. H., Beinart, R. A., Hewson, I., White, A. E., Johnson, K. S., Carlson, C. A., et al. (2010). Unicellular cyanobacterial distributions broaden the oceanic N2 fixation domain. *Science* 327, 1512–1514. doi: 10.1126/science.1185468
- Moisander, P. H., Beinart, R. A., Voss, M., and Zehr, J. P. (2008). Diversity and abundance of diazotrophic microorganisms in the south China sea during intermonsoon. *ISME J.* 2, 954–967. doi: 10.1038/ismej.2008.51
- Moisander, P. H., Benavides, M., Bonnet, S., Berman-Frank, I., White, A. E., and Riemann, L. (2017). Chasing after non-cyanobacterial nitrogen fixation in marine pelagic environments. *Front. Microbiol.* 8:1736. doi: 10.3389/fmicb.2017.01736
- Moisander, P. H., Zhang, R., Boyle, E. A., Hewson, I., Montoya, J. P., and Zehr, J. P. (2011). Analogous nutrient limitations in unicellular diazotrophs and Prochlorococcus in the south Pacific ocean. *ISME J.* 6, 733–744. doi: 10.1038/ismej.2011.152
- Monteiro, F. M., Dutkiewicz, S., and Follows, M. J. (2011). Biogeographical controls on the marine nitrogen fixers. *Global Biogeochem. Cycles* 25:GB003902
- Monteiro, F. M., Follows, M. J., and Dutkiewicz, S. (2010). Distribution of diverse nitrogen fixers in the global ocean. *Global Biogeochem. Cycles* 24:GB3017. doi: 10.1029/2009GB003731
- Montoya, J. P., Holl, C. M., Zehr, J. P., Hansen, A., Villareal, T. A., and Capone, D. G. (2004). High rates of N2 fixation by unicellular diazotrophs in the oligotrophic Pacific ocean. *Nature* 430, 1027–1031.
- Moonsamy, P. V., Williams, T., Bonella, P., Holcomb, C. L., Hoglund, B. N., Hillman, G., et al. (2013). High throughput HLA genotyping using 454 sequencing and the fluidigm access array system for simplified amplicon library preparation. *Tissue Antigens* 81, 141–149. doi: 10.1111/tan.12071
- Moore, C. M., Mills, M. M., Achterberg, E. P., Geider, R. J., Laroche, J., Lucas, M. I., et al. (2009). Large-scale distribution of Atlantic nitrogen fixation controlled by iron availability. *Nat. Geosci.* 2, 867–871. doi: 10.1038/NGEO667
- Moreira-Cuello, V., Mouríño-Carballido, B., Marañón, E., Fernández-Carrera, A., Bode, A., and Varela, M. M. (2017). Biological N2 fixation in the upwelling region off NW iberia: magnitude, relevance, and players. *Front. Mar. Sci.* 4:303. doi: 10.3389/fmars.2017.00303
- Mulholland, M. R., Bernhardt, P. W., Blanco-García, J. L., Mannino, A., Hyde, K., Mondragon, E., et al. (2012). Rates of dinitrogen fixation and the abundance of diazotrophs in north American coastal waters between cape hatteras and georges bank. *Limnol. Oceanogr.* 57, 1067–1083. doi: 10.4319/lo.2012.57.4.1067
- Mulholland, M. R., and Capone, D. G. (1999). Nitrogen fixation, uptake, and metabolism in natural and cultured populations of *Trichodesmium* spp. *Mar. Ecol. Prog. Ser.* 188, 33–49. doi: 10.3354/meps188033
- Norman, J. S., and Friesen, M. L. (2017). Complex N acquisition by soil diazotrophs: how the ability to release exoenzymes affects N fixation by terrestrial free-living diazotrophs. *ISME J.* 11, 315–326. doi: 10.1038/ismej.2016.127
- O’Neil, J. M. (1998). The colonial cyanobacterium *Trichodesmium* as a physical and nutritional substrate for the harpacticoid *Macrosetella gracilis*. *J. Plankton Res.* 20, 43–59. doi: 10.1093/plankt/20.1.43
- O’Neil, J. M., Metzler, P. M., and Gilbert, P. M. (1996). Ingestion of 15N2-labelled *Trichodesmium* spp. and ammonium regeneration by the harpacticoid copepod *Macrosetella gracilis*. *Mar. Biol.* 125, 89–96.

- Pasulka, A. L., Landry, M. R., Taniguchi, D. A., Taylor, A. G., and Church, M. J. (2013). Temporal dynamics of phytoplankton and heterotrophic protists at station ALOHA. *Deep Sea Res. Part II Top. Stud. Oceanogr.* 93, 44–57. doi: 10.1016/j.dsr2.2013.01.007
- Quast, C., Pruesse, E., Yilmaz, P., Gerken, J., Schweer, T., Yarza, P., et al. (2013). The SILVA ribosomal RNA gene database project: improved data processing and web-based tools. *Nucleic Acids Res.* 41, D590–D596. doi: 10.1093/nar/gks1219
- R Development Core Team (2012). *R: A Language and Environment for Statistical Computing. Foundation for Statistical Computing*. Available at: <http://www.r-project.org/>
- Reddy, K., Haskell, J., Sherman, D., and Sherman, L. (1993). Unicellular, aerobic nitrogen-fixing cyanobacteria of the genus *Cyanothecae*. *J. Bacteriol.* 175, 1284–1292. doi: 10.1128/jb.175.5.1284-1292.1993
- Sargent, E. C., Hitchcock, A., Johansson, S. A., Langlois, R., Moore, C. M., Laroche, J., et al. (2016). Evidence for polyploidy in the globally important diazotroph *Trichodesmium*. *FEMS Microbiol. Lett.* doi: 10.1093/femsle/fnw244 [Epub ahead of print].
- Scavotto, R. E., Dziallas, C., Bentzon-Tilia, M., Riemann, L., and Moisander, P. H. (2015). Nitrogen-fixing bacteria associated with copepods in coastal waters of the north Atlantic ocean. *Environ. Microbiol.* 17, 3754–3765. doi: 10.1111/1462-2920.12777
- Schade, J. D., Espeleta, J. F., Klausmeier, C. A., McGroddy, M. E., Thomas, S. A., and Zhang, L. (2005). A conceptual framework for ecosystem stoichiometry: balancing resource supply and demand. *Oikos* 109, 40–51. doi: 10.1111/j.0030-1299.2005.14050.x
- Schmoker, C., Hernández-León, S., and Calbet, A. (2013). Microzooplankton grazing in the oceans: impacts, data variability, knowledge gaps and future directions. *J. Plankton Res.* 35, 691–706. doi: 10.1093/plankt/fbt023
- Shilova, I., Mills, M., Robidart, J., Turk-Kubo, K., Björkman, K., Kolber, Z., et al. (2017). Differential effects of nitrate, ammonium, and urea as N sources for microbial communities in the north Pacific ocean. *Limnol. Oceanogr.* 62, 2550–2574. doi: 10.1002/lno.10590
- Shiozaki, T., Bombar, D., Riemann, L., Hashihama, F., Takeda, S., Yamaguchi, T., et al. (2017). Basin scale variability of active diazotrophs and nitrogen fixation in the north pacific, from the tropics to the subarctic bering Sea. *Global Biogeochem. Cycles* 31, 996–1009. doi: 10.1002/2017GB005681
- Shiozaki, T., Fujiwara, A., Ijichi, M., Harada, N., Nishino, S., Nishi, S., et al. (2018). Diazotroph community structure and the role of nitrogen fixation in the nitrogen cycle in the chukchi sea (western Arctic Ocean). *Limnol. Oceanogr.* doi: 10.1002/lno.10933 [Epub ahead of print].
- Sohm, J. A., Hilton, J. A., Noble, A. E., Zehr, J. P., Saito, M. A., and Webb, E. A. (2011a). Nitrogen fixation in the south Atlantic gyre and the Benguela upwelling system. *Geophys. Res. Lett.* 38:L16608. doi: 10.1029/2011GL048315
- Sohm, J. A., Subramanian, A., Gunderson, T. E., Carpenter, E. J., and Capone, D. G. (2011b). Nitrogen fixation by *Trichodesmium* spp. and unicellular diazotrophs in the north Pacific subtropical gyre. *J. Geophys. Res. Biogeosci.* 116:G03002. doi: 10.1029/2010JG001513
- Sommer, U. (1984). The Paradox of the plankton - fluctuations of phosphorus availability maintain diversity of phytoplankton in flow-through cultures. *Limnol. Oceanogr.* 29, 633–636. doi: 10.4319/lo.1984.29.3.0633
- Sunagawa, S., Coelho, L. P., Chaffron, S., Kultima, J. R., Labadie, K., Salazar, G., et al. (2015). Structure and function of the global ocean microbiome. *Science* 348:1261359. doi: 10.1126/science.1261359
- Taniuchi, Y., Chen, Y. -L. L., Chen, H. -Y., Tsai, M. -L., and Ohki, K. (2012). Isolation and characterization of the unicellular diazotrophic cyanobacterium Group C TW3 from the tropical western Pacific ocean. *Environ. Microbiol.* 14, 641–654. doi: 10.1111/j.1462-2920.2011.02606.x
- Thompson, A., Carter, B. J., Turk-Kubo, K., Malfatti, F., Azam, F., and Zehr, J. P. (2014). Genetic diversity of the unicellular nitrogen-fixing cyanobacteria UCYN-A and its prymnesiophyte host. *Environ. Microbiol.* 16, 3238–3249. doi: 10.1111/1462-2920.12490
- Thompson, A. W., Foster, R. A., Krupke, A., Carter, B. J., Musat, N., Vaulot, D., et al. (2012). Unicellular cyanobacterium symbiotic with a single-celled eukaryotic alga. *Science* 337, 1546–1550.
- Tripp, H. J., Bench, S. R., Turk, K. A., Foster, R. A., Desany, B. A., Niazi, F., et al. (2010). Metabolic streamlining in an open-ocean nitrogen-fixing cyanobacterium. *Nature* 464, 90–94. doi: 10.1038/nature08786
- Turk-Kubo, K. A., Achilles, K. M., Serros, T. R., Ochiai, M., Montoya, J. P., and Zehr, J. P. (2012). Nitrogenase (*nifH*) gene expression in diazotrophic cyanobacteria in the tropical north Atlantic in response to nutrient amendments. *Front. Microbiol.* 3:386. doi: 10.3389/fmicb.2012.00386
- Turk-Kubo, K. A., Farnelid, H. M., Shilova, I. N., Henke, B., and Zehr, J. P. (2017). Distinct ecological niches of marine symbiotic N₂-fixing cyanobacterium *candidatus atelocyanobacterium thalassa* sublineages. *J. Phycol.* 53, 451–461. doi: 10.1111/jpy.12505
- Turk-Kubo, K. A., Frank, I. E., Hogan, M. E., Desnues, A., Bonnet, S., and Zehr, J. P. (2015). Diazotroph community succession during the VAHINE mesocosm experiment (New Caledonia lagoon). *Biogeosciences* 12, 7435–7452. doi: 10.5194/bg-12-7435-2015
- Turk-Kubo, K. A., Karamchandani, M., Capone, D. G., and Zehr, J. P. (2014). The paradox of marine heterotrophic nitrogen fixation: abundances of heterotrophic diazotrophs do not account for nitrogen fixation rates in the eastern tropical south Pacific. *Environ. Microbiol.* 16, 3095–3114. doi: 10.1111/1462-2920.12346
- Villareal, T. A. (1989). *Ecology of Oceanic Diatoms: Investigations of Symbioses, Suspension and Growth Dynamics of Selected Rhizosolenia Species*. Kingston, RI: University of Rhode Island.
- Villareal, T. A. (1990). Laboratory culture and preliminary characterization of the nitrogen-fixing Rhizosolenia-Richelia symbiosis. *Mar. Ecol.* 11, 117–132. doi: 10.1111/j.1439-0485.1990.tb00233.x
- Villareal, T. A. (1992). “Marine nitrogen-fixing diatom – cyanobacteria symbioses,” in *Marine Pelagic Cyanobacteria: Trichodesmium and other Diazotrophs*, eds E. J. Carpenter, D. G. Capone and J. G. Rueter (Dordrecht: Kluwer Academic Publishers), 163–175.
- Vu, T. T., Stolyar, S. M., Pinchuk, G. E., Hill, E. A., Kucek, L. A., Brown, R. N., et al. (2012). Genome-scale modeling of light-driven reductant partitioning and carbon fluxes in diazotrophic unicellular cyanobacterium *Cyanothecae* sp. ATCC 51142. *PLoS Comput. Biol.* 8:e1002460. doi: 10.1371/journal.pcbi.1002460
- Ward, B. A., Dutkiewicz, S., Moore, C. M., and Follows, M. J. (2013). Iron, phosphorus, and nitrogen supply ratios define the biogeography of nitrogen fixation. *Limnol. Oceanogr.* 58, 2059–2075. doi: 10.4319/lo.2013.58.6.2059
- Welschmeyer, N. A. (1994). Fluorometric analysis of chlorophyll a in the presence of chlorophyll b and phaeopigments. *Limnol. Oceanogr.* 39, 1985–1992. doi: 10.4319/lo.1994.39.8.1985
- Wilson, S. T., Aylward, F. O., Ribalet, F., Barone, B., Casey, J. R., Connell, P. E., et al. (2017). Coordinated regulation of growth, activity and transcription in natural populations of the unicellular nitrogen-fixing cyanobacterium *Crocospaera*. *Nat. Microbiol.* 2:17118. doi: 10.1038/nmicrobiol.2017.118
- Zehr, J. P., and Bombar, D. (2015). “Marine nitrogen fixation: organisms, significance, enigmas, and future directions,” in *Biological Nitrogen Fixation*, ed. F. J. de Bruijn (Santa Cruz, CA: University of California), 855–872. doi: 10.1002/9781119053095.ch84
- Zehr, J. P., Montoya, J. P., Jenkins, B. D., Hewson, I., Mondragon, E., Short, C. M., et al. (2007). Experiments linking nitrogenase gene expression to nitrogen fixation in the North Pacific subtropical gyre. *Limnol. Oceanogr.* 52, 169–183. doi: 10.4319/lo.2007.52.1.01069
- Zhang, J., Kobert, K., Flouri, T., and Stamatakis, A. (2014). PEAR: a fast and accurate illumina paired-end reAd mergeR. *Bioinformatics* 30, 614–620. doi: 10.1093/bioinformatics/btt593.
- Conflict of Interest Statement:** The authors declare that the research was conducted in the absence of any commercial or financial relationships that could be construed as a potential conflict of interest.
- The handling Editor declared a past co-authorship with one of the authors KT-K.
- Copyright © 2018 Turk-Kubo, Connell, Caron, Hogan, Farnelid and Zehr. This is an open-access article distributed under the terms of the Creative Commons Attribution License (CC BY). The use, distribution or reproduction in other forums is permitted, provided the original author(s) and the copyright owner(s) are credited and that the original publication in this journal is cited, in accordance with accepted academic practice. No use, distribution or reproduction is permitted which does not comply with these terms.



Dynamics of *Prochlorococcus* and *Synechococcus* at Station ALOHA Revealed through Flow Cytometry and High-Resolution Vertical Sampling

Ger J. van den Engh^{1,2*}, Joseph K. Doggett², Anne W. Thompson³, Martina A. Doblin⁴, Carla N. G. Gimpel² and David M. Karl²

¹ Center for Marine Cytometry, Concrete, WA, United States, ² Daniel K. Inouye Center for Microbial Oceanography: Research and Education, University of Hawai'i at Manoa, Honolulu, HI, United States, ³ Department of Biology, Portland State University, Portland, OR, United States, ⁴ Climate Change Cluster, University of Technology, Sydney, NSW, Australia

OPEN ACCESS

Edited by:

Matthew J. Church,
University of Montana, United States

Reviewed by:

Luke Thompson,
Southwest Fisheries Science Center
(NOAA), United States

Rui Zhang,
Xiamen University, China

*Correspondence:

Ger J. van den Engh
ger.engh@me.com

Specialty section:

This article was submitted to
Aquatic Microbiology,
a section of the journal
Frontiers in Marine Science

Received: 07 July 2017

Accepted: 25 October 2017

Published: 27 November 2017

Citation:

van den Engh GJ, Doggett JK,
Thompson AW, Doblin MA,
Gimpel CNG and Karl DM (2017)
*Dynamics of Prochlorococcus and
Synechococcus at Station ALOHA
Revealed through Flow Cytometry and
High-Resolution Vertical Sampling.*
Front. Mar. Sci. 4:359.
doi: 10.3389/fmars.2017.00359

The fluorescence and scattering properties of *Prochlorococcus* and *Synechococcus* at Station ALOHA as measured by flow cytometry (termed the FCM phenotype) vary with depth and over a variety of time scales. The variation in FCM phenotypes may reflect population selection or physiological acclimation to local conditions. Observations before, during, and after a storm with deep water mixing show a short-term homogenization of the FCM phenotypes with depth, followed by a return to the stable pattern over the time span of a few days. These dynamics indicate that, within the upper mixed-layer, the FCM phenotype distribution represents acclimation to ambient light. The populations in the pycnocline (around 100 m and below), remain stable and are invariant with light conditions. In samples where both cyanobacteria coexist, fluorescence properties of *Prochlorococcus* and *Synechococcus* are tightly correlated providing further evidence that FCM phenotype variability is caused by a common environmental factor or factors. Measurements of the dynamics of FCM phenotypes provide insights into phytoplankton physiology and adaptation. Alternatively, FCM phenotype census of a water mass may provide information about its origin and illumination history.

Keywords: flow cytometry, *Prochlorococcus*, *Synechococcus*, Station ALOHA, thermocline, population dynamics, light acclimation

INTRODUCTION

Prochlorococcus is the numerically dominant photosynthetic organism in the warm oligotrophic waters of the North Pacific Subtropical Gyre (NPSG; Campbell and Vault, 1993). In surface waters, *Prochlorococcus* cells make up more than 98% of the chlorophyll-containing particles that are detected by flow cytometry (FCM). At a relative abundance of about 1%, *Synechococcus* is a distant second. Larger cells, mostly pigmented picoeukaryotes (1–3 μ m), make up the remainder of the chlorophyll-containing particles that are counted by a flow cytometer. If phytoplankton groups are ranked by their contribution to total chlorophyll fluorescence, the balance shifts toward the larger organisms. Even then, despite its diminutive size, *Prochlorococcus* accounts for more than half

of the chlorophyll present in the upper 200 m of the subtropical and tropical North Pacific Ocean (Campbell et al., 1994; Partensky et al., 1999). Because of their abundance, *Prochlorococcus* and *Synechococcus* represent a significant compartment of autotrophic biomass and carbon fixation in the NPSG.

The niche spaces of *Prochlorococcus* and *Synechococcus* straddle two distinct physical environments (Karl and Church, 2014). A warm surface layer with relatively homogeneous physical properties that are maintained by turbulence, floats on a stratified column, the pycnocline, which is stabilized by a density gradient that is the net result of opposite gradients in temperature and salinity. The upper, mixed-layer is relatively depleted in inorganic nitrogen (<10 nM) and other nutrients (Karl et al., 2001). The top of the pycnocline starts around a depth of 100 m (\pm 30 m) where the photosynthetically available radiation (PAR) is reduced to about 2% of the surface irradiance. With strong winds or surface cooling, the mixed-layer may extend well into the pycnocline, especially in winter, causing a sharp transition between the mixed and the stratified environments. In calm weather, an intermediate transition zone with a slight temperature gradient may form between the surface mixed-layer and the top of the permanent pycnocline.

FCM provides an accurate, quantitative description of the individuals that make up a phytoplankton community (Trask et al., 1982). The term FCM phenotype will be used for the aggregate of optical properties that characterizes a particle by flow cytometry. The *Prochlorococcus* and *Synechococcus* cells that are found across the two environments exhibit a wide range of FCM phenotypes, covering an almost 2-decade range in signal intensities (Vaulot et al., 1995). Broadly, chlorophyll fluorescence, and to a lesser extent forward light scatter (an approximate proxy for cell size), increase with depth. There are two explanations for the gradient in phenotypes. The increase in chlorophyll content may represent photo-acclimation: the organisms adjust their chlorophyll content, size, and shape to compensate for the changes in irradiance with increasing depth (Vaulot et al., 1995; Bricaud et al., 1999; Moore and Chisholm, 1999; Partensky et al., 1999; Mann and Chisholm, 2000). More often, the observed phenotypic variation is attributed to heterogeneity in genotype. *Prochlorococcus* has two main ecotypes (Partensky et al., 1999; West and Scanlan, 1999; Rocap et al., 2003; Bouman et al., 2006; Kettler et al., 2007; Zwirglmaier et al., 2008; Martiny et al., 2009) with at least 12 genomic clades (Biller et al., 2014), each with hundreds of subpopulations (Kashtan et al., 2014). Laboratory studies show that representatives of the two main ecotypes differ in light requirements for growth and consequently have been termed high-light (HL) and low-light (LL) adapted ecotypes (Moore and Chisholm, 1999). From the genomics perspective, a light gradient could cause a gradient of eco-genotypes each with a characteristic phenotype that can be distinguished with flow cytometry (Rocap et al., 2003; Zwirglmaier et al., 2008). Many reports indeed show *Prochlorococcus* genotype segregation with depth in the water column (Malmstrom et al., 2010). Genotype stratification could be the cause of gradients in FCM phenotype. Thus, there are two distinct, not necessarily mutually exclusive, mechanisms that may contribute to the

FCM phenotype gradients of *Prochlorococcus* and *Synechococcus* observed at Station ALOHA: the local environment selects for best-fit genotypes, each with a different, distinct phenotype, or phenotype transcends the genotype and the heterogeneous cells, through a process of physiological acclimation, assume a similar shape and pigment expression to better match the requirements of ambient conditions. The relative contributions of these two mechanisms in wild type populations need to be clarified.

To complicate matters, the distribution patterns of *Prochlorococcus* are usually described in relation to sampling depth. Depth does not represent a reliable descriptor of the local environment. The stratified layers at Station ALOHA are subject to considerable vertical movements. Tidal and inertial forces and passing weather fronts transmit large amounts of energy along the mixed layer-pycnocline interface. This energy dissipates through subsurface waves that temporarily heave the pycnocline toward the surface and cause high-velocity shearing of adjacent density layers (Mann and Lazier, 1991; Knauss, 1996; Stewart, 2008). Consequently, the inhabitants of different water layers are not permanently fixed to one depth or isolume, but swing up and down, often 50 m or more, as a result of passing internal waves. During this process cells experience large changes in light exposure over unpredictable and often relatively short time periods (Karl et al., 2002). When considering the interplay of phenotype, genotype, acclimation, niche selection and light conditions, the dynamics of water masses must be taken into account.

The fluorescence and scatter traits of FCM phenotypes are associated with local light intensity and other environmental conditions. Analysis of FCM phenotypes in the context of a dynamic environment may reveal aspects of acclimation physiology and genome selection that shape phytoplankton communities. Such studies may also be helpful in following the movement of water masses or the dynamics of mesoscale features such as eddies. Acclimation and ecotype selection of phytoplankton populations must take place at characteristic time scales. Knowledge of the time constants at which phenotype adjustment occurs may be used to reconstruct the illumination history of a water mass. Dusenberry (1995) and Dusenberry et al. (1999) supplied evidence that acclimation-dependent phenotype differences can be used as biological markers for the dynamics of the water column. Bidigare et al. (2014) proposed an analogous approach in which ratios of specific pigments from the water column can be used to estimate mixing rates within the upper euphotic zone. Here we attempt to identify water mass characteristics by describing its individual plankton constituents through their FCM phenotypes.

During the period of 2010–2015, we acquired a large number of high-resolution depth profiles of FCM phenotypes of *Prochlorococcus* and *Synechococcus* at Station ALOHA. Under the prevailing light weather conditions, depth profiles collected throughout the year, show a characteristic gradient of FCM phenotypes. In 2014 and 2015 we observed deep mixing events that rearranged the FCM phenotype patterns. These disturbances and the subsequent return to the steady-state, confirm the notion that acclimation, whether through physiological response or genetic ecotype segregation, plays a major role in FCM phenotype

distribution patterns. The results demonstrate that fine-scale sampling, in both space and time, provides valuable information identifying environmental factors that control phytoplankton abundance, biology, and ecology, and that high-resolution FCM depth profiles contain information about the circulation history of the water mass in which the phytoplankton resides.

METHODS AND MATERIALS

Sample Collection

Samples were obtained during several expeditions to Station ALOHA (6 nautical mile radius around 22° 45' N, 158° 00' W, Karl and Lukas, 1996) conducted on September 30–October 4, 2013 (HOT255), March 11–25, 2014 (KM1409), and December 15–19, 2014 (HOT268) using a 24-bottle CTD rosette. Water from the CTD was collected in 15 mL polypropylene tubes after three rinses with sample water. In our experience, the finer details of the pico-phytoplankton FCM phenotype rapidly degrade with established fixation and storage procedures. To avoid loss of resolution due to fixation and freezing, samples were stored in the dark without treatment at room temperature until analysis as soon as possible but no longer than 2 h after collection.

Environmental Data

The CTD rosette sensors captured *in situ* temperature (T), conductivity (salinity), dissolved oxygen (DO) concentration, and fluorescence for each cast. DO concentrations were calibrated with discrete water samples collected for Winkler titration and fluorescence data were calibrated with samples collected for total chlorophyll determinations. Density (sigma theta) was calculated from (potential) temperature and salinity. Mixed-layer depth (MLD) was calculated using three independent methods (MLD1–3). MLD1 and MLD3 were set at the depth where the density anomaly (density – 1.000 × 10³) was 0.125 greater than at 1 decibar (db) or more than 0.03 greater than at 10 db, respectively. MLD2 was set at the depth where temperature was 0.05 degrees C offset from that at 1 db. Wind speed data at Station ALOHA were obtained from the Woods Hole Oceanographic Institution Hawai'i Ocean Time-series Station (WHOTS) buoy for the period of interest (<http://www.soest.hawaii.edu/whots/>).

Flow Cytometry Configurations

Flow cytometry analysis was performed at sea in a purpose-built laboratory van mounted on the ship's deck. An inFlux cell sorter (Cytopeia, 2005, presently manufactured by Becton Dickinson, USA) fit with a low-glow, black ceramic nozzle tip, with 457 nm and 488 nm lasers, and a small-particle forward scatter detector (FSC), was used for marine particle analysis (Petersen et al., 2012). Forward and side scatter signals (FSC and SSC) were collected from the 488 nm illumination beam. Red fluorescence (692/40 nm bandpass filter) and orange fluorescence (572/27 nm bandpass filter) were collected for both the 457 nm and the 488 nm excitation lasers. Data collection of all parameters was triggered by the 488 nm scatter signal. The trigger threshold was set well below the lowest scatter signals from surface *Prochlorococcus* cells. Spurious scatter events and

scatter-to-fluorescence cross-talk were minimized by setting the polarization of the excitation laser perpendicular to the axis of flow. At these settings, measurements of sheath fluid alone registered fewer than 10 events s⁻¹. If higher background counts were detected, the instrument was thoroughly cleaned with 5% bleach or Contrad 90 detergent (Decon Laboratories, UK) and rinsed until the background counts fell below 10 events s⁻¹.

Sheath fluid was prepared from concentrated BioSure 8X sheath fluid (BioSure, Grass Valley, CA) diluted to 1X concentration with DI water produced from the ship's reverse osmosis system and filtered through a 0.2 μm pore size Sterivex filter (Millipore, Billerica, MA). Flow rate was monitored with a Sensirion liquid flow meter (Sensirion, Switzerland) placed in the sample line. Samples were run at a differential pressure that yielded a flow rate of ~20 μl min⁻¹.

Scatter and fluorescence signals were collected with user-built detector assemblies with an extended range. The detectors cover a signal range of more than 6 decades by combining the signals from two photomultipliers that operate at different gains. The relative gain settings (~100x) are calibrated by a regression analysis of the events that fall within the linear window of both detectors. After analog-to-digital conversion, the list-mode data from two detectors are combined into one plot with custom software. This approach allows simultaneous detection and display of all phytoplankton sizes ranging from dim surface dwelling *Prochlorococcus* to bright picoeukaryotes.

Optical alignments of lasers, lenses, and stream were conducted as follows for optimal and consistent flow cytometry while minimizing the effects of the movements of a ship at sea. After loading and pressurizing the sheath fluid, beer (Heineken, Amsterdam, The Netherlands¹) was sampled for the first step of alignment. Beer fluoresces when excited by 488 nm and 457 nm lasers, is biocompatible, and has good batch-to-batch reproducibility. For these reasons it is the reagent of choice for imaging the sample stream within the sheath jet. One-mL aliquots of calibration beer may be stored at -20°C. The fluorescence of the beer sample stream, when illuminated by the laser, allows quick and optimal alignment of the spatial pinhole filter in the inFlux optical system and sample stream. Low sample flow rates (less than 1 psi difference between sample and sheath pressure) were maintained to restrict the width of the sample stream (and therefore the path of the enclosed particles) within the focal depth of the inFlux collection optics. Ultra-rainbow beads (1 μm diameter, Spherotech, USA) were used for the next stage of cytometer alignment. If needed, further adjustments to the stream, lasers, and/or small particle detectors were carried out by monitoring pulse amplitude, shape and position within the image-plane pinholes on an oscilloscope.

For relative fluorescence estimates, samples were spiked with a dilute stock of 1 μm ultra-rainbow beads. Optical alignment was confirmed and, if needed, adjusted at 30 min intervals during sampling. However, if the alignment procedures described were

¹Full disclosure: one of the authors (GvdE) hails from Amsterdam. His Dutch roots may have played a role in the selection of Heineken brand beer. In our experience, all lager labels, irrespective of gustatory qualities, are equally suitable for the calibration and alignment of flow cytometry equipment.

carried out correctly, even energetic movement of the ship did not disturb laser and stream alignments. Samples were analyzed in random order to prevent data bias due to any changes in alignment and sensitivity during data collection from an entire water column profile. Data from 100 μl of seawater were collected for each sample.

Flow cytometry data were collected in list-mode with "Spigot" software (created by Juno Cho and Barclay Purcell, no longer available through Becton-Dickinson). Stored FCM files were plotted and analyzed with custom programs written in Python. Counts of *Prochlorococcus* and *Synechococcus* populations were determined by gates drawn in bivariate distributions of 457 nm and 488 nm excited chlorophyll fluorescence.

Calculation of Light Exposure of a Particle Circulation between the Surface and a Depth of 100 m

To estimate the light exposure of cells circulating in the mixed-layer (top 100 m), we used the Beer-Lambert law where light intensity (I) decreases exponentially with depth (x):

$$I(x) = I_0 e^{-\alpha x} = I_0 e^{-\frac{x}{A}}$$

The average extinction coefficient (α) at Station ALOHA has been empirically determined to be:

$$\alpha = 0.04 \quad (\text{Letelier et al., 2004})$$

For integration we introduce a standard depth, A , where the light intensity is $1/e$ of the surface intensity:

$$A = 1/\alpha = 25 \text{ m}$$

Thus, the integrated light exposure of a particle traveling at a uniform velocity from the surface to a depth of 100 m ($4A$) is:

$$\int_0^{4A} e^{-x/A} dx = -Ae^{-x/A} \Big|_0^{4A} = -Ae^{-4} + A = A(1 - e^{-4})$$

The average light intensity factor per depth unit is

$$\frac{A(1 - e^{-4})}{4A} = \frac{(1 - e^{-4})}{4} = 0.2454$$

which is equivalent to permanent residence at a depth of ~ 35 m.

RESULTS

The Phytoplankton Profile at Station ALOHA

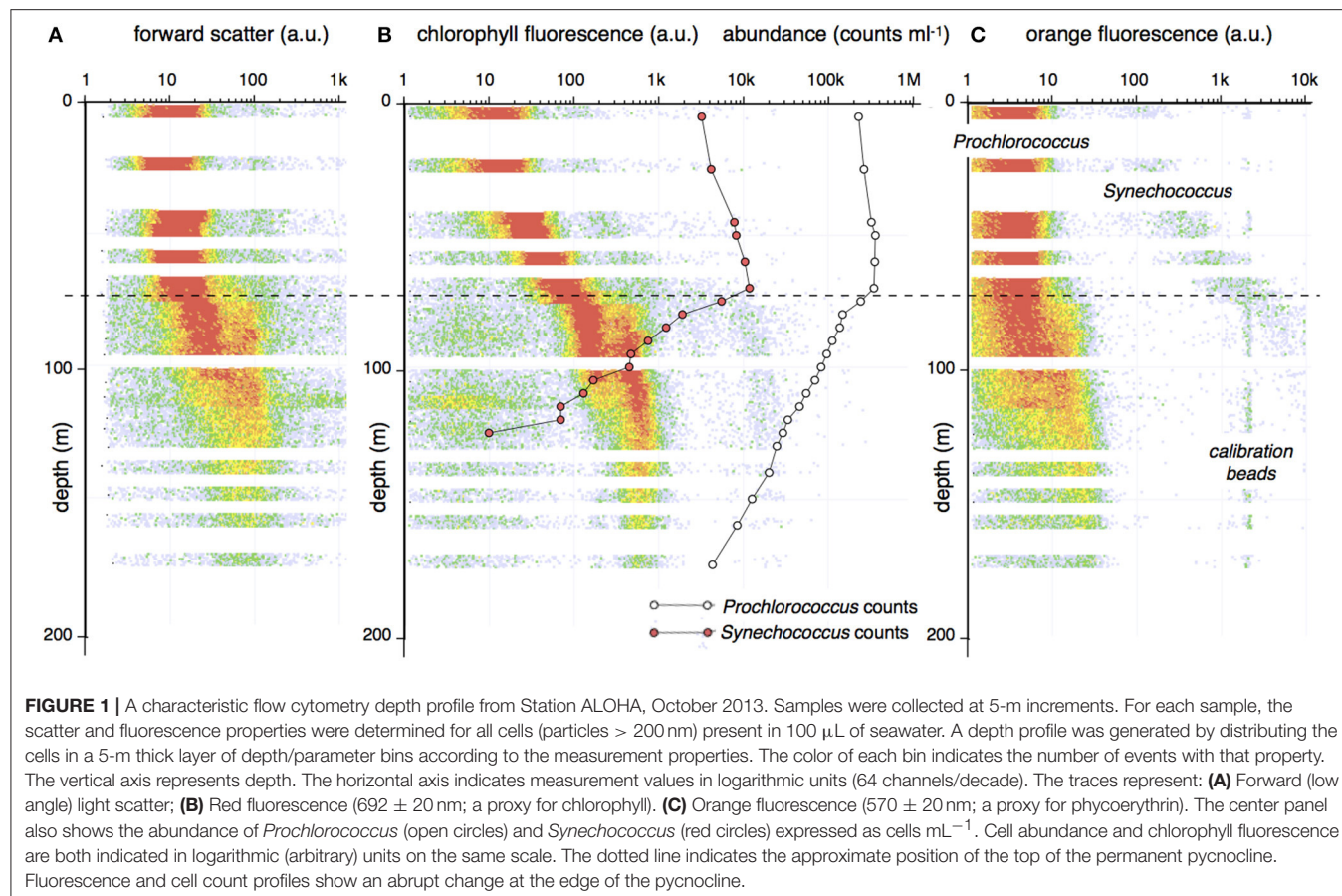
Flow cytometry provides a quantitative description of the cell distribution and optical properties of microbial communities (Trask et al., 1982). **Figure 1** illustrates the FCM phenotypes of the plankton community at Station ALOHA. A forward scatter detector registers all particles greater than 200 nm (**Figure 1A**). Less than half of the scattering particles naturally contain fluorescent molecules (e.g., chlorophyll, phycoerythrin) and therefore also register on one or more of the fluorescence detectors. These representative profiles for samples taken at 5-m

depth intervals were obtained during a period of calm weather in October 2013 (HOT255).

The cell counts, light scattering, and fluorescence properties of *Prochlorococcus* and *Synechococcus* vary with depth. The distribution pattern has two distinct phases (**Figure 1B**). In the upper mixed layer (~ 80 m shown as a dashed line in **Figure 1**), the chlorophyll fluorescence shows a gradual, monotonic increase with depth while *Synechococcus* and *Prochlorococcus* counts increase by about 2-fold. At a depth of 80 m, there is a transition in the abundance and in the optical properties of both cell types. Beyond this depth, the population counts decline exponentially, while the chlorophyll fluorescence assumes a bimodal distribution. The position of the two modes remains relatively constant down to 175 m. Below 80 m, a dim but distinct orange fluorescence signal becomes apparent (**Figure 1C**) and the scatter signals of *Prochlorococcus*, both forward and perpendicular scatter (latter not shown), increase by an order of magnitude. Between a depth of 80 and 115 m, *Prochlorococcus* presents as two groups with distinct scatter and chlorophyll fluorescence properties (**Figure 2**). These observed distribution patterns are consistent with previous reports (Campbell et al., 1994; Binder et al., 1996; Partensky et al., 1999; Malmstrom et al., 2013).

Changes in Phytoplankton Profiles during a Wind-Driven Mixing Event

Daily high-resolution profiles collected over a period of 2 weeks in March 2014, during which there was a deep mixing event, provide insights into the dynamics of *Prochlorococcus* and *Synechococcus* populations at Station ALOHA. CTD casts performed at regular intervals before and after the wind-driven mixing event, document the rearrangement of the water column and the associated changes in the phytoplankton assemblage (**Figure 3**). After a period of relatively low wind-speeds ending near day 4, the average wind speed increased over a period of a few hours, then gradually decreased over several days (**Figure 3**). Before the mixing event, the surface zone of uniform temperature and salinity was relatively shallow ranging from 10 to 50 m. A temperature gradient between the homogeneous surface and the start of the stratified pycnocline (~ 100 m) supported an intermediate zone of higher salinity (**Figures 4, 6A**). Before the mixing event, surface temperatures were greater than 24°C . After the mixing event the surface temperatures dropped below 24°C and temperature and salinity became uniform throughout the mixed-layer (**Figures 4, 6B**). An abrupt inflection point in the temperature profile marked the bottom of the mixed-layer and the top of the permanently stratified thermocline/pycnocline interface. At samplings taken only a few hours apart, the depth of this temperature inflection point varied by as much as 50 m indicating the presence of subsurface waves at the mixed-layer/pycnocline interface. These large changes in the physical properties of the water column provide an excellent context in which to explore the dynamics of *Prochlorococcus* and *Synechococcus* abundances and the distribution of their phenotypes.



Dynamics of *Prochlorococcus* and *Synechococcus* Abundance before and after Deep Mixing

Over the 15 casts before, during, and after the deep mixing event, the cell count profiles of *Prochlorococcus* and *Synechococcus* were qualitatively similar, displaying a pattern with two distinct phases (Figure 4A). Throughout the mixed-layer, *Prochlorococcus* and *Synechococcus* counts were relatively constant varying less than a factor of two within each cast with only a few points marginally outside of this range. In contrast, below the mixed-layer, within the thermocline, *Prochlorococcus* and *Synechococcus* declined exponentially with depth (Figure 4B). *Synechococcus* declined at a rate of $0.07\text{--}0.09 \text{ m}^{-1}$ and *Prochlorococcus* declined at 0.05 m^{-1} . The rate of decline in cell count remained constant until the populations fell below the limit of detection (fewer than 10 cells per $100 \mu\text{L}$ seawater). Over the 2-week time course, the start of the exponential decline in *Prochlorococcus* and *Synechococcus* numbers oscillated between a depth of 60–120 m, with the greatest variability in the onset of exponential decline in the period after the mixing event. Throughout these oscillations, the depth of onset of the exponential decline remained correlated with the depth of the thermocline (Figure 5).

Though the overall shapes of the profiles were similar, total abundances of *Prochlorococcus* and *Synechococcus* in the surface

mixed-layer were lower immediately after the mixing event in March 2014 (Figure 4B). Throughout the surface layer, the concentrations of *Prochlorococcus* ranged between 1 and $3 \times 10^5 \text{ mL}^{-1}$. Out of ~ 250 samples from the mixed zone, which were taken during both calm weather and gale force winds with deep water mixing, only a few points fell outside of a 2-fold range (Figure 4B). *Synechococcus* abundances showed a larger variation. The mean pre- and post-wind event values differ by about a factor of 3. Again, for individual traces, only a few points fell outside a 2-fold range (Figure 4B).

Patterns and Dynamics of *Prochlorococcus* FCM Phenotypes after a Deep Mixing Event

The *Prochlorococcus* FCM phenotype over the depth range sampled, varied with changing environmental features. Before the wind event (Figure 6A), when the water column had a shallow mixed-layer transitioning via a temporary temperature gradient into the permanent pycnocline, *Prochlorococcus* optical characteristics followed the general pattern as shown in Figure 1. Chlorophyll fluorescence of cells steadily increased by nearly two orders of magnitude with depth well into the thermocline. At the point where *Prochlorococcus* abundance began to decline, forward scatter increased (not shown),

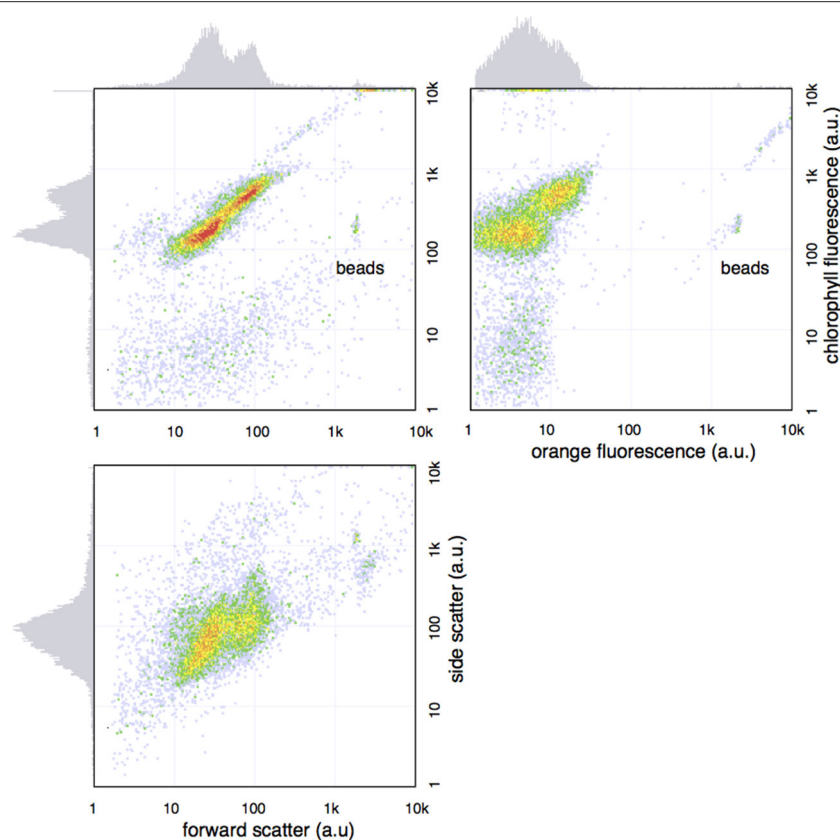


FIGURE 2 | Bimodal distribution of *Prochlorococcus* seen in the sample from 90 m in the cast of **Figure 1**. The bivariate plot show two populations with distinct FCM phenotype, as seen by light scatter and fluorescence profiles on the x- and y-axes.

and cells started to exhibit a dim orange fluorescence, with chlorophyll fluorescence remaining relatively constant with depth (**Figure 6A**). As in **Figure 1**, the gradual changes in chlorophyll fluorescence matched the transition into the pycnocline.

While the mixing event was ongoing (**Figure 6B**), a sharp mixed-layer boundary at 100 m depth, was observed with a corresponding change in the *Prochlorococcus* phenotype and abundance with depth. In contrast to a well-stratified water column where red fluorescence increased gradually with depth (**Figure 6A**), chlorophyll fluorescence was constant throughout the depth of the mixed-layer before beginning a substantial increase within the thermocline (**Figure 6B**). In contrast to the gradual changes in the stratified column, the increase in forward scatter, red fluorescence, orange fluorescence and the exponential decay in population counts is now restricted to the pycnocline below the mixed surface 100 m.

As the winds subsided, the homogeneous chlorophyll fluorescence in the top 100 m gradually re-established its depth-related gradient where cell fluorescence increases instep with light attenuation (**Figures 7, 8**). For the next 4 days, the passing of internal waves, as evident from large amplitude oscillations

in the mixed-layer/pycnocline interface (**Figure 3**) and the discontinuities in the temperature and salinity profiles, was also reflected in *Prochlorococcus* abundance patterns. During the large swings in the position of the mixed-layer/pycnocline interface, the inflection point in the *Prochlorococcus* cell count remained correlated with the top of the pycnocline (**Figure 5**).

Several post-storm profiles had discontinuous anomalies in the *Prochlorococcus* and *Synechococcus* profiles that were most clearly observed in the chlorophyll fluorescence traces. In these profiles a pattern normally seen at a shallower depth appears to be repeated in a deep zone (**Figures 7, 8**). Such repeats or inversion anomalies were always accompanied by large discontinuities in the salinity profile (**Figure 7**) as well as breaks in the temperature profile, indicating a vertical water column structure that had not yet returned to the calm-weather equilibrium state. When such repeats in population characteristics happened, all features of the deep layer—abundance of *Prochlorococcus* and *Synechococcus*, scatter, orange/red fluorescence—recapitulated the properties of a population closer to the surface. A week after the storm, the characteristics of the *Prochlorococcus* and *Synechococcus* populations re-established the characteristic pattern of the pre-mixing-event distributions, although some evidence of salinity anomalies was still present. The final trace again showed a double

population at the mixed-zone/permanent pycnocline interface (**Figure 8**).

An Example of a Very Deep Mixing Event

Further evidence that *Prochlorococcus* and *Synechococcus* properties are constant throughout a well-mixed layer but vary

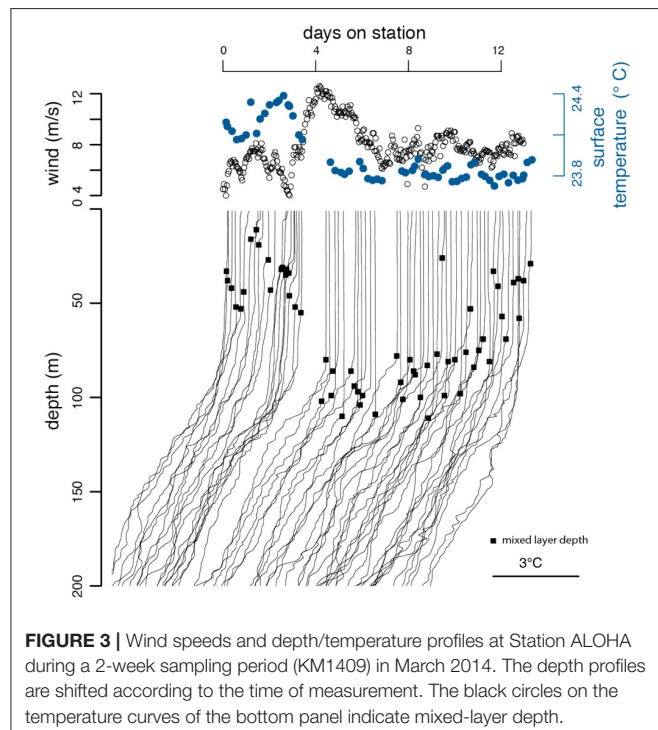


FIGURE 3 | Wind speeds and depth/temperature profiles at Station ALOHA during a 2-week sampling period (KM1409) in March 2014. The depth profiles are shifted according to the time of measurement. The black circles on the temperature curves of the bottom panel indicate mixed-layer depth.

with depth under stratified conditions were obtained on HOT cruise 268 in December 2014 (**Figure 9**). Four profiles were taken following a deep mixing event that descended into the previously established pycnocline, as evidenced by the temperature profile. This short time-series provides no evidence of a transition between the surface and the deep *Prochlorococcus* populations. Abundance (between 50 and 150×10^3 cell mL $^{-1}$) and FCM phenotype of *Prochlorococcus* in the mixed layer were relatively constant. Below the transition into the pycnocline the optical properties were abruptly different, exhibiting the high forward scatter, chlorophyll fluorescence, and orange fluorescence signals that are typical for the deep water population. As in the other profiles, the *Prochlorococcus* population counts decreased exponentially with sample depth.

DISCUSSION

Cyanobacteria in the Intermittent Thermocline: The Top 100 m

The dynamics of *Prochlorococcus* and *Synechococcus* populations at Station ALOHA, before, during, and after a wind-driven mixing event, indicate that the gradient of phenotypes that is observed using flow cytometry (**Figures 1, 6A**) represents acclimation to local light conditions.

Under prolonged conditions of stable, calm weather the chlorophyll fluorescence pattern inversely matches the attenuation of light with depth over a range of nearly 2 decades. For example, the two ridges in the chlorophyll fluorescence profile of **Figure 1** (the ridge near the surface and the one around 100 m) differ by a factor of 50. The reported extinction coefficient at Station ALOHA is 0.04 (Letelier et al., 2004) which

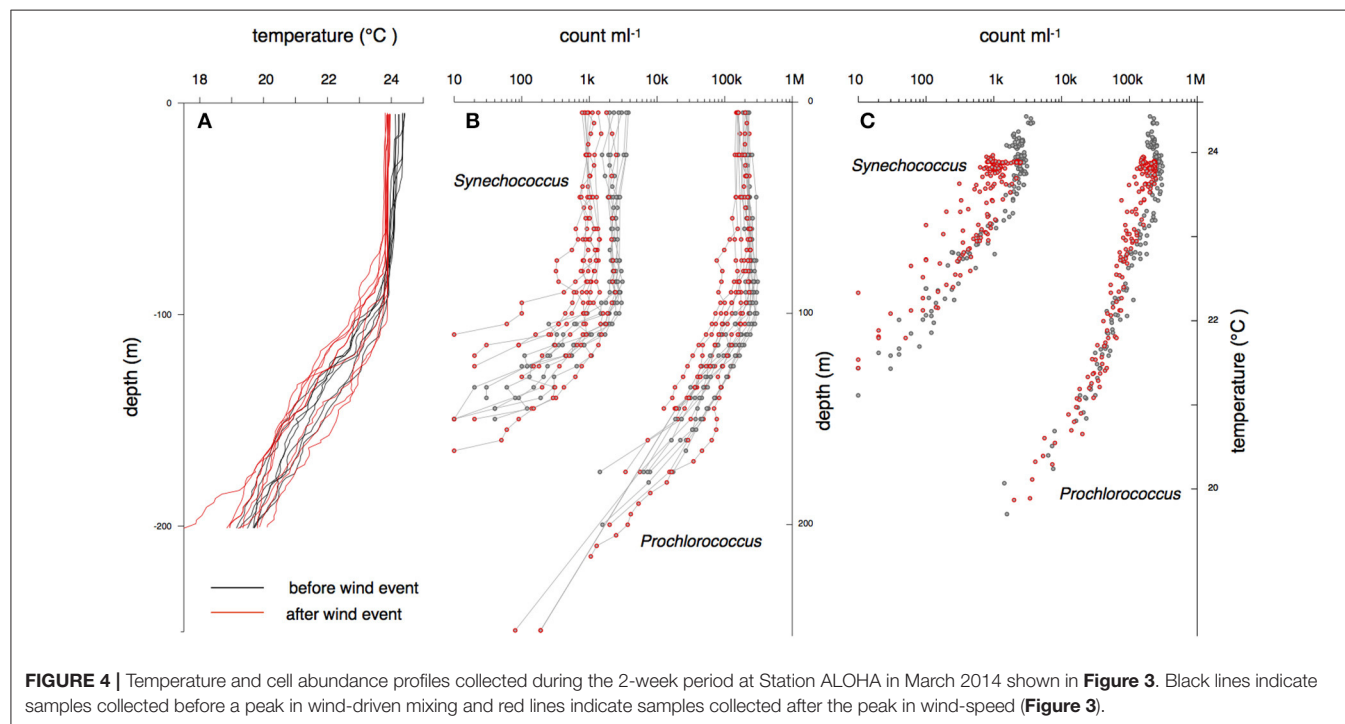
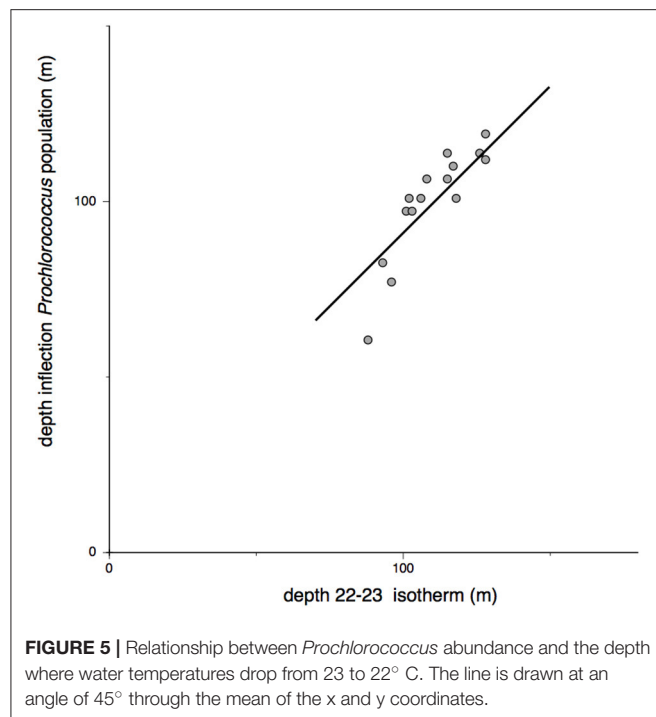


FIGURE 4 | Temperature and cell abundance profiles collected during the 2-week period at Station ALOHA in March 2014 shown in **Figure 3**. Black lines indicate samples collected before a peak in wind-driven mixing and red lines indicate samples collected after the peak in wind-speed (**Figure 3**).



corresponds to a 50-fold decrease in PAR over 100 m. In all profiles where the column is stable and stratification takes place, the mean fluorescence profile follows the 0.04 extinction profile within the 5-m sampling resolution. The close agreement between chlorophyll fluorescent intensity and the extinction coefficient of seawater is not likely to be coincidental.

After a storm, in which the top 100 m is thoroughly mixed as evidenced by uniform temperature (Figures 6B, 7, 8), the chlorophyll fluorescence signals from individual *Prochlorococcus* and *Synechococcus* cells become invariant with depth and assume a value intermediate to the signals of the surface and deep populations before mixing. This uniform chlorophyll expression pattern is reached within 24 hrs. In the aftermath of a mixing event, when the upper column again develops a shallow thermocline, the chlorophyll/depth relationship is re-established in 3–4 days (Figure 8).

Prochlorococcus and *Synechococcus* are reported to divide once per day (Vaulot et al., 1995; Marie et al., 1997; confirmed at Station ALOHA by Liu et al., 1995, 1997; Doggett and van den Engh, unpublished). The time scale of the changes in chlorophyll expression indicates that *Prochlorococcus* and *Synechococcus* adjust their FCM phenotype to ambient conditions rather than being replaced by a population with a different genetic makeup. After mixing of the upper water column, *Prochlorococcus* and *Synechococcus* cell abundances are lower (*Prochlorococcus* ~70%, *Synechococcus* ~30% of pre-storm numbers, Figure 4). During the subsequent re-establishment of the chlorophyll-expression gradient the abundance of both species does not change significantly. The changes in the FCM phenotype of the population occur over the span of a few cell generations (one generation to become homogeneous and at most 4 to reestablish

the phenotype gradient). It is difficult to generate a plausible scenario that replaces the majority of a population by sub-population selection while maintaining a constant population size in 1–3 cell divisions. The linearization of the chlorophyll depth gradient and the subsequent re-establishment must represent physiological adaptation of the individuals in the population rather than population replacement.

Further evidence that chlorophyll expression patterns of cyanobacteria are a response to environmental factors is supplied by the observation that chlorophyll fluorescence signals of *Prochlorococcus* and *Synechococcus* are tightly correlated over a wide range of depths and environmental conditions. Figure 10 compares the chlorophyll fluorescence of *Prochlorococcus* and *Synechococcus* in all samples in which both species were present, that were collected before, during, and after the wind-driven mixing event (over 200 samples). Considering the large genomic and physiological differences between these cyanobacteria, the remarkable correlation in chlorophyll expression patterns of *Prochlorococcus* and *Synechococcus* again strongly suggests that the phenotype changes represent a response to local environmental conditions.

Cyanobacteria in the Permanent Pycnocline

While the population sizes of cyanobacteria in the surface layers are relatively constant, the cell counts in the pycnocline diminish exponentially with depth. From about 100 m to 200 m, *Prochlorococcus* counts decrease by about 5 decades in magnitude (from 2×10^6 cell mL⁻¹ to ~ 10 cell mL⁻¹, Figures 1, 6). The exponential decrease in cell abundance is much steeper than the reduction of available light (<2 decades over the same range). Within the pycnocline, with cell numbers decreasing, the chlorophyll content of cells no longer matches ambient light, but becomes invariant with depth.

The transition point in the biphasic population pattern (constant population density in the surface zone; decreasing numbers at depths with less than 2% surface PAR) coincides with the depth of the top of the pycnocline. Figure 5 exhibits the point of intersection between the population plateau phase and the line through the exponential decay phase in profiles before, during, and after the storm event of 2014. Within the time span sampled, the position of the pycnocline underwent large vertical movements over a period of 12 h (Figure 3). The interpolation points move up and down in association with the position of the pycnocline. With a diel division cycle, constant cell numbers indicate that daily cell production is balanced by an equal loss in cell numbers.

Chlorophyll Acclimation Implies a Constant Energy Harvest

Acclimation to ambient light may explain how *Prochlorococcus* and *Synechococcus* in the mixed layers are able to maintain a relatively constant population size despite a gradient in PAR. Within the upper 100 m, mean chlorophyll content of individual *Prochlorococcus* and *Synechococcus* cells increases inversely with a decrease in available light (Figures 1, 6A, 8)

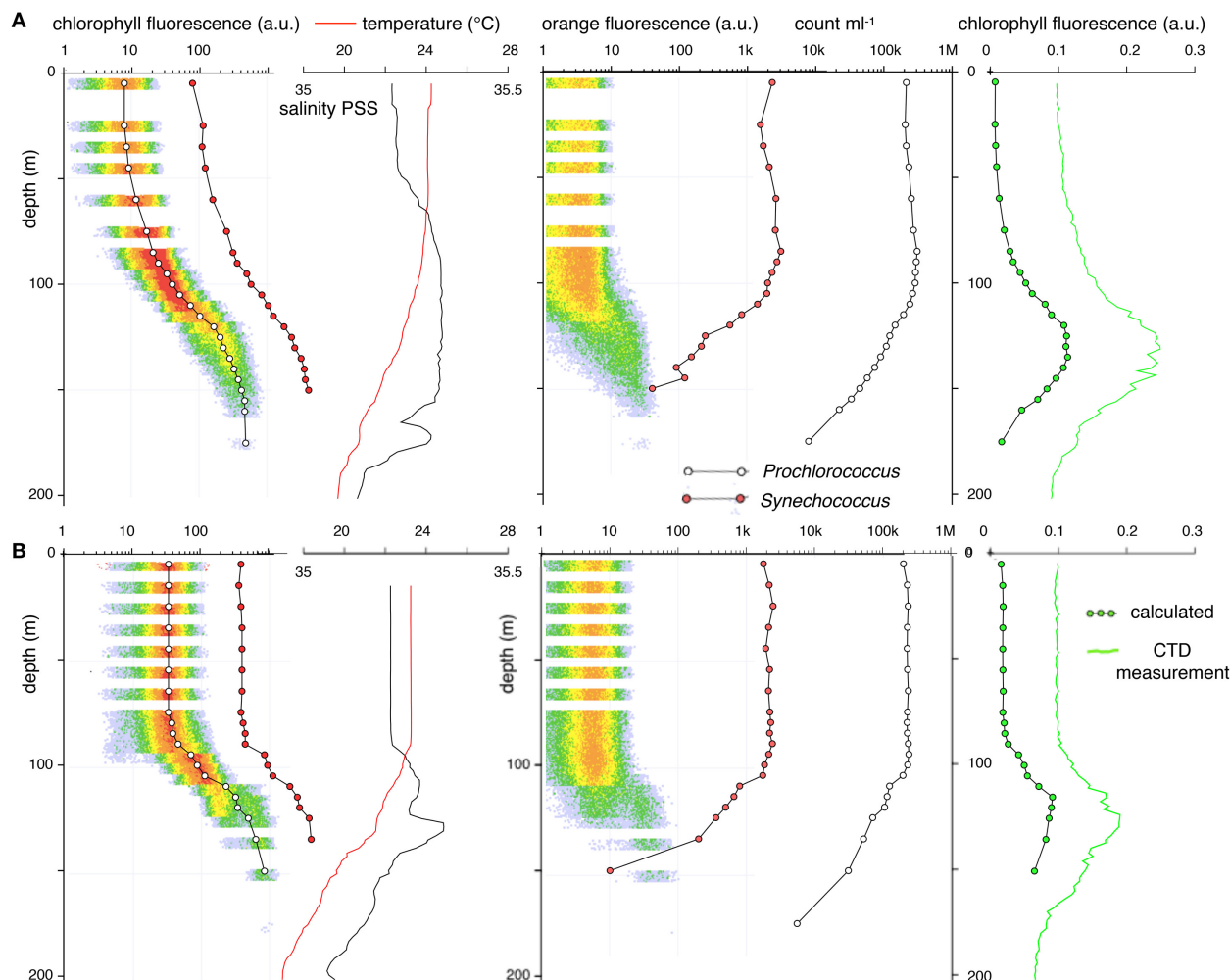


FIGURE 6 | Abundance and optical properties of *Prochlorococcus* (open circles) and *Synechococcus* (red circles) measured by flow cytometry at Station ALOHA. The solid red line indicates temperature; the black line indicates salinity. The open circles represent the mean fluorescence and abundance of *Prochlorococcus*. Solid red circles represent those values for *Synechococcus*. The green line represents bulk fluorescence as measured by the CTD. The solid green circles represent the product of the mean *Prochlorococcus* fluorescence and the cell counts. **(A)** Depth profile in calm weather (March 14, 2014, 20:45 HST). **(B)** Depth profile after a deep mixing event (March 16, 2014, 18:10 HST). Before the mixing event, the mean fluorescence of *Prochlorococcus* and *Synechococcus* increases monotonically over a 50-fold range with depth. Within 24 h after homogenization of the upper water column, as evidenced by the straight salinity and temperature measurements, the fluorescence of *Prochlorococcus* and *Synechococcus* are invariant with depth at a value intermediate to the surface and deep measurements obtained just before the storm. During these changes, there is no appreciable change in *Prochlorococcus* or *Synechococcus* abundance.

with little change in the forward light scatter signal (~size, Figure 1). By modulating their chlorophyll content in this manner, the photosynthetic cells in the mixed-layer zone increase their light-gathering capacity to compensate for the decrease in irradiance and maintain a constant rate of photon capture (Letelier et al., 2017). Despite a light intensity gradient of almost 2 decades, the cells are able to collect the amount of energy that is required for a daily division cycle. To maintain constant growth under decreasing light conditions, the overall light harvesting capacity per cell must increase, but since the number of collected photons per cell is constant, the mechanism that turns excited photons into chemical energy does not need to be adjusted. Therefore, the number of photo-reaction centers

per cell can be expected to remain the same, resulting in an increasing ratio of chlorophyll per reaction center. Differences in chlorophyll/reaction center ratios may explain the paradoxical observation that photosynthesis rates do not correlate with chlorophyll content (Laws et al., 2016). It should be noted here that a flow cytometer measures chlorophyll fluorescence at an extremely high excitation irradiance. Fluorescence photons represent excess photons that cannot be processed by the reaction centers. Under such saturation conditions, fluorescence emission becomes proportional to the number of chlorophyll molecules. In contrast, photosynthesis rate measurements are determined by the number of reaction centers and, under saturating light conditions, are independent of light intensity (Kirk, 2011).

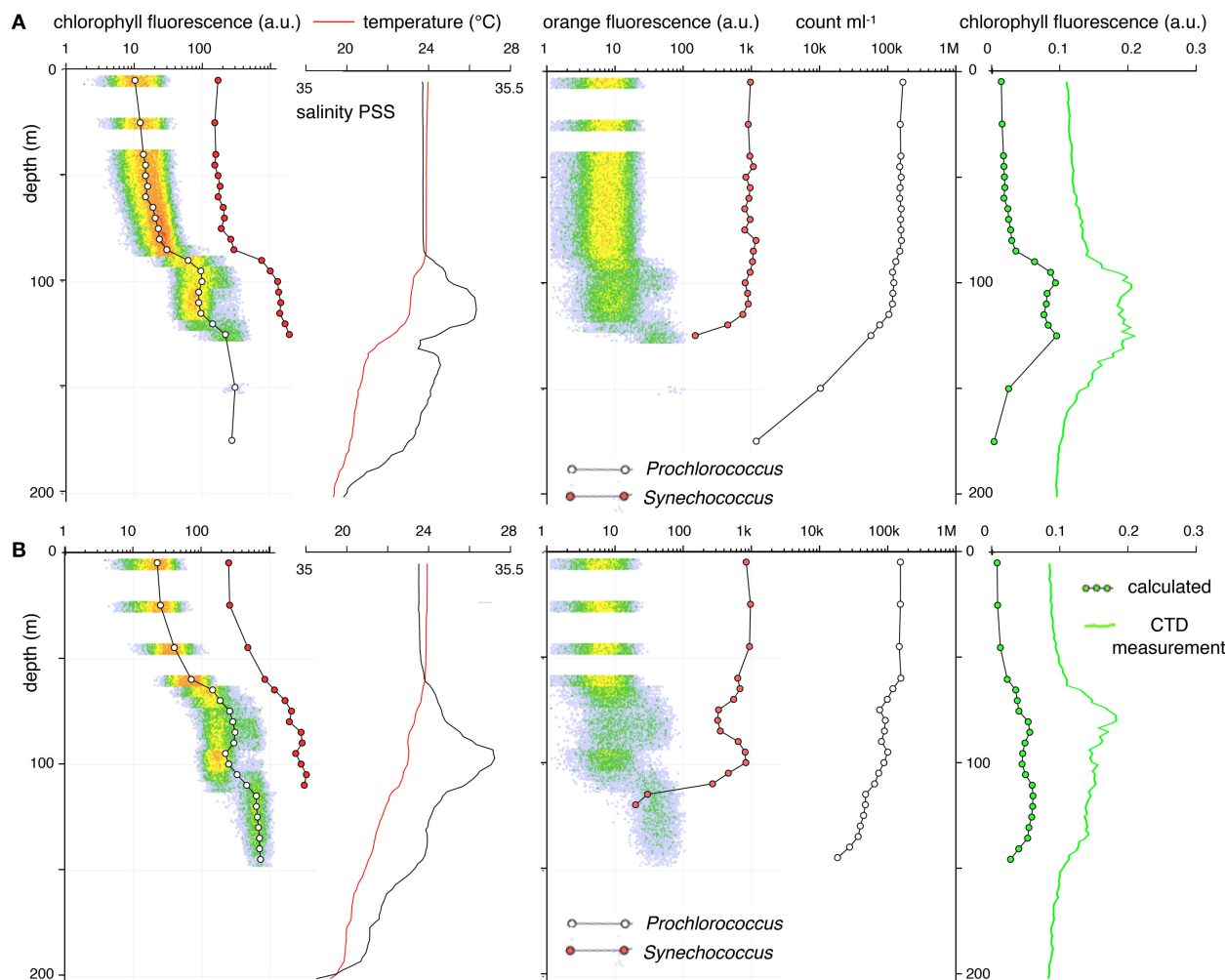


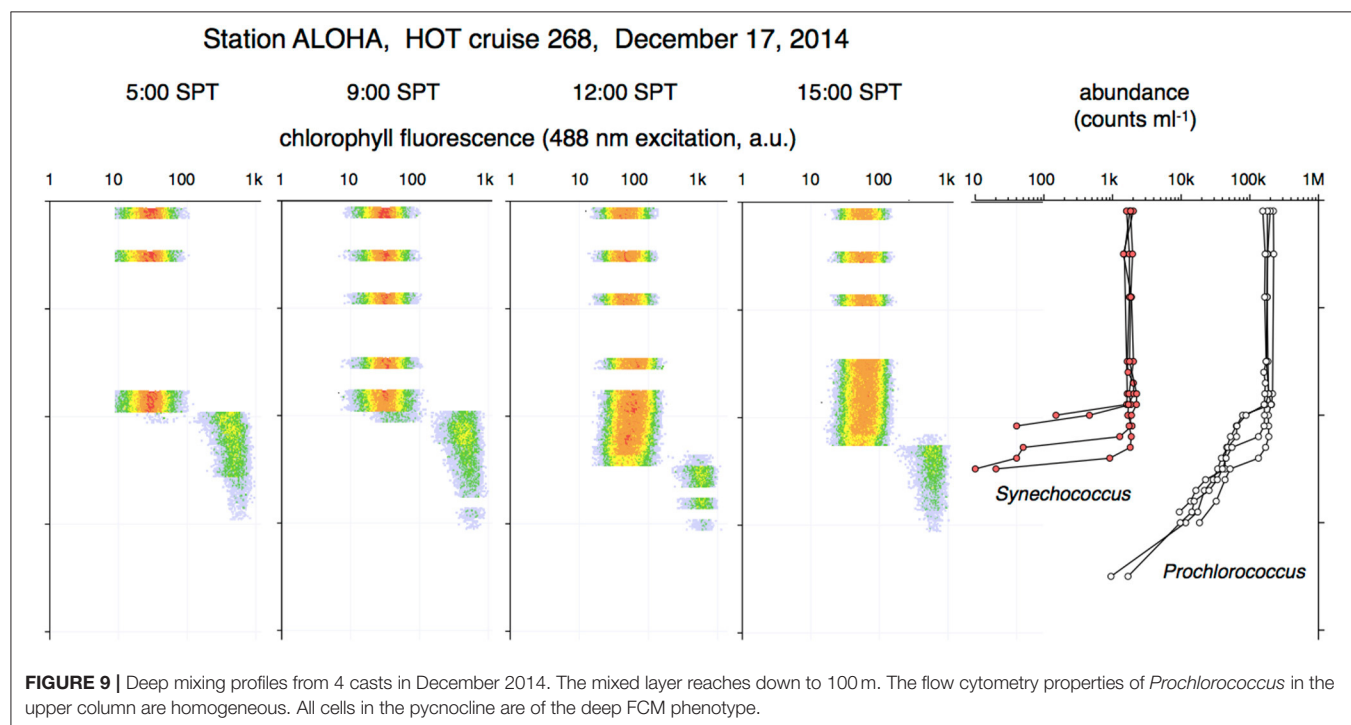
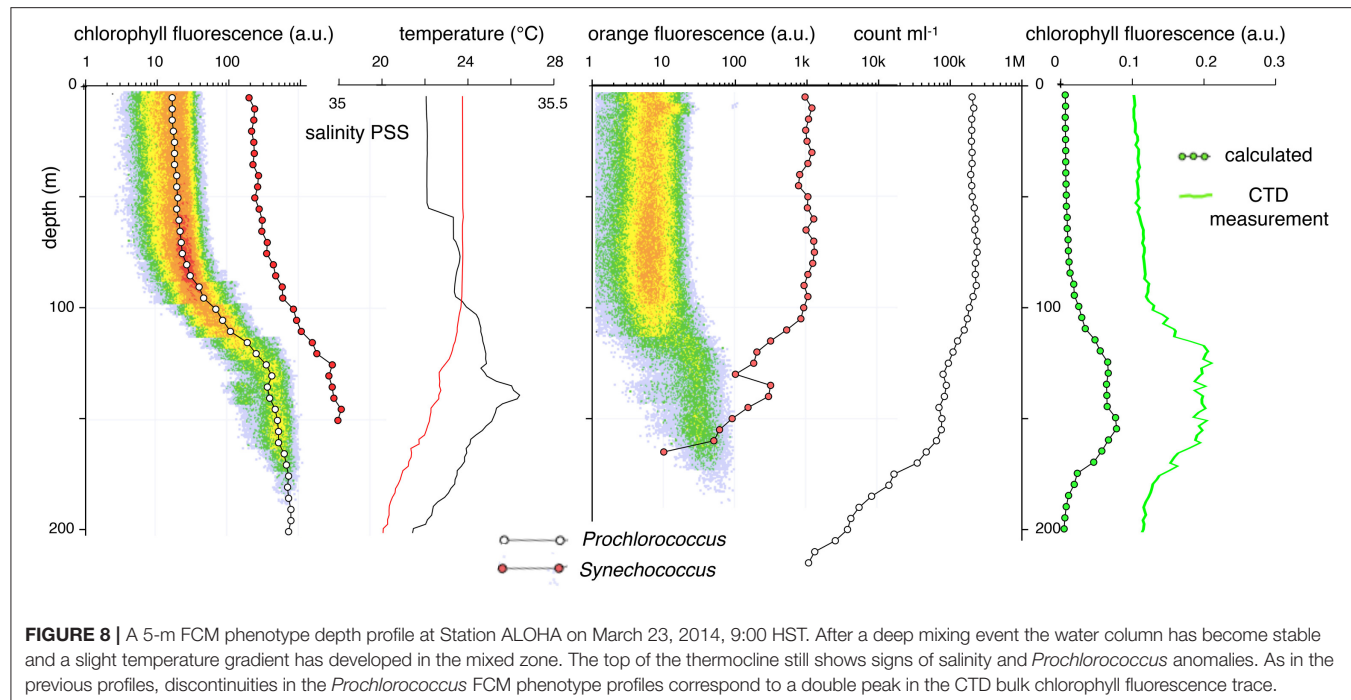
FIGURE 7 | Two examples of 5-m resolution flow cytometry profiles of *Prochlorococcus* and *Synechococcus* that show local inversion patterns that correlate with salinity/temperature anomalies. Symbol and line coloring as in **Figure 6**. As the temperature of the high salinity layers equilibrates with that of the surrounding layers, the salt anomaly will descend and will be diluted by mixing with the lower salt layer underneath. The salinity/temperature anomalies correlate with discontinuities in the *Prochlorococcus* and *Synechococcus* fluorescence and abundance profiles. **(A)** March 19, 2014, 16:40 HST; **(B)** March 21, 2014, 17:00 HST.

A large variance in chlorophyll signal combined with a near-constant population size (both in number and in volume) implies that bulk chlorophyll fluorescence measurements with CTD sensors cannot directly relate to phytoplankton population size (Cullen, 2014). The total amount of chlorophyll associated with the *Prochlorococcus* and *Synechococcus* at different depth layers can be estimated by multiplying the mean per cell chlorophyll fluorescence with the volumetric cell counts. Calculated profiles are in good agreement with the profile of the bulk chlorophyll fluorescence measured by the CTD sensor (**Figures 6–8**). When the CTD sensors register a double chlorophyll peak (**Figures 7A,B**), the calculated profile also has a bimodal shape. In all profiles, both the measured and calculated chlorophyll profiles reach a maximum just below the top of the pycnocline where the cell numbers have already started a significant decline. At the depth of the maximum chlorophyll signal (which is often

used as a marker to guide depth sampling) the *Prochlorococcus* counts are about 1/3 and the *Synechococcus* counts are about 1/10 of the plateau values in the mixed-layer zone. In populations with a daily cell division, productivity must relate to population size. Since the population maximum is reached when chlorophyll measurements are still rising, bulk chlorophyll measurements cannot be expected to correlate with productivity (Cullen, 2014; Laws et al., 2016).

Irradiance in a Dynamic Environment

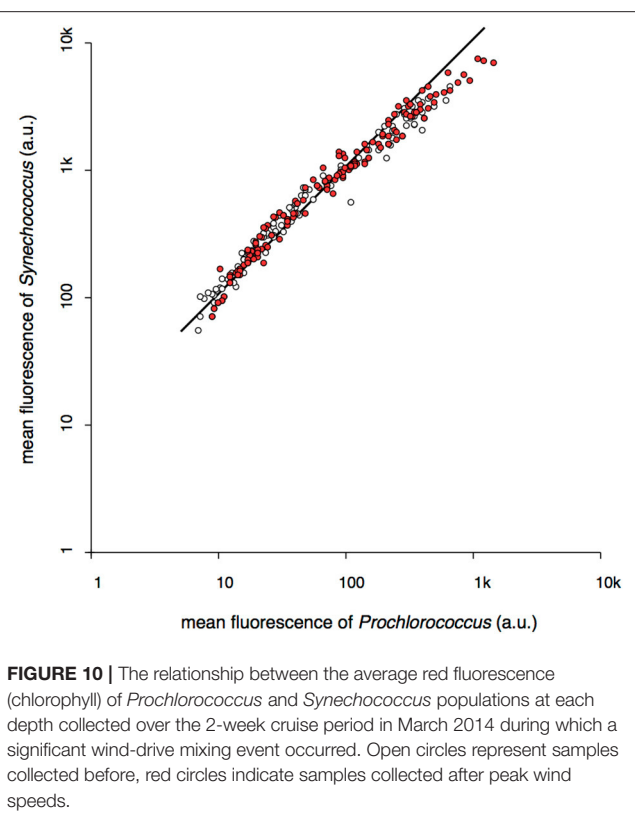
The previous discussion describes the properties of cyanobacteria in relation to sampling depth, as if the marine environment is a static system. However, wind events and subsurface waves frequently cause rearrangement of the water layers. Periodic wind-driven deep mixing events and/or episodes with significant subsurface waves may disturb the static conditions and may



greatly affect light exposure. In a stratified ocean, *Prochlorococcus* and *Synechococcus* at a depth of 100 m receive only about 2% of the light compared to the individuals near the surface (Letelier et al., 2004). Under complete dynamic mixing, when all individuals circulate throughout the mixed zone and spend an equal time at all depths, each inhabitant would receive an integrated light dose of about 25% the surface dose or the

equivalent of a stationary exposure at a depth of about 35 m (calculations in Methods and Materials). Consequently, during a deep mixing event the majority of cells will experience a significantly higher illumination dose than under stable stratified conditions.

The layers of the permanent pycnocline are not subject to vertical circulation but still may experience dynamic changes



in light regime. Tidal or storm-related subsurface waves may lift and lower the top of the pycnocline by as much as 50 m corresponding to a 10–20-fold change in photon flux with in a period of 31 h (Karl and Church, 2017, **Figures 3, 4, 7**). Thus, the inhabitants of the deep pycnocline will experience episodic exposure to high-light conditions. The irradiance regime in the pycnocline is different from that in the upper column. The latter will experience exposure with a diel periodicity. The light exposure in the pycnocline has a random, unpredictable component leading to a variability in irradiance including periods of relatively low photon fluxes (Letelier et al., 1996; Karl et al., 2002).

The differences in optical properties across depth profiles of *Prochlorococcus* and *Synechococcus* are often (implicitly) attributed to genomic ecotypes that segregate at different depths (Johnson et al., 2006; Zwirglmaier et al., 2008). The designation of low-light (LL) and high-light (HL) ecotypes suggests that light intensity at different depths is the determining factor (Moore and Chisholm, 1999). However, as the storm observation data show, the FCM phenotype segregation is restored within the time span of a few cell cycles after a mixing event takes place, giving little time for genotype segregation by competitive proliferation. The frequency at which the upper water column is scrambled and the speed at which equilibrium of FCM phenotype gradients are re-established indicate that acclimation and plasticity of genome expression are likely to be more important. If niche selection of genomes adapted to different niches in the water column plays a role, it is most likely to occur in the stable

pycnocline where populations remain segregated over longer periods (weeks to month, or longer). Light intensity is not the only, or even the major defining difference between the periodically mixed-layer and the stable pycnocline (Braakman et al., 2017). Compared to the mixed-layer zone, the pycnocline has higher nutrient concentrations with a different composition (Karl and Church, 2017). The inhabitants of the pycnocline are not always in the dark but may experience elevated light conditions of an aperiodic, random nature due to subsurface waves. If there are differences in genomic traits between mixed-layer and pycnocline inhabitants, they can be expected to include metabolic requirements (Björkman et al., 2015) and adaptations to a diel light cycle in the mixed-layer zone vs. a random irradiance regime in the pycnocline (Ottesen et al., 2014).

Interpretation of Scatter and Chlorophyll-Fluorescence Signals of Phytoplankton

One more aspect must be considered. In living organisms, fluorescence intensity is not necessarily proportional to chromophore content (van den Engh and Farmer, 1992; Asbury et al., 2000; Uy et al., 2004). Light collection for photosynthesis involves pigment complexes that dissipate energy along multiple pathways. Photon energy moves among pigment molecules by resonant energy transfer. The energy may be used for photosynthesis or may be released as fluorescence or heat. Energy transfer depends to the sixth power on molecular distances (Jovin, 1979). Therefore, small changes in molecular arrangements may have a large effect on the ratio of photon capture vs. fluorescence emission. In addition, phototrophs express variable amounts of compounds (e.g., zeaxanthin) that quench chlorophyll's excited state, further affecting the relationship between fluorescence and photosynthetic activity (Bricaud et al., 1995; Falkowski and Raven, 1997). If cyanobacteria are capable of adjusting their chlorophyll content to match ambient conditions, the cells may also be able to modulate their absorption efficiency. This could be accomplished by adjusting the molecular arrangement or composition of their light harvesting complex, thereby affecting the efficiency of chlorophyll fluorescence. More information about fluorescence spectra and efficiencies is needed for an accurate quantitative interpretation of *in situ* chlorophyll fluorescence signals.

Implications

This study demonstrates the potential of high-resolution depth profiling and single cell analysis by flow cytometry in analyzing marine microbial community structure and dynamics. Fine-scale features, both temporal and spatial, reveal intricate relationships and dependencies between phototrophic microbes and their dynamic physical environment that are easily missed with samples collected at a few standard depths. Our observations show that microbial community structure may undergo sudden, dramatic changes within a narrow depth range, especially when crossing boundary layers. Understanding of the nature and cause of such changes may reveal hidden mechanisms and patterns of phytoplankton behavior. High-resolution sampling combined

with detailed single cell analysis of phenotype, metabolic activity, genomic identity and functional gene capacity will be valuable in deciphering the rules of genetic adaptation and metabolic acclimation that determine the differences in lifestyles of *Prochlorococcus* and *Synechococcus* in the open ocean.

AUTHOR CONTRIBUTIONS

GvdE: primary author, designed experimental equipment, participated in all experiments. JD: participated in all experiments, reviewed and contributed to manuscript. AT: participated in crucial experiments, made major contributions to manuscript. MD: participated in crucial experiments, reviewed and made major contributions to manuscript. CG, participated in crucial experiments, reviewed and contributed to manuscript. DK: made major contributions to experimental design and final content of manuscript.

ACKNOWLEDGMENTS

We thank the officers and crews of the R/V Kilo Moana and Kaimikai-O-Kanaloa, and the scientists aboard for their assistance in sample collection. Funding was provided by the National Science Foundation (grant #OCE-1260164) and (award #1646709 to AT), the Gordon and Betty Moore Foundation (award #3794 to DK), and the Simons Foundation (SCOPE award #329108 to DK). CG is a recipient of a Fulbright fellowship and received support from Fondecyt, Chile. MD's participation in this research was funded by the Australian Government through the Australian Research Council (LE130100019). During a period of this study AT and GvdE were employed by BD BioSciences. The opportunity to do research that is not directly linked to BD's commercial mission is greatly appreciated. We thank Andy Siegel (Foster School of Business, UW) for checking the calculation of the light exposure of circulating particles.

REFERENCES

- Asbury, C. L., Uy, J. L., and van den Engh, G. (2000). Polarization of fluorescence and scatter signals in flow cytometry. *Cytometry* 40, 88–101. doi: 10.1002/(SICI)1097-0320(20000601)40:2<88::AID-CYTO2>3.0.CO;2-J
- Bidigare, R. R., Buttler, F. R., Christensen, S. J., Barone, B., Karl, D. M., and Wilson, S. T. (2014). Evaluation of the utility of xanthophyll cycle pigment dynamics for assessing upper ocean mixing processes at Station ALOHA. *J. Plankton Res.* 36, 1423–1433. doi: 10.1093/plankt/fbu069
- Biller, S. J., Berube, P. M., Berta-Thompson, J. W., Kelly, L., Roggensack, S. E., Awad, L., et al. (2014). Genomes of diverse isolates of the marine cyanobacterium *Prochlorococcus*. *Sci. Data.* 1:140034. doi: 10.1038/sdata.2014.34
- Binder, B. J., Chisholm, S. W., Olson, R. J., Frankel, S. L., and Worden, A. Z. (1996). Dynamics of picophytoplankton, ultraphytoplankton and bacteria in the central equatorial Pacific. *Deep-Sea Res. Part II* 4–6, 907–931. doi: 10.1016/0967-0645(96)00023-9
- Björkman, K. M., Church, M. J., Doggett, J. K., and Karl, D. M. (2015). Differential assimilation of inorganic carbon and leucine by *Prochlorococcus* in the oligotrophic North Pacific Subtropical Gyre. *Front. Microbiol.* 17:1401. doi: 10.3389/fmicb.2015.01401
- Bouman, H. A., Ulloa, O., Scanlan, D. J., Zwirglmaier, K., Li, W. K. W., Platt, T., et al. (2006). Oceanographic basis of the global surface distribution of *Prochlorococcus* ecotypes. *Science* 312, 918–921. doi: 10.1126/science.112692
- Braakman, R., Follows, M. J., and Chisholm, S. W. (2017). Metabolic evolution and the self-organization of ecosystems. *Proc. Natl. Acad. Sci. U.S.A.* 114, E3091–E3100. doi: 10.1073/pnas.1619573114
- Bricaud, A., Allali, K., Morel, A., Marie, D., Veldhuis, M. J. W., Partensky, F., et al. (1999). Divinyl chlorophyll a-specific absorption coefficients and absorption efficiency factors for *Prochlorococcus marinus*: kinetics of photoacclimation. *Mar. Ecol. Prog. Ser.* 188, 21–32. doi: 10.3354/meps188021
- Bricaud, A., Babin, M., Morel, A., and Claustre, H. (1995). Variability of chlorophyll specific absorption coefficient of natural plankton: analysis and parameterization. *J. Geophys. Res.* 109, C11010. doi: 10.1029/2004JC002419
- Campbell, L., Nolla, H. A., and Vaulot, D. (1994). The importance of *Prochlorococcus* to community structure in the central North Pacific Ocean. *Limnol. Oceanogr.* 39, 954–961. doi: 10.4319/lo.1994.39.4.0954
- Campbell, L., and Vaulot, D. (1993). Photosynthetic picoplankton community structure in the subtropical North Pacific Ocean near Hawaii (station ALOHA). *Deep-Sea Res. Part I* 40, 2043–2060. doi: 10.1016/0967-0637(93)90044-4
- Cullen, J. J. (2014). Subsurface chlorophyll maximum layers: enduring enigma or mystery solved? *Annu. Rev. Mar. Sci.* 7, 207–239. doi: 10.1146/annurev-marine-010213-135111
- Dusenberry, J. A. (1995). *Picophytoplankton Photoacclimation and Mixing in the Surface Oceans*. Ph.D. thesis, MIT.
- Dusenberry, J. A., Olson, R. J., and Chisholm, S. W. (1999). Frequency distributions of phytoplankton single-cell fluorescence and vertical mixing in the surface ocean. *Limnol. Oceanogr.* 44, 431–435. doi: 10.4319/lo.1999.44.2.0431
- Falkowski, P. G., and Raven, J. A. (1997). *Aquatic Photosynthesis*. Oxford: Blackwell Science.
- Johnson, Z. I., Zinser, E. R., Coe, A., McNulty, N. P., Woodward, E. M. S., and Chisholm, S. W. (2006). Niche partitioning among *Prochlorococcus* ecotypes along ocean-scale environmental gradients. *Science* 311, 1737–1740. doi: 10.1126/science.1118052
- Jovin, T. M. (1979). “Fluorescence polarization and energy transfer: theory and application,” in *Flow Cytometry and Sorting*, eds M. R. Melamed, P. F. Mullaney, and M. L. Mendelsohn (New York, NY: Wiley and Sons), 137–166.
- Karl, D., Bidigare, R., and Letelier, R. M. (2002). “Sustained seasonal and interannual variability of phytoplankton processes in the NPSG,” in *Phytoplankton Productivity: Carbon Assimilation in Marine and Freshwater Ecosystems*, eds P. J. LeB, W. D. N. Thomas, and C. Reynolds (Oxford: Blackwell Science Ltd.), 222–264.
- Karl, D. M., Björkman, K. M., Dore, J. E., Fujiki, L., Hebel, D. V., Houlihan, T., et al. (2001). Ecological nitrogen-to-phosphorus stoichiometry at Station ALOHA. *Deep-Sea Res. Part II* 48, 1529–1566. doi: 10.1016/S0967-0645(00)00152-1
- Karl, D. M., and Church, M. J. (2014). Microbial oceanography and the Hawaii Ocean Time-series programme. *Nat. Rev. Microbiol.* 12, 699. doi: 10.1038/nrmicro3333
- Karl, D. M., and Church, M. J. (2017). Ecosystem structure and dynamics in the North Pacific Subtropical Gyre: new views of an old ocean. *Ecosystems* 20, 433–457. doi: 10.1007/s10021-017-0117-0
- Karl, D. M., and Lukas, R. (1996). The Hawaii Ocean Time-series (HOT) program: background, rationale and field implementation. *Deep-Sea Res. Part II* 43, 129–156. doi: 10.1016/0967-0645(96)00005-7
- Kashtan, N., Roggensack, S. E., Rodrigue, S., Thompson, J. W., Biller, S. J., and Coe, A. (2014). Single-cell genomics reveals hundreds of coexisting subpopulations in wild *Prochlorococcus*. *Science* 344, 416–420. doi: 10.1126/science.1248575
- Kettler, G. C., Martiny, A. C., Huang, K., Zucker, J., Coleman, M. L., and Rodrigue, S. (2007). Patterns and implications of gene gain and loss in the evolution of *Prochlorococcus*. *PLoS Genet.* 3:e231. doi: 10.1371/journal.pgen.0030231
- Kirk, J. T. O. (2011). *Light and Photosynthesis in Aquatic Ecosystems*. Cambridge: University Press.

- Knauss, J. A. (1996). *Introduction to Physical Oceanography*. Upper Saddle River, NJ: Prentice Hall.
- Laws, E. A., Bidigare, R. R., and Karl, D. M. (2016). Enigmatic relationship between chlorophyll a concentrations and photosynthetic rates at Station ALOHA. *Heliyon* 2, 2–15. doi: 10.1016/j.heliyon.2016.e00156
- Letelier, R. M., Dore, J. E., Winn, C. D., and Karl, D. M. (1996). Seasonal and interannual variations in photosynthetic carbon assimilation at Station ALOHA. *Deep-Sea Res. Part II* 43, 467–490. doi: 10.1016/0967-0645(96)00006-9
- Letelier, R. M., Karl, D. M., Abbott, M. R., and Bidigare, R. R. (2004). Light driven seasonal patterns of chlorophyll and nitrate in the lower euphotic zone of the North Pacific Subtropical Gyre. *Limnol. Oceanogr.* 49, 508–519. doi: 10.4319/lo.2004.49.2.0508
- Letelier, R. M., White, A. E., Bidigare, R. R., Barone, B., Church, M. J., and Karl, D. M. (2017). Light absorption by phytoplankton in the North Pacific subtropical gyre. *Limnol. Oceanogr.* 62, 1526–1540. doi: 10.1002/lo.10515
- Liu, H., Campbell, L., and Landry, M. R. (1995). Growth and mortality rates of *Prochlorococcus* and *Synechococcus* measured with a selective inhibitor technique. *Mar. Ecol. Prog. Series* 116, 277–287.
- Liu, H., Nolla, H., and Campbell, L. (1997). *Prochlorococcus* growth rate and contribution to primary production in the equatorial and subtropical North Pacific Ocean. *Aquat. Microb. Ecol.* 12, 39–47. doi: 10.3354/ame012039
- Malmstrom, R. R., Coe, A., Kettler, G. C., Martiny, A. C., Frias-Lopez, J., and Zinser, E. R. (2010). Temporal dynamics of *Prochlorococcus* ecotypes in the Atlantic and Pacific oceans. *ISME J.* 4, 1252–1264. doi: 10.1038/ismej.2010.60
- Malmstrom, R. R., Rodriguez, S., Huang, K. H., Kelly, L., Kern, S. E., Thompson, A., et al. (2013). Ecology of uncultured *Prochlorococcus* clades revealed through single-cell genomics and biogeographic analysis. *ISME J.* 7, 184–198. doi: 10.1038/ismej.2012.89
- Mann, E. L., and Chisholm, S. W. (2000). Iron limits the cell division rate of *Prochlorococcus* in the eastern equatorial Pacific. *Limnol. Oceanogr.* 45, 1067–1076. doi: 10.4319/lo.2000.45.5.1067
- Mann, K. H., and Lazier, J. R. N. (1991). *Dynamics of Marine Ecosystems: Biological-Physical Interactions in the Oceans*. Cambridge, MA: Blackwell Scientific Publications.
- Marie, D., Partensky, F., Jacquet, S., and Vaulot, D. (1997). Enumeration and cell cycle analysis of natural populations of marine picoplankton by flow cytometry using the nucleic acid stain SYBR Green I. *Appl. Environ. Microbiol.* 63, 186–193.
- Martiny, A. C., Kathuria, S., and Berube, P. M. (2009). Widespread metabolic potential for nitrite and nitrate assimilation among *Prochlorococcus* ecotypes. *Proc. Natl. Acad. Sci. U.S.A.* 106, 10787–10792. doi: 10.1073/pnas.0902532106
- Moore, L. R., and Chisholm, S. W. (1999). Photophysiology of the marine cyanobacterium *Prochlorococcus*: ecotypic differences among cultured isolates. *Limnol. Oceanogr.* 44, 628–638. doi: 10.4319/lo.1999.44.3.0628
- Ottesen, E. A., Young, C. R., Gifford, S. M., Eppley, J. M., Marin, R., Schuster, S. C., et al. (2014). Multispecies diel transcriptional oscillations in open ocean heterotrophic bacterial assemblages. *Science* 345, 207–212. doi: 10.1126/science.1252476
- Partensky, F., Hess, W. R., and Vaulot, D. (1999). *Prochlorococcus*, a marine photosynthetic prokaryote of global significance. *Microbiol. Molec. Biol. Rev.* 63, 106–127.
- Petersen, T. W., Harrison, B., Horner, D. N., and van den Engh, G. (2012). Flow cytometric characterization of marine microbes. *Methods* 57, 350–358. doi: 10.1016/j.ymeth.2012.07.001
- Rocap, G., Larimer, F. W., Lamerdin, J., Malfatti, S., Chain, P., and Ahlgren, N. A. (2003). Genome divergence in two *Prochlorococcus* ecotypes reflects oceanic niche differentiation. *Nature* 424, 1042–1047. doi: 10.1038/nature01947
- Stewart, R. H. (2008). *Introduction to Physical Oceanography*. College Station, TX: Texas A and M.
- Trask, B. J., van den Engh, G. J., and Elgershuizen, J. H. B. W. (1982). Analysis of phytoplankton by flow cytometry. *Cytometry* 2, 258–264. doi: 10.1002/cyto.990020410
- Uy, J. L., Asbury, C. L., Petersen, T. W., and van den Engh, G. (2004). The polarization of fluorescence of DNA stains depends on the incorporation density of the dye molecules. *Cytometry* 61A, 18–25. doi: 10.1002/cyto.a.20059
- van den Engh, G. J., and Farmer, C. (1992). Photo-bleaching and photon saturation in flow cytometry. *Cytometry* 13, 669–677. doi: 10.1002/cyto.990130702
- Vaulot, D., Marie, D., Olson, R. J., and Chisholm, S. W. (1995). Growth of *Prochlorococcus*, a photosynthetic prokaryote, in the equatorial Pacific Ocean. *Science* 268, 1480–1482. doi: 10.1126/science.268.5216.1480
- West, N. J., and Scanlan, D. J. (1999). Niche-partitioning of *Prochlorococcus* populations in a stratified water column in the Eastern North Atlantic Ocean. *Appl. Environ. Microbiol.* 65, 2585–2591.
- Zwirglmaier, K., Jardillier, L., Ostrowski, M., Mazard, S., Garczarek, L., and Vaulot, D. (2008). Global phylogeography of marine *Synechococcus* and *Prochlorococcus* reveals a distinct partitioning of lineages among oceanic biomes. *Environ. Microbiol.* 10, 147–161. doi: 10.1111/j.1462-2920.2007.01440.x

Conflict of Interest Statement: At the time when the experiments were conducted GvdE and AT were employed by BD BioSciences, a major developer and distributor of flow cytometry equipment. The article may be perceived as promoting a specific model of flow cytometer that is manufactured and sold by BD. GvdE and AT no longer have any financial interest in the company.

The other authors declare that the research was conducted in the absence of any commercial or financial relationships that could be construed as a potential conflict of interest.

Copyright © 2017 van den Engh, Doggett, Thompson, Doblin, Gimpel and Karl. This is an open-access article distributed under the terms of the Creative Commons Attribution License (CC BY). The use, distribution or reproduction in other forums is permitted, provided the original author(s) or licensor are credited and that the original publication in this journal is cited, in accordance with accepted academic practice. No use, distribution or reproduction is permitted which does not comply with these terms.



Temporal Variability of *Trichodesmium* spp. and Diatom-Diazotroph Assemblages in the North Pacific Subtropical Gyre

Angelicque E. White^{1*}, Katie S. Watkins-Brandt¹ and Matthew J. Church²

¹ College of Earth, Ocean, and Atmospheric Sciences, Oregon State University, Corvallis, OR, United States, ² Flathead Lake Biological Station, University of Montana, Polson, MT, United States

OPEN ACCESS

Edited by:

Rex Malmstrom,
Joint Genome Institute (DOE),
United States

Reviewed by:

Julie Robidart,
National Oceanography Centre
Southampton, United Kingdom
Rachel Ann Foster,
Stockholm University, Sweden

*Correspondence:

Angelicque E. White
angelicque.white@gmail.com

Specialty section:

This article was submitted to
Aquatic Microbiology,
a section of the journal
Frontiers in Marine Science

Received: 31 October 2017

Accepted: 18 January 2018

Published: 14 February 2018

Citation:

White AE, Watkins-Brandt KS and
Church MJ (2018) Temporal Variability
of *Trichodesmium* spp. and
Diatom-Diazotroph Assemblages in
the North Pacific Subtropical Gyre.
Front. Mar. Sci. 5:27.
doi: 10.3389/fmars.2018.00027

In oligotrophic ocean regions such as the North Pacific Subtropical Gyre (NPSG), N₂ fixation (i.e., diazotrophy) by a diverse consortium of microorganisms has been shown to contribute significantly to new production and particle export. In 2015 and 2016, we measured near-monthly abundances of the large cell-sized (> 10 µm) diazotrophic genera *Trichodesmium* and diatom-associated *Richelia* and *Calothrix* spp. in the NPSG via microscopy and quantitative PCR of *nifH* genes. Of these genera, we find *Trichodesmium* to be the more abundant over our study period, with cell concentrations in the upper water column (0–45 m) ranging from 1 to 5,988 cells L⁻¹, while the sum of *Richelia* and *Calothrix* spp. abundances ranged from 4 to 157 heterocysts L⁻¹. Significant discrepancies between absolute abundances were noted between cell and gene-based approaches to biomass determination (*nifH* copies L⁻¹ were up to 10²–10³ higher than cell concentrations). Potential explanations for these striking discrepancies are discussed. Using the maximum N fixation rates per cell found in the existing literature for these genera, we estimate potential N₂ fixation rates via these large diazotroph communities to be between 0.01 and 1.5 nmol N L⁻¹ d⁻¹. When comparing these rates to available ¹⁵N₂ tracer measurements, we conclude that large diazotrophs were generally minor (<10%) contributors to bulk N₂ fixation in the surface ocean during our study period. Conversely, high concentrations of *Trichodesmium* observed in fall-winter of 2015 and 2016 were estimated to drive >50% of measured N₂ fixation rates. While these large cell-sized and heterogeneously distributed organisms may still disproportionately contribute to export, cell-abundance based rate estimates suggests that other diazotrophs are largely responsible for N₂ fixation rates measured in bottle-based incubations.

Keywords: nitrogen fixation, *Trichodesmium*, North Pacific Subtropical Gyre, *Richelia*, qPCR

INTRODUCTION

The biological reduction of dinitrogen gas (N₂) into ammonia (termed N₂ fixation or diazotrophy) by certain genera of oceanic microorganisms represents the largest incoming flux of nitrogen to the global ocean (Galloway et al., 2004). As such, biological N₂ fixation plays a significant role in the regulation of oceanic productivity and the export of carbon and nitrogen (N) out of the sun-lit

surface waters (Capone and Carpenter, 1982). In open ocean habitats, ambient concentrations of bioavailable N are low (typically 100's of nmol L⁻¹). Hence, the capacity to utilize atmospheric N₂ allows diazotrophs to fulfill their N requirements for growth and subsequently contribute new N to the system via trophic transfer, sinking, (Scharek et al., 1999), or the release of ammonia and dissolved organic matter rich in N (Mulholland and Capone, 2001). More than just a conduit for inputs of new N, these organisms can also form large surface blooms, thereby transiently dominating both primary productivity and N cycling (Bowman and Lancaster, 1965; Karl et al., 1992; Capone et al., 1998).

In the oligotrophic North Pacific Subtropical Gyre (NPSG), isotopic models indicate that N₂ fixation is directly or indirectly responsible for 26–47% of the particulate N that is exported from the euphotic zone (Böttjer et al., 2017). Diazotrophic organisms in this ecosystem range from unicellular cyanobacterial symbionts (termed Group A, Zehr et al., 1998, 2001) to small and generally free-living cyanobacteria such as *Crocospaera* spp. and heterotrophic diazotrophs (Church et al., 2005; Gradovalle et al., 2017b), to more conspicuous and large cell-sized diazotrophs such as *Trichodesmium* and symbioses of *Richelia* and *Calothrix* with various diatoms (termed DDAs, diatom-diazotroph assemblages). These latter, larger organisms have been recognized as important contributors to upper ocean productivity and the annual flux of organic matter to the mesopelagic of the NPSG (Scharek et al., 1999; Dore et al., 2002; Karl et al., 2012).

Despite the knowledge of the importance of diazotrophy to new production in the NPSG, there have been few studies assessing the temporal variability of diazotroph biomass in the upper euphotic zone where they predominately reside. Using a quantitative PCR-based (qPCR) time series (2004–2007) targeting the *nifH* gene, which encodes a component of the nitrogenase enzyme that catalyzes N₂ fixation, Church et al. (2009) reported highly variable diazotroph assemblages in the NPSG. Unicellular diazotrophs were typically found to be most abundant whereas episodic increases of DDAs and *Trichodesmium* were noted. Similar *nifH* gene-based surveys in the region (Robidart et al., 2014) report highly patchy diazotroph assemblages, with *Trichodesmium* gene-copies varying up to three orders of magnitude over <30 km and <2 d time scales. While powerful, relationships between gene and cellular abundances remain largely unknown for naturally-occurring marine diazotrophs. Moreover, like several other cyanobacterial classes (Griese et al., 2011), diazotrophs such as *Trichodesmium* have recently been suggested to be polyploidal (Sargent et al., 2016) and nitrogenase gene-copies per cell can also vary for *Richelia* spp. (Foster and O'Mullen, 2008) such that gene-based measurements may overestimate cell abundances.

In this study we enumerated the abundance of large diazotrophs in the upper ocean of the NPSG via epifluorescence microscopy and qPCR over a 2-year period (2015–2016). From our measurements of the cellular abundance of these diazotrophs and published values of their N fixation rate per cell, we estimate the potential contributions of these organisms

to coincident measurements of ¹⁵N₂ fixation and N export. All samples were collected at Station ALOHA (A Long-term Oligotrophic Habitat Assessment), the field site for the Hawaii Ocean Time-series (HOT) program. The aim of this work was to describe the temporal variability of large diazotrophs and estimate their potential contributions to new production in the region.

MATERIALS AND METHODS

Diazotroph Cell Counts

Between April 2015 and December 2016, in coordination with the HOT program, samples were collected to enumerate the abundance of large (> 10 µm) diazotrophs at Station ALOHA (22.75°N, 158°W) in the upper water column. At each depth (5, 25, and 45 m), the entire volume of a PVC rosette bottle was drained directly into clean ~10 L carboys fitted with spigots in order to avoid underestimation of cells due to positive or negative buoyancy (Carpenter et al., 2004). Carboys were covered in dark cloth and the volume was gravity filtered through a 47-mm diameter, 10 µm pore size, black polycarbonate filter with a Sterlitech polyester drain disk (PETEDD47100) as a backing filter. All filtrations lasted <2 h. Following filtration, filter holders were fit with a short section of tubing and a syringe leur fitting on one side and a 2-way valve on the outflow side. For each filter, 5 ml of 2% glutaraldehyde was slowly injected onto the filter and samples were allowed to fix for 30 min. Fixative was drained after this time and 60 ml of air was used to flush all filters. Polycarbonate filters were then mounted onto 3" × 2" glass slides with Cargille Series A immersion oil, cover slides were added, and the edges of each cover slip were sealed with quick dry nail polish. All slides were stored at -20°C and counted within 60 days of collection.

Enumeration of diazotrophic taxa was performed using epifluorescence microscopy of phycoerythrin autofluorescence (548 nm excitation/561 nm emission) under 10–40× magnification using an Olympus epifluorescence BX61 microscope fit with a Cooke Sensicam camera. The entire area of the slide was counted (1735 mm³), such that the detection limit would effectively be ~0.1 cell L⁻¹ for all classes of organisms enumerated. The heterocysts of the diatom-associated genera *Richelia* and *Calothrix* were counted and the associated diatom was noted. These included diatoms of the following genera: *Rhizosolenia*, *Hemiaulus*, and *Chaetoceros*. Heterocysts of free *Richelia intracellularis* were also counted. For ease of presentation, we present total heterocysts L⁻¹, i.e., the sum of *Richelia* and *Calothrix*. *Trichodesmium* filaments were enumerated and the length of each filament was recorded. *Trichodesmium* cell number was then calculated by dividing filament length by the mean cell length (10 ± 2.5 µm, n = 200). For calculation of cells per filament, as in Letelier and Karl (1996), we consider only intact filaments with rounded apical ends in order to avoid underestimation of cells per filament. For colony morphologies, including puffs and tufts (see Figure 1 for morphology), cell numbers were estimated by counting the number of filaments per colony and dividing by mean cell length.

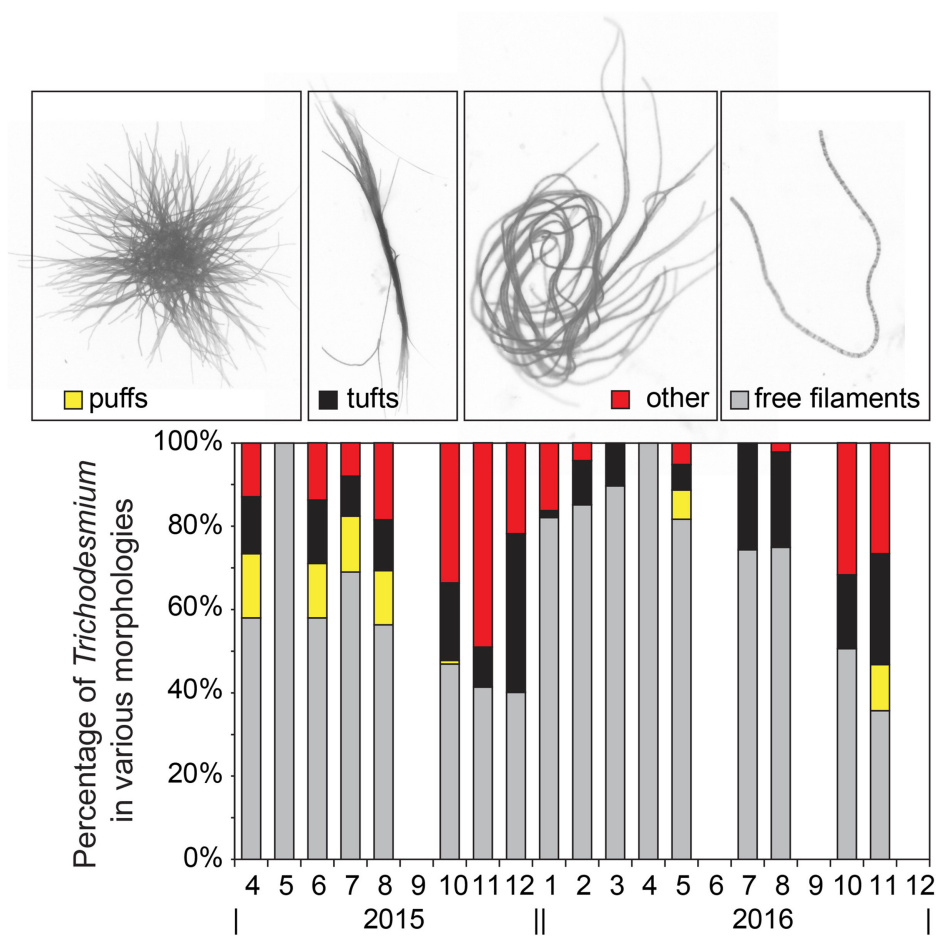


FIGURE 1 | Percentage of *Trichodesmium* cells in the various morphologies shown in the micrographs on top from left to right: puffs (yellow stacked bar), tufts (black stacked bar), other colonial morphologies (red stacked bar), and free filaments (gray stacked bar).

Quantification of *nifH* Genes

Abundances of nitrogenase genes (*nifH*) were quantified by quantitative polymerase chain reaction (qPCR) following procedures described in Church et al. (2009). Seawater for subsequent extraction of DNA was subsampled from CTD rosette bottles (5, 25, and 45 m) into acid-washed, polyethylene 4 L bottles. In the shipboard laboratory, seawater (typically 2 L) was filtered onto 25 mm diameter, 0.2 μ m pore size polyethersulfone filters (Pall Supor®) using a peristaltic pump. Filters were placed into 2 mL microcentrifuge tubes containing lysis buffer AP1 (Qiagen) and glass beads (0.1 mm and 0.5 mm), and stored at -80°C until extraction. DNA was extracted and purified using the Qiagen DNeasy Plant Mini Kit, including a bead-beating step. Standards for qPCR assays consisted of dilution series of plasmids containing the target *nifH* genes; primers and probes for *Trichodesmium*, Het1, Het2, and Het3 are described in Church et al. (2005, 2008, 2009). Detection limits for these reactions corresponded to ~ 50 genes L^{-1} of seawater.

Nitrogen Fixation Rates and Ancillary Data

Rates of N_2 fixation were measured during all cruises using the $^{15}\text{N}_2$ assimilation technique (Wilson et al., 2012; Böttjer et al., 2017). To inoculate the seawater samples with the gaseous tracer, the ^{15}N -labeled gas was dissolved in degassed, filtered seawater prior to its addition as per Wilson et al. (2012). The “ $^{15}\text{N}_2$ -enriched seawater” was prepared using filtered surface seawater collected at Station ALOHA and $^{15}\text{N}_2$ gas sourced from Cambridge Isotope Laboratories. The quantity of N isotopes (i.e., N masses equivalent to 28, 29, and 30) was measured in each batch of $^{15}\text{N}_2$ -enriched seawater using membrane inlet mass spectroscopy (Kana et al., 1994) using a one-point calibration to air. To conduct the rate measurements in the field, 200 ml of the $^{15}\text{N}_2$ -enriched seawater was added to a ~ 4 L bottle which had been filled with water collected from 5 depths between 5 and 125 m with Niskin bottles attached to a CTD rosette. These bottles were attached to an array and incubated *in situ* at their approximate collection depths from dawn to dawn. Note that cell

counts are only available in the upper 45 m for comparison to rate measurements (5, 25, and 45 m).

Upon termination of all incubations, the entire contents of the ~4 L bottle were filtered via peristaltic pump onto a pre-combusted glass microfiber (Whatman 25 mm GF/F) filter and stored in the -20°C freezer. On land, the filters were dried, pelletized in tin and silver boats, and analyzed for the total mass of N and the $\delta^{15}\text{N}$ composition analysis using an elemental analyzer-isotope ratio mass spectrometer (Carlo-Erba EA NC2500 coupled with Thermo Finnigan Delta S) at the Stable Isotope Facility of the University of Hawaii as per methods described in Wilson et al. (2012). Internal standards consisting of dried plankton material were included in the analytical run to evaluate instrument drift during analysis.

Station ALOHA records of surface chlorophyll (Chl) concentrations, water column temperature, ^{14}C primary productivity, and sediment trap-based particulate N export at 150 m were obtained from the HOT program (<http://hahana.soest.hawaii.edu/hot/>). These latter data were only available for 2015.

Estimated Contributions of Large Diazotrophs to Nitrogen Fixation Rates

We have estimated the potential magnitude of N_2 fixation associated with these large diazotrophs via a simple biomass-based approach (Tyrrell et al., 2003; Poulton et al., 2009) where the estimated rate is the product of the measured cell concentrations, the upper estimate for the daily duration of N_2 fixation (12-h), and cell-specific N_2 -based N fixation rates derived from the existing literature. For *Trichodesmium* spp., we consider the upper limit of cell-specific N fixation rates reported by Hutchins et al. (2007) for Pacific and Atlantic isolates of *Trichodesmium* (25×10^{-6} nmol N cell $^{-1}$ h $^{-1}$), whereas for *Richelia* and *Calothrix* spp. we use the heterocyst-specific rates (71.5×10^{-6} nmol N heterocyst $^{-1}$ h $^{-1}$) reported by Foster et al. (2011). We have modeled rates using these upper limits and assumed a 12 h photoperiod such that N fixation rates in units nmol N L $^{-1}$ d $^{-1}$ are calculated as:

$$\begin{aligned} \text{Trichodesmium N fixation} &\approx [\text{cells L}^{-1}] \\ &\quad \times 3 \times 10^{-4} \text{ nmol N cell}^{-1} \text{d}^{-1} \end{aligned} \quad (1)$$

$$\begin{aligned} \text{Heterocystous N fixation} &\approx [\text{heterocysts L}^{-1}] \\ &\quad \times 8.6 \times 10^{-4} \text{ nmol N heterocyst}^{-1} \text{d}^{-1} \end{aligned} \quad (2)$$

We then compared estimated rates to *in situ* $^{15}\text{N}_2$ fixation measurements made in the upper 45 m of the water column as well as particulate N export at 150 m as recorded by sediment traps (see Karl and Letelier, 2008 for methods).

RESULTS AND DISCUSSION

Trichodesmium Morphology

We have presented all *Trichodesmium* volumetric concentrations in units of cells L $^{-1}$; this required consideration of the highly variable morphology of *Trichodesmium*. For free filaments, we measured the length of each filament from apical end to end ($n = 7,586$ filaments for the full data record) and divided that length

by the mean individual cell length measured from a subset of filaments ($10 \pm 2.5 \mu\text{m}$, range = 4–15 μm , $n = 200$) to estimate cells per filament. Filament length and width measurements were made using the program Image-Pro Plus, with distance calibrated at each magnification using a standard micrometer. This method follows that of Hynes (2009). Accurate cell length is clearly critical to this calculation. At Station ALOHA, a number of recent papers have observed Clade I to dominate *Trichodesmium* spp. assemblages (Rouco et al., 2016; Gradoville et al., 2017a). Clade I includes *T. thiebautii*, *T. tenuis*, *T. hildebrandtii*, and *T. spiralis* (Hynes et al., 2012). Within this clade, morphological analyses of seven cultured strains indicate individual cell lengths of 5–22 μm (Hynes et al., 2012). Our measured mean cell length is consistent with these ranges for Clade I species and strains; however, the measured range in cell length (4–15 μm) adds an uncertainty of ~30% to our estimated *Trichodesmium* cell concentrations.

Measured filament length (i.e., the length of a chain of cells) was log-normally distributed with a mean filament length of 90 μm and a range of 12–6801 μm . Using the measured mean cell length, this equates to a geometric mean and standard deviation of 13.2 ± 2.3 cells filament $^{-1}$ (range 1.2–685 cells filament $^{-1}$). This result is significantly less than the mean of 100 cells filament $^{-1}$ used in modeling studies such as Luo et al. (2012) and reports by Letelier and Karl (1996) for Station ALOHA (100 cells filament $^{-1}$ average with a range 6–250 cells filament $^{-1}$, $n = 22$), which were each based on smaller sample sizes. While the range of filament size we observe is consistent with the oft-used average of 100 cells filament $^{-1}$, the variability indicates that enumeration of filaments rather than cells will lead to large uncertainties in *Trichodesmium* biomass.

Of the various morphologies, free filaments dominated the morphological distribution of cells, accounting for $71 \pm 26\%$ of all cells on average. The puff and tuft morphologies accounted for $5 \pm 15\%$ and $12 \pm 16\%$, respectively, while aggregations not clearly matching either morphological category accounted for the remaining $13 \pm 18\%$ (Figure 1). This finding is consistent with Letelier and Karl (1996), where *Trichodesmium* cells associated with a colony morphology accounted for only $12 \pm 11\%$ ($n = 11$) of the total *Trichodesmium* biomass. Given that cells were gravity filtered, the possibility of mechanical disruption of colonies and hence overestimation of free filaments is considered low.

In the NPSG, it is clear that free filaments dominate the morphological distribution of *Trichodesmium* spp. (Maruyama et al., 1970; Marumo and Asaoka, 1974; Letelier and Karl, 1996) and that colonies are observed less frequently. That said, there is no current accepted paradigm for why or how *Trichodesmium* forms colonies. In culture, there are strains that predominately form colonies (e.g., H-9, Hynes et al., 2012) and there are strong species-specific differences in colony shape (e.g., “puffs” and “tufts”), however the ecological advantages of these differences in morphology are not understood. Unraveling this aspect of *Trichodesmium* auto-ecology may be the key to understanding bloom formation and decline. A potential clue to colony formation in *Trichodesmium*, or at least a testable hypothesis, may come from recent research with the freshwater cyanobacteria, *Microcystis* spp., which showed that certain distinct “specialist bacteria” may trigger extracellular

polysaccharide production and colony formation of otherwise single cells of *Microcystis* spp. (Shen et al., 2011).

Seasonality of Large Diazotrophs

Between 2015 and 2016, cell concentrations for *Trichodesmium* spp. were $< 1,000$ cells L^{-1} , with the exception of October–December of 2015 and November of 2016 when significant increases ($> 2,000$ cells L^{-1}) were observed (Table 1, Figure 2). While we do not anticipate absolute cell abundances and gene abundances to agree due to polyploidy (Sargent et al., 2016), variable sampling methodologies, and potential amplification of moribund genetic material from cells that would not be enumerated via epifluorescence, qPCR-based abundances also record high abundances of *Trichodesmium* gene copies in October–December of 2015 and November of 2016 (Table 1). The ratio of *Trichodesmium* gene copies to cell abundances (Figure 4) is 130 ± 239 (range = 1.4–1,405) and is higher but not inconsistent with the degree of polyploidy reported by Sargent et al. (2016) (range = 1–120). Notably, the *Trichodesmium* spp. gene abundances measured in Oct.–Nov. of 2015, when cell abundances were also elevated, were among the highest ever recorded by the HOT program (Church et al., 2009), indicating that qPCR is a sufficient indicator of relative *Trichodesmium* abundance.

The persistent elevation of *Trichodesmium* spp. cell counts and gene copies observed in late 2015 was unexpected as blooms of this organism are thought to be more episodic and generally occurring in summer-fall months coincident with warm temperatures and strong water column stratification (Capone and Carpenter, 1982; Church et al., 2009). During these bloom phases (Oct.–Dec. 2015), colonial morphologies were also more abundant, accounting for $57 \pm 12\%$ of cells when puff, tuft, and other aggregates were summed, relative to the time-series

mean of $29 \pm 26\%$ for *Trichodesmium* cells occurring in aggregations (Figure 1). The abundance of colonies appeared to increase after an extended period of water column stratification in 2015 (Table 2, mixed layer depth < 40 m in June–August) and were associated with an increase in fluorometric Chl *a* (Table 2, 0.16 – $0.29 \mu\text{g L}^{-1}$ between October and December 2015) as well as elevated ^{14}C -based production rates (Table 2, $8.3 \pm 0.1 \text{ mg C m}^{-3} \text{ d}^{-1}$ in Oct. and $6.3 \pm 1.8 \text{ mg C m}^{-3} \text{ d}^{-1}$ in December). These values are slightly higher than their respective climatological means: Oct.–Dec. mean Chl = 0.17 – $0.22 \mu\text{g L}^{-1}$ while the climatological mean for production is $6.7 \text{ mg C m}^{-3} \text{ d}^{-1}$ in Oct. and $5.5 \text{ mg C m}^{-3} \text{ d}^{-1}$ in Dec. This finding of an increase in colony morphologies during periods of enhanced *Trichodesmium* biomass is consistent with that of Rodier and Le Borgne (2008) who reported a similar shift to colonial morphologies during bloom periods in the lagoons of New Caledonia in the South Pacific. By virtue of a high-frequency sampling strategy, these authors were able to show that growth as well as aggregation led to increased *Trichodesmium* biomass in the surface mixed layer however colonies accumulated only at the sea surface and not within the mixed layer. Here we cannot discriminate between growth and the potential concentration of cells from deeper in the euphotic zone into the mixed layer, nonetheless it is clear that these blooms coincided with periods when phytoplankton biomass and production were elevated, possibly due to excretion of bioavailable N sources from diazotrophs which fueled non-diazotrophic growth. We also note that our sampling methodology (bottle-based) may have missed surface-trapped cells that would have been captured via net tows.

In comparison, the temporal variability of summed *Richelia* and *Calothrix* heterocyst concentrations was less pronounced (Figure 3), with heterocyst abundances in the upper 45 m ranging from 4 to 157 heterocysts L^{-1} . When evaluating specific

TABLE 1 | Depth-averaged mean and standard deviation of large diazotroph abundance in the upper 45 m as determined via microscopy and qPCR with the depth integrated (\int) abundances of the summed organism classes as determined from microscopy based cell counts.

Month-Year	<i>Trichodesmium</i> cells L^{-1}	<i>Trichodesmium nifH</i> copies L^{-1}	heterocysts L^{-1}	Het1-3 <i>nifH</i> copies L^{-1}	$\int_{0-45\text{m}}$, cells $\text{m}^{-2} \times 10^7$
Apr-15	409 ± 523	1081 ± 1043	34 ± 18	7914 ± 6004	2
May-15	19 ± 13	759 ± 746	31 ± 17	4462 ± 471	0.2
Jun-15	395 ± 287	$51,457 \pm 203,587$	18 ± 7	9477 ± 4691	2
Jul-15	689 ± 393	$697,578 \pm 778,228$	62 ± 26	$124,485 \pm 63,972$	3
Aug-15	1016 ± 945	$229,836 \pm 241,607$	65 ± 54	$54,450 \pm 64,205$	5
Oct-15	3406 ± 1393	$738,231 \pm 547,465$	64 ± 41	$107,087 \pm 51,575$	16
Nov-15	4131 ± 553	$1,458,663 \pm 214,315$	35 ± 35	$10,892 \pm 3470$	19
Dec-15	2621 ± 131	$164,223 \pm 75,820$	15 ± 5	5998 ± 7305	12
Jan-16	315 ± 448	$92,190 \pm 89,605$	21 ± 17	4559 ± 2534	2
Feb-16	345 ± 491	1801 ± 897	21 ± 14	4376 ± 2320	2
Mar-16	60 ± 48	1038 ± 898	18 ± 4	2498 ± 2142	0.4
Apr-16	8 ± 6	593 ± 354	14 ± 6	5526 ± 908	0.1
May-16	200 ± 156	2748 ± 1415	28 ± 16	1664 ± 2397	1
Jul-16	485 ± 197	8374 ± 9888	46 ± 11	$8638 \pm 10,669$	2
Aug-16	266 ± 9	$10,229 \pm 10,166$	13 ± 6	2773 ± 1433	1
Oct-16	4031 ± 372	$59,106 \pm 7475$	29 ± 8	6238 ± 3051	18
Nov-16	737 ± 465	4233 ± 2853	22 ± 6	148 ± 338	3

Standard deviations are calculated from samples collected at 5, 25, and 45 m for each cruise.

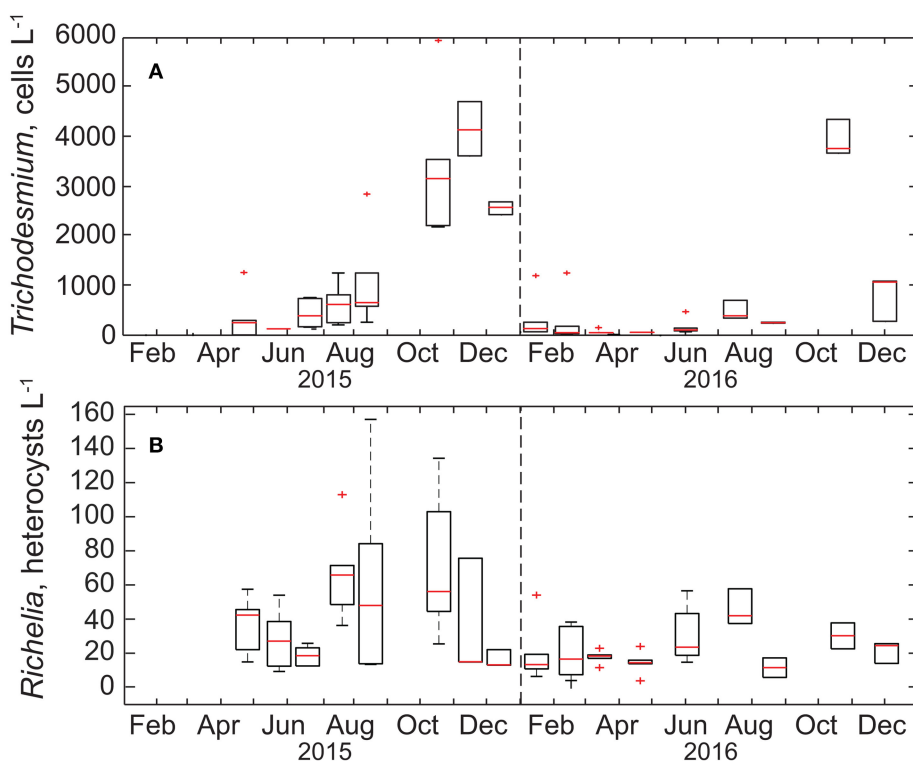


FIGURE 2 | Box-plots of the monthly time-series of **(A)** *Trichodesmium* cells and **(B)** *Richelia* + *Calothrix* heterocysts (the sum of free and diatom-associated heterocysts) in the upper 45 m at Stn. ALOHA. The range of each box spans the 25th–75th percentile of data for each month whereas whiskers are ± 2.7 standard deviations, the red line is the median, and plus symbols are outliers. The dashed vertical line in each panel is the demarcation between years.

TABLE 2 | Mixed layer depth, mean fluorometric Chl a concentrations (Chl), sea surface temperature (SST), average ^{14}C fixation rates between 5–45 m, and sediment trap particulate N export (at 150 m) for 2015 as recorded by the HOT program.

Month-Year	Mixed layer depth, m	Avg. Chl, mg m^{-3}	Avg. SST, $^{\circ}\text{C}$	^{14}C fixation, $\text{mg C m}^{-3} \text{d}^{-1}$	Sediment trap N export $\mu\text{mol N m}^{-2} \text{d}^{-1}$	$\int_{0-45 \text{ m}} \text{Lg. diazo NFR } \mu\text{mol N m}^{-2} \text{d}^{-1}$	$\int_{0-45 \text{ m}} ^{15}\text{N}_2 \text{ fix } \mu\text{mol N m}^{-2} \text{d}^{-1}$	% N_2 fix by lg. diazo
Apr-15	31 ± 15	0.141	24.20	6.0	771	5.7	175	3%
May-15	53 ± 31	0.155	24.50	7.3	206	1.4	140	1%
Jun-15	39 ± 7	0.102	25.45	7.1	455	5.0	100	5%
Jul-15	37 ± 4	0.105	26.48	7.9	375	9.8	84	11%
Aug-15	37 ± 5	0.13	26.71	11.3	249	13.4	102	12%
Oct-15	50 ± 16	0.163	26.09	8.34	320	39.2	69	56%
Nov-15	74 ± 11	0.292	25.86	ND	ND	46.0	ND	ND
Dec-15	61 ± 15	0.161	25.75	7.0	ND	28.9	42	70%
Jan-16	86 ± 12	0.205	24.97	6.8	NA	4.2	50	8%
Feb-16	45 ± 20	0.182	24.52	6.7	NA	4.5	18	25%
Mar-16	105 ± 8	0.165	24.34	ND	NA	1.3	ND	ND
Apr-16	79 ± 9	0.12	24.40	6.5	NA	0.6	ND	ND
May-16	30 ± 11	0.101	25.82	6.8	NA	3.3	65	5%
Jul-16	60 ± 16	0.11	25.83	5.7	NA	7.0	98	7%
Aug-16	37 ± 8	0.133	26.19	6.4	NA	3.4	ND	ND
Oct-16	64 ± 8	0.16	26.21	5.9	NA	44.7	89	50%
Nov-16	88 ± 11	0.22	24.96	NA	NA	8.8	ND	ND

The 0–45 m depth integrated *in situ* $^{15}\text{N}_2$ fixation rate (N_2 fix) measurements is shown and the estimated contribution of large diazotrophs to integrated rates (% N_2 fix by lg. diazo) is calculated as the quotient of N_2 fix estimated for all groups and the measured 0–45 m integrated $^{15}\text{N}_2$ fixation rates. ND indicates months when rates of N_2 fixation were not measured. ND indicates values were not determined whereas NA indicates data not yet available.

diatom-symbiont associations (including *Rhizosolenia* spp., *Hemiaulus* spp., and *Chaetoceros* spp.) we found no difference in the percentage of heterocysts associated with individual diatom genera, with the overall mean for heterocysts associated with *Rhizosolenia*, *Hemiaulus*, and *Chaetoceros*, respectively, to be $29 \pm 18\%$, $35 \pm 21\%$, and $29 \pm 22\%$ of the total observed and the remaining $2.0 \pm 5.0\%$ observed as free filaments. In late summer-fall we do observe elevated abundances of *Rhizosolenia-Richeliea* and *Chaetoceros-Richeliea* particularly in 2015 but also in 2016 for *Rhizosolenia-Richeliea* (**Figure 3**).

Note though that abundances of heterocysts were on average (33 ± 28 heterocysts L^{-1}) significantly lower than that observed for *Trichodesmium* cells ($932 \pm 1,364$ cells L^{-1}), with the mean concentration of heterocysts associated with *Rhizosolenia*, *Hemiaulus*, and *Chaetoceros*, respectively, to be 9 ± 9 heterocysts L^{-1} , 11 ± 13 heterocysts L^{-1} , and 11 ± 9 heterocysts L^{-1} . When integrating over the upper 45 m, areal distributions of large diazotrophs (*Trichodesmium* + heterocysts) were on the order of 10^6 - 10^8 cells m^{-2} (**Table 1**). These values are consistent with the geometric mean (10^8 cells m^{-2}) for the sum of *Trichodesmium*

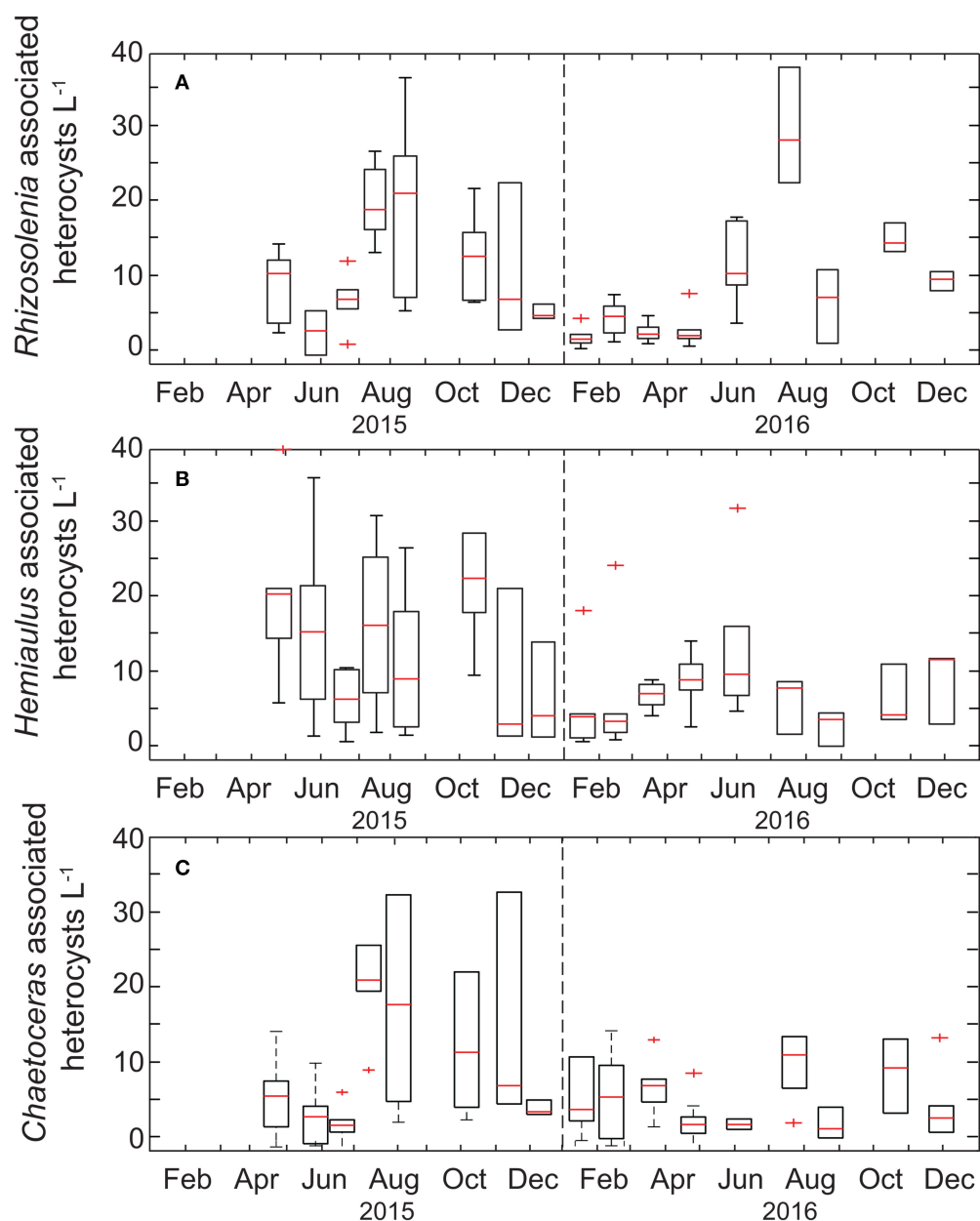


FIGURE 3 | Box-plots of the monthly time-series of heterocysts associated with diatom genera **(A)** *Rhizosolenia*, **(B)** *Hemiaulus*, and **(C)** *Chaetoceros*. The range of each box spans the 25th–75th percentile of data for each month whereas whiskers are ± 2.7 standard deviations, the red line is the median, and plus symbols are outliers.

+ heterocysts presented in a recently assembled global database (Luo et al., 2012).

Notably, gene-based abundances of heterocystous diazotrophs are orders of magnitude greater than cell concentrations (**Table 1**, **Figure 4**) although relative change of the two proxies are consistent. A portion of this difference is due to our restriction of cell counts to heterocysts without inclusion of vegetative cells, however given 3–5 vegetative cells per trichome on average (Foster et al., 2007), this methodological difference alone cannot explain the large discrepancy (gene copies: heterocyst counts = 542 ± 811 , $n = 51$). Significantly different volumes were also examined (2 L for qPCR and 10 L for microscopy) and samples were not collected on the same cast such that the natural heterogeneity of these large organisms in the water column may play a role in the observed differences. However, one would expect the larger the volume filtered, the higher the probability of capturing rare or heterogeneously distributed cells. We find the opposite with qPCR suggesting higher cell concentrations than observed via microscopy. The most likely explanation for the discrepancies are variable gene copies per cell. Heterocystous cyanobacteria are known to have more than one gene copy per genome (Foster and O'Mullen, 2008) although it is unclear how variable the relationship between

nifH gene copies and cell abundance is *in situ*. If we adjusted our heterocyst counts by a factor of 5 to include gene copies in vegetative cells, qPCR based abundance are on average more than a $100 \times$ higher than cell-based estimates. Other potential explanations for this disparity include (1) the potential for non-specificity of het-1 and het-2 primers and probes as described in Foster et al. (2007), (2) omission of heterocysts that may have been embedded in *Trichodesmium* colonies and hence not readily visible via microscopy (Momper et al., 2015), and (3) amplification of moribund DNA that would not have been detected by epifluorescence microscopy. The lack of agreement between gene and cell based abundances is a topic that clearly needs further study.

While large diazotrophs were recorded in every sample collected over our study period (**Table 1**) our findings indicate that neither DDA's nor *Trichodesmium* spp. were major contributors to plankton biomass. Considering the more abundant of the two classes and the *Trichodesmium* Chl *a* content per cell reported by Letelier and Karl (2.6 pg chl *a* cell $^{-1}$), the maximum observed *Trichodesmium* densities in our study would account for <5% of the standing stock of Chl *a*, significantly less than mean 18% reported by Letelier and Karl (1996) for 1991–1992. Assuming that we have not underestimated large diazotroph biomass, for example by missing surface-trapped cells, our findings indicate that while these relatively rare organisms would not be expected to appreciably contribute to bulk biomass measures, aperiodic enhancement of diazotroph biomass may fuel “echo blooms” as a result of the input of new nitrogen (Walsh and Steidinger, 2001). In contrast to our findings here, other studies have observed significant contributions of large diazotrophs to bulk organic matter. Specifically, Pasulka et al. (2013) microscopically estimated *Trichodesmium* spp. biovolume at Station ALOHA (2004–2009) in small volume samples (0.5 L filtered and a minimum of 10 ml volume imaged) and concluded that *Trichodesmium* in the upper 50 m could account for 20–50% of total carbon in late summer to early fall. These authors do note that observations of *Trichodesmium* were relatively rare events and when observed they were clumped and unevenly distributed on the filters. Additionally, Venrick (1974) recorded up to 2,000 heterocysts L $^{-1}$ in early transects of the NPSG, and gene-based abundance herein and elsewhere have also reported *nifH* phylotypes belonging to heterocystous symbionts on the order of ~ 1000 's L $^{-1}$ (Church et al., 2009; Shiozaki et al., 2017). Keeping in mind the large differences in methodology between prior studies and our own, heterogeneity and aperiodicity appear to be the norm for these large diazotrophs. Future work is necessary to evaluate the environmental triggers that lead to accumulations of these keystone species.

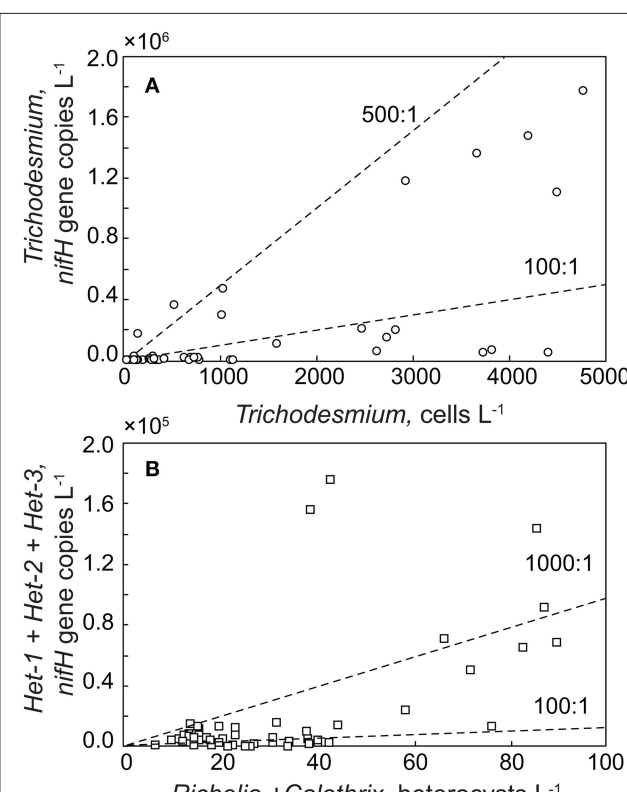


FIGURE 4 | Relationship between cell abundance and gene copies for (A) *Trichodesmium* and (B) heterocystous cyanobacteria collected in the upper 45 m from Station ALOHA. Note that for heterocystous cells, microscopy-based counts only considered the heterocyst while there are known to be *nifH* copies in the vegetative cells as well. Isolines of gene copies: cell abundance ratios are noted as dashed lines.

Estimated Contributions of New Production

During the 2015 and 2016 winter blooms, we estimate the upper limit of N fixation rates by *Trichodesmium* spp. to be ~ 1.4 nmol N L $^{-1}$ d $^{-1}$. During non-bloom periods, rates potentially driven by this genus are estimated to be $0.12 \pm$

0.21 nmol N L⁻¹ d⁻¹. When N fixation rates measured via ¹⁵N₂ tracer additions were available (Table 1), we estimate that *Trichodesmium* productivity generally accounted for ~5% of the measured 0–45 m integrated N₂ fixation rates, with the 2015 bloom accounting for 30–90% of measured ¹⁵N₂ fixation in the upper 45 m. Given the lower abundances of heterocystous diazotrophs compared to *Trichodesmium*, we estimate reduced group-specific rates of N fixation by these organisms, ranging from 0.01 to 0.13 nmol N L⁻¹ d⁻¹ with contributions to measured ¹⁵N₂ fixation never exceeding 11%. We have chosen not to make these same calculations using gene-based abundances due to known variability in *nifH* gene copies per cell. These findings are very similar to findings in the North Atlantic where Martinez-Perez et al. (2016) use single-cell analyses to show that *Trichodesmium* spp. are generally minor contributors to N fixation (<20%). Importantly these authors (Martinez-Perez et al., 2016) also report high percentages (46%) of non-N₂ fixing *Trichodesmium* spp. and caution that “the large variability observed in *Trichodesmium* cellular activities indicates that N₂ fixation estimates based on the mere abundance should be treated with caution.” If this is the case at Station ALOHA, then our biomass-based rates may over-estimate actual contributions to new production by this enigmatic microorganism.

Particulate N export rates are also available from HOT sediment trap deployments conducted in 2015 (Table 2). We have compared the summed rates of N fixation estimated for these diazotrophs and integrated these rates over the upper 45 m. Comparison of these rates to N export indicate that large diazotrophs would contribute 0.3–17% of the new production reaching the 150 m horizon. These estimates are far less than that predicted by isotopic mass balance (26–47%, Böttjer et al., 2017) indicating that other diazotrophs such as *Crocospaera* spp. or Group-A cyanobacteria may fuel the much of the N₂ driven new production in this region. This assertion of course assumes our 2-year sampling record is representative of the mean state in the NPSG.

CONCLUSIONS

The study of large cell-sized phytoplankton in the oligotrophic ocean is effectively the study of rare species (Chisholm, 1992). While significantly less abundant than the small cyanobacteria that dominate autotrophic community structure in the NPSG (e.g., *Prochlorococcus* and *Synechococcus* spp. Campbell and Vaulot, 1993), these large diazotrophs serve unique ecosystem functions. Specifically, these include acting as habitat for a wide array of species, from bacteria to metazoans (O’Neil, 1998; Sheridan et al., 2002; Hewson et al., 2009; Gradoville et al., 2017a) and as a source of “new” nitrogen to an otherwise N starved upper ocean (Karl et al., 1997). Hence, these rare organisms have a disproportionate impact on the ocean metabolism relative to their abundance. By enumerating the cell-based concentrations of *Trichodesmium* spp. and DDAs over a 2-year period we have characterized the temporal variability of these populations and estimated their impact on measured rates of ¹⁵N₂ fixation and the export of particles. There are four major findings of our

work: (1) the abundance of *Trichodesmium* spp., is highly variable at monthly time-scales whereas we observed reduced variability and lower concentrations of DDAs in the mixed layer; (2) gene-based and cell-based metrics of diazotroph abundance diverge widely for reasons not fully understood albeit at least in part due to polyploidy and variable genetic content per cell; (3) while colonial morphologies of *Trichodesmium* spp. generally comprise a minor fraction of the total *Trichodesmium* cell counts, they are significantly more abundant during bloom periods, and (4) assuming maximum cell-specific N fixation rates from the literature (Hutchins et al., 2007; Foster et al., 2011), we conclude that these large diazotrophs were generally minor contributors to bulk rates of ¹⁵N₂ fixation as well as N export to 150 m. The exception to this last finding are aperiodic *Trichodesmium* blooms which appeared to strongly impact upper water column biomass and production in winter months of 2015–2016.

Our first two findings are largely to be expected in the NPSG. Patchiness is a hallmark of *Trichodesmium* and DDA ecology in oligotrophic regimes (Maruyama et al., 1970; Venrick, 1974; Shiozaki et al., 2017). The more surprising finding of this work is the conclusion that these large diazotrophs are typically minor contributors to both bottle-based ¹⁵N₂ fixation measurements in this region as well as N export. This conclusion is not isolated; prior studies also indicate a generally minor role for large diazotrophs as contributors to new production. Size-fractionated ¹⁵N₂ fixation measurements at Station ALOHA indicate that ¹⁵N₂ fixation in the >10 μm size class accounts for 0–83% of bulk rates with mean contributions of 5, 35, 33, and 12% when seasonally binned for spring, summer, fall, and winter, respectively (Church et al., 2009). Similarly in the West Pacific, Kitajima et al. (2009) measured the abundance of both *Trichodesmium* cells and *Richelia* heterocysts ranging from 0 to 436 cells L⁻¹ and report that these genera could only account for <0.7% of the whole-water activity. And as already discussed, recent single-cell analyses in the North Atlantic indicate that *Trichodesmium* are not uniformly active and contribute generally <20% to total N fixation (Martinez-Perez et al., 2016).

The conundrum then is that a hallmark of Station ALOHA is a predictable and efficient summer export pulse to the deep ocean, presumably driven by large diazotrophs (Karl et al., 2012). Here we try to reconcile these disparate views. Karl et al. (2012) have shown that deep sediment traps record an annual summer pulse of N to ~4000 m in the NPSG which is isotopically, genetically, and elementally consistent with DDA export. Specifically, these authors observed a surface diazotroph community dominated by Group A cyanobacteria whereas *nifH* genes quantified from particulate matter at 4000 m were dominated by heterocystous phylotypes characteristic of endosymbiotic cyanobacteria. This summer export pulse is thus hypothesized to be driven by rapid, high efficiency export of DDA assemblages in summer (Karl et al., 2012). As a “back of envelope” calculation we can compare the estimated rates of N fixation by the sum of large diazotrophs in the upper water column (~1–46 μmol N m⁻² d⁻¹) to measured rates of N export at 4000 m assuming a range of export ratios (export flux/production; Figure 5). Note that the maximum carbon based export ratio at Station ALOHA is 0.15 (measured between 1989 and 2009, Karl et al., 2012). The increase

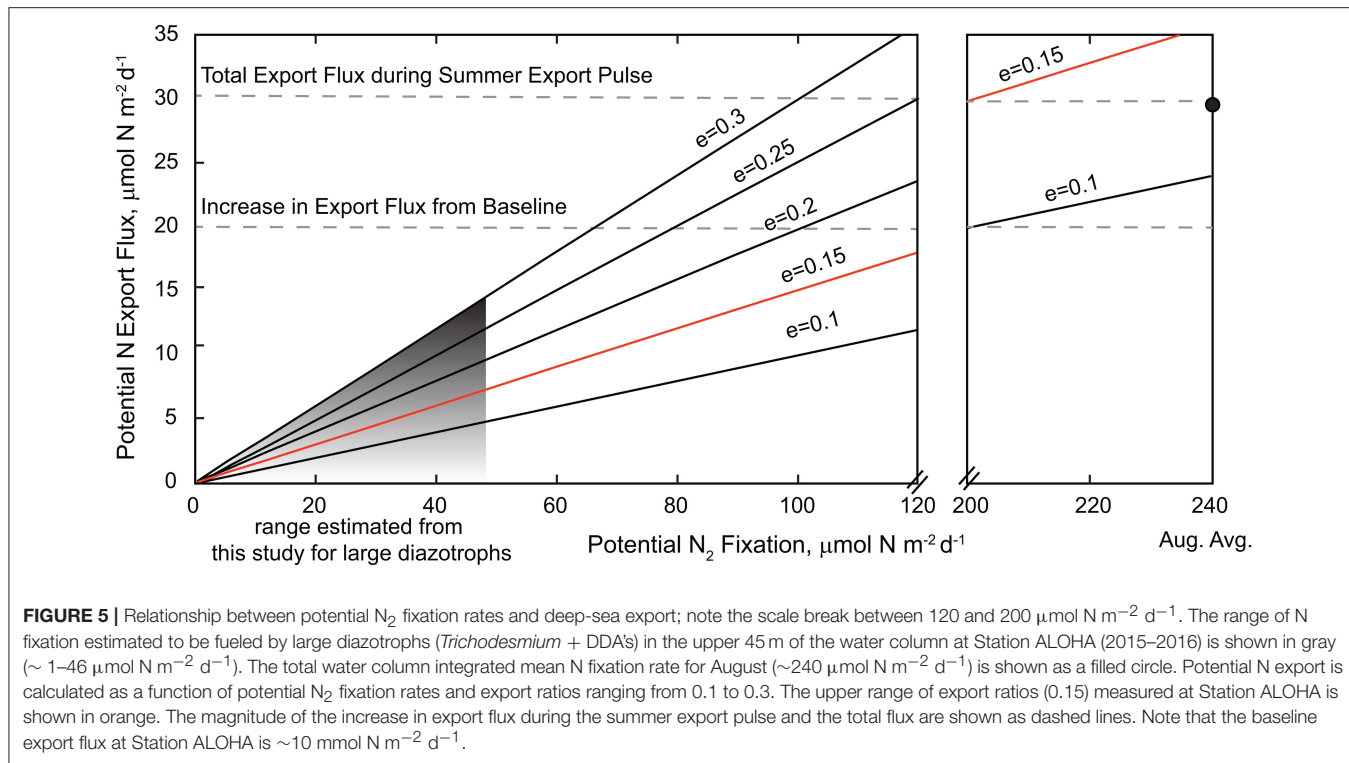


FIGURE 5 | Relationship between potential N_2 fixation rates and deep-sea export; note the scale break between 120 and 200 $\mu\text{mol N m}^{-2} \text{d}^{-1}$. The range of N_2 fixation estimated to be fueled by large diazotrophs (*Trichodesmium* + DDA's) in the upper 45 m of the water column at Station ALOHA (2015–2016) is shown in gray (~ 1 – $46 \mu\text{mol N m}^{-2} \text{d}^{-1}$). The total water column integrated mean N fixation rate for August ($\sim 240 \mu\text{mol N m}^{-2} \text{d}^{-1}$) is shown as a filled circle. Potential N export is calculated as a function of potential N_2 fixation rates and export ratios ranging from 0.1 to 0.3. The upper range of export ratios (0.15) measured at Station ALOHA is shown in orange. The magnitude of the increase in export flux during the summer export pulse and the total flux are shown as dashed lines. Note that the baseline export flux at Station ALOHA is $\sim 10 \mu\text{mol N m}^{-2} \text{d}^{-1}$.

in N flux recorded during the summer export pulse at Station ALOHA is on order of $\sim 20 \mu\text{mol N m}^{-2} \text{d}^{-1}$ (Karl et al., 2012). In order for estimated production by large diazotrophs alone to account for the level of N export observed in deep traps, the export efficiency would need to be extremely high, e.g., $>30\%$. Alternately, if the export ratio is more consistent with measured ratios ($e = 0.02$ – 0.15), then either large diazotroph production would need to be an order of magnitude greater than what we have estimated or other N_2 -fixing organisms are directly or indirectly contributing to the summer export pulse. While not observed in our study period, there is precedent in the literature for an order of magnitude increase in the concentration of large diazotrophs as discussed earlier (Venrick, 1974; Church et al., 2009; Pasulka et al., 2013; Shiozaki et al., 2017) and presumably their contribution to production and export. And so, while DDA cell abundances were relatively low over our study period and the disparity between cell- and gene-based abundance needs to be reconciled, there are historical records of abundances that are more consistent with summer DDA-driven export than ours. However, given the current knowledge of export ratios, it seems more likely that other smaller diazotrophs may be contributing to the summer export pulse directly or via stimulation of “echo blooms” of non-diazotrophic diatom assemblages. In fact, the water column integrated $^{15}\text{N}_2$ fixation rate measured at Station ALOHA ($\sim 240 \mu\text{mol N m}^{-2} \text{d}^{-1}$), would only require a modest e -ratio (< 0.1) to account for the measured increase in N flux. While we do not yet know if a summer export pulse was recorded during our study period, our data indicate that either extremely high export ratios would be required to fuel the observed magnitude of summer export pulses or the abundance

and activity of large diazotrophs would need to be significantly greater than observed in this study. Further study of diazotroph abundances in conjunction with cell-specific rate measurements and imaging based records of cell export (e.g., Durkin et al., 2015) in this region is necessary to elucidate the linkages between growth and community structure of diazotrophs in the surface ocean and their relative contributions to particle export.

DATA AVAILABILITY STATEMENT

All data are available via the Simons Collaboration on Ocean Processes and Ecology data page (<http://scope.soest.hawaii.edu/data/hot/>).

AUTHOR CONTRIBUTIONS

AW: Designed the study and wrote the manuscript; KW-B: Performed all diazotroph cell counts; MC: Contributed nitrogen fixation rate measurements and gene abundances; All authors contributed to editing and revision of the manuscript.

ACKNOWLEDGMENTS

This work was funded by the Simons Foundation (Award 329108 to AW and MC) and made possible via National Science Foundation support of the HOT program (OCE1260164 to MC and DMK). We thank Tara Clemente and the SCOPE operations team for sample collection and shipping. No authors declare any real or perceived financial conflicts of interests.

REFERENCES

- Böttjer, D., Dore, J. E., Karl, D. M., Letelier, R. M., Mahaffey, C., Wilson, S. T., et al. (2017). Temporal variability of nitrogen fixation and particulate nitrogen export at Station ALOHA. *Limnol. Oceanogr.* 62, 200–216. doi: 10.1002/lno.10386
- Bowman, T. E., and Lancaster, L. J. (1965). A bloom of the planktonic blue-green algae, *Trichodesmium erythraeum*, in the Tonga Islands. *Limnol. Oceanogr.* 10, 291–293. doi: 10.4319/lo.1965.10.2.0291
- Campbell, L., and Vaulot, D. (1993). Photosynthetic picoplankton community structure in the subtropical North Pacific Ocean near Hawaii (station ALOHA). *Deep Sea Res. I Oceanogr. Res. Pap.* 40, 2043–2060. doi: 10.1016/0967-0637(93)90044-4
- Capone, D. G., and Carpenter, E. J. (1982). Nitrogen fixation in the marine environment. *Science*, 217, 1140–1142. doi: 10.1126/science.217.4565.1140
- Capone, D. G., Subramaniam, A., Montoya, J. P., Voss, M., Humborg, C., Johansen, A. M., et al. (1998). An extensive bloom of the N₂-fixing cyanobacterium *Trichodesmium erythraeum* in the central Arabian Sea. *Mar. Ecol. Progr. Ser.* 172, 281–292. doi: 10.3354/meps172281
- Carpenter, E. J., Subramaniam, A., and Capone, D. G. (2004). Biomass and primary productivity of the cyanobacterium *Trichodesmium* spp. in the tropical N Atlantic ocean. *Deep Sea Res. I Oceanogr. Res. Pap.* 51, 173–203. doi: 10.1016/j.dsr.2003.10.006
- Chisholm, S. W. (1992). "Phytoplankton size," in *Primary Productivity and Biogeochemical Cycles in the Sea. Environmental Science Research*, Vol. 43, eds P. G. Falkowski, A. D. Woodhead, and K. Vivirito (Boston, MA: Springer).
- Church, M., Björkman, K., Karl, D., Saito, M., and Zehr, J. (2008). Regional distributions of nitrogen-fixing bacteria in the Pacific Ocean. *Limnol. Oceanogr.* 53:63. doi: 10.4319/lo.2008.53.1.0063
- Church, M., Jenkins, B., Karl, D., and Zehr, J. (2005). Vertical distributions of nitrogen-fixing phylotypes at Stn ALOHA in the oligotrophic North Pacific Ocean. *Aquat. Microb. Ecol.* 38, 3–14. doi: 10.3354/ame038003
- Church, M., Mahaffey, C., Letelier, R., Lukas, R., Zehr, J., and Karl, D. (2009). Physical forcing of nitrogen fixation and diazotroph community structure in the North Pacific subtropical gyre. *Global Biogeochem. Cycles* 23, GB2020. doi: 10.1029/2008GB003418
- Dore, J., Brum, J., Tupas, L., and Karl, D. M. (2002). Seasonal and interannual variability in sources of nitrogen supporting export in the oligotrophic subtropical North Pacific Ocean. *Limnol. Oceanogr.* 47, 1595–1607. doi: 10.4319/lo.2002.47.6.1595
- Durkin, C. A., Estapa, M. L., and Buesseler, K. O. (2015). Observations of carbon export by small sinking particles in the upper mesopelagic. *Mar. Chem.* 175, 72–81. doi: 10.1016/j.marchem.2015.02.011
- Foster, R. A., Kuypers, M. M., Vagner, T., Paerl, R. W., Musat, N., and Zehr, J. P. (2011). Nitrogen fixation and transfer in open ocean diatom-cyanobacterial symbioses. *ISME J.* 5, 1484–1493. doi: 10.1038/ismej.2011.26
- Foster, R., and O'Mullen, G. (2008). "Nitrogen-fixing and nitrifying symbioses in the marine environment," in *Nitrogen in the Marine Environment*, eds D. Capone, D. Bronk, M. Mulholland, and E. Carpenter (San Diego, CA: Academic Press/Elsevier), 1197–1218.
- Foster, R., Subramaniam, A., Mahaffey, C., Carpenter, E., Capone, D., and Zehr, J. (2007). Influence of the Amazon River plume on distributions of free-living and symbiotic cyanobacteria in the western tropical north Atlantic Ocean. *Limnol. Oceanogr.* 52, 517–532. doi: 10.4319/lo.2007.52.2.0517
- Galloway, J. N., Dentener, F. J., Capone, D. G., Boyer, E. W., Howarth, R. W., Seitzinger, S. P., et al. (2004). Nitrogen cycles: past, present, and future. *Biogeochemistry* 70, 153–226. doi: 10.1007/s10533-004-0370-0
- Gradoville, M. R., Crump, B. C., Hase, C., Letelier, R., Zehr, J. P., and White, A. E. (2017b). Diversity and activity of nitrogen-fixing communities across ocean basins. *Limnol. Oceanogr.* 62, 1895–1909. doi: 10.1002/lno.10542
- Gradoville, M. R., Crump, B. C., Letelier, R., Church, M. J., and White, A. E. (2017a). Microbiome of *Trichodesmium* colonies from the north pacific subtropical gyre. *Front. Microbiol.* 8:1122. doi: 10.3389/fmicb.2017.01122
- Griese, M., Lange, C., and Soppa, J. (2011). Ploidy in cyanobacteria. *FEMS Microbiol. Lett.* 323, 124–131. doi: 10.1111/j.1574-6968.2011.02368.x
- Hewson, I., Poretsky, R. S., Dyhrman, S. T., Zielinski, B., White, A. E., Tripp, H. J., et al. (2009). Microbial community gene expression within colonies of the diazotroph, *Trichodesmium*, from the Southwest Pacific Ocean. *ISME J.* 3, 1286. doi: 10.1038/ismej.2009.75
- Hutchins, D. A., Fu, F., Zhang, Y., Warner, M. E., Feng, Y., Portune, K., et al. (2007). CO₂ control of *Trichodesmium* N₂ fixation, photosynthesis, growth rates, and elemental ratios: implications for past, present, and future ocean biogeochemistry. *Limnol. Oceanogr.* 52, 1293–1304. doi: 10.4319/lo.2007.52.4.1293
- Hynes, A. M. (2009). *Diversity of the Marine Cyanobacterium Trichodesmium: Characterization of the Woods Hole Culture Collection and Quantification of Field Populations*. Woods Hole, MA: MIT/WHOI.
- Hynes, A. M., Webb, E. A., Doney, S. C., and Waterbury, J. B. (2012). Comparison of cultured *Trichodesmium* (cyanophyceae) with species characterized from the field. *J. Phycol.* 48, 196–210. doi: 10.1111/j.1529-8817.2011.01096.x
- Karl, D. M., Church, M. J., Dore, J. E., Letelier, R. M., and Mahaffey, C. (2012). Predictable and efficient carbon sequestration in the North Pacific Ocean supported by symbiotic nitrogen fixation. *Proc. Natl. Acad. Sci. U.S.A.* 109, 1842–1849. doi: 10.1073/pnas.1120312109
- Kana, T. M., Darkangelo, C., Hunt, M. D., Oldham, J. B., Bennett, G. E., and Cornwell, J. C. (1994). Membrane inlet mass spectrometer for rapid high-precision determination of N₂, O₂, and Ar in environmental water samples. *Anal. Chem.* 66, 4166–4170.
- Karl, D. M., Letelier, R. M., Hebel, D. V., Bird, D. F., and Winn, C. D. (1992). "Trichodesmium blooms and new nitrogen in the North Pacific gyre," in *Marine Pelagic Cyanobacteria: Trichodesmium and Other Diazotrophs*, ed E. J. Carpenter, D. G. Capone, and J. G. Rueter (Dordrecht: Springer), 219–237.
- Karl, D., and Letelier, R. (2008). Nitrogen fixation-enhanced carbon sequestration in low nitrate, low chlorophyll seascapes. *Mar. Ecol. Progr. Ser.* 364, 257–268. doi: 10.3354/meps07547
- Karl, D., Letelier, R., Tupas, L., Dore, J., Christian, J., and Hebel, D. (1997). The role of nitrogen fixation in biogeochemical cycling in the subtropical North Pacific Ocean. *Nature*, 388, 533–538. doi: 10.1038/41474
- Kitajima, S., Furuya, K., Hashihama, F., Takeda, S., and Kanda, J. (2009). Latitudinal distribution of diazotrophs and their nitrogen fixation in the tropical and subtropical western North Pacific. *Limnol. Oceanogr.* 54:537. doi: 10.4319/lo.2009.54.2.0537
- Letelier, R. M., and Karl, D. M. (1996). Role of *Trichodesmium* spp. in the productivity of the subtropical North Pacific Ocean. *Mar. Ecol. Progr. Ser.* 133, 1–3. doi: 10.3354/meps133263
- Luo, Y.-W., Doney, S. C., Anderson, L. A., Benavides, M., Berman-Frank, I., Bode, A., et al. (2012). Database of diazotrophs in global ocean: abundances, biomass and nitrogen fixation rates. *Earth Syst. Sci. Data* 4, 47–73. doi: 10.5194/essd-4-47-2012
- Martinez-Perez, C., Mohr, W., Löscher, C. R., Dekaezemacker, J., Littmann, S., Yilmaz, P., et al. (2016). The small unicellular diazotrophic symbiont, UCYN-A, is a key player in the marine nitrogen cycle. *Nat. Microbiol.* 1:16163. doi: 10.1038/nmicrobiol.2016.163
- Marumo, R., and Asaoka, O. (1974). Distribution of pelagic blue-green algae in the North Pacific Ocean. *J. Oceanogr. Soc. Japan* 30, 77–85. doi: 10.1007/BF02112896
- Maruyama, Y., Taga, N., and Matsuda, O. (1970). Distribution of nitrogen fixing bacteria in the central Pacific Ocean. *J. Oceanogr. Soc. Japan* 26, 360–366. doi: 10.1007/BF02753907
- Momper, L. M., Reese, B. K., Carvalho, G., Lee, P., and Webb, E. A. (2015). A novel cohabitation between two diazotrophic cyanobacteria in the oligotrophic ocean. *ISME J.* 9, 882–893. doi: 10.1038/ismej.2014.186
- Mulholland, M. R., and Capone, D. G. (2001). Stoichiometry of nitrogen and carbon utilization in cultured populations of *Trichodesmium* IMS101: implications for growth. *Limnol. Oceanogr.* 46, 436–443. doi: 10.4319/lo.2001.46.2.0436
- O'Neil, J. M. (1998). The colonial cyanobacterium *Trichodesmium* as a physical and nutritional substrate for the harpacticoid copepod *Macrocetella gracilis*. *J. Plankton Res.* 20, 43–59. doi: 10.1093/plankt/20.1.43
- Pasulka, A. L., Landry, M. R., Taniguchi, D. A., Taylor, A. G., and Church, M. J. (2013). Temporal dynamics of phytoplankton and heterotrophic protists at station ALOHA. *Deep Sea Res. II Top. Stud. Oceanogr.* 93, 44–57. doi: 10.1016/j.dsr2.2013.01.007

- Poulton, A. J., Stinchcombe, M. C., and Quartly, G. D. (2009). High numbers of *Trichodesmium* and diazotrophic diatoms in the southwest Indian Ocean. *Geophys. Res. Lett.* 36:L15610. doi: 10.1029/2009GL039719
- Robidart, J. C., Church, M. J., Ryan, J. P., Ascani, F., Wilson, S. T., Bombar, D., et al. (2014). Ecogenomic sensor reveals controls on N2-fixing microorganisms in the North Pacific Ocean. *ISME J.* 8, 1175–1185. doi: 10.1038/ismej.2013.244
- Rodier, M., and Le Borgne, R. (2008). Population dynamics and environmental conditions affecting *Trichodesmium* spp. (filamentous cyanobacteria) blooms in the south-west lagoon of New Caledonia. *J. Exp. Mar. Biol. Ecol.* 358, 20–32. doi: 10.1016/j.jembe.2008.01.016
- Rouco, M., Haley, S. T., and Dyhrman, S. T. (2016). Microbial diversity within the *Trichodesmium* holobiont. *Environ. Microbiol.* 18, 5151–5160. doi: 10.1111/1462-2920.13513
- Sargent, E. C., Hitchcock, A., Johansson, S. A., Langlois, R., Moore, C. M., LaRoche, J., et al. (2016). Evidence for polyploidy in the globally important diazotroph *Trichodesmium*. *FEMS Microbiol. Lett.* 363:fnw244. doi: 10.1093/femsle/fnw244
- Scharek, R., Tupas, L., and Karl, D. M. (1999). Diatom fluxes to the deep sea in the oligotrophic North Pacific gyre at Station ALOHA. *Mar. Ecol. Prog. Ser.* 182, 55–67. doi: 10.3354/meps182055
- Shen, H., Niu, Y., Xie, P., Tao, M., and Yang, X. (2011). Morphological and physiological changes in *Microcystis aeruginosa* as a result of interactions with heterotrophic bacteria. *Freshw. Biol.* 56, 1065–1080. doi: 10.1111/j.1365-2427.2010.02551.x
- Sheridan, C. C., Steinberg, D. K., and Kling, G. W. (2002). The microbial and metazoan community associated with colonies of *Trichodesmium* spp.: a quantitative survey. *J. Plankton Res.* 24, 913–922. doi: 10.1093/plankt/24.9.913
- Shiozaki, T., Bombar, D., Riemann, L., Hashihama, F., Takeda, S., Yamaguchi, T., et al. (2017). Basin scale variability of active diazotrophs and nitrogen fixation in the North Pacific, from the tropics to the subarctic Bering Sea. *Global Biogeochemical Cycles.* 31, 996–1009. doi: 10.1002/2017GB005681
- Tyrrell, T., Maranon, E., Poulton, A. J., Bowie, A. R., Harbour, D. S., and Woodward, E. M. S. (2003). Large-scale latitudinal distribution of *Trichodesmium* spp. in the Atlantic Ocean. *J. Plankton Res.* 25, 405–416. doi: 10.1093/plankt/25.4.405
- Venrick, E. L. (1974). The distribution and significance of *Richelia intracellularis* Schmidt in the North Pacific Central Gyre. *Limnol. Oceanogr.* 19, 437–445. doi: 10.4319/lo.1974.19.3.0437
- Walsh, J. J., and Steidinger, K. A. (2001). Saharan dust and Florida red tides: the cyanophyte connection. *J. Geophys. Res. Oceans* 106, 11597–11612. doi: 10.1029/1999JC000123
- Wilson, S. T., Böttjer, D., Church, M. J., and Karl, D. M. (2012). Comparative assessment of nitrogen fixation methodologies, conducted in the oligotrophic North Pacific Ocean. *Appl. Environ. Microbiol.* 78, 6516–6523. doi: 10.1128/AEM.01146-12
- Zehr, J. P., Mellon, M. T., and Zani, S. (1998). New nitrogen-fixing microorganisms detected in oligotrophic oceans by amplification of nitrogenase (nifH) genes. *Appl. Environ. Microbiol.* 64, 3444–3450.
- Zehr, J. P., Waterbury, J. B., Turner, P. J., Montoya, J. P., Omorogie, E., Steward, G. F., et al. (2001). Unicellular cyanobacteria fix N₂ in the subtropical North Pacific Ocean. *Nature* 412, 635–616. doi: 10.1038/35088063

Conflict of Interest Statement: The authors declare that the research was conducted in the absence of any commercial or financial relationships that could be construed as a potential conflict of interest.

The reviewer RAF declared a past collaboration and co-authorship with one of the authors, AW.

Copyright © 2018 White, Watkins-Brandt and Church. This is an open-access article distributed under the terms of the Creative Commons Attribution License (CC BY). The use, distribution or reproduction in other forums is permitted, provided the original author(s) and the copyright owner are credited and that the original publication in this journal is cited, in accordance with accepted academic practice. No use, distribution or reproduction is permitted which does not comply with these terms.

Advantages of publishing in Frontiers



OPEN ACCESS

Articles are free to read for greatest visibility and readership



FAST PUBLICATION

Around 90 days from submission to decision



HIGH QUALITY PEER-REVIEW

Rigorous, collaborative, and constructive peer-review



TRANSPARENT PEER-REVIEW

Editors and reviewers acknowledged by name on published articles



REPRODUCIBILITY OF RESEARCH

Support open data and methods to enhance research reproducibility



DIGITAL PUBLISHING

Articles designed for optimal readership across devices



FOLLOW US
@frontiersin



IMPACT METRICS
Advanced article metrics track visibility across digital media



EXTENSIVE PROMOTION
Marketing and promotion of impactful research



LOOP RESEARCH NETWORK
Our network increases your article's readership

Frontiers

Avenue du Tribunal-Fédéral 34
1005 Lausanne | Switzerland

Visit us: www.frontiersin.org

Contact us: info@frontiersin.org | +41 21 510 17 00